TECHNICAL REPORT STANDARD TITLE PAGE

1. Report No.	2. Government Accession No.	3. Recipient's Catalog No.
FHWATX-77-7-2F		

4. Title and Subtitle	5. Report Date
STRENGTH AND STIFFNESS OF REINFORCED CONCRETE COLUMNS UNDER BIAXIAL BENDING	November 1976
	6. Performing Organization Code
7. Author(s)	8. Performing Organization Report No.
V. Mavichak and R. W. Furlong	Research Report 7-2F
9. Performing Organization Name and Address	10. Work Unit No.
Center for Highway Research The University of Texas at Austin Austin, Texas 78712	11. Contract or Grant No. Research Study 3-5-73-7
	13. Type of Report and Period Covered
12. Sponsoring Agency Name and Address	Final
Texas State Department of Highways and Public Transportation; Transportation Planning Division P. O. Box 5051 Austin, Texas 78763	14. Sponsoring Agency Code

15. Supplementary Notes

Work done in cooperation with the U. S. Department of Transportation, Federal Highway Administration.
Research Study Title: "Design Parameters for Columns in Bridge Bents"

16. Abstract

The strength and stiffness behavior of reinforced concrete columns subjected to biaxial bending and compression was investigated. In order to provide data points on biaxial interaction surfaces, nine rectangular cross section columns and fifteen partial circular cross section columns were loaded to failure as moments were increased while thrust was maintained at a constant value. Test data included longitudinal strain profiles as well as transverse displacement measurements at all levels of load. Test measurements were compared with a discrete element analytical model that was modified to provide results that were in favorable agreement with measured response. Test results from other investigators were included in the data against which analytical results were checked. The reciprocal thrust equation was selected as the simplest analytical expression that provided approximations of strength that were consistent with test results. The influence of slenderness effects in skew bending was examined. The moment magnifier method was used for approximate analysis of slenderness. Member stiffness relationships recommended by the ACI Building Code were studied in addition to alternate approximations of EI. The ACI procedures were found to five safe results at low thrust levels only if ACI Eq (10-7) was used. Moment magnification used separately for each principal axis of bending appeared to give rational reflections of biaxial behavior. The discrete element analytical model was also used to produce more analytical data for comparison with the approximate methods of analysis. Simple approximations of EI were not found to be consistent with test data when thrust levels varied and when slenderness ratios were large.

17. Key Words	18. Distribution Statement
columns, reinforced concrete, strength, stiffness, biaxial bending, compression	No restrictions. This document is available to the public through the National Technical Information Service, Springfield, Virginia 22161.

19. Security Classif. (of this report)	20. Security Classif. (of this page)	21. No. of Pages	22. Price
Unclassified	Unclassified	242	

Form DOT F 1700.7 (8-69)

STRENGTH AND STIFFNESS OF REINFORCED CONCRETE COLUMNS UNDER BIAXIAL BENDING

by

V. Mavichak and R. W. Furlong

Research Report 7-2F

Project 3-5-73-7
Design Parameters for Columns in Bridge Bents

Conducted for

Texas
State Department of Highways and Public Transportation

In Cooperation with the
U. S. Department of Transportation
Federal Highway Administration

by

CENTER FOR HIGHWAY RESEARCH
THE UNIVERSITY OF TEXAS AT AUSTIN

November 1976

The contents of this report reflect the views of the authors, who are responsible for the facts and the accuracy of the data presented herein. The contents do not necessarily reflect the official views or policies of the Federal Highway Administration. This report does not constitute a standard, specification, or regulation.

There was no invention or discovery conceived or first actually reduced to practice in the course of or under this contract, including any art, method, process, machine, manufacture, design or composition of matter, or any new and useful improvement thereof, or any variety of plant which is or may be patentable under the patent laws of the United States of America or any foreign country.

A B S T R A C T

The strength and stiffness behavior of reinforced concrete columns subjected to biaxial bending and compression was investigated. In order to provide data points on biaxial interaction surfaces, nine rectangular cross section columns and fifteen partial circular cross section columns were loaded to failure as moments were increased while thrust was maintained at a constant value. Test data included longitudinal strain profiles as well as transverse displacement measurements at all levels of load. Test measurements were compared with a discrete element analytical model that was modified to provide results that were in favorable agreement with measured response. Test results from other investigators were included in the data against which analytical results were checked.

The reciprocal thrust equation:

$$\frac{1}{P_i} = \frac{1}{P_x} + \frac{1}{P_y} - \frac{1}{P_o}$$

was selected as the simplest analytical expression that provided approximations of strength that were consistent with test results. The influence of slenderness effects in skew bending was examined. The moment magnifier method was used for approximate analysis of slenderness. Member stiffness relationships recommended by the ACI Building Code (ACI 318-71) were studied in addition to alternate approximations of EI. The ACI procedures were found to give safe results at low thrust levels only if ACI Eq. (10-7) was used. Moment magnification used separately for each principal axis of bending appeared to give rational reflections of biaxial behavior. The discrete element analytical model was also used to produce more analytical data for comparison with the approximate methods of analysis. Simple

approximations of EI were not found to be consistent with test data when thrust levels varied and when slenderness ratios were large.

A deflection limit method for computing member strength was introduced. The method involved assigning to the nominal eccentricity an additional eccentricity that is a function of the slenderness ratio. An empirical equation and a procedure for computing member strength were proposed on the basis of agreement with experimental data.

KEY WORDS: columns, reinforced concrete, strength, stiffness, biaxial bending, compression

S U M M A R Y

All reinforced concrete columns must be proportioned to resist compression thrust that is assumed to act at some degree of eccentricity away from the longitudinal centroid of the column. This report contains an analytic and laboratory investigation of concrete columns that are required to resist thrust that is eccentric about both principal axes of member cross sections. Heretofore, the design of columns to resist biaxially eccentric thrust has been dependent upon largely unverified analytic combinations of design procedures for uniaxial thrust.

The investigation incorporates results from other laboratories where columns with square cross sections were tested. Since the shape of columns in bridge structures frequently is rectangular or partially circular (rectangular with circular ends), nine rectangular specimens and fifteen partially circular specimens were tested as a part of this investigation.

The investigation revealed that cross section strength and cross section ductility are significantly undervalued analytically if the customary Whitney constant stress block model is used to represent the limit strength of concrete on nonrectangular compression zones. The investigation indicated that biaxially eccentric thrust capacity P_i can be analyzed more accurately in terms of uniaxial thrust capacities P_x and P_y, and a squash load strength P_o in the following equation of reciprocals

$$\frac{1}{P_i} = \frac{1}{P_x} + \frac{1}{P_y} - \frac{1}{P_o} \qquad \text{(A)}$$

The effects of slenderness can be incorporated through moment magnification factors applied separately to each uniaxial thrust capacity P_x and P_y. The skew bending tendency to twist the column was found to be negligible. Values of flexural stiffness of cross sections under thrusts less than $0.4P_o$ should reflect the effects of cracking and reinforcement percentage.

Simplified general formulas for flexural stiffness must reflect lower bound resistance to deflection, and consequently they become useless for moment magnifier applications to extremely slender members. An analysis technique that employs a deflection limit as a supplementary eccentricity is proposed in lieu of moment magnification for extremely slender columns.

I M P L E M E N T A T I O N

Specific recommendations for design procedures have been made as a result of this study. For many conditions of column design, the cross sections and reinforcement can be selected on the basis of a uniaxial bending load condition, and subsequent analysis must be made to assure adequate strength for biaxial bending load cases. The analysis for biaxial bending should employ the reciprocal thrust equation and should not use any of the strength approximations now employed for moment "contours" under constant thrust. Applications of the reciprocal thrust equation can be programmed for use in column design or analysis computer subroutines, or applications can be based on uniaxial strength interaction diagram design aids.

If biaxial bending load conditions are likely to represent the most severe loading condition, an equivalent uniaxial moment can be used for the preliminary selection of a cross section shape and for longitudinal reinforcement. The equation for the equivalent uniaxial moment is simply a crude adaptation of a moment contour function for rectangular cross sections.

The biaxial bending capacity of prismatic slender columns can be analyzed in terms of moment magnification factors. Two moment magnification factors must be determined, one for each principal axis of the column cross section and unsupported length. Thrust values P_x and P_y in the reciprocal thrust interaction equation must represent capacities under magnified eccentricities about each principal axis.

Implementation of the design and analytic verification recommendations including slenderness effects could be expedited by means of a computer program subroutine for the design of prismatic reinforced

concrete columns. The design subroutine should be programmed to include its own evaluation of cross section strength for selected general shapes of columns. Equations for the analysis of slenderness effects and for biaxially eccentric thrust load cases are given in the report.

C O N T E N T S

LIST OF TABLES

L I S T O F F I G U R E S

Figure | Page

Figure Page

Figure | Page

NOTATION

b	Width of the column section
C_m	A factor that reflects the effect of end moments in slender column moment magnification $C_m = 0.6 + 0.4M_1/M_2 \geq 0.4$
E_c	Modulus of elasticity of concrete according to ACI 318-71[1]
E_o	Initial slope of the stress-strain curve of concrete
E_s	Modulus of elasticity of reinforcing steel
EI	Flexural stiffness of the cross section
$EI_{measured}$	Measured flexural stiffness of the cross section
e_c	End eccentricity due to end rotation
e_{cs}	Strong axis eccentricity due to end rotation
e_{cw}	Weak axis eccentricity due to end rotation
e_{end}	Total eccentricity at end of the column including the applied moment
e_i	Initial end eccentricity of the axial load ram
e_{is}	Strong axis eccentricity of the axial load ram
e_{iw}	Weak axis eccentricity of the axial load ram
e_{max}	Maximum eccentricity corresponding to maximum moment along the column
e_x	Eccentricity of load P_u in x-direction
e_y	Eccentricity of load P_u in y-direction
f_c	Concrete stress at strain ϵ_c
f'_c	Compressive strength of 6 in. by 12 in. cylinder
G	Shear modulus of the concrete column
I_g	Gross moment of inertia about the axis of bending of the column section
I_s	Moment of inertia of reinforcement about the axis of bending
J	Polar moment of inertia of the column section
k	Effective length factor

k_2	Ratio of the transformation of axis used by Ramamurthy,[37] $k_2 = M_{xo}/M_{yo}$
$k\ell$	Effective length for compression member
L, ℓ	Length of the column
$M\text{-}\varphi$	Moment-curvature relationship of the column section
M_1	Value of smaller design end moment on compression member
M_2	Value of larger design end moment on compression member
M_c	Design moment of compression member including amplification factor
M_d	Failure moment when P_u acts along the diagonal axis of the section
M_{end}	Moment at end of the column
M_{max}	Maximum moment on the column
M_{ru}	Resultant moment on the section, $M_{ru} = \sqrt{M_{xu}^2 + M_{yu}^2}$
M_{so}	First order moment about strong axis applied at end of the column
M_{wo}	First order moment about weak axis applied at end of the column
M_{xb}	Uniaxial failure moment about x-axis at balanced condition
M_{xo}	Uniaxial moment capacity about x-axis when axial load P_u acts with eccentricity producing moment about x-axis only
M_{xu}	Failure moment about x-axis under failure thrust P_u
M_{yb}	Uniaxial failure moment about y-axis at balanced condition
M_{yo}	Uniaxial moment capacity about y-axis when axial load P_u acts with eccentricity producing moment about y-axis only
M_{yu}	Failure moment about y-axis under failure thrust P_u
N	Constant defining the deviation of M_d from M_{yo}
P	Compression thrust on the columns
P_A	Applied thrust from the axial ram
p_b	Failure thrust at balanced condition on the uniaxial interaction diagram for thrust and moment
P_{cr}	Critical load, $P_{cr} = \pi^2 EI/(k\ell)^2$
P_i	Approximate load capacity of column section using reciprocal load equation

P_o	Load-carrying capacity of column section under concentric axial compression, i.e., squash strength of the column section
P_S	Applied thrust from the strong axis moment ram
P_T	Total applied thrust on the column
P_W	Applied thrust from the weak axis moment ram
P_u	Ultimate thrust capacity of column
P_x	Load-carrying capacity of column section under compression with uniaxial eccentricity e_y
P_y	Load-carrying capacity of column section under compression with uniaxial eccentricity e_x
R	Radius of the hemispherical ball used as the loading head in the tests
r	Radius of gyration of the section about the axis of bending
S	Shape function of the deviation of the contour line of the failure surface to the circular arc of radius equal to M_{yo}
T	Torque on the column section
T_c	Torsional capacity for concrete in a section
t	Thickness of the column section
v_{tc}	Allowable shear stress for torsion for plain concrete
y	Shape function of the column under load P
y'	Slope at any point along the column under load P
α_1	Exponent in load contour equation, Eq. 1.2
β_1	Exponent in load contour equation, Eq. 1.2
β_2	Transformed load angle (by Ramamurthy[37])
β_3	Ordinate of the load contour at the point where related moments M_{xu}/M_{xo} and M_{yu}/M_{yo} are equal
β_d	Sustained load factor
Δ	Deflection at midheight of the column under load P; assigned deflection by deflection limit method in Chapter 5
δ	Moment magnification factor for compression member
ϵ_c	Strain in concrete corresponding stress f_c
ϵ_o	Strain in concrete at maximum stress on the stress-strain curve of concrete

θ Load angle measured from strong axis of bending

$$\theta = \tan^{-1} \frac{M_{\text{strong axis}}}{M_{\text{weak axis}}}$$

θ_1 Transformed load angle (by Pannell[32])

θ_2 Load angle used by Ramamurthy[37]

θ_A Slope at end of the column under load P

ρ Ratio between steel area and cross section area

φ Neutral axis angle measured from weak axis of bending

φ_1 Ratio for the transformation of axis used by Pannell[30,32]
$\varphi_1 = M_{yb}/M_{xb}$

φ_2 Neutral axis angle used by Ramamurthy[37]

φ_t Twist angle per unit length

CHAPTER 1

INTRODUCTION

1.1 General Review

A column that is subjected to axial compression and bending moments about both major axes presents a biaxial bending problem in the column. The problem always occurs in the design of monolithic building frames, at corner columns. The corner column of a reinforced concrete frame must resist biaxial bending because moments are introduced from beams which frame to the column from both directions of the major axes of the column. In many cases the beam from one direction predominates the total skew bending moment, but both directions must resist moment.

For esthetic appearance, a single column bridge bent, as shown in Fig. 1.1, has come into favor in the design of highway bridges. Single column bridge bents require only one set of forms at a time. Single columns that support bent caps in highway bridges are always loaded with moments about both principal axes of column cross sections. Moments are introduced to the column in one direction by the cantilever action of the beam, as shown in Fig. 1.2(a). In the perpendicular direction, longitudinal braking forces create moments in addition to moment that is introduced from torsion when stringers from only one side of the bent cap are loaded as suggested in Fig. 1.2(b).

Although numerous studies of columns under uniaxial bending have been made and many design aids are available, the biaxial bending problem has not benefited from as much research. Empirical and analytical approaches to the problem have led to complex and difficult design aids from which the precision of results have yet to be demonstrated by physical tests.

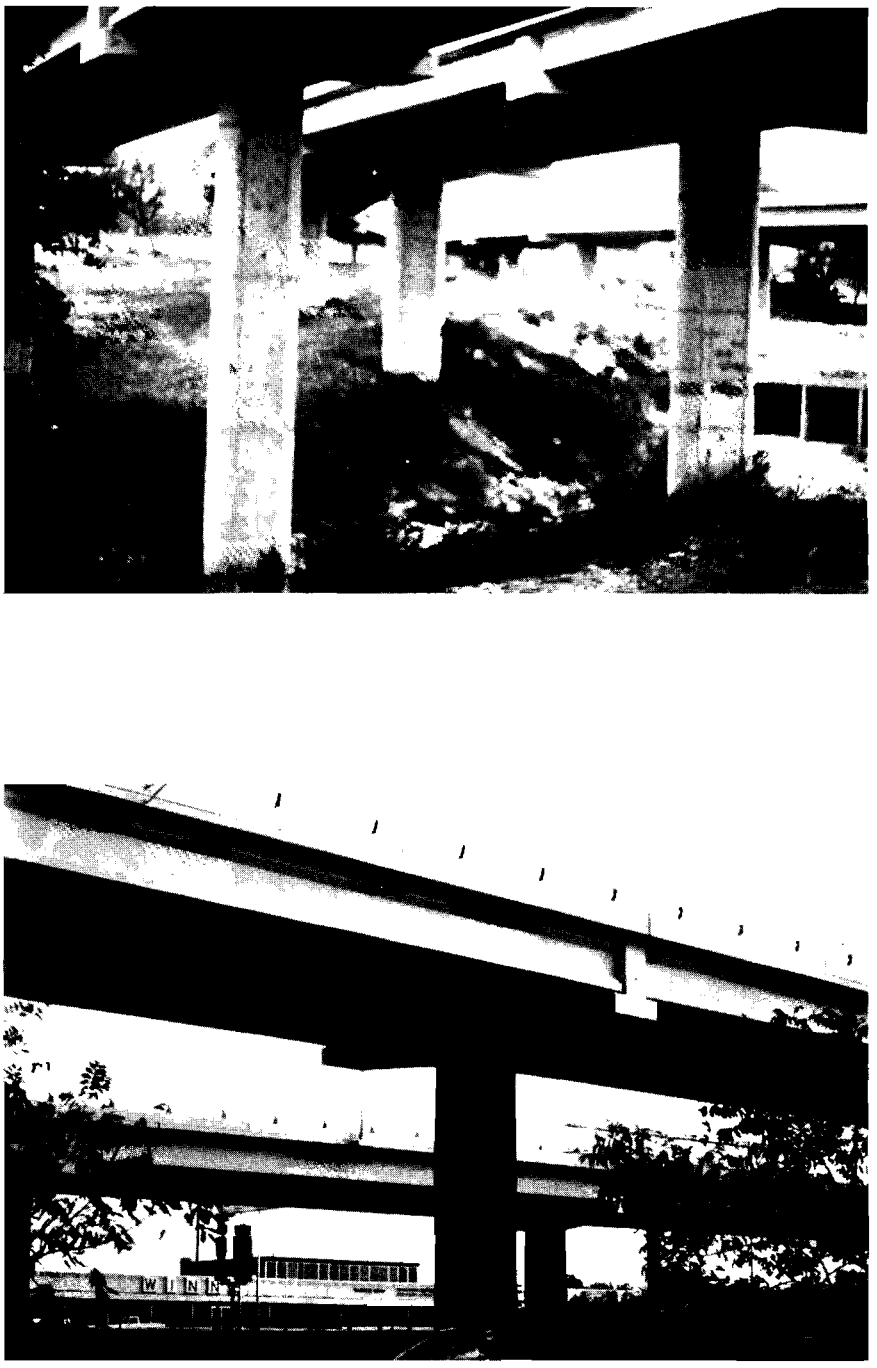

Fig. 1.1 Single column bridge bents

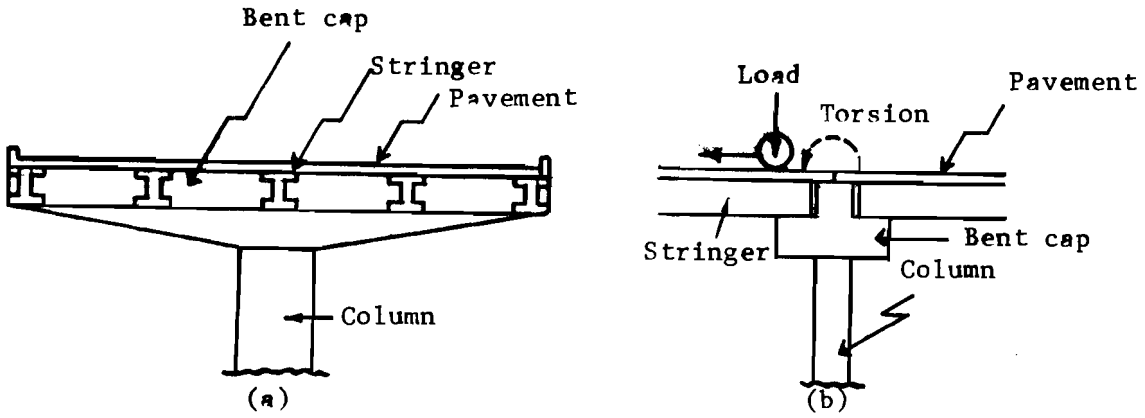

Fig. 1.2 Sketch of highway bridge

1.2 Review of Research on Biaxial Bending of Concrete Columns

The ultimate strength design of columns with uniaxial bending logically follows the concepts of nonlinear behavior as a basis for concrete design. The special problem of biaxial bending was given less attention, but several investigators suggested analytic and design techniques.

1.2.1 The Investigation of Strength of Short Columns. In 1952, Craemer[11] reported using the idea of plasticity to solve the problem of skew bending for both beams and columns by an iteration method. He assumed that compressive stress at the extreme fiber of

---

*Superscript numbers refer to references at the end of this dissertation.

of the member equals f'_c but the average stress of $0.85f'_c$ on the compression zone was used for the calculations.

Tung Au[3] presented a procedure and design charts for rectangular sections under skew bending. He assumed a uniform stress of $k_1 f'_c$ over the compression zone bounded by the edges of the extreme compressive corner and a line parallel to the neutral axis with an equivalent depth measured from the extreme compressive corner taken equal to $k_1 h$, where h is the distance from the corner to the neutral axis. The value of k_1 was taken not greater than 0.85 and it was to be reduced at the rate of 0.05 per 1000 psi concrete strength in excess of 5000 psi.

Kuang-Han Chu[9] treated the analysis of biaxially loaded reinforced concrete columns by separating the compression zone of concrete into a plastic portion and an elastic portion. By trial and error, the location of the neutral axis was located using the equilibrium of forces and moments on the section.

1.2.1.1 Concept of the Failure Surface. If the failure interaction diagrams of load and moment about all axes of the column cross section are plotted using the same axis for thrust but with different orientations of moment axes according to the moment angles, a three-dimensional failure surface is formed.[23] Every point on this surface represents a failure load-moment condition for the cross section. In 1960, Bresler[5] used the failure surface concept to propose two equations which would represent approximately the failure surface.

(a) Reciprocal Load Equation. When the inverse of the failure load, $1/P_u$, is plotted on one axis and the eccentricities, e_x and e_y of the two major axes on the other two axes, as shown in Fig. 1.3, the approximate equation for this failure surface is:

$$\frac{1}{P_i} = \frac{1}{P_x} + \frac{1}{P_y} - \frac{1}{P_o} \qquad 1.1$$

where P_i = Approximate load capacity of the section (i.e., $P_i \approx P_u$) when subjected to eccentricities e_x and e_y

P_x, P_y = Load-carrying capacities of the section under compression with uniaxial eccentricity e_y and e_x, respectively

P_o = Load-carrying capacity of the section under concentric axial compression

Bresler indicated that a formula similar to Eq. 1.1 is given in the Russian Specification, but no reference is available for the derivation of this equation.

(b) Load Contour Equation. Bresler described another failure surface which is shown in Fig. 1.4. The failure thrust is plotted against the associated failure moments, M_{xu} and M_{yu}, about two major axes. At a level of axial load, P_u, the failure moments corresponding to that load can be related as:

$$\left[\frac{M_{xu}}{M_{xo}}\right]^{\alpha_1} + \left[\frac{M_{yu}}{M_{yo}}\right]^{\beta_1} = 1.0 \qquad 1.2$$

where M_{xu}, M_{yu} = moments at failure load, P_u, about x-axis and y-axis, respectively

M_{xo} = Failure moment about x-axis when axial load, P_u, acts with uniaxial eccentricity producing moment about the x-axis only (i.e., $M_y = 0$)

M_{yo} = Failure moment about y-axis when axial load, P_u, acts with uniaxial eccentricity producing moment about the y-axis only (i.e., $M_x = 0$)

α_1, β_1 = Exponents depending on column dimensions, amount and distribution of steel and properties of concrete

Bresler tested some specimens and made calculations to evaluate the validity of the proposed equations. He found that for rectangular sections, α_1 and β_1 in Eq. 1.2 could be assumed equal, so Eq. 1.2 becomes

$$\left(\frac{M_{xu}}{M_{xo}}\right)^{\alpha_1} + \left(\frac{M_{yu}}{M_{yo}}\right)^{\alpha_1} = 1.0 \qquad 1.3$$

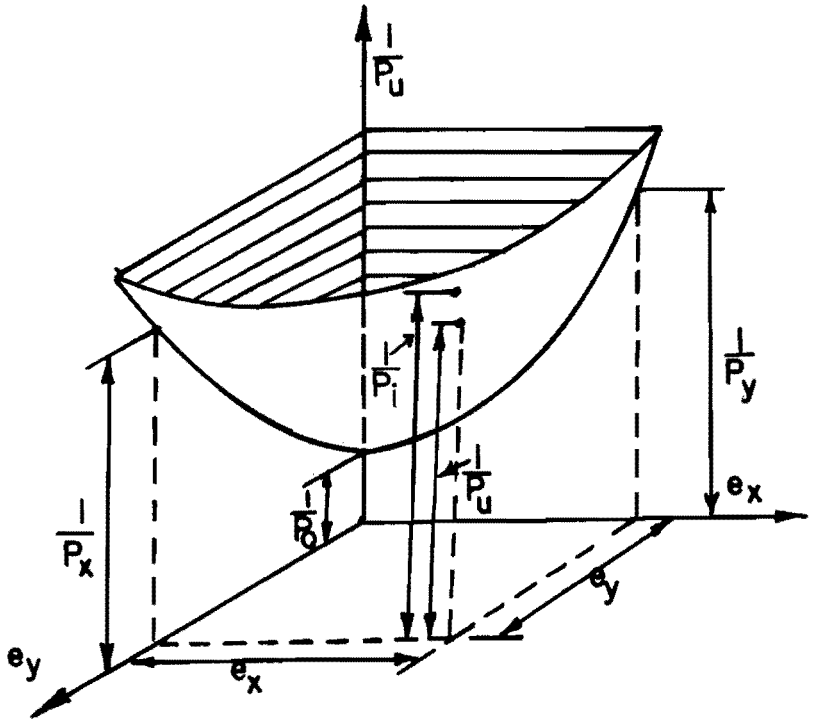

Fig. 1.3 Failure surface ($1/P_u$, e_x, e_y), the Reciprocal Load Method

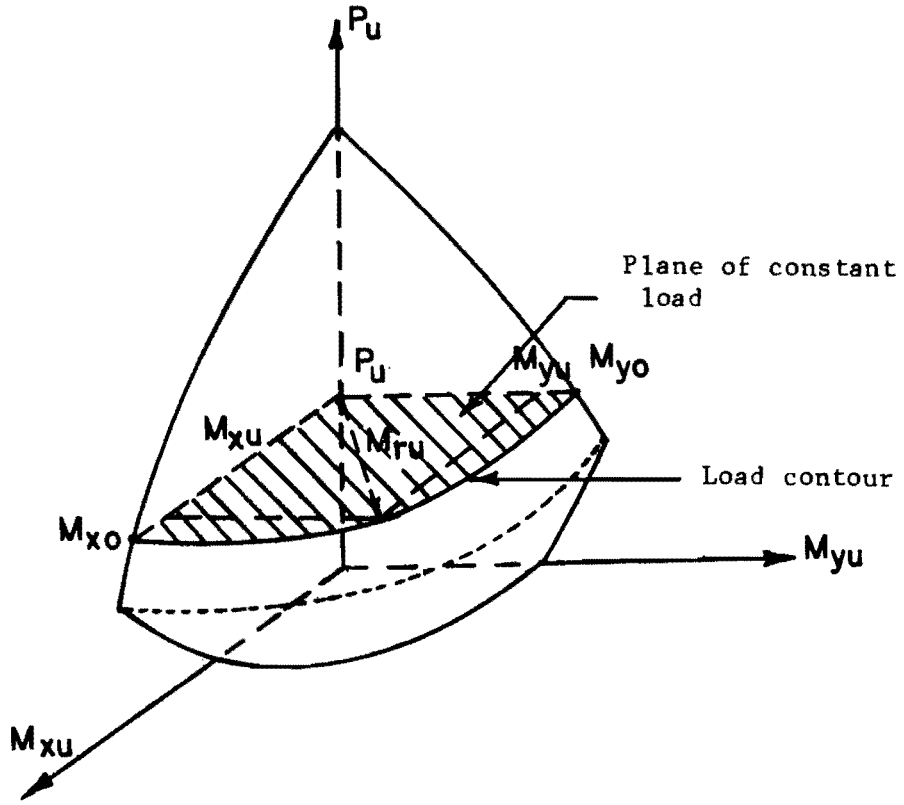

Fig. 1.4 Failure surface (P_u, M_{yu}, M_{xu}), Load Contour Method

With α_1 varied from 1.15 and 1.55, a good result could be obtained. From Eq. 1.1, P_i gave excellent agreement with tested and analytical results.

1.2.1.2 Transformation of Axis. Pannell[30,31,32] showed that an interaction surface at any load level, P_u, of a rectangular cross section, as shown in Fig. 1.5(a), could be transformed into an equivalent interaction surface of a square section. If the interaction surface in Fig. 1.5(a) is distorted by multiplying the minor axis coordinate [i.e., M_{xu} in Fig. 1.5(a)] by the ratio M_{yo}/M_{xo}, then it will transform to coincide with the interaction surface of square sections in Fig. 1.5(b), where M_{yo} and M_{xo} are the uniaxial failure moments at load P_u eccentric about the major and minor axes, respectively.

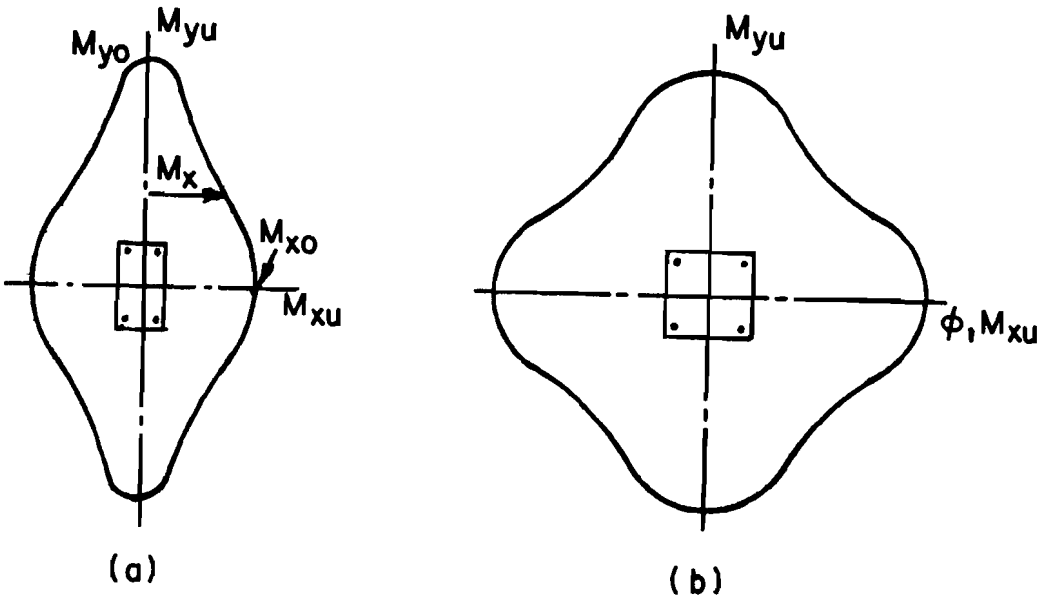

Fig. 1.5 Horizontal section of interaction surface; for rectangular column (left); for square column (right)

It was also confirmed that the ratio of M_{yo}/M_{xo} at all load levels for the cross section was effectively a constant and might be represented by the ratio of $\varphi_1 = M_{yb}/M_{xb}$ of "balanced" failure moments about the major and minor axes. When the square column interaction surface is used, it is possible to calculate the failure moment about the diagonal, M_d. With three points, M_{yo}, M_d, and $\varphi_1 M_{xo}$ in Fig. 1.6, Pannell drew a smooth continuous curve "A" tangent to these points and used the curve to define the entire failure surface.

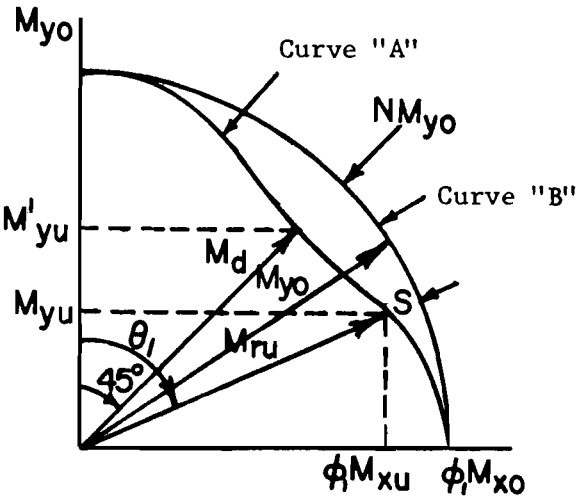

Fig. 1.6 Horizontal section of quadrant of actual failure surface and surface of revolution

Also shown in Fig. 1.6 is the circular arc "B" which resulted from revolving the uniaxial failure moment, M_{yo}, about the origin. At the load angle of 45^o, the deviation from the diagonal failure moment, M_d, to the circular arc can be found as $M_{yo} - M_d$ or NM_{yo}, where $N = 1 - M_d/M_{yo}$. Pannell gave the equation of the deviation "S" of curve "A" to the circular arc "B" as

$$S = NM_{yo} \sin^2 \theta_1 \qquad 1.4$$

where θ_1 is the load angle.

At any point on the failure surface "A" with the load P_u and resulting moment M_{ru} of $\varphi_1 M_{xu}$ and M_{yu}, Pannell showed that the required uniaxial moment capacity is

$$M_{yo} = \frac{M_{yu} \sec \theta_1}{1 - N \sin^2 \theta_1} \qquad 1.5$$

in which $\theta_1 = \tan^{-1} \varphi_1 M_{xu}/M_{yu}$

Pannell also included a chart for the value of N calculated from the basic equation of equilibrium of the section. He tried to compare his method with Bresler's load contour equation (Eq. 1.3) by rewriting the equation in the form that follows:

$$\left[\frac{M_{xu}}{M_{xo}}\right]^{\alpha_1} + \left[\frac{M_{yu}}{M_{yo}}\right]^{\alpha_1} = 1$$

$$\left[\frac{\varphi_1 M_{xu}}{M_{yo}}\right]^{\alpha_1} + \left[\frac{M_{yu}}{M_{yo}}\right]^{\alpha_1} = 1$$

$$[M_{yo}]^{\alpha_1} = (\varphi_1 M_{xu})^{\alpha_1} + (M_{yu})^{\alpha_1} \qquad 1.6$$

After the comparison, Pannell concluded that his proposed Eq. 1.5 gave better accuracy than Eq. 1.6 and was easier to use. The exponent α_1 of Eq. 1.6 was difficult to determine because it varied within a wide range and it was sensitive to the condition of eccentricity. Pannell also claimed that his method was practical for design, because only one major axis interaction curve was needed.

Ramamurthy,[37] in 1965 presented his study in biaxial bending at the 61st Annual American Concrete Institute Convention. He first investigated square columns and reported that for columns with eight or more bars, the neutral axis is approximately perpendicular to the line from the centroid of the section to the load point (i.e., $\theta_2 = \varphi_2$ in Fig. 1.7, where θ_2 is the load angle and φ_2 is the neutral axis angle).

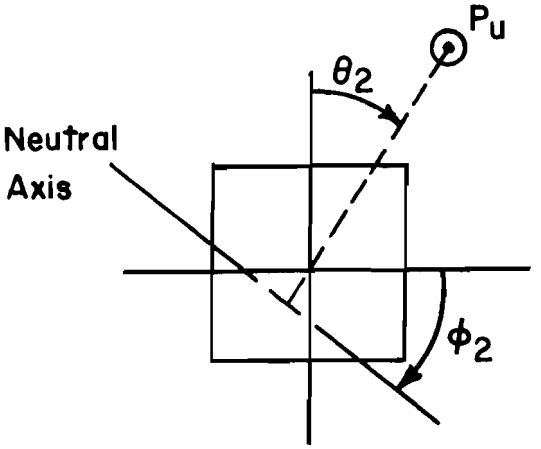

Fig. 1.7 Load angle and neutral axis angle

Ramamurthy also observed that in any load contour for the square column, the relationship between M_{xu} and M_{xo} of the same load level can be expressed approximately as

$$M_{xu} = M_{xo}(1 - \sin^3 \omega_2) \qquad 1.7$$

where M_{xu} is the greater of the moments about the major axis. With $\omega_2 \approx \theta_2$, Eq. 1.7 gives

$$M_{ru} = M_{xu} \sec \theta_2$$

then $$M_{ru} = M_{xo}(1 - \sin^3 \omega_2) \sec \omega_2$$

where M_{ru} = the resulting moment on the section

The simplified equation becomes

$$M_{ru} = M_{xo}(1 - 0.1 \frac{\theta_2}{45}) \qquad 1.8$$

in which θ_2 is the load angle expressed in degree or $\theta_2 = \tan^{-1} e_x/e_y$

For rectangular columns, Ramamurthy used the transformation of axis technique to change the section into an equivalent square section and Eq. 1.8 had been adjusted to read:

$$M_{ru} = M_{xo}\left[1 - 0.15\,\frac{\beta_2}{45}\right]\sqrt{\cos^2\beta_2 + \frac{\sin^2\beta_2}{k_2^2}} \qquad 1.9$$

where $k_2 = \dfrac{M_{xo}}{M_{yo}}$

$\tan\beta_2 = k_2 \tan\theta_2$

= transformed load angle

Values of k_2 were also recommended for various aspect ratios t/b for the rectangular sections.

The inclination of the neutral axis in rectangular columns under biaxial bending also was studied by Ramamurthy and the values of θ_2 and φ_2 were tabulated. The conclusion of the study indicated the variation in θ_2 and φ_2 is small, so the proposed relation of $\theta_2 = \varphi_2$ can be used. Some specimens were tested to verify his method. The reciprocal load Eq. 1.1 was also used and it was said to give a reasonable result.

In 1967, H. Eloseily[16] of Switzerland reported on rectangular reinforced concrete sections under biaxial bending. He also transformed the rectangular section into a square section and constructed design charts and tables for many cases of concrete strength, steel strength, amounts of reinforcement and various arrangements of steel bars.

1.2.1.3 Simplification of Load Contour Equation. After Bresler introduced the idea of a failure surface and the load contour equation, some investigators developed a more practical criteria for design purposes.

Furlong[23] studied the problem of square columns using the rectangular stress block for ultimate strength analysis in concrete under compression. He constructed interaction diagrams and load contours. His study concluded that for the design of ultimate moment capacity in square columns at a particular load level, P_u, the limit of the skew moment should not exceed an ellipse whose axes are the

uniaxial moment capacities for the load P_u. His equation took the form of Eq. 1.3 with $\alpha_1 = 2$.

$$\left(\frac{M_{xu}}{M_{xo}}\right)^2 + \left(\frac{M_{yu}}{M_{yo}}\right)^2 \leq 1.0 \qquad 1.10$$

Furlong recommended that if $|P_u - P_b|/P_b \leq 1.0$, the limit should be reduced from 1.0 to 0.85 or 0.9, where P_b is the load capacity at a balanced condition.

Meek[29] tested nine square columns and recommended that for design purposes, the description of a load contour interaction curve required another point in addition to the uniaxial moment capacities (M_{xo}, M_{yo}). He suggested using the case of equal eccentricities or the moment about the 45^o diagonal. Then a straight line interpolation could be used between the moment about the diagonal and the moment about a principal axis. Figure 1.8 shows Meek's approximated load contour.

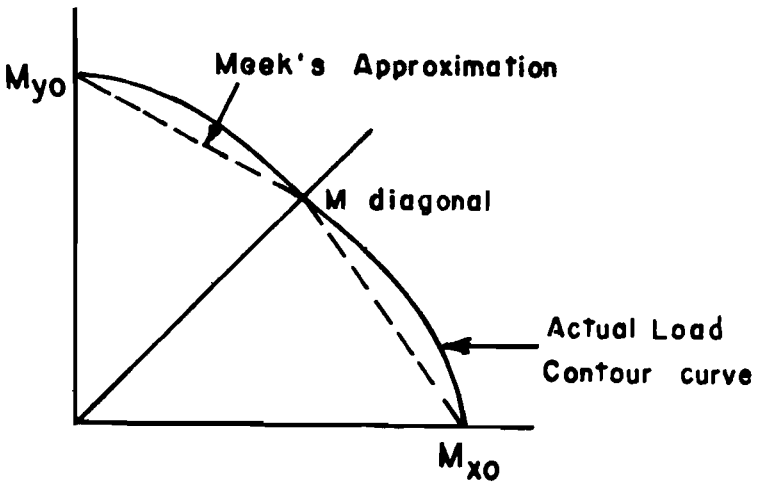

Fig. 1.8 Meek's approximation of load contour

In 1965, Fleming and Werner[19] presented a set of design charts for square sections with different f'_c and f_y values. Weber[45] also constructed a set of design charts for diagonal bending in square columns and used Meek's idea of linear interpolation between the uniaxial bending and the diagonal bending in order to design square columns with any load angles.

Parme[33,34] related Bresler's load contour equation to the logarithmic form

$$\left[\frac{M_{xu}}{M_{xo}}\right]^{\frac{\log 0.5}{\log \beta_3}} + \left[\frac{M_{yu}}{M_{yo}}\right]^{\frac{\log 0.5}{\log \beta_3}} = 1.0 \qquad 1.11$$

where β_3 = the ordinate of the load contour at the point at which the moments, M_{xu}/M_{xo} and M_{yu}/M_{yo}, are equal. β_3 values range between 0.5 and 1.0.

When compared to the theoretical curve, for columns with various bar arrangements and different aspect ratios, Eq. 1.11 gave results that agreed within 5 percent. Parme also pointed out that β_3 was a function of the amount, distribution, and location of the reinforcement, the dimensions of the section, and the properties of materials. He found that β_3 was dependent primarily on the ratio of the load level, P_u/P_o, bar arrangement, and the strength of the steel. The parameters b/t, amount of cover or edge distance, and f'_c had a minor effect on β_3.

More simplifications were made for PCA Publication No. 18.[34] As shown in Fig. 1.9, two straight lines intersecting at the point on the load contour where the relative moments are equal (i.e., $M_{xu}/M_{xo} = M_{yu}/M_{yo} = \beta_3$) were used to approximate a load contour surface. The two straight lines can be expressed:

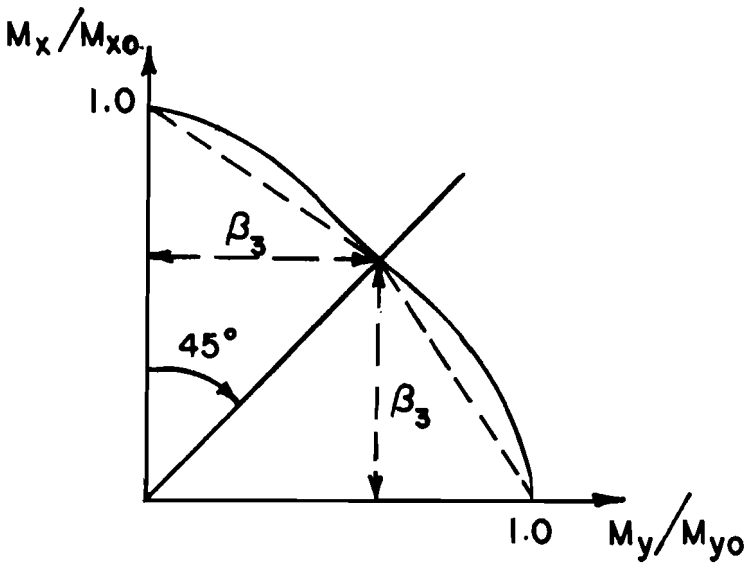

Fig. 1.9 PCA approximation

$$\frac{M_{yu}}{M_{yo}} + \frac{M_{xu}}{M_{xo}} \frac{(1 - \beta_3)}{\beta_3} = 1 \qquad \text{when } \frac{M_{yu}}{M_{yo}} > \frac{M_{xu}}{M_{xo}} \tag{1.12}$$

$$\frac{M_{xu}}{M_{xo}} + \frac{M_{yu}}{M_{yo}} \frac{(1 - \beta_3)}{\beta_3} = 1 \qquad \text{when } \frac{M_{xu}}{M_{xo}} > \frac{M_{xu}}{M_{yo}} \tag{1.13}$$

For rectangular cross sections, these equations were

$$M_{yu} + M_{xu}\, b/t \frac{(1 - \beta_3)}{\beta_3} \approx M_{yo} \text{ when } \frac{M_{yu}}{M_{yo}} > \frac{M_{xu}}{M_{xo}} \tag{1.14}$$

and

$$M_{xu} + M_{yu}\, t/b \frac{(1 - \beta_3)}{\beta_3} \approx M_{xo} \text{ when } \frac{M_{xu}}{M_{xo}} > \frac{M_{yu}}{M_{yo}} \tag{1.15}$$

where M_{xu} was the moment about the strong axis and t was the depth of the section.

The values of β_3 with various bar arrangements, steel strengths, and different load levels were also presented in this report.

In PCA Publication No. 20[35] more tables were included for designing biaxially loaded columns. This publication also contained materials for the section with unequal bar arrangements on the faces and for rectangular cross sections.

Fleming,[20] in 1974, used a discretization of a cross section to analyze cross sections and he compared his results with experimental data available for short columns loaded with biaxial bending. He tried to analyze the problem using various stress-strain functions for concrete. His results showed that the equivalent rectangular stress-block gave a reasonable strength representation of concrete behavior in skew bending. Fleming recommended that if an α_1 value for Eq. 1.3 were available, Bresler's load contour equation would be easy to apply. However, without the aid of a computer, he concluded that Bresler's reciprocal load equation was the simplest and it provided results as accurate as any analysis he had studied.

The studies that have been described treat only the analysis and design of cross sections. Most of the investigators used as a basis of "correctness" the results of an analysis that employed Whitney's concept of a rectangular stress block to represent concrete in compression prior to failure. Investigators recognized that more accurate results would require a more accurate representation of concrete strength. The strength influence of slenderness was not considered by these investigators. Slenderness effects have been studied, and the most promising analytic techniques have used digital computer programs.

1.2.2 Numerical Analysis Methods. Research has been pursued on the problem of skew bending, including length effects, using numerical analysis methods. The method of analysis usually consists of three steps: (1) find the load-moment-curvature (P-M-ϕ) relationship for all cross sections, (2) use moment-curvature functions to find the deflected shape, and (3) verify the deflected shape by iteration.

Warner and Brettle[6] developed a partitioned element method for studying the ultimate strength of hollow colums. The plane of strain in the cross section was defined in terms of maximum corner strain, minimum corner strain, and the neutral axis angle. The cross section was divided into small grid elements. The strain at the centroid of each grid then was defined and the stress at each element was obtained by using stress-strain relationships of the materials. Forces and moments on the section then could be calculated by integrating all forces and moments from the elements. For a given load and skew bending moment, the proper plane of strain could be searched by iteration. Warner[44] made further studies on biaxial columns with square and rectangular cross sections. He generated P-M-ζ curves for a constant neutral axis angle by increasing P, or maximum corner strain, before finding the resultant force and corresponding curvature.

Farah and Huggins[17] defined the plane of strain by using three corner strains. With the stress-strain relationship, the force of each grid element could be found and integrated for the values of total moment and force on the section in terms of the three corner strains. The column was divided into small segments along the length. With an assumed initial deflected shape, the curvature at each section corresponding to the forces could be obtained. These curvatures then were used to describe a new deformation of the column. An iteration method was used for predicting each new deflected shape until the predicted and the resultant shapes were the same within acceptable tolerances.

Drysdale[14] studied the behavior of slender columns under biaxial loading. He tested columns under both sustained load and short term loading and the results gave good agreement with the analytical results estimated by Farah and Huggins' method.

Wu,[47] in 1973, studied the effect of the volume/surface ratio or sustained loading behavior of biaxially loaded square slender columns. Wu analyzed the problem by partitioning the cross section

into strips parallel to the neutral axis in order to calculate the P-M-φ relationship of cross sections. He assumed that the neutral axis angle and the load angle were orthogonal. He used a differential equation which was solved by an approximate method in order to compute the deflected shape, eventually yielding a continuous function for the deflected shape.

Redwine[38] used Farah and Huggins' method to study the behavior of biaxially loaded rectangular columns. His analytic study included possible twisting of the section as well as slenderness effects. He concluded that torsional effects could be negligible. He found that the difference between the neutral axis angle and nominal load angle, M_y/M_x, increased with the cross section aspect ratio, b/t, and reached the greatest difference when the neutral axis was closest to the corner of the maximum compressive strain. For deflection studies, he found that the tendency for nonplanar behavior (neutral axis orientation changes along the length of the column) increased with slenderness, for small aspect ratios and for larger eccentricities, e/t. However, he concluded that in general nonplanar behavior was of minor significance. Redwine used Eqs. (10-7) and (10-8) in the ACI Building Code (ACI 318-71)[1] for calculating the stiffnesses of slender members, then magnified separately the moment about each major axis and computed the resultant moment by using the equation

$$M_R = [(\delta_x M_x)^2 + (\delta_y M_y)^2]^{1/2} \qquad 1.16$$

He observed that the use of these equations for stiffness gave a smaller load capacity of the column than did the numerical analysis. Thus, he concluded that ACI rules gave safe values for column design. Using the analyzed load as a correct strength, he reported that the safety ratio when using the ACI Code ($P_{analyzed}/P_{ACI}$) would be smallest for large ratios e/t. For smaller e/t ratios, an increase in slenderness decreased the safety ratio, but for larger e/t ratios slenderness had less effect on the safety ratio.

1.3 Scope of This Investigation

Previous studies have shown that Bresler's idea of failure surfaces and his proposed equations were the most convenient design methods for approaching the problem of columns under biaxial load. Several tests indicated that both the reciprocal load equation (Eq. 1.1) and the load contour equation (Eq. 1.3) gave results that agree with experimental work. Most of the experiments were done on square short columns. A small number of tests were conducted on rectangular shaped columns. Although Fleming[20] indicated that non-rectangular shapes should exhibit good agreement analytically using Bresler's equations, no physical test had been done to confirm his prediction.

The load contour equation (Eq. 1.3) is easy to apply if the exponential, α_1, is known, but to find the value of α_1 is a difficult problem because many parameters are involved. The reciprocal load equation is easier to apply but less research has been directed toward it than that directed toward perfecting parameters for Eq. 1.3.

In the ACI Building Code (318-71)[1] it is required that for all compression members subjected to bending about both principal axes, the moment about each axis must be amplified by a moment magnification factor δ, computed from the corresponding conditions of restraint about each axis (ACI 318-71, Sec. 10.11.5.2). No experimental data are available in support of this requirement.

The scope of the investigation reported here included the development of an analytical capacity for studying long concrete columns under biaxially eccentric thrust. Laboratory tests of columns with rectangular and oval-shaped cross sections were monitored both for strength and stiffness data. The oval shape consisted of a 5 in. diameter semicircle at each end of a 5 in. by 6 in. rectangle, and will be called a partial circle or oval cross section in this report.

At a relatively high thrust level, Furlong[23] observed that the contour lines of the complete failure interaction surface could be

represented by an ellipse whose axes were the ultimate moment capacities with the load P_u acting along the principal axes of the column cross section. Thus, if moment capacity can be predicted for bending about both principal axes at high thrust levels, intermediate or biaxial moment capacity can be predicted also. In order to reveal irregular aspects of the interaction surface, the thrust levels used for physical tests in this report were set at thrust levels of $0.2P_o$, $0.35P_o$, and $0.5P_o$, where P_o is here defined as the axial load capacity of the section, $P_o = A_g f'_c + A_s f_y$. The concrete cylinder strength f'_c was used without the usual reduction factor 0.85 for strength calculations even though specimens were cast in the vertical position and the majority of failure regions were above midheight of the specimens. The absence of a reduction factor 0.85 kept analytical expressions for stress-strain functions consistent for all load levels, and none of the biaxial bending tests involved failures near the top of specimens. For axial load levels below $0.6P_o$, the strength analysis of cross sections is relatively insensitive to the precise value of P_o, and all physical tests involved total axial loads less than $0.6P_o$.

The analytic computer programs were modified to produce results consistent with physical test data from these tests, as well as tests reported by others. Finally, the reliability of some approximate analysis techniques useful for design were checked against analytic as well as test results.

CHAPTER 2

PHYSICAL TESTS AND MEASUREMENTS

2.1 General

Twenty-four columns with two different shapes but the same length were tested to failure. Nine specimens with rectangular cross section were designated RC-1 through RC-9. Fifteen partial circular columns were called C-1 through C-15. During the sequence of loading, thrust was maintained at one of three different load levels, $0.2P_o$, $0.35P_o$, or $0.5P_o$, while eccentric loads were increased to produce failure. P_o was the squash load capacity of the section. Each type of cross section for the column was tested with one of three nominal skew load angles, $22\text{-}1/2^o$, 45^o, or $67\text{-}1/2^o$, and at one of the three axial load levels. Uniaxial bending tests were made on partial circular columns, but not on rectangular columns.

2.2 Type of Specimens

Test specimens were intended to represent one-sixth to one-eighth scale models of bridge pier columns with low reinforcement ratios for longitudinal steel. There were two different shapes in the test columns but all specimens were the same length of 72 in. The rectangular cross section had the nominal exterior dimension of 5 in. by 9 in. The partial circular columns had two semicircles 5 in. in diameter, located 6 in. apart, making the total depth of 11 in. with a 5-in. width. Figure 2.1 shows the dimensions and details of both cross sections. The longitudinal reinforcement was 6 mm diameter deformed bar, 14 bars for the partial circular and 10 bars for the rectangular columns. The reinforcement ratio was 0.01 for rectangular sections and 0.0138 for partial circle sections. All the reinforcing

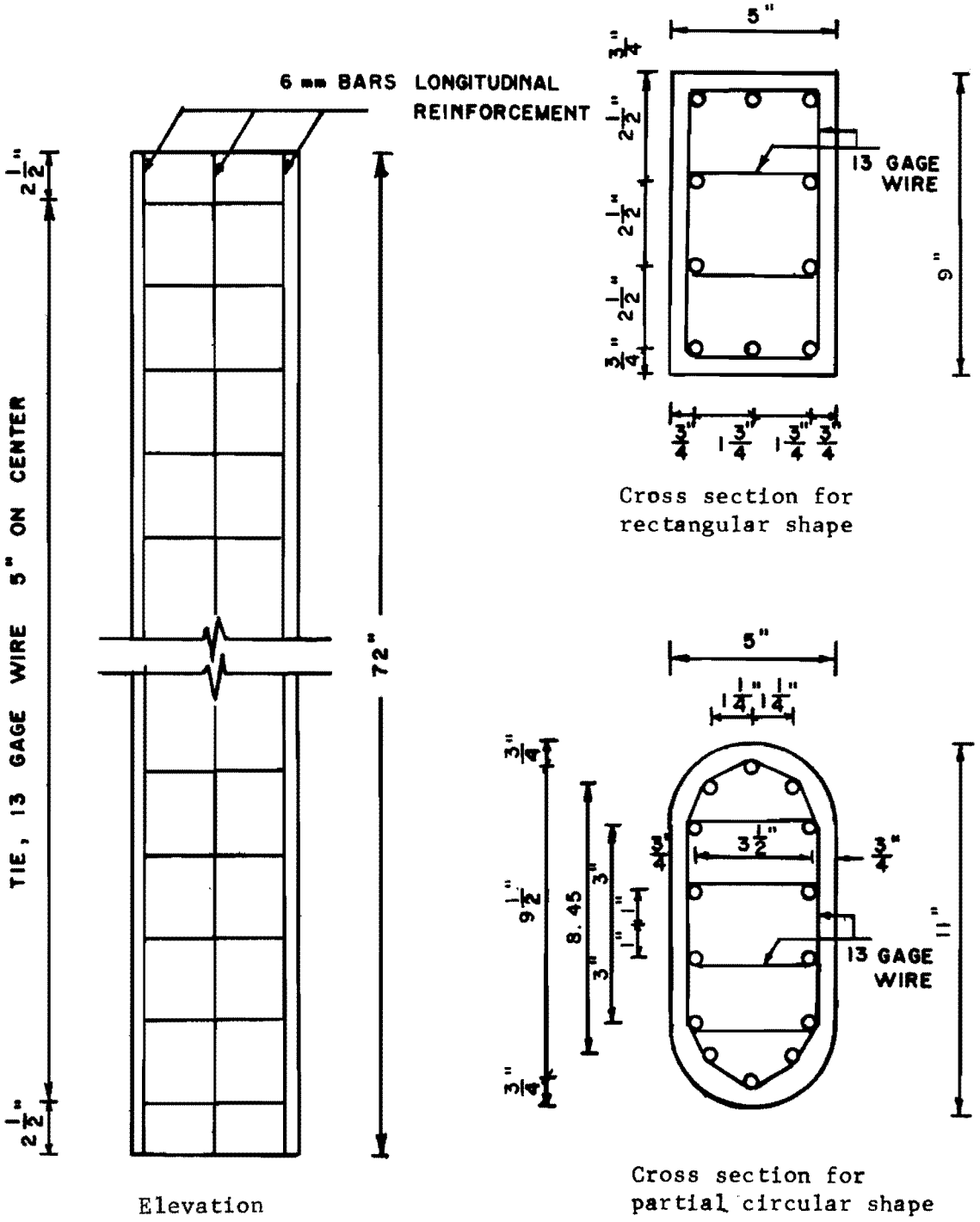

Elevation

Cross section for rectangular shape

Cross section for partial circular shape

O = 6 mm diameter bar

Fig. 2.1 Details of specimens

bars were 72 in. long, placed 5/8 in. from the surface of the columns. The longitudinal bars were tied with 13 gage steel wire spaced at 5 in. centers along the length of the columns.

2.3 Materials and Fabrication

2.3.1 Concrete. The prototype concrete mix was designed for a strength of f'_c = 4000 psi, according to the State Department of Highways and Public Transportation Specification.[41] The actual mix model contained a maximum size of coarse aggregate of 3/8 in. Type 1 portland cement was used for all specimens. The typical proportions of the concrete mix are shown in Table 2.1. Concrete was placed with the column form in the vertical position. Cylinder forms also were filled with concrete simultaneously so that the cylinders would represent the concrete in the batch. The concrete was placed and vibrated in approximately 2-ft. lifts. The cylinders also were machine vibrated. Table 2.2 shows the listing of the average cylinder strength for every specimen. Each cylinder strength in the table represents an average from ten cylinder tests conducted on the same day that the column was loaded to failure. Also shown in Table 2.2 are the standard deviation and coefficient of variation for ten cylinders tested with each specimen.

2.3.2 Reinforcing Steel. Deformed steel bars 72 in. long and 6 mm (0.24 in.) in diameter were used as longitudinal reinforcing bars, and 13 gage wire was used as tie reinforcement at a spacing of 5 in. on centers. A typical stress-strain relationship of the 6 mm bar is shown in Fig. 2.2. The average of ten tension test specimens gave a yield strength based on an 0.2 percent offset equal to 65.5 ksi, with the values ranged between 64.3 ksi to 66.3 ksi, and the modulus of elasticity was 30,000 ksi. The ultimate strength of the reinforcing bars was 94.3 ksi. The average cross-sectional area was 0.049 sq.in.

2.3.3 Fabrication. A steel form was used for rectangular columns. For partial circular columns, the form for the circular

TABLE 2.1 PROPORTIONS OF THE CONCRETE MIX FOR 6 CU.FT.

Material	Weight (lbs)
Cement (Type I)	125.5
Water	45.0
Sand	264.0
Aggregate	424.0
Septair	40.0 cc

TABLE 2.2 AVERAGE CYLINDER STRENGTH OF SPECIMENS

Specimen	Average* Cylinder Strength (psi)	Std.* Devia. σ (psi)	Coef.* of Variation	Specimen	Average* Cylinder Strength (psi)	Std.* Devia. σ (psi)	Coef.* of Variation
RC-1	4886	126	0.026	C-4	4831	169	0.035
RC-2	4871	246	0.051	C-5	4340	131	0.031
RC-3	5210	255	0.049	C-6	4396	270	0.061
RC-4	5181	228	0.044	C-7	4403	157	0.036
RC-5	5012	297	0.059	C-8	4760	269	0.057
RC-6	4425	132	0.032	C-9	4534	173	0.038
RC-7	4350	211	0.049	C-10	4425	107	0.024
RC-8	4446	135	0.030	C-11	4830	84	0.017
RC-9	4700	282	0.060	C-12	5091	188	0.037
C-1	4783	280	0.059	C-13	5397	115	0.021
C-2	4460	155	0.035	C-14	5514	381	0.069
C-3	4386	167	0.038	C-15	5468	295	0.054

*From 10 cylinder tests

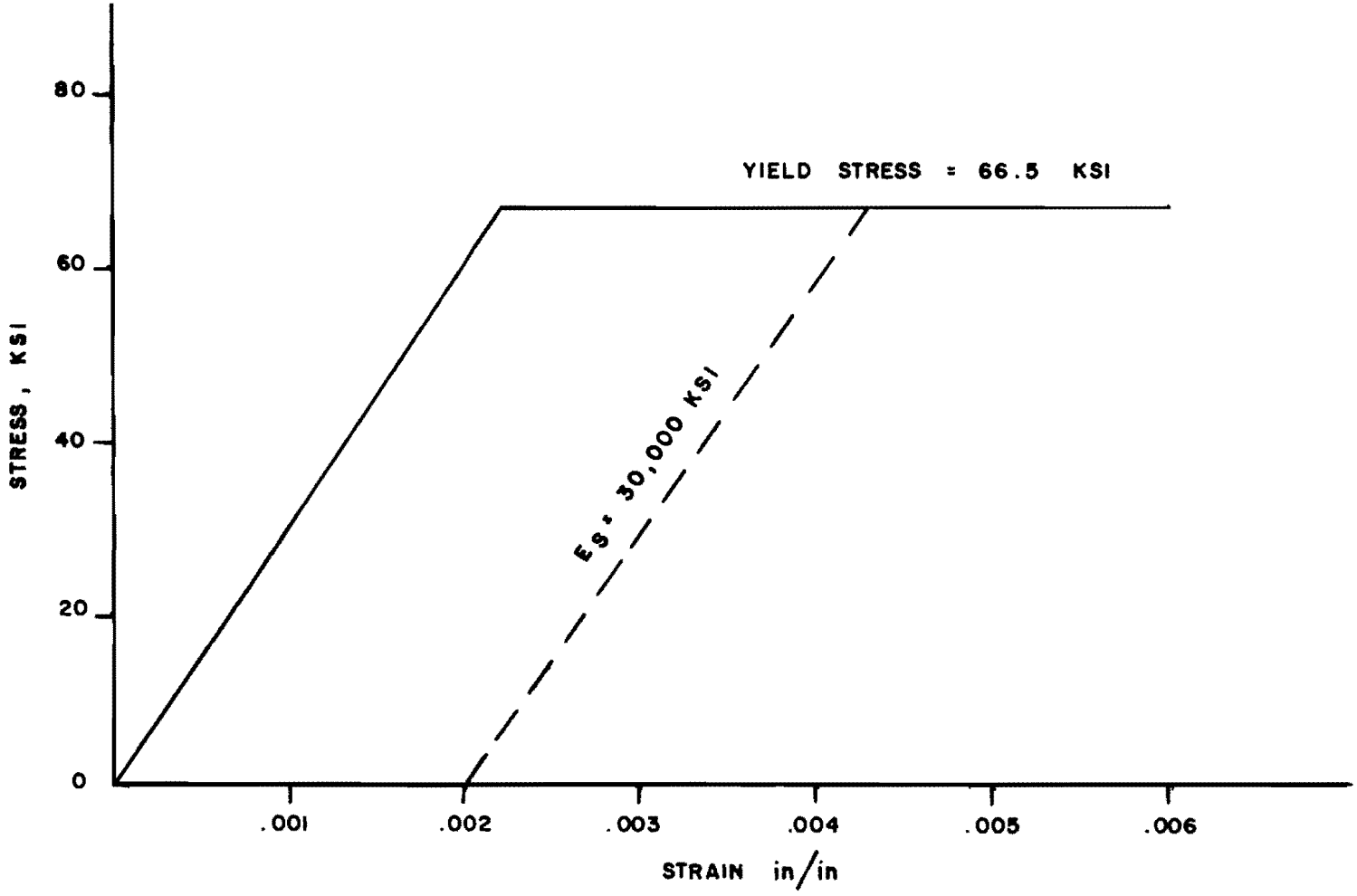

Fig. 2.2 Stress-strain curve for 6mm deformed bar

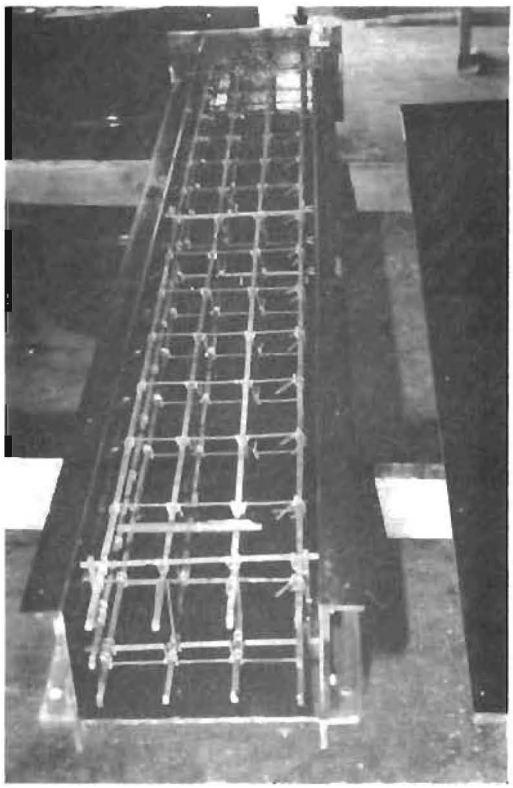

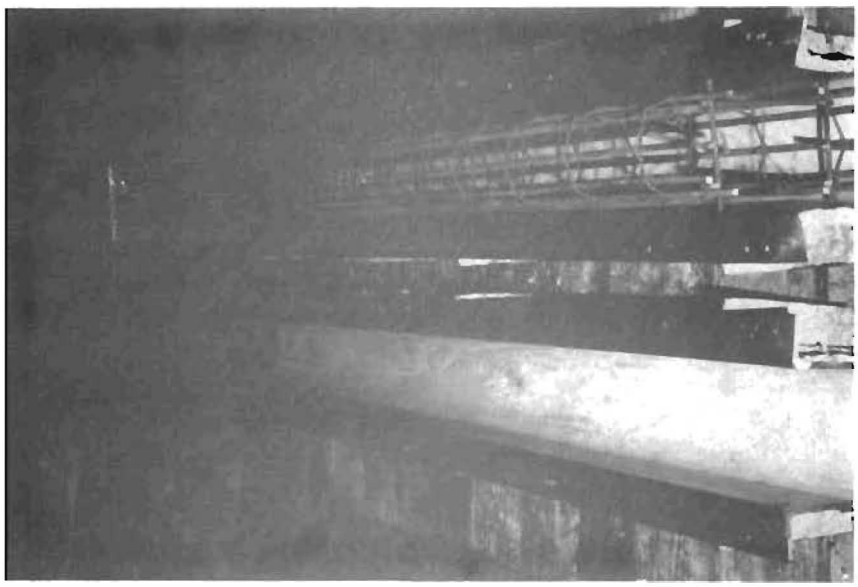

Fig. 2.3 Steel cages of rectangular column and partial circular column

Fig. 2.4 Column after casting, forms have not been taken out

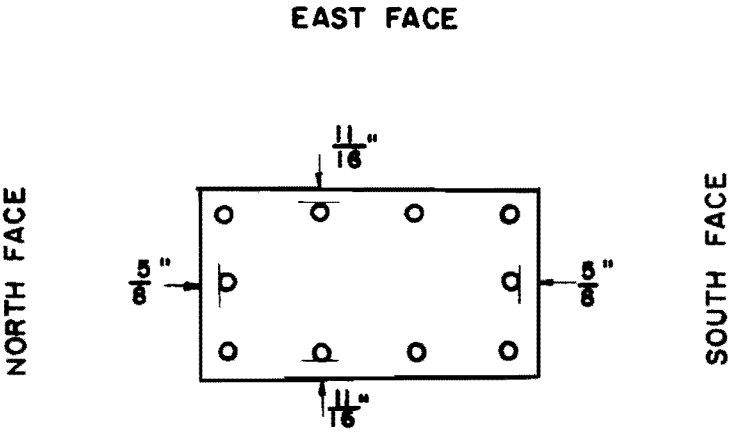

(a) at 21 inches from top of the column

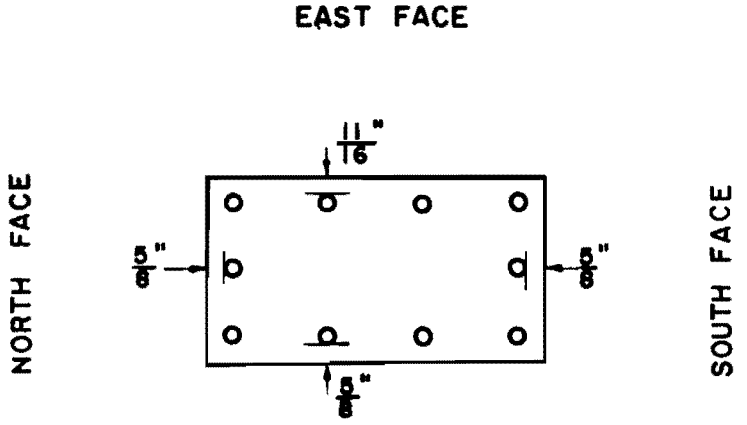

(b) at 57 inches from top of the column

Fig. 2.5 Actual clear cover of RC-6

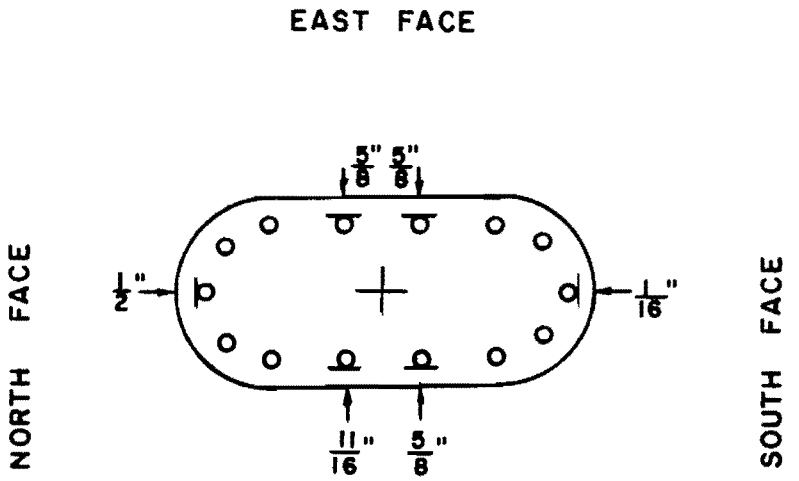

(a) at 21 inches from top of the column

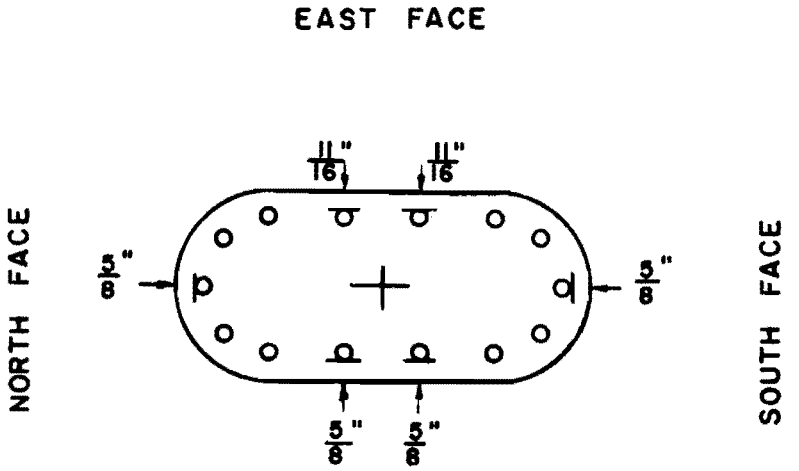

(b) at 51 inches from top of the column

Fig. 2.6 Actual clear cover of C-1

TABLE 2.3 SURFACE DIMENSION OF RC-2

Section	Distance from Top	North Face	South Face	East Face	West Face
1	3 in.	5 in.	5-1/16 in.	9-1/32 in.	9-1/16 in.
2	9	5-1/32	5-1/16	9-1/32	9-1/16
3	15	5-1/32	5-1/16	9-1/16	9-1/32
4	21	5-1/32	5-1/16	9-1/16	9-1/32
5	27	5-1/16	5-1/16	9-1/32	9-1/32
6	33	5-1/16	5-3/32	9-1/32	9-1/32
7 ℄	36	5-1/16	5-3/32	9-1/32	9-1/32
8	39	5-1/16	5-3/32	9-1/32	9-1/32
9	45	5-1/16	5-3/32	9-1/32	9-1/32
10	51	5-1/16	5-1/16	9-1/32	9-1/32
11	57	5-1/16	5-1/16	9-1/32	9-1/32
12	63	5-1/16	5-1/16	9-1/32	9-1/32

TABLE 2.4 SURFACE DIMENSION OF C-1

Section	Distance from Top (in.)	Overall Width (in.)	Overall Depth (in.)
1	3	5,5	11
2	9	4-31/32,4-31/32	10-31/32
3	15	5,4-31/32	10-31/32
4	21	4-31/32,4-31/32	10-15/16
5	27	4-15/16,4-15/16	10-31/32
6	33	5,4-15/16	11
7 ℄	36	4-15/16,4-15/16	10-31/32
8	39	4-15/16,4-15/16	11
9	45	4-29/32,4-7/8	11-1/16
10	51	4-15/16,4-31/32	11
11	57	4-31/32,4-31/32	11
12	63	4-15/16,4-15/16	11-1/16
13	69	4-15/16,4-15/16	11-1/16

shape was made from a 5-in. diameter plastic tube. The tube was cut longitudinally into halves and screwed to steel plates which were used as sidewall forms for the straight sides of the column. Figure 2.3 shows the pictures of the forms with a reinforcement cage inside. The cage was held in position with some small wire chairs to provide 5/8-in. clear cover on longitudinal bars.

All columns were cast in the vertical position to represent the actual field condition. Figure 2.4 shows the picture of both rectangular and oval shape columns after the concrete was cast, but before the forms had been removed. The form was stripped within two days of casting and the specimen and cylinders were cured under plastic covers.

The actual dimensions of the columns varied slightly due to the imperfections in forming and the flexibility of the plastic tube. Actual width and depth were measured at 6-in. intervals along the columns. No significant dimensional error was detected. The maximum error from desired member cross section was less than ±2.5 percent. Tables 2.3 and 2.4 show the actual dimensions of Specimens RC-2 and C-1.

After the tests, some attempts were made to measure the actual concrete cover of the reinforcing bars. It was found that the covering was almost the same as the nominal cover. For subsequent calculations the position of the reinforcing bars was assumed to be the same as the nominal position, as shown in Fig. 2.1. Shown in Figs. 2.5 and 2.6 are the actual clear cover of the concrete for Specimens RC-6 and C-1, respectively.

2.4 Loading System

The main axial thrust was applied by a 200 kip double acting hydraulic ram along the centroid of the column cross section. Thrust was transmitted to the specimen through a hemispherical head welded to a flat plate. Loading tended to flatten the hemispherical shape. Two 20-kip single acting rams were used to induce moment about

each principal axis. These moment rams were connected to one hand pump in order to ensure that the eccentric loads in both rams remained very near the same level. The schematic diagram of the loading system is shown in Fig. 2.7.

Two loading heads were placed over the ends of the column to transmit load from bearings and rams to the column. The heads were made from 5/8-in. steel plates welded together to form a shape of the cross section of the column. Two wide flange beam sections were butt-welded to the side of each column loading head. Eccentric loads were applied at the outside of the wide flange beams. The location of the loading points on the eccentric moment arms were designed to produce the assigned moment angles. The moment angle has been defined as:

$$\theta = \tan^{-1} \frac{M_{\text{strong axis}}}{M_{\text{weak axis}}}$$

$$= \tan^{-1} \frac{P \times \text{strong axis moment arm}}{P \times \text{weak axis moment arm}}$$

$$= \tan^{-1} \frac{\text{strong axis moment arm}}{\text{weak axis moment arm}}$$

In this test program there were five different moment angles, 90°, $67\text{-}1/2^{\circ}$, 45°, $22\text{-}1/2^{\circ}$, and 0°. Figure 2.8 shows a diagram of the assembled loading system. Figure 2.9 is a picture of the column with loading heads and rams in place.

2.5 Specimen Preparation

The following steps were taken in order to put the column into its testing position:

(a) The faces of the column were marked into 6-in. segments beginning 3 in. from midheight. The marking served to identify points at which the actual size of the column was measured and then served as reference lines for attaching measuring devices.

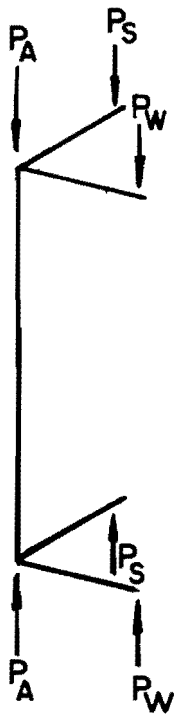

Fig. 2.7 Schematic of load system

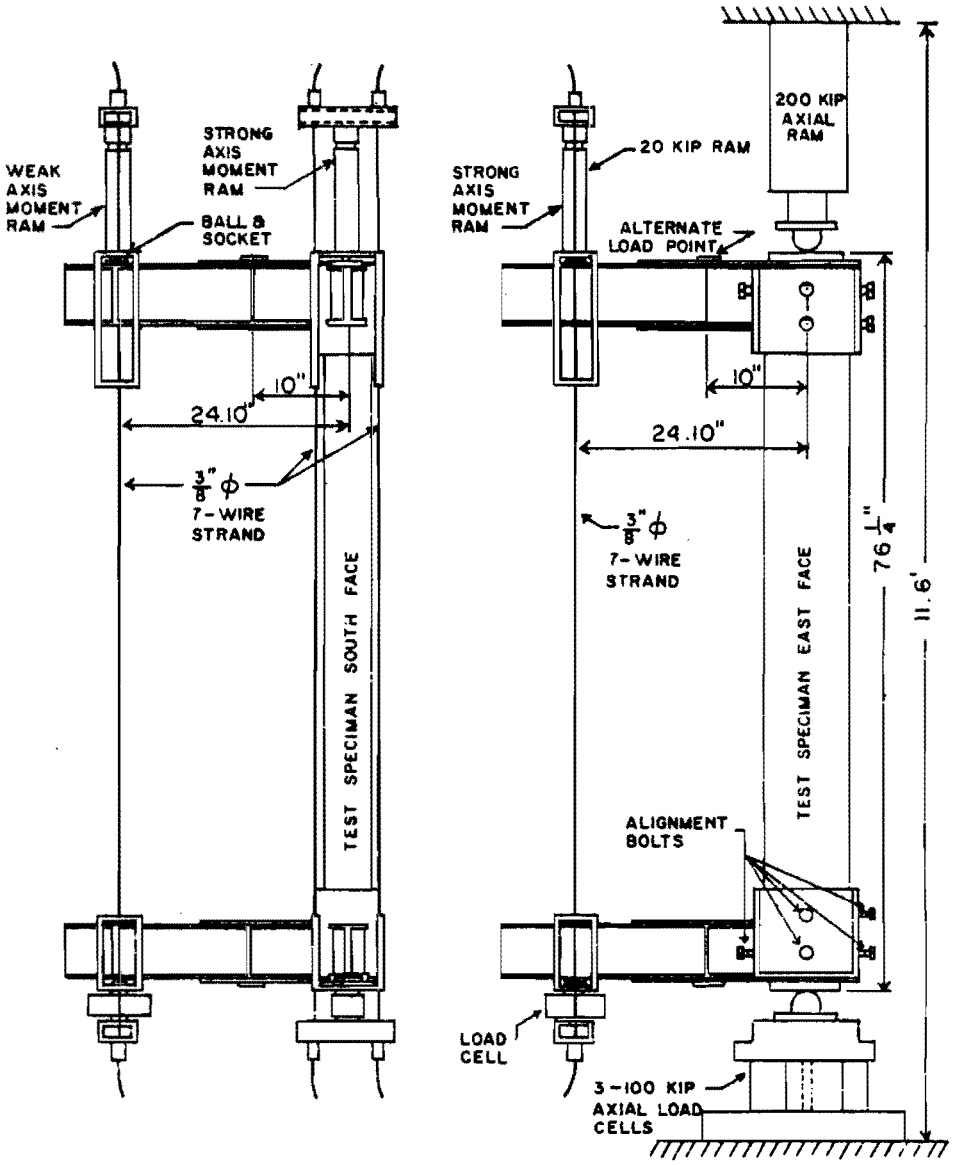

Fig. 2.8 Diagram of loading frame

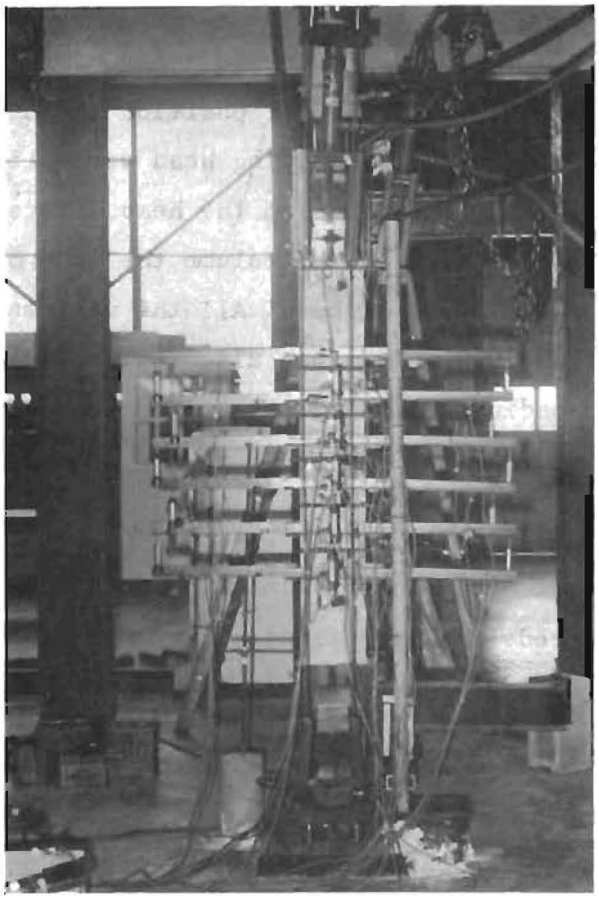

Fig. 2.9 Specimen in testing position

(b) Loading heads were attached to the column in the following manner:

1. The top loading head was set on the floor with the open side up and the moment arms were leveled.

2. The top of the column was lowered into the loading head with the aid of an overhead hoist. The column was adjusted into the proper position so that the center of the column and the loading head were aligned. By matching the punched marks on the head with some longitudinal reference lines on the column the load points on the head also were aligned. All the alignment adjustments could be made with some alignment bolts on the sides of the loading head.

3. The column was pulled out of the head after the alignment bolts had been loosened one turn.

4. Hydrastone was poured into the box and the column was replaced. After a final adjustment of the alignment, the hydrastone was allowed to set.

5. The column was turned end for end and the procedure was repeated for attaching the bottom end of the column.

(c) The column then was placed in the loading position in the loading frame. Overall alignment was aided by using a plumb bob located so that the hemispherical head at both top and bottom of the specimen would be positioned through the vertical centroidal axis of the column.

2.6 Instrumentation Devices

Three types of data, the magnitude of applied loads, the surface deformations, and the lateral deformations were collected during the test.

2.6.1 Magnitude of Applied Loads. The axial load that was applied at the centroid of the column was monitored by three 100 kip

load cells. The load cells were placed side by side under a bearing plate beneath the bottom hemispherical head. The three load cells provided a stable support for the column and also sufficient capacity for the highest load near 300 kips. A hydraulic pressure transducer also was used to monitor the axial load and to provide the electrical signal necessary for remote recording. In addition, visual observation of a pressure gage dial on the hydraulic pump provided a record and continual control of the axial centroidal load.

The loads of the two small rams on the moment arms were also monitored by two 10-kip capacity load cells located in the bottom of the load saddles. One pressure transducer together with a pressure gage dial were used to measure for recording the force in the two rams which were connected to the same pump.

The loading devices were calibrated in so far as possible under the same conditions as those of the actual test. Each load arrangement of ram, pump, hemisphere bearing, pressure transducer, load cell, and bearing plate was assembled in the same arrangement for calibration and for the tests.

2.6.2 Lateral Deformation. Deflections in the direction of each principal axis were measured by using linear potentiometers. The potentiometers were placed along the 24-in. midheight portion of the column at 6-in. intervals providing five measuring stations in the midheight region.

Torsional displacements were measured at three positions in the horizontal plane, one at the top, one at the bottom, and one at midheight. The three measurements could be converted to records of twist and the displacement in the direction of the minor axis. Twist near the top of the column was monitored by two potentiometers mounted 6 in. apart on the longer face of the column at 11 in. below the top end. Two dial gages were used to measure the twist near the bottom end, also mounted 6 in. apart on the west face at 11 in. above the bottom end. Another pair of dial gages was used for measuring twist at

midheight of the column. The gages were placed 8 in. out from the shorter faces of the column at midheight providing a longer twisting arm.

All the deflection measuring devices were mounted on a 2-1/2 in. steel pipe vertical post supported on the laboratory floor. All movement recorded, therefore, would be relative to the post, which was assumed fixed in position and direction.

2.6.3 Surface Deformation. Six steel frame strain meters (Fig. 2.10) were mounted on the column at 6 in. intervals through the 30 in. midheight portion of the column. The steel frames were attached to the column by a bolt at each side. The bolts were tightened to the column against aluminum bearing plates, which were glued to the column at the desired points. A linear potentiometer was placed between corresponding legs at adjacent frames. The records from the potentiomeyers indicated the change in longitudinal position between two adjacent frames. Similar frames were used by Chang,[7] Breen,[4] Furlong,[22] and Green,[24] et al., except that the system used here was expanded in order to measure biaxial longitudinal deformation.

All data from load cells and poteniometers were recorded onto magnetic tape and paper tape by a VIDAR data acquisition system which also provided a printed teletyped output when one was desired. The pressure transducer readings, dial gage readings, and pressure gage readings were recorded on the data collection sheets. The linear potentiometers and dial gages that were used gave an accuracy for the readings to the nearest 0.001 in. The strain indicator which was used to record the change in pressure transducer readings could give readings as accurate as±5 microstrains. The pressure gage gave readings to within ±50 psi. A column with all devices attached and in the position ready to be tested is shown in Fig. 2.9.

2.7 Test Procedure

The loading procedure in the test program was designed so that the total amount of axial load would be maintained at a constant

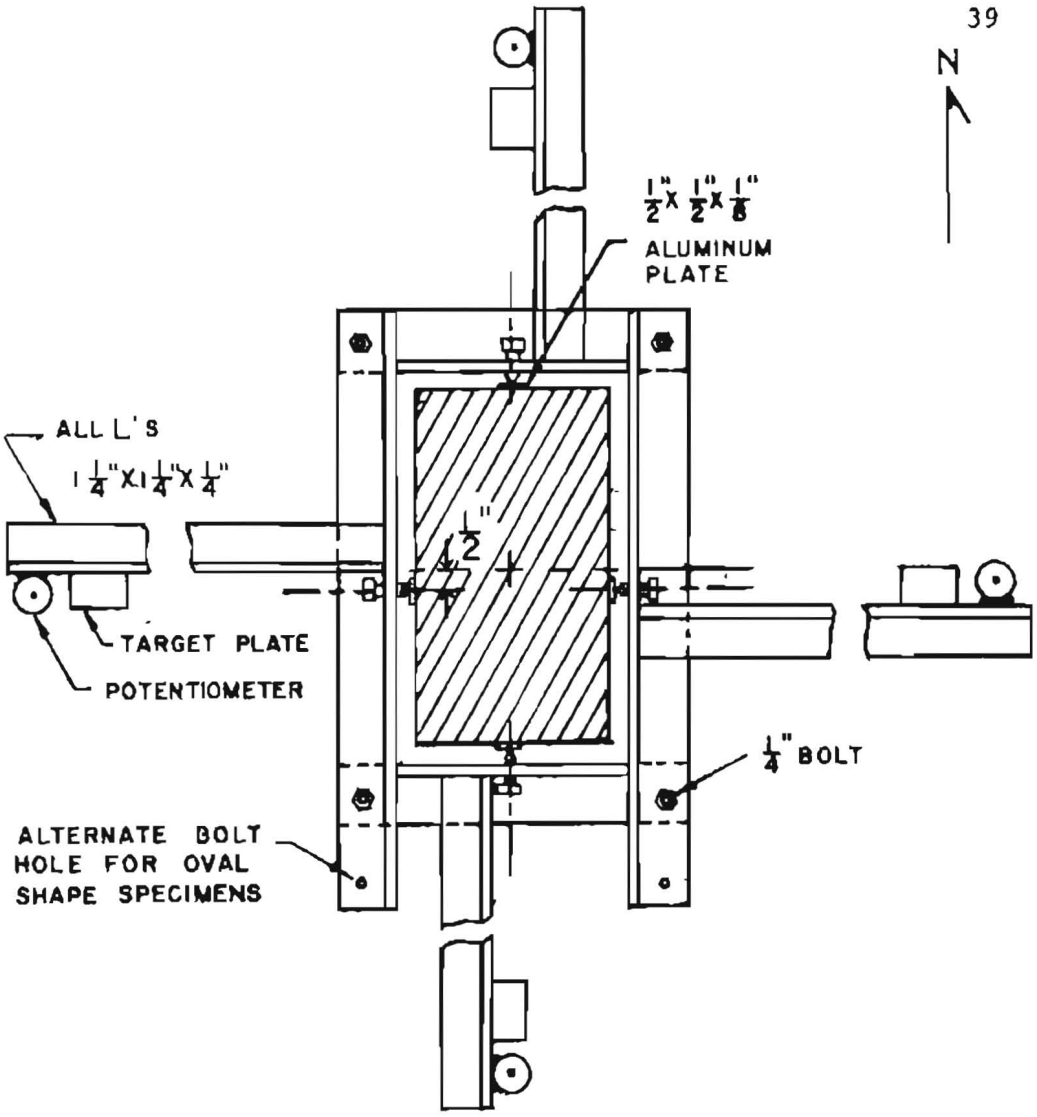

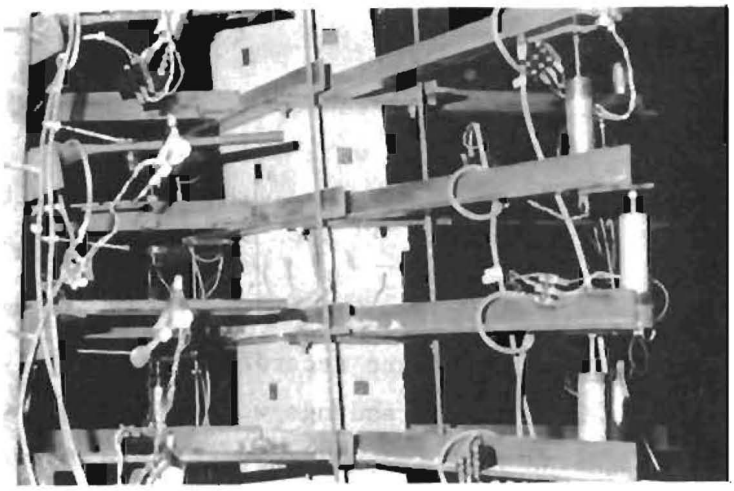

Fig. 2.10 Diagram and photo of deformation measuring frame

level while the moments would increase until failure. With this type of loading, the eccentricity would increase, moving outward from the centroid of the column along a nominally straight line.

After all devices had been connected and checked, pressure was applied to the axial ram for about 10 percent of the desired axial load level and then the load was released. This procedure helped to seat the measuring devices and the column bearings. After seating, the axial ram was loaded in about ten increments until the desired thrust level was reached. After each increment of axial load a set of data was recorded.

After the desired axial thrust level had been reached, the eccentric moment load about both strong and weak axis was applied. The loading points on the moment arms were located so that the nominal eccentricity angle would be either 0°, $22\text{-}1/2^{\circ}$, 45°, $67\text{-}1/2^{\circ}$, or 90°. The rams on each moment arm were loaded simultaneously from the same pump. The increment of the ram load was very small at the first few eccentric loadings. A graph of moment load and centerline deflection on the weak axis was maintained during the loading sequence. The magnitude of the load increment was adjusted according to the non-linearity of this graph. After the column reached the inelastic range, the load increment was kept very small, and readings were made only after the column could maintain steadily a level of load for several minutes.

The axial load was checked occasionally to keep the thrust level constant. Adjustments of load were made to the axial ram only if the total thrust varied more than 5 percent from the preferred level.

During the test cracks were observed and each was marked after each load stage. All data were recorded after each loading before marking the cracks. While readings were made and the cracks were marked, some creep and relaxation occurred. When it was noted that the creep was significant, another set of readings was taken before the next load increment was applied.

As the column reached ultimate load, the moment ram load could not be increased; because of the loss of stiffness the column ceased to resist greater load, and the dial gage at the midheight of the column showed increasing lateral deformation without any additional load increments. The VIDAR-recorded data readings could be taken continuously until failure occurred. Moment rams were pumped until failure of the column took place. It was found that the column failure sometimes damaged the potentiometers. Consequently, for the oval-shaped columns, loading was stopped after load instability of the column was observed (i.e., centerline deflection increased rapidly while the column could not maintain a constant moment). Figures 2.11 and 2.12 show pictures of some specimens after failure.

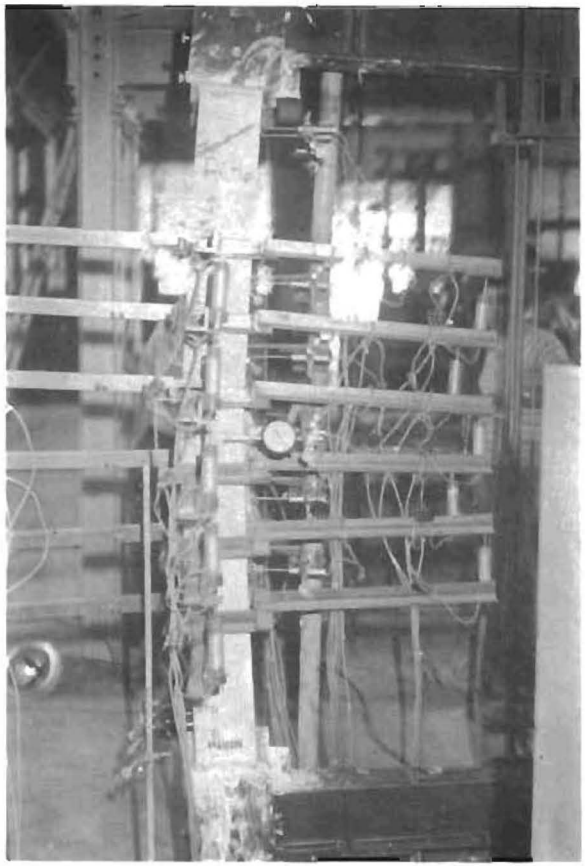

Fig. 2.11 Specimen RC-6 after failure, before measuring devices were taken off

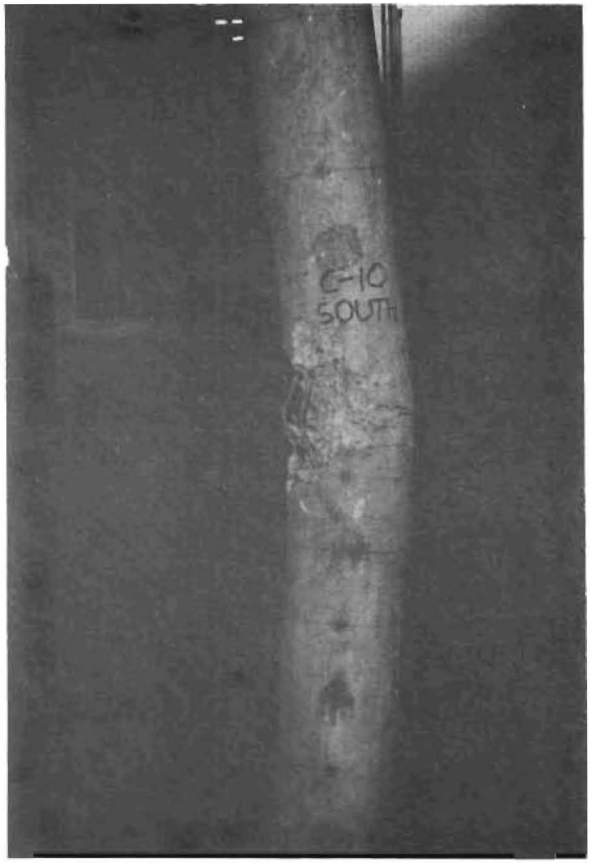

Fig. 2.12 Specimen C-10 after failure, all instruments were taken off

CHAPTER 3

ANALYSIS OF DATA

3.1 General

Three types of data were collected during the tests: lateral deflection, concrete surface deformation, and load measurement. Deformation and load cell readings were recorded on magnetic tape. A standard VIDAR program decoded the information and converted the readings to a reduced form of engineering units. Data files of this reduced information have been stored on magnetic tapes as well as punched cards. Computer programs have been written to reduce the data to the form of axial load, applied moments, skew angle, deflections, eccentricities, and surface strains. Another program has been prepared to analyze the surface strains and compute the forces, moments, and curvatures. Comparison of load and moments among different types of load indicators has been made to verify the reliability of the measured data.

3.2 Deflection

The deflected shapes in both weak axis and strong axis directions have been plotted for every load stage. These graphs show some aspects of behavior of the column during the test which would affect the analysis of the magnitude of the load.

3.2.1 Initial Position of Column. It had been observed that during each load stage the top and bottom of the column moved. This resulted in the changing of the position of the column. As higher moments were applied to the column, the movement decreased and the position of the ends stabilized finally at loads lower than eventual failure loads. Figures 3.1 and 3.2 show the movement and the stable position of RC-5 and C-11.

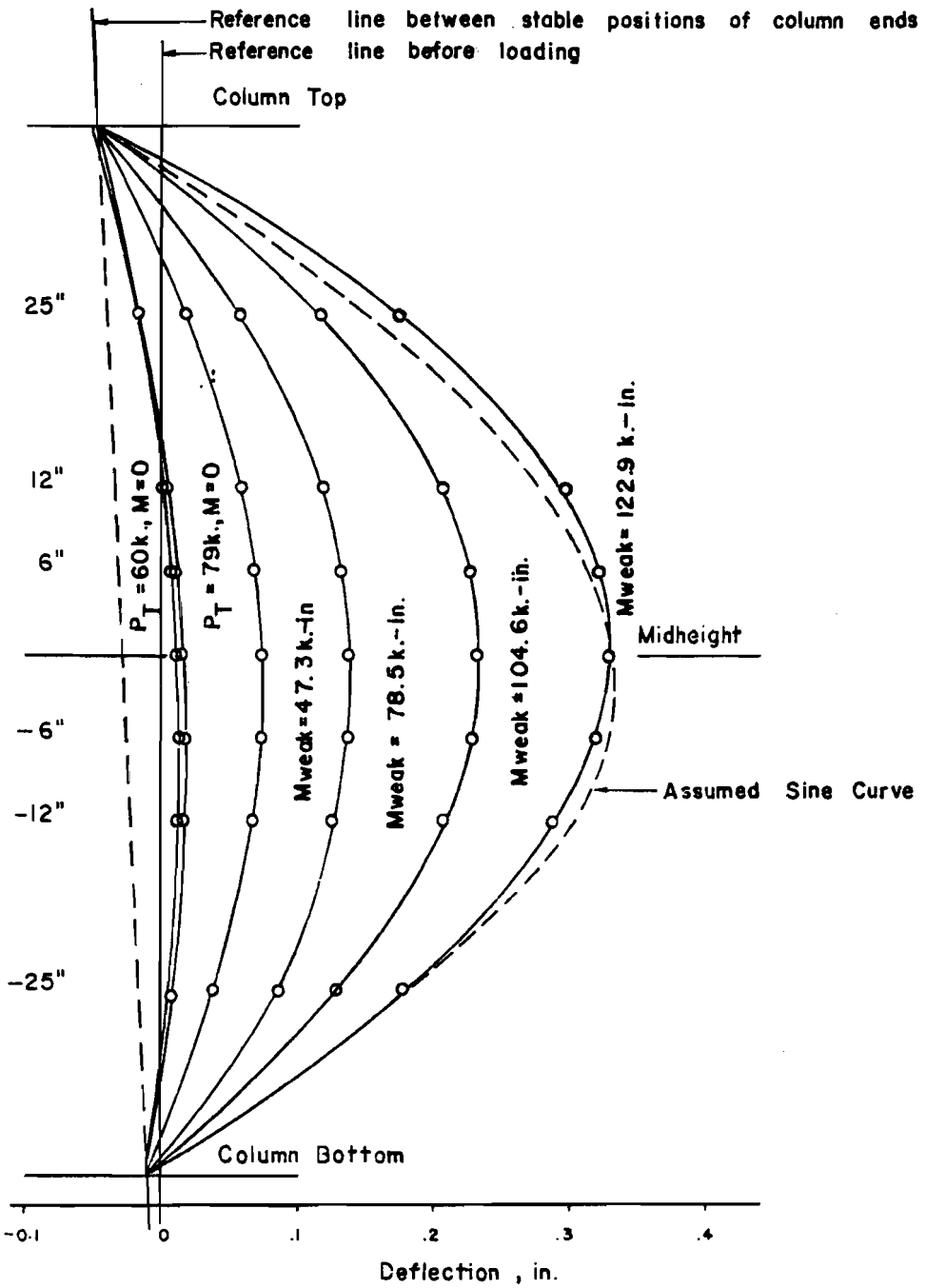

Fig. 3.1 Deflected shape of RC-5 (weak axis)

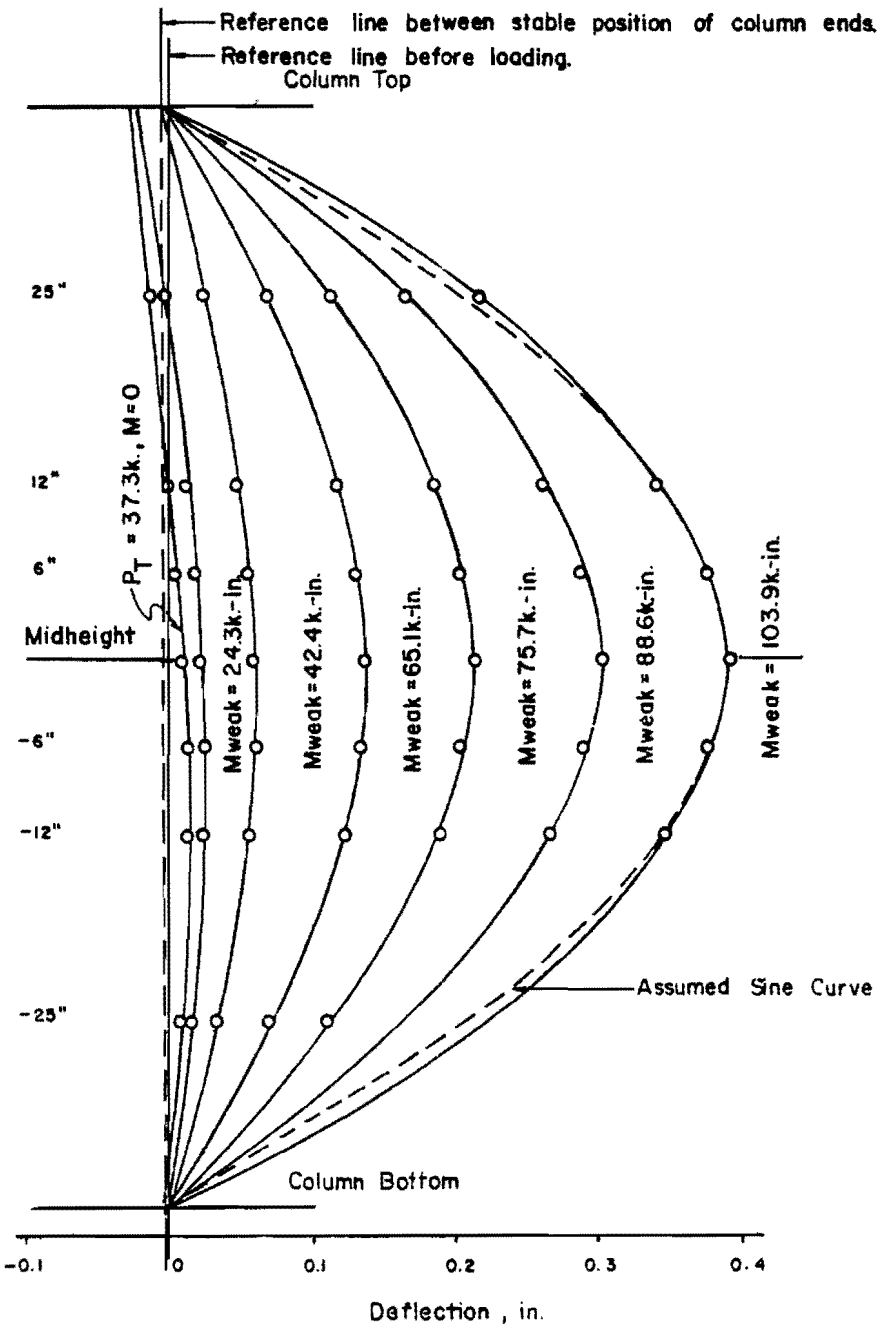

Fig. 3.2 Deflected shape of C-11 (weak axis)

For computer input the reference position of the column has been taken for the load stage at which no further movement of the column heads was noted. All the readings after the stabilized load stage have been corrected to a reference axis through the stable positions of the ends of the specimens. The stable positions of the ends of each specimen are tabulated in Table 3.1(a) as well as the deflections at midheight at failure of each column.

No measurement of column crookedness was made. It was assumed that the columns were straight because of the use of straight steel forms. Any error due to column crookedness was neglected. Specific measurement of movement of the top end of the column during the test was not attempted, but instead the column deflections were referred to the estimated position of the chord between column ends.

3.2.2 End Eccentricity. Eccentricity of Axial Load Ram. Axial loads were applied through hemispherical bearings located as near as possible along the longitudinal centroid of the specimens. Even with some flattening, the bearings could not transmit flexural forces, and the applied axial force had to act along a line between end bearings. The actual eccentricity of end bearings from the longitudinal axis of the specimen was estimated from measured deformations at midheight of the specimen under the "axial load only" condition. Subsequent application of flexural loads involved no change in the position of end bearings for axial load rams.

A midheight correction e_i for axial load end eccentricity was computed on the basis of the elastic deformation of a beam column as illustrated in Fig. 3.3 and defined by Eq. 3.1. The effect of Eq. 3.1 was to average the influence of end eccentricity at opposite ends of the specimen for an estimate of the overall influence at midheight before the application of flexural forces with accurately measured eccentricities.

$$e_i = \frac{\Delta EI}{PL^2} \left[\frac{u^2 \cos u}{2(1 - \cos u)}\right] \qquad 3.1$$

where $u = \frac{L}{2}\sqrt{P/EI}$

EI = Stiffness of the section

Δ = Midheight deflection taken as the lateral distance from column centroid to the reference line between "final" position of ends of column

L = Length of the column

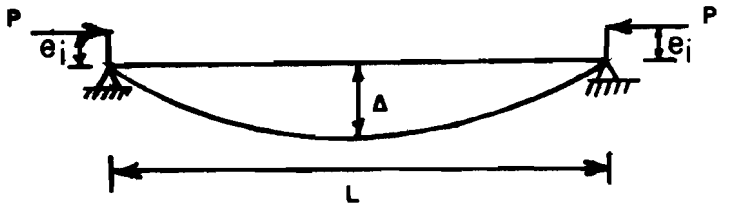

Fig. 3.3 End eccentricity due to misalignment

The magnitude of centerline deflection and axial load at the last load stage before moment load was to be applied had been used in Eq. 3.1 to calculate initial end eccentricity in each direction. These eccentricities are tabulated with every column in Table 3.1 (a).

Eccentricity due to End Rotation. As the column deflected, the contact point between the hemispherical ball and the bearing plate at the end of the column changed with respect to the column axis. Rotation of the loaded ends created the change in end eccentricity, as shown in Fig. 3.4.

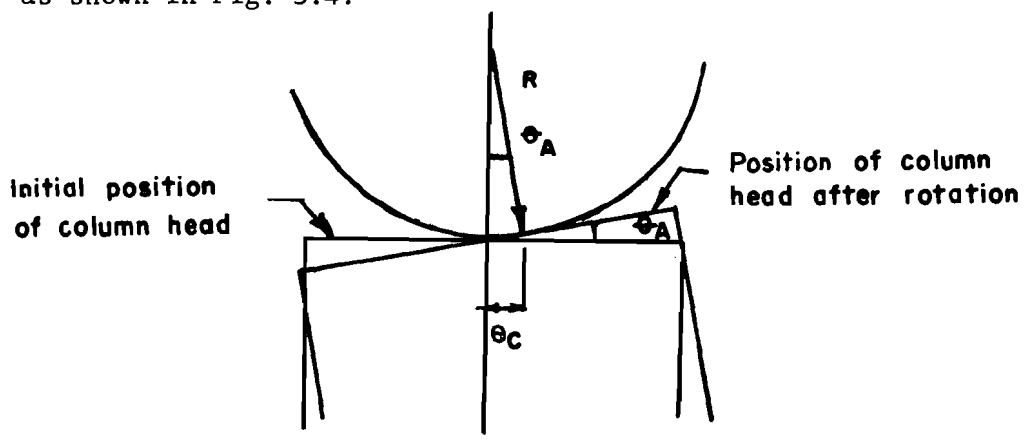

Fig. 3.4 End eccentricity due to end rotation

The change in eccentricity can be determined if the end slope of the deflected column is known. It is assumed that the deflected shape was one-half of the sine wave with the amplitude equal to centerline deflection. The deflected shape then can be expressed as

$$y = \Delta \sin \frac{\pi x}{L} \qquad 3.2$$

the slope $$y' = \frac{dy}{dx} = \frac{\pi}{L} \Delta \cos \frac{\pi x}{L}$$

at end, $x = 0$ $$y' = \frac{\pi}{L} \Delta = \theta_A \qquad 3.3$$

As illustrated in Fig. 3.4, if R equals the radius of the hemispherical ball, the end eccentricity, e_c is

$$e_c = R \tan \theta_A$$

If θ_A is small so that $\tan \theta_A = \theta_A$

$$e_c = R \theta_A$$

$$e_c = R \Delta \frac{\pi}{L} \qquad 3.4$$

In Figs. 3.1 and 3.2 a curve of the half sine wave adjusted with the amplitude set equal to the centerline deflection is plotted as a dashed line for comparison with the maximum measured deflected shape that is shown.

Green[25] measured the radius of the bearing surface of the ball and found that R = 18 in. appeared to be the most reasonable value. The column length, L, of 76.25 in. was measured between end bearings of the specimen and was used in Eq. 3.4. The end eccentricities due to end rotation changed during the test because the centerline deflection changed according to the applied moment.

Effects of misalignment and end rotation have been included in the computer program that calculated applied force and effective total moments. Table 3.1(a) also shows an example of the eccentricities due to end rotation at the very last load stage in the experiment.

The end eccentricity due to misalignment of the axial ram on the strong axis was small enough to be neglected for some specimens. However, the misalignment eccentricity was found to be a significant factor in calculating the total eccentricity at midheight of some

TABLE 3.1 FAILURE MOMENTS AND DEFLECTIONS

(a) End Eccentricities and Deflections at Failure Load Stage

Specimen	Measured Deflection at Midheight		Position of Column Ends, Strong Axis		Position of Column Ends, Weak Axis		Adjusted Deflection at Center Portion*		Eccentricity due to Misalignment		Eccentricity due to End Rotation	
	Strong Axis (in.)	Weak Axis (in.)	Top (in.)	Bottom (in.)	Top (in.)	Bottom (in.)	Δ_{strong} (in.)	Δ_{weak} (in.)	e_{is} (in.)	e_{iw} (in.)	e_{cs} (in.)	e_{cw} (in.)
RC-1	0.124	0.586	0.044	-0.026	-0.007	-0.019	0.109	0.506	0.000	0.122	-0.087	-0.242
RC-2	0.234	0.571	0.175	0.020	-0.009	0.038	0.138	0.537	0.000	0.129	-0.105	-0.416
RC-3	0.210	0.588	0.105	0.063	-0.030	0.011	0.148	0.569	0.000	0.116	-0.115	-0.443
RC-4	0.304	0.507	0.053	0.003	-0.016	-0.013	0.263	0.490	0.000	0 141	-0.205	-0.387
RC-5	0.090	0.726	0.033	-0.005	-0.048	-0.010	0.073	0.719	-0.176	0.209	-0.056	-0.560
RC-6	0.093	0.868	0.022	-0.004	-0.016	-0.051	0.080	0.847	0 000	0.186	-0.062	-0.669
RC-7	0.250	0.898	0.056	0.001	-0.002	-0 025	0.209	0.861	-0.646	0.134	-0.165	-0.676
RC-8	0.404	0.581	0.010	0.025	0.038	0.038	0.364	0.507	0 000	0.000	-0.287	-0.402
RC-9	0.366	0.498	0.009	0.063	-0.002	0.018	0.313	0.466	0.000	0.000	-0.246	-0.363
C-5	0.095	0.512	-0.036	-0.086	0.032	-0.047	0.150	0.490	0.716	-0.108	-0.114	-0.383
C-6	0.157	0.596	-0.062	-0.036	0.083	-0.013	0.264	0.529	0.182	-0.214	-0.154	-0.416
C-7	0.118	0.617	-0.007	-0.065	0.086	0.016	0.164	0.541	0.106	-0.048	-0.114	-0.420
C-8	0.063	0.891	0.004	-0.046	0.069	-0.013	0.092	0.814	0.000	0,000	-0.062	-0.640
C-9	0.082	0.735	-0.023	-0.011	0.043	0.020	0.091	0.721	0.000	0.000	-0.076	-0.565
C-10	0.050	0.634	-0.072	-0.046	0.019	-0.001	0.098	0.593	0.000	0.272	-0 081	-0.464
C-11	0.327	0.685	-0.087	-0.023	-0.005	-0.005	0.381	0.634	0.353	0.426	-0.283	-0.512
C-12	0.472	0.612	-0.083	-0.054	0.021	-0.002	0.320	0.569	0.173	0.450	-0.197	-0 447
C-13	0.133	0.394	-0 100	-0.050	-0.002	0.024	0.230	0.369	0.117	0.233	-0.154	-0.284
C-1	-	0.796	-	-	-0.016	0.007	-	0.737	-	0.282	-	-0.593
C-2	-	0.480	-	-	0.001	0.006	-	0.444	-	0.000	-	-0.353
C-15	-	0.771	-	-	-0.051	-0.048	-	0.779	-	-0.146	-	-0.609
C-3	0.618	-	0.028	0.010	-	-	0.591	-	0.000	-	-0.465	-
C-4	0.347	-	0.033	0.007	-	-	0.307	-	0.000	-	-0 243	-
C-14	0.451	-	-0.034	-0.046	-	-	0.442	-	0.000	-	-0.364	-

*Averaged along 24 in portion at midheight

(b) Moments at Failure Load Stage

Specimen	Axial Thrust* (k)	Applied Moment		Moment due to Ram Misalignment		Moment due to End Rotation		Total End Moment		Maximum Moment at Midheight**	
		M_{strong} (k-in.)	M_{weak} (k-in.)	$P_u \times e_{is}$ (k-in.)	$P_u \times e_{iw}$ (k-in.)	$P_u \times e_{cs}$ (k-in.)	$P_u \times e_{cw}$ (k-in.)	M_{so} (k-in.)	M_{wo} (k-in.)	M_s (k-in.)	M_w (k-in.)
RC-1	119.2	57.9	138.0	0.0	14.5	-10.4	-28.8	47.5	123.7	60.6	184.0
RC-2	120.3	120.1	124.0	0.0	15.5	-12.6	-50.0	107.5	89.5	124.0	154.1
RC-3	94.3	125.0	127.6	0.0	10.9	-10.8	-41.6	114.2	96.7	128.2	150.4
RC-4	128.8	221.4	96.0	0.0	18.2	-26.4	-49.8	195.0	64.4	228.9	127.4
RC-5	87.1	54.2	128.7	-15.3	18.2	-4.9	-48.8	34.0	98.1	46.3	160.8
RC-6	53.9	51.2	126.2	0.0	10.0	-3.3	-36.0	47.9	100.2	52.2	145.9
RC-7	40.4	110.9	108.4	-26.1	5.4	-6.7	-27.3	78.1	86.5	86.6	121.3
RC-8	40.4	187.3	82.2	0.0	0.0	-11 6	-16.2	175.7	66.0	190.4	86.4
RC-9	85.8	211.8	93.2	0.0	0.0	-21.1	-31.1	190.7	62.1	217.5	102.0
C-5	49.5	101.1	113.6	35.6	-5.3	-5.6	-19.0	131.1	89.3	138.3	113.5
C-6	92.2	144.4	156.4	16.8	-19.7	-14.2	-38.4	147.0	98.3	171.3	147.1
C-7	139.7	143.3	151.4	14.8	-6.7	-15.9	-58.8	142.2	85.9	165.1	161.6
C-8	57.1	62.7	158.1	0.0	6.9	-3.5	-36.5	59.2	121.6	64.4	168.0
C-9	96.2	66.4	164.1	0.0	0.0	-7.3	-54.4	59.1	109.7	67.8	179.1
C-10	138.2	54.7	132.5	0 0	37.6	-11.2	-64.1	43.5	106.0	57.1	188.6
C-11	53.2	227.9	99.6	18.8	22.7	-15.1	-27.2	231.6	95.1	251.9	128.8
C-12	99.2	213.8	98.9	17.2	44.6	-19.5	-44.3	211.5	99.2	243.1	155.6
C-13	152.5	238.8	99.1	17.8	35.5	-23.5	-43.3	233.1	91.3	268.2	147.7
C-1	60.7	-	139.7	-	17.1	-	-36.0	-	120.8	-	165.5
C-2	135.6	-	141.7	-	0.0	-	-47.9	-	93.8	-	154.1
C-15	109.2	-	191.5	-	-15.9	-	-66.5	-	109.1	-	194.2
C-3	58.4	364.8	-	0.0	-	-27.2	-	337.6	-	372.2	-
C-4	155.8	414.3	-	0.0	-	-37.9	-	376.4	-	424.2	-
C-14	119.2	445.9	-	0.0	-	-43.4	-	402.5	-	455.2	-

*From ram pressure reading

**Averagedalong 24 in. portion at midheight

columns. For example, Specimen RC-5 was found to have an end eccentricity due to misalignment in the strong axis direction of 0.176 in., which produced moment equal to 38 percent of the total moment at midheight at the failure load. The weak axis misalignment of the axial load ram was computed for every specimen. The maximum end eccentricity due to misalignment about the weak axis was 0.45 in. for Specimen C-12, creating 29 percent of the total moment at midheight at the failure load stage.

The end rotation always was an important factor in the calculation of the total eccentricity. The ratio between moment due to end rotation and the total moment at midheight was smaller for strong axis than for the weak axis bending. At the failure load stage, a maximum ratio of 20 percent was found in Specimen C-10 in the strong axis direction. The maximum ratio of 39 percent was found in the weak axis direction of Specimen RC-4. The moments due to misalignment and due to end rotation at failure load are shown in Table 3.1(b).

3.3 Axial Load and Moments

The total axial thrust, P_T, is the combination of the loads from three rams, one ram P_A at the longitudinal axis of the specimen and two rams P_S and P_W on the eccentric thrust arms.

$$P_T = P_A + P_S + P_W \tag{3.5}$$

where P_T = Total axial load
P_A = Load on axial ram
P_W = Load on weak axis moment ram
P_S = Load on strong axis moment ram

Applied moments for each principal axis were determined as the combination of eccentric thrust from each ram, including the corrections for alignment of the major force P_A.

$$M_{so} = P_S \times \text{strong axis moment arm} + P_A(e_{is} + e_{cs}) \tag{3.6}$$

$$M_{wo} = P_W \times \text{weak axis moment arm} + P_A(e_{iw} + e_{cw}) \tag{3.7}$$

where M_{so}, M_{wo} = Strong axis moment and weak axis moment applied at ends of the column

e_{is}, e_{iw} = Strong and weak axis eccentricity of the axial load ram

e_{cs}, e_{cw} = Strong and weak axis eccentricity due to end rotation

The moments along the 24 in. middle portion of the column were the sum of the applied moment at the end and the additional second order moment due to thrust and lateral deflection. Table 3.1(b) also shows the tabulation of total end moment and the moment at mid-height at the failure load stage for every column.

3.3.1 Applied Loads Measured from Load Cells and from Ram Hydraulic Pressure. There were two methods for measuring ram load: the reading from load cells and the reading from the ram pressure transducer. At the time the load cell calibration was made, the system consisted of an axial load ram, bottom hemispherical ball, bottom bearing plate, three load cells, and a pressure transducer. The total load obtained from the load cells and from the pressure transducer were nearly identical, as shown in Table 3.2. In the actual column tests, although careful adjustment of alignment was attempted, the readings in load cells indicated that each of the three load cells did not carry equal load. Even the sum of different load cell readings differed from loads indicated by the pressure transducers. Comparisons between load cell readings and pressure readings have been made at several load stages for each column. The average of the ratio between load cell data and pressure data for each column is shown in Table 3.3. Data in Table 3.3 indicate that the ram pressure load was generally lower than the sum of load cell readings. During any specimen loading, the ratios between ram pressure load and load cell readings remained within 5 percent of a constant or mean value. For uniaxial bending tests of partial circle specimens (Load Angle = 0° or 90° in Table 3.3), both measuring systems indicated loads that were within 4 percent of one another.

TABLE 3.2 CALIBRATION OF LOAD CELLS AND PRESSURE TRANSDUCER READING FOR AXIAL RAM

Actual Ram Load* (kips)	Load in Individual Load Cell			Total Load from Load Cell	Load from Pressure Transducers
	L.C. #4 (kips)	L.C. #5 (kips)	L.C. #6 (kips)	(kips)	(kips)
0	0	0	0	0	0
5.01	3.544	1.731	1.266	6.541	5.269
16.87	6.201	4.588	5.526	16.315	16.017
20.86	8.269	5.670	7.467	21.406	20.969
30.30	11.433	7.704	11.644	30.781	30.488
40.32	17.761	10.041	16.242	44.044	40.780
49.92	17.339	12.465	20.123	49.927	50.404
60.10	22.064	15.278	24.426	61.768	60.801
70.07	22.908	17.832	28.307	69.047	71.233
80.36	27.843	20.472	32.695	80.940	80.541
90.50	30.628	23.242	36.787	90.657	90.516
100.60	33.117	25.622	40.542	99.281	100.597
110.28	36.492	28.046	44.718	109.256	110.116
121.18	41.006	31.249	49.823	122.078	121.005
131.31	43.326	33.975	54.210	131.511	131.056
141.07	46.996	36.226	58.007	141.229	140.920
151.61	49.359	39.299	63.070	151.728	150.650
161.60	52.565	42.026	67.726	162.217	160.801

*Indicated from calibration machine

TABLE 3.3 RATIO BETWEEN LOAD CELL READINGS AND RAM PRESSURE LOAD

Specimen	Load Level (P_o)	Load Angle ($\tan^{-1} M_s/M_w$) (degree)	Load on Ram / Load on Load Cell (average)	Range of the Ratio within Specimen		No. of Reading
				Max.	Min.	
C-1	0.2	0	1.023	1.039	0.996	10
C-15	0.4	0	0.963	0.981	0.958	7
C-2	0.6	0	0.982	0.996	0.974	10
C-3	0.2	90	1.003	1.037	0.959	11
C-14	0.4	90	0.983	1.007	0.961	12
C-4	0.6	90	1.007	1.028	1.005	9
C-5	0.2	45	0.971	0.979	0.946	4
C-6	0.4	45	0.963	0.979	0.940	8
C-7	0.6	45	0.980	0.985	0.972	8
C-8	0.2	22½	0.944	0.971	0.911	9
C-9	0.4	22½	0.969	0.995	0.935	9
C-10	0.6	22½	0.956	0.958	0.947	6
C-11	0.2	67½	0.946	0.996	0.919	11
C-12	0.4	67½	0.915	0.930	0.892	11
C-12	0.6	67½	0.921	0.940	0.894	11
RC-6	0.2	22½	0.881	0.907	0.869	14
RC-5	0.4	22½	0.899	0.915	0.892	12
RC-1	0.6	22½	0.847	0.880	0.838	18
RC-7	0.2	45	0.876	0.930	0.841	11
RC-3	0.4	45	0.914	0.972	0.899	13
RC-2	0.6	45	0.896	0.923	0.870	17
RC-8	0.2	67½	0.825	0.850	0.808	9
RC-9	0.4	67½	0.824	0.833	0.821	8
RC-4	0.6	67½	0.907	0.923	0.899	18

Relationships between nominal load angle and the ratio of axial thrust measured from ram pressure and load cells are also plotted in Fig. 3.5. The plot shows that specimens with oval-shaped cross section had better agreement between load cell readings and pressure readings than did rectangular cross section specimens. For biaxially loaded specimens, specimens with a nominal load angle of $67\text{-}1/2^{\circ}$ showed the largest difference between load cell readings and pressure readings, while specimens with a load angle of 45° had the best agreement.

For biaxial bending tests, the test with an eccentric load angle of $67\text{-}1/2^{\circ}$ on rectangular specimens gave the maximum differences. The lowest value of the ratio between the load from ram pressure and the load from load cells is 0.824. Since load indicated from load cell involved the sum of three load cell readings, the effect of eccentricity at bearings would be more prominent from load cells. Data in Table 3.3 indicate maximum difference in total load measurements when the load angle was $67\text{-}1/2^{\circ}$. Load cell sensitivity to eccentric force through the load cell was considered to be the source of observed variations between ram pressure data and the sum of load cell readings. Consequently, the ram pressures were used as the reported value of load for all strength studies. The values read from pressure transducers were found to agree within 50 psi with the visual observations of pressures from a gage in the hydraulic system.

From Table 3.3, RC-8 and RC-7 have the maximum difference of the average ratio between pressure load and the load cell load. Also, the ranges of the ratio are greatest for these two specimens. The ratio of load cell reading and pressure transducer reading for several load stages of RC-8 is listed in Table 3.4. The statistical analysis of the data for RC-8 in Table 3.4 shows that the variations of the measuring systems are not large. For RC-8, the standard deviation of 0.0116 and the coefficient of variation of 0.014 have been computed when the ratios of ram pressure load to the load cell loads were used as population in the analysis. With the maximum error of three

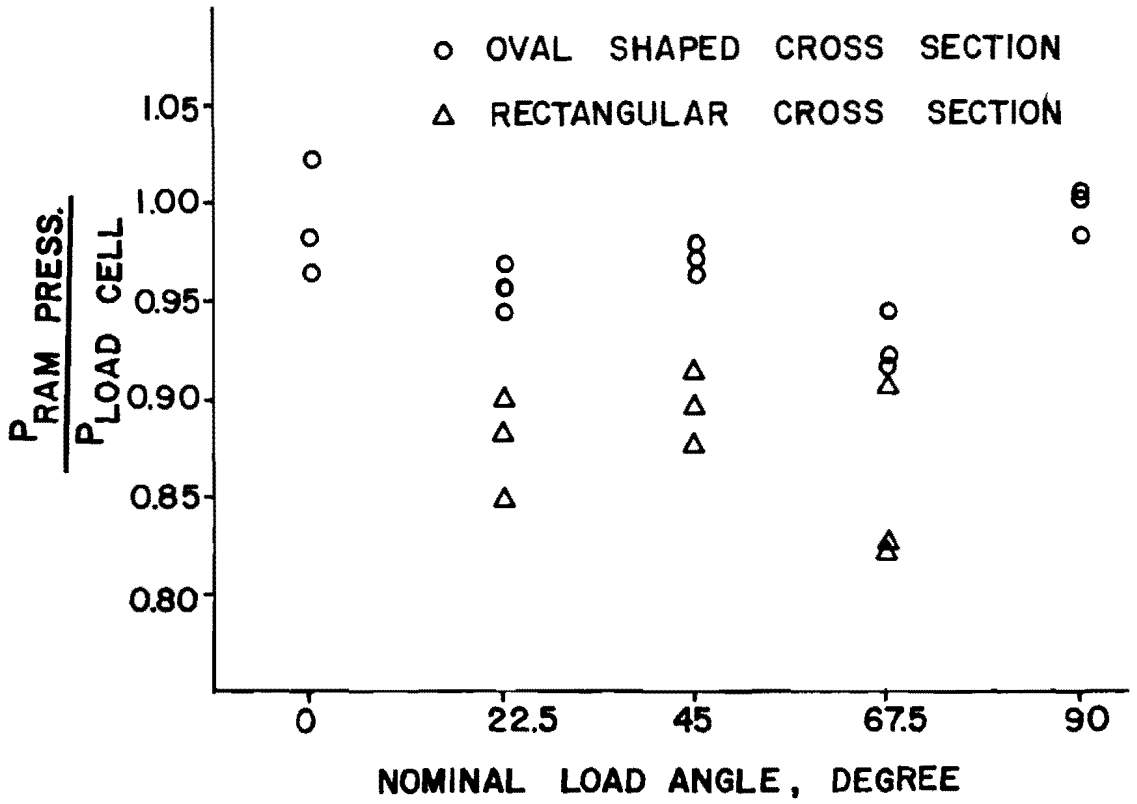

Fig. 3.5 Load angle vs. ratio of thrust from ram pressure and load cell

TABLE 3.4 INDIVIDUAL STATISTICAL ANALYSIS FOR $P_{pressure}/P_{load\ cell}$ OF RC-8

Reading No.	$\frac{P_{pressure}}{P_{load\ cell}}$ (x)	$(x - \bar{x})$	$(x - \bar{x})^2$
1	0.827	0.0016	0.00000256
2	0.808	-0.0174	0.00030276
3	0.819	-0.0064	0.00004096
4	0.823	-0.0024	0.00000576
5	0.818	-0.0074	0.00005476
6	0.850	0.0246	0.00060516
7	0.830	0.0046	0.00002116
8	0.831	0.0056	0.00003136
9	0.823	-0.0024	0.00000576

$\Sigma_x = 7.429$ $\Sigma = 0.00107024$

$\bar{x} = 0.8254$

Standard Deviation $\sigma = \sqrt{\frac{\Sigma(x - \bar{x})^2}{n - 1}} = 0.011566$

Code of Variation $\frac{\sigma}{\bar{x}} = 0.014$

standard deviations, or ±3.5 percent, most of the data of RC-8 can be represented by the mean value of the ratio. Similar analyses were conducted for other columns, and the results indicated that the average of the ratio can be used to represent the difference between the load cell reading and the ram pressure reading. The data from pressure transducers could not be read at the load near failure, whereas the load cell readings were available on magnetic tape until failure. Load cell data were corrected in proportion to the average ratio between ram pressure data and load cell data at lower levels of load where ram pressure data were available. With corrections for end eccentricity of spherical bearings, rotation of loading heads, and a dual set of end thrust measurements, it is felt that reported thrusts and moments are within ±10 percent of a "true" value.

Computer programs were written to compute the total axial load, end moment, moment along the column due to secondary effect from deflections, the eccentricities and the effective angle of eccentricity for every load stage of every specimen.

Although the axial load from the computer output shows that the load cell reading and the ram pressure load reading are different, the flexural effect of concentric thrust P_A was minor and the computed moments are almost the same. Figure 3.6 shows the comparison between the centerline moments of Specimen RC-9 determined with concentric thrust from load cells and from ram pressures plotted on the same scale. Note that even though thrust measurements differed by 20 percent, differences in end moments cannot be detected.

3.4 Analysis of Surface Deformation

Throughout the 30 in. center portion of each column, the surface deformations were measured at five stations of 6-in. gage length. Four potentiometer readings for each section were recorded, one for each face of the column. The potentiometers were attached to the end of the arms of steel frames which were described in Chapter 2.

3.4.1 Plane of Strain. At each 6-in. station, four deformation readings were available. Only three were needed to compute an

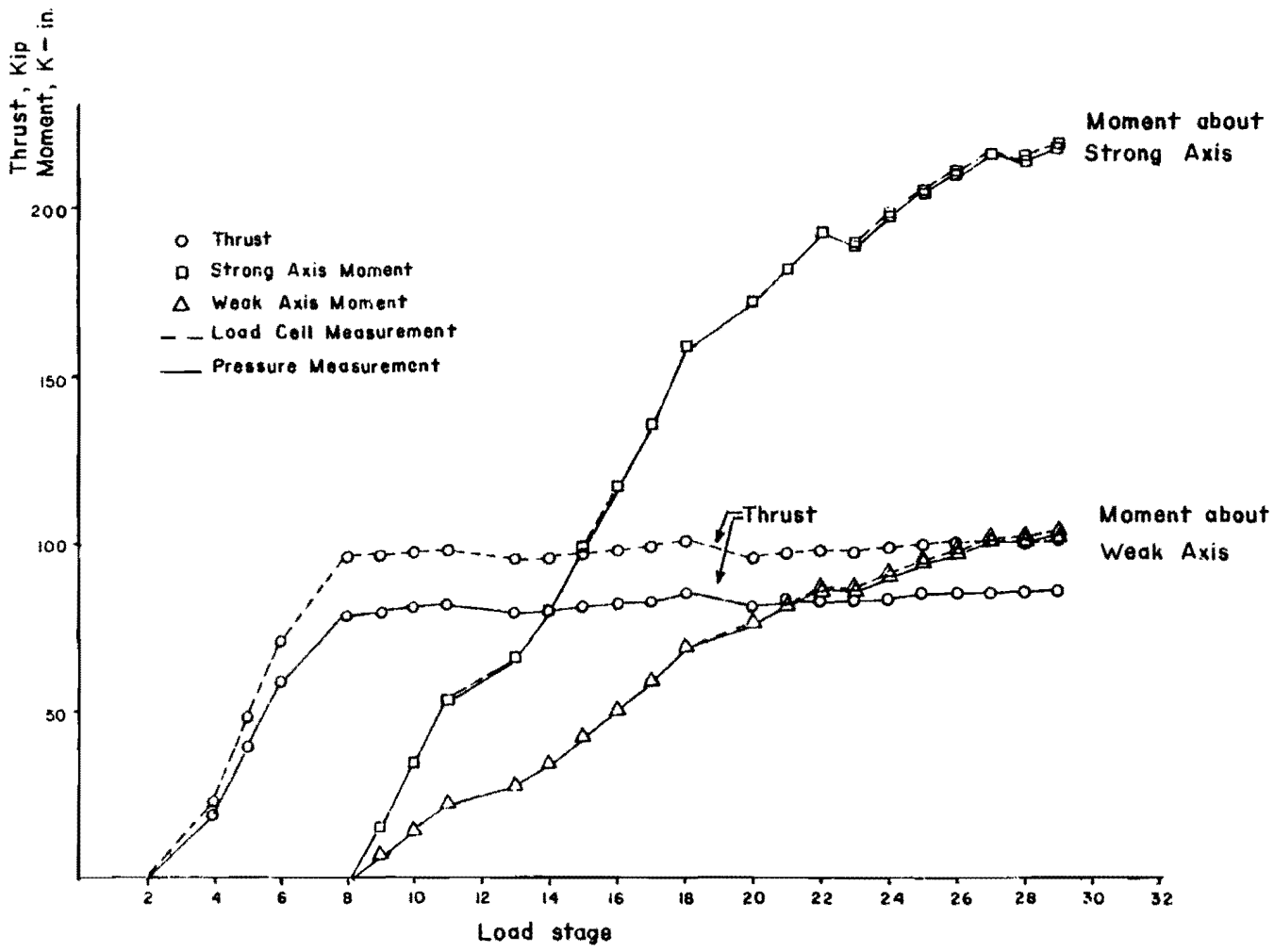

Fig. 3.6 Load cell measurement and ram pressure measurement for Specimen RC-9

equation of the deformed plane. Figure 3.7 shows the planes of strain before load and the deformed plane after loading. It has been assumed that plane sections before loading remain plane after the load was applied. The validity of this assumption will be discussed later in this section.

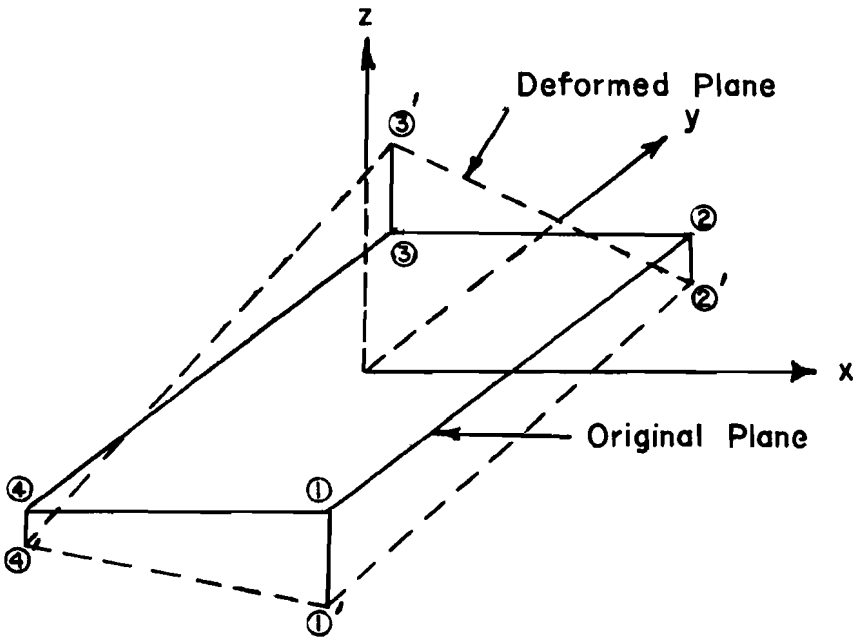

Fig. 3.7 Planes of strain

In Fig. 3.7, 1 1′, 2 2′, 3 3′, and 4 4′ represent the strains at each corner of the section. The three potentiometer readings that showed the most compressive deformation were used to define the plane. The fourth point, which was frequently a tension deformation, was used as a check point. Using the coordinates as shown in Fig. 3.7, the Z direction represents longitudinal deformation. An equation of the deformed plane can be developed as follows:

The general equation of the plane is

$$A_x + B_y + C_z + D = 0 \qquad 3.8$$

or

$$A(x_1 - x_2) + B(y_1 - y_2) + C(z_1 - z_2) = 0 \qquad 3.9$$

$$A(x_2 - x_3) + B(y_2 - y_3) + C(z_2 - z_3) = 0 \qquad 3.10$$

$$A(x_3 - x_1) + B(y_3 - y_1) + C(z_3 - z_1) = 0 \qquad 3.11$$

With the data available for x, y, and z values, the three simultaneous equations 3.9, 3.10, and 3.11 can be solved for the value of constants A, B, and C. The general equation of strain was used to determine the strain of the section at any point simply by input coordinates x, y of the point.

A computer program was coded to reduce the potentiometer readings into the strains at the middle of each side of the measuring station. This program also averaged the strain along all five stations. The average strain for each face of every load has been printed onto the magnetic tape permanent file for later studies with the computer system.

The validity of the assumption that strains varied in a plane was examined by comparing at the fourth measuring station the observed strain and the strain which was computed from observations at the other three stations. Data for three different load levels on two specimens are shown in Table 3.5. These data are representative for all specimens. The table shows at each measuring station the difference of values and an error ratio taken as the ratio between the difference and the measured value. After each set of values for five longitudinal positions along the specimen, the average of all five strain values is shown. Error ratios were larger generally before moment loading was applied, and the error ratios tended to become smaller as moment loading was increased. The error ratio of 0.053 for the sum of all stations at the first cracking load on Specimen C-5 is considerably smaller than ratios as high as 0.544 at Station 1 under the same load, indicating the local influence of cracks that cross from one station to another. Under high moment loading near failure in each test, the error ratio for the sum of all stations was never greater than 0.1 and usually less than 0.05, a range within which the assumption of a plane variation of strain is acceptable. The error ratio for the sum of all stations of each specimen at the failure load stage is shown in Table 3.6.

TABLE 3.5 COMPARISON OF MEASURED AND COMPUTED STRAINS AT 4th POINT

Load Stage	Level	East Deformation		Difference	Error*
		Computed	Measured		
		Specimen RC-1			
16	1	0.00056	0.00030	0.00025	0.829
(Before moment	2	0.00164	0.00132	0.00023	0.249
load was	3	0.00288	0.00020	0.00268	13.249
applied)	4	0.00168	0.00088	0.00080	0.903
	5	0.00619	0.00381	0.00238	0.624
	Sum	0.01295	0.00651	0.00644	
	Avg.	0.00259	0.00130	0.00129	0.988
25	1	0.03593	0.03875	-0.00282	-0.073
(1st crack)	2	0.04367	0.04158	0.00209	0.050
	3	0.04525	0.04380	0.00144	0.033
	4	0.03557	0.03688	-0.00132	0.036
	5	0.04746	0.04601	0.00145	0.031
	Sum	0.20787	0.20702	0.00085	
	Avg.	0.04157	0.04140	0.00017	0.004
30	1	0.07910	0.09414	-0.01504	-0.160
(Failure)	2	0.11514	0.10637	0.00877	0.083
	3	0.11093	0.11062	0.00031	0.003
	4	0.09709	0.10097	-0.00388	-0.039
	5	0.10912	0.10756	0.00156	0.015
	Sum	0.51137	0.51965	-0.00828	
	Avg.	0.10227	0.10393	-0.00166	-0.016
		Specimen C-5			
9	1	-0.00297	-0.00243	-0.00055	0.183
(before moment	2	-0.00156	-0.00172	0.00017	-0.106
load was	3	-0.00231	-0.00253	0.00022	-0.097
applied)	4	-0.00196	-0.00192	-0.00004	0.020
	5	-0.00023	-0.00074	0.00051	-2.198
	Sum	-0.00903	-0.00934	-0.00031	
	Avg.	-0.00181	-0.00186	-0.00006	-0.034
13	1	0.01661	0.02565	-0.00904	-0.544
(1st crack)	2	0.03023	0.02407	0.00615	0.204
	3	0.02907	0.03136	-0.00229	-0.079
	4	0.02011	0.02330	-0.00319	-0.159
	5	0.02909	0.02767	0.00141	0.049
	Sum	0.12510	0.13206	-0.00696	
	Avg.	0.02502	0.02641	-0.00139	-0.053
22	1	0.06744	0.07749	-0.01005	-0.149
(Failure)	2	0.08849	0.08433	0.00417	0.047
	3	0.11029	0.10707	0.00322	0.029
	4	0.07351	0.07829	-0.00478	-0.065
	5	0.08824	0.08418	0.00406	0.046
	Sum	0.42797	0.43136	-0.00339	
	Avg.	0.08559	0.08627	-0.00068	-0.008

*Error = Difference/Measured

TABLE 3.6 AVERAGE VALUE OF ERROR OF THE 4th POINT COMPARISON AT FAILURE LOAD STAGE

Specimen	Average value of error at failure* %	Specimen	Average value of error at failure* %
RC-1	1.59	C-5	0.79
RC-2	2.75	C-6	3.61
RC-3	2.97	C-7	8.62**
RC-4	1.81	C-8	0.78
RC-5	5.11	C-9	3.20
RC-6	1.34	C-10	1.28
RC-7	4.47	C-11	2.14
RC-8	1.74	C-12	0.46
RC-9	2.05**	C-13	5.81

*Average error = Sum of the differences between measured and computed value of every level divided by sum of the measured values of the 4th point strains of every level.

**Average from four levels only because of bad potentiometer at one level.

Wu[47] also showed that it was evident that the strain distribution was almost linear even at high loads by plotting strain profiles of the cross sections under various loadings. The assumption of linear strain distribution was accepted also by Wu on the basis of his observations.

The calculation of loads that correspond to measured strains was based on the average value of strain along the five measuring stations. It may also be implied that the strain in the steel bars could be determined from the equation of plane of deformation. In this test program there was no measurement of strain in steel bars; all calculations of stress and strain in steel, therefore, were made after the calculation of Eq. 3.8.

3.4.2 Discretization of a Cross Section. After the plane of strain has been defined, the strain was used to compute the force, moment, and curvature of the deformed section. The section was discretized into small grid elements. The grid system made it convenient to analyze for both rectangular sections and partial circular sections. Strain at the centroid of each element was computed, and a stress-strain function of the material, either steel or concrete, was used in order to get the stress and the force at that element. Integrating the force and moment over the whole section yielded the internal force and moments at each particular load stage.

3.4.3 Stress-Strain Relationship of Materials. For reinforcing steel, the stress-strain curve has been shown in Chapter 2. An idealized stress-strain curve was used with no consideration of strain hardening in reinforcing bars. The same stress-strain relationship was used for both compression and tension.

Several stress-strain functions for concrete were tried in the analyses. The relationship proposed by Hognestad,[27] Todeschini et al.,[43] Chang,[8] and Kent and Park[28] were used and the results were compared to the test results. The functions proposed by Hognestad and Todeschini were quoted from Fowler's report[21] on the study of reinforced concrete columns governed by concrete compression. It was found that better agreement was achieved from all four stress-strain

functions when the full cylinder strength of concrete, f'_c, was used instead of a reduced maximum such as $0.85f'_c$. The stress-strain functions which were used in the calculations are shown graphically in Fig. 3.8. More details on these stress-strain functions are displayed in Appendix B. The summary of the load and moments at failure of each specimen analyzed from strain measurements with different type of stress-strain functions is shown in Table 3.7(a), (b), and (c).

Two more stress-strain functions were used in the analysis of strain, the "Modified Hognestad stress-strain function," and the "Parabolic-Rectangular stress-strain function." The details of these two stress-strain functions are discussed in the following sections:

Modified Hognestad Stress-Strain Function. Hognestad's stress-strain relationship consisted of two parts. The initial parabolic curve is defined by the equation:

$$f_c = f''_c \left[2 \frac{\epsilon_c}{\epsilon_o} - \left(\frac{\epsilon_c}{\epsilon_o}\right)^2\right] \qquad 3.12$$

where f''_c = Maximum compression stress of concrete in flexure
$= 0.85f'_c$

ϵ_c = Strain in concrete corresponding to stress, f_c

ϵ_o = Strain in concrete at maximum stress

$$\epsilon_o = \frac{2f''_c}{E_o} \qquad 3.13$$

E_o = Initial slope of the curve

Beyond the maximum value of stress where the slope of the parabola becomes horizontal and strain equals ϵ_o, the curve is represented by a straight line which falls to the value of $0.85f''_c$ at a strain of 0.0038. Some modifications to Eq. 3.12 were studied.

Breen[4] suggested that for horizontal cast columns if the maximum stress were taken as the cylinder stress ($f''_c = f'_c$), the function gives a reasonably good agreement for the theoretical values when compared to the experimental values. Sargin[40] recommended that the initial modulus of elasticity, E_o may be taken as

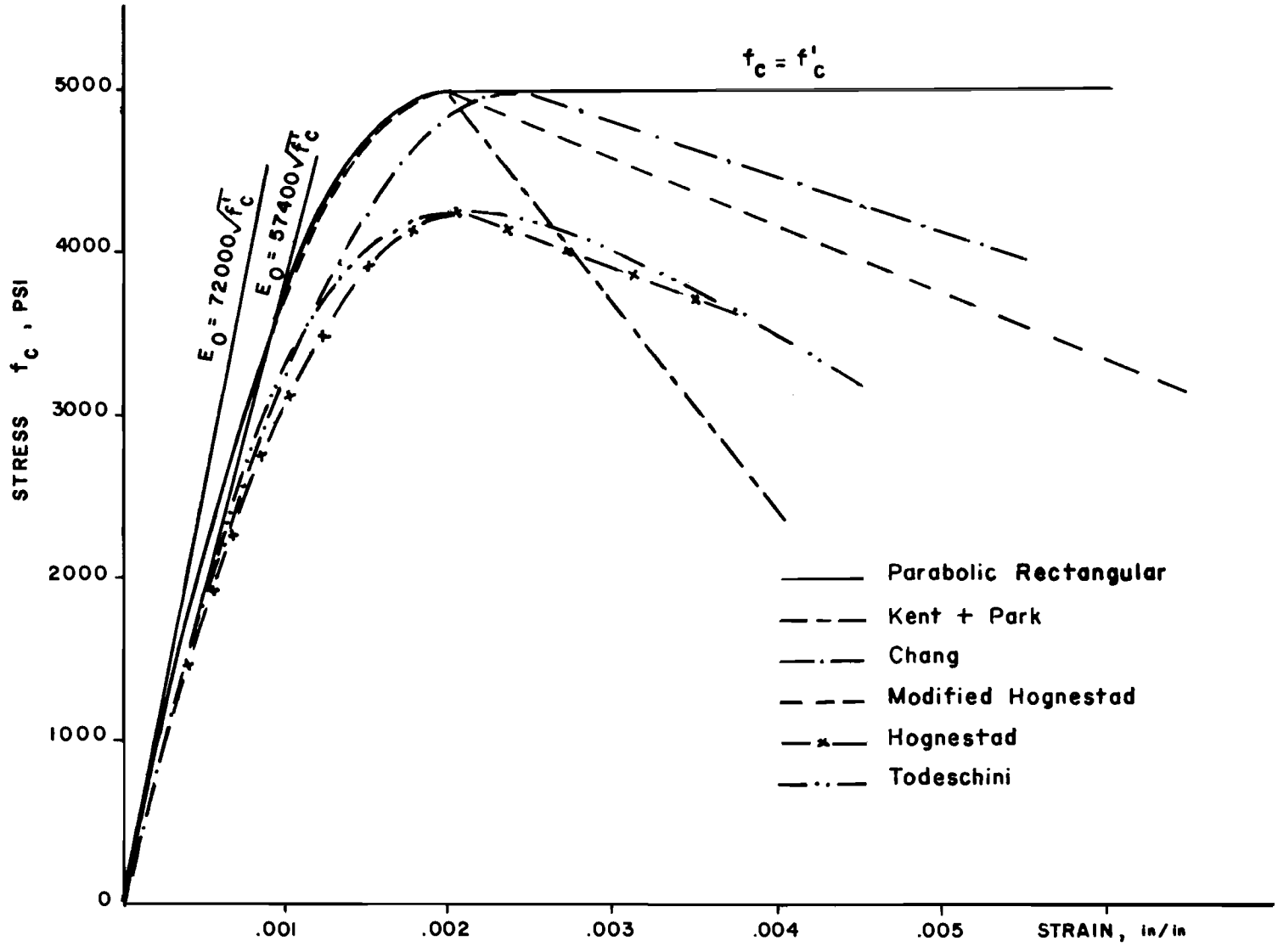

Fig. 3.8 Stress-strain relationship of concrete (for f'_c = 5000 psi)

TABLE 3.7 COMPARISON BETWEEN APPLIED LOAD AND LOAD COMPUTED FROM STRAIN AT FAILURE

Specimen	Applied Thrust* P_T test k	P_T computed from strain/P_T test					
		Modified Hognestad	Parabolic Rectangular	Todeschini	Hognestad	Kent & Park	Chang
			(a) Thrust				
RC-1	119.2	0.908	0.907	0.790	0.766	0.884	0.841
RC-2	120.3	0.872	0.876	0.758	0.734	0.838	0.811
RC-3	94.3	0.991	1.002	0.858	0.827	0.971	0.905
RC-4	128.8	0.755	0.769	0.655	0.632	0.725	0.700
RC-5	87.1	0.799	0.799	0.681	0.657	0.786	0.724
RC-6	53.9	0.732	0.709	0.606	0.579	0.698	0.650
RC-7	40.4	0.768	0.750	0.624	0.595	0.710	0.688
RC-8	40.4	0.756	0.741	0.617	0.587	0.716	0.674
RC-9	85.8	0.887	0.894	0.764	0.740	0.833	0.828
C-5	49.5	0.993	0.935	0.840	0.794	0.935	0.845
C-6	92.2	1.022	0.996	0.887	0.858	0.983	0.933
C-7	139.7	0.961	0.954	0.842	0.821	0.916	0.906
C-8	57.1	0.771	0.756	0.632	0.601	0.750	0.670
C-9	96.2	0.930	0.917	0.804	0.778	0.896	0.859
C-10	138.2	0.913	0.906	0.799	0.779	0.873	0.860
C-11	53.2	0.930	0.942	0.773	0.742	0.867	0.856
C-12	99.2	0.837	0.841	0.719	0.692	0.819	0.758
C-13	152.5	0.979	0.991	0.856	0.825	0.979	0.885
C-1	60.7	0.823	0.817	0.684	0.656	0.795	0.743
C-2	135.6	0.898	0.877	0.785	0.761	0.872	0.822
C-15	109.2	0.833	0.851	0.715	0.690	0.819	0.765
C-3	58.4	0.799	0.800	0.661	0.639	0.737	0.747
C-4	155.8	0.917	0.924	0.804	0.783	0.880	0.869
C-14	119.2	1.103	1.155	0.962	0.934	1.014	1.066
Mean		0.8824	0.8795	0.7548	0.7279	0.8457	0.8085
Standard Deviation		0.0973	0.1034	0.0958	0.0952	0.0935	0.0998
Coefficient of Variation		0.110	0.118	0.127	0.131	0.111	0.123

Specimen	Applied Strong Axis Moment* M_s test k-in.	M_s computed from strain/M_s test					
		Modified Hognestad	Parabolic Rectangular	Todeschini	Hognestad	Kent & Park	Chang
			(b) Strong Axis Moment				
RC-1	60.6	0.946	0.981	0.857	0.846	0.877	0.971
RC-2	124.0	0.890	0.924	0.801	0.794	0.821	0.904
RC-3	128.2	0.918	0.940	0.825	0.815	0.871	0.914
RC-4	228.9	0.869	0.894	0.778	0.765	0.814	0.854
RC-5	40.3	0.838	0.860	0.763	0.755	0.796	0.856
RC-6	52.2	0.710	0.724	0.643	0.638	0.691	0.716
RC-7	86.6	0.942	0.958	0.850	0.843	0.897	0.933
RC-8	190.4	0.827	0.825	0.749	0.735	0.794	0.792
RC-9	217.5	0.938	0.959	0.841	0.826	0.877	0.918
C-5	138.3	0.948	0.920	0.853	0.831	0.920	0.872
C-6	171.3	0.882	0.883	0.794	0.784	0.861	0.859
C-7	165.1	0.806	0.833	0.724	0.719	0.755	0.815
C-8	64.4	0.638	0.639	0.577	0.568	0.627	0.616
C-9	67.8	0.867	0.880	0.788	0.779	0.835	0.860
C-10	57.1	1.147	1.182	1.035	1.026	1.076	1.157
C-11	251.9	0.861	0.876	0.782	0.770	0.819	0.840
C-12	243.1	0.931	0.940	0.841	0.826	0.910	0.896
C-13	268.2	0.915	0.924	0.812	0.800	0.901	0.878
C-3	372.2	0.879	0.886	0.801	0.791	0.840	0.861
C-4	424.2	0.856	0.879	0.768	0.760	0.809	0.860
C-14	455.2	0.951	1.001	0.861	0.847	0.845	0.963
Mean		0.8838	0.9004	0.7973	0.7866	0.8398	0.8731
Standard Deviation		0.0991	0.1050	0.0888	0.0876	0.0893	0.1025
Coefficient of Variation		0.112	0.117	0.111	0.111	0.106	0.117

*From ram pressure

TABLE 3.7 (Continued)

Specimen	Applied Weak Axis Moment* M_w test k-in.	M_w computed from strain/M_w test					
		Modified Hognestad	Parabolic Rectangular	Todeschini	Hognestad	Kent & Park	Chang
		(c) Weak Axis Moment					
RC-1	184.0	0.834	0.842	0.740	0.728	0.809	0.809
RC-2	154.1	0.922	0.938	0.820	0.806	0.878	0.898
RC-3	150.4	0.972	0.986	0.865	0.846	0.946	0.927
RC-4	127.4	0.895	0.921	0.799	0.784	0.840	0.876
RC-5	160.8	0.968	0.970	0.865	0.848	0.953	0.917
RC-6	145.9	0.844	0.833	0.760	0.744	0.824	0.798
RC-7	121.3	0.880	0.875	0.796	0.781	0.845	0.841
RC-8	86.4	0.861	0.860	0.775	0.761	0.812	0.826
RC-9	102.0	0.922	0.949	0.824	0.814	0.856	0.910
C-5	113.5	0.945	0.913	0.849	0.822	0.913	0.860
C-6	147.1	0.930	0.923	0.832	0.817	0.906	0.890
C-7	161.6	0.858	0.879	0.767	0.735	0.771	0.860
C-8	168.0	0.860	0.854	0.778	0.762	0.849	0.809
C-9	179.1	0.911	0.912	0.820	0.807	0.887	0.882
C-10	188.0	0.826	0.815	0.740	0.733	0.792	0.823
C-11	128.8	0.900	0.915	0.817	0.803	0.857	0.875
C-12	155.6	0.867	0.874	0.779	0.763	0.848	0.826
C-13	147.7	0.843	0.852	0.746	0.733	0.830	0.806
C-1	165.5	0.929	0.929	0.842	0.827	0.910	0.890
C-2	154.1	0.977	0.972	0.867	0.855	0.962	0.940
C-15	194.2	0.989	1.004	0.891	0.875	0.965	0.953
	Mean	0.9016	0.9055	0.8082	0.7926	0.8692	0.8674
	Standard Deviation	0.0505	0.0532	0.0453	0.0448	0.0569	0.0471
	Coefficient of Variation	0.056	0.059	0.056	0.057	0.065	0.054

*From ram pressure

$$E_o = 72{,}000 \sqrt{f'_c} \qquad 3.14$$

The stress-strain relationship used in this investigation was a combination of those proposed above. The parabolic part can be expressed as

$$f_c = f'_c \left[\frac{2\epsilon_c}{\epsilon_o} - \left(\frac{\epsilon_c}{\epsilon_o}\right)^2 \right] \qquad 3.15$$

which is the same as the Hognestad curve except that f'_c is the cylinder strength instead of $0.85f'_c$. Values of ϵ_o and E_o are defined in Eqs. 3.13 and 3.14, respectively.

At strains beyond ϵ_o, the straight line with the same slope as the Hognestad curve was used. The stress falls from f'_c at ϵ_o to $0.85f'_c$ at a strain of 0.0038, but the function was allowed to go beyond the strain of 0.0038 with no limiting strain. The Modified Hognestad Stress-Strain Curve is shown in Fig. 3.8.

Parabolic Rectangular Stress-Strain Function. The Comité Européen du Béton (CEB)[10] recommends a concrete stress-strain function consisting of a parabola plus a zero slope straight line. The parabolic portion has the same equation as Hognestad's curve, but the maximum concrete stress, f_c equals $0.85f'_c$ at a strain of $\epsilon_o = 0.002$. Beyond the strain of 0.002, a constant stress can be used up to the failure strain of 0.0035. Analysis using this stress-strain relationship underestimated results compared to the test values. A modification of this type of curve was made so that the maximum stress at the strain of $\epsilon_o = 0.002$ is f'_c instead of $0.85f'_c$. Also, the constant stress of f'_c was used for strains beyond 0.002 with no limit to the failure strain. Thus, the first portion had a parabolic path with the same equation as the Modified Hognestad curve in Eq. 3.15, except that ϵ_o was always 0.002 (and $E_o = 2f'_c/0.002$), and there was no reduction of stress beyond the strain of ϵ_o. The graphical representation of the Parabolic Rectangular Stress-Strain Function is also shown in Fig. 3.8.

The strain analyses using the full cylinder strength of concrete, f'_c, gave a better result for both thrust and moments than the stress-strain function which used only $0.85f'_c$ as a maximum compressive stress. The Hognestad stress-strain curve and the Todeschini et al. function which used $0.85f'_c$ gave much lower values of thrust and moments than the applied load measured from ram pressure. The thrust, moment about the strong axis, and the moment about the weak axis at the failure load stage analyzed from strains using several types of stress-strain function are listed in Table 3.7. Also shown in this table is the thrust and moment measured from ram pressure, which was used as the applied load.

The comparison between applied thrusts and thrusts computed from measured strains are shown in Table 3.7(a). The applied thrusts were always higher than the computed thrusts regardless of the assumed stress variation for concrete, except for Specimens C-14 and C-6 when the Modified Hognestad stress-strain function was used. The Modified Hognestad and Parabolic Rectangular stress-strain functions gave the highest values among all stress functions used in the comparison. The mean values of $P_{computed}/P_{test}$ were about 0.88 for both functions with the standard deviation of about 0.10. The comparison of thrust showed that if the value of thrust from load cell readings was used for applied thrust, the deviation would be greater because load cells always gave higher readings than ram pressure readings, as discussed in Sec. 3.3.1.

A similar comparison for measured and computed moments is shown in Table 3.7(b) and (c). The observed moments again were always larger than the computed moments for both strong and weak axis bending, except for strong axis moments of Specimens C-10 and C-14 when the applied moments were smaller than the moments computed with some of the stress-strain functions. The Parabolic Rectangular stress function gave the best agreement with the applied moment, giving a mean value for $M_{computed}/M_{test}$ of 0.90 for strong axis bending and 0.91 for

weak axis bending. The coefficient of variation of the comparison for all stress functions was almost the same regardless of concrete stress function, varying in a range of 0.11 to 0.12 for strong axis moment and 0.05 to 0.07 for weak axis moment.

It should be noted that when the stress-strain functions used full strength of cylinder stress, f'_c, the differences in calculated forces were small, although different stress-strain functions were used with the strain analyses. Similarly, the reduction of stress beyond the strain ϵ_o had a minor effect on results, and the best result was from the function with no reduction of stress beyond the strain of ϵ_o.

It could be concluded in this study that the stress-strain functions using nominal cylinder strength of concrete, f'_c, should be used in analysis, at least for short-time loading. The first part of the function should be a parabola and the tail of the curve beyond maximum stress can be considered constant with strain limit or decrement of stress. Analysis for sustained load with some creep of concrete cannot be derived from data considered in these studies.

3.4.4 Superposition of Stress-Strain Relationship onto the Discretized Deformed Section. The average longitudinal strains of the cross sections at each load stage were stored on magnetic tape. The equation of the strain plane was computed. For each grid element of the discretized section, the strain at the centroid of each element was calculated. The average stress on each element was found from the stress-strain function.

Figure 3.9 shows the superposition of concrete stress-strain relationships onto the cross section. At element A in the section, the strain is ϵ_c. A stress of f_c was found and the force in the element was simply the product of the stress and the area of that element. Tension in concrete was neglected.

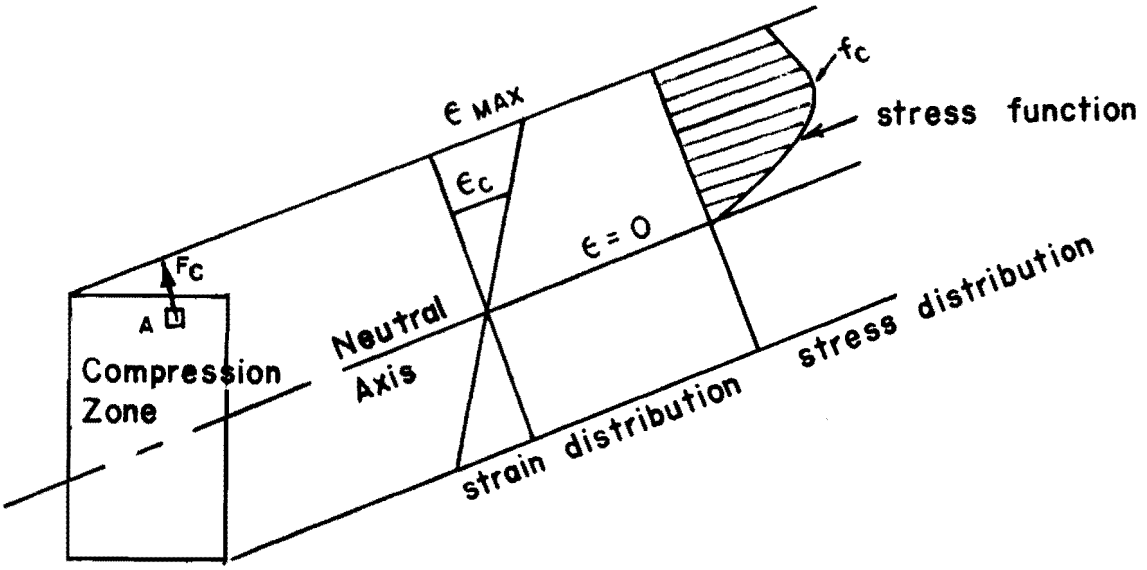

Fig. 3.9 Superposition of stress-strain relationship on the cross section

3.4.5 Force and Moments from Strain Measurement. The total force corresponding to measured strains was obtained by integrating all the element forces. Moments about each axis were determined by summing the product of each element force and its distance from each principal axis.

A computer program called GRID used the geometry of the section, the area and coordinates of the reinforcing bars, and the location of the strains which were to be read from the tape. Strains at each load stage were input. The procedure to find the plane of strain, to discretize the cross section, and to relate the stress-strain functions were coded into the program. Alternate subroutines for different stress-strain functions could be used in the program. The final results from each set of output were the axial force, moments about the strong and weak axis, curvature about each axis, moment angle, neutral axis angle, and the maximum compressive strain and its location.

3.5 Comparisons between Applied Forces and Theoretical Forces Computed from Strains

In Figs. 3.10 to 3.33, graphs of thrust, moment about the strong axis and moment about the weak axis are plotted against curvatures; strong axis moment is shown with strong axis curvature and weak axis moment with weak axis curvatures. Thrust values are plotted against total curvature about the skewed axis. Solid line graphs represent observed data and dotted line graphs represent data computed from the average of strain profile along five stations in the 30 in. midheight portion of each specimen. The Parabolic Rectangular Stress-strain Function was used for all computed forces on concrete.

Graphs for rectangular cross section columns are in Figs. 3.10 to 3.18. Thrusts computed from strains were always lower than the applied thrust. Although at the beginning of loading Specimen RC-3 showed higher thrust analyzed from strains than thrust from the ram, but as the moments increased the thrust analyzed from strain dropped to a lower value than the ram pressure thrust. The maximum difference between the analyzed thrust and the applied thrust was about 30 kips

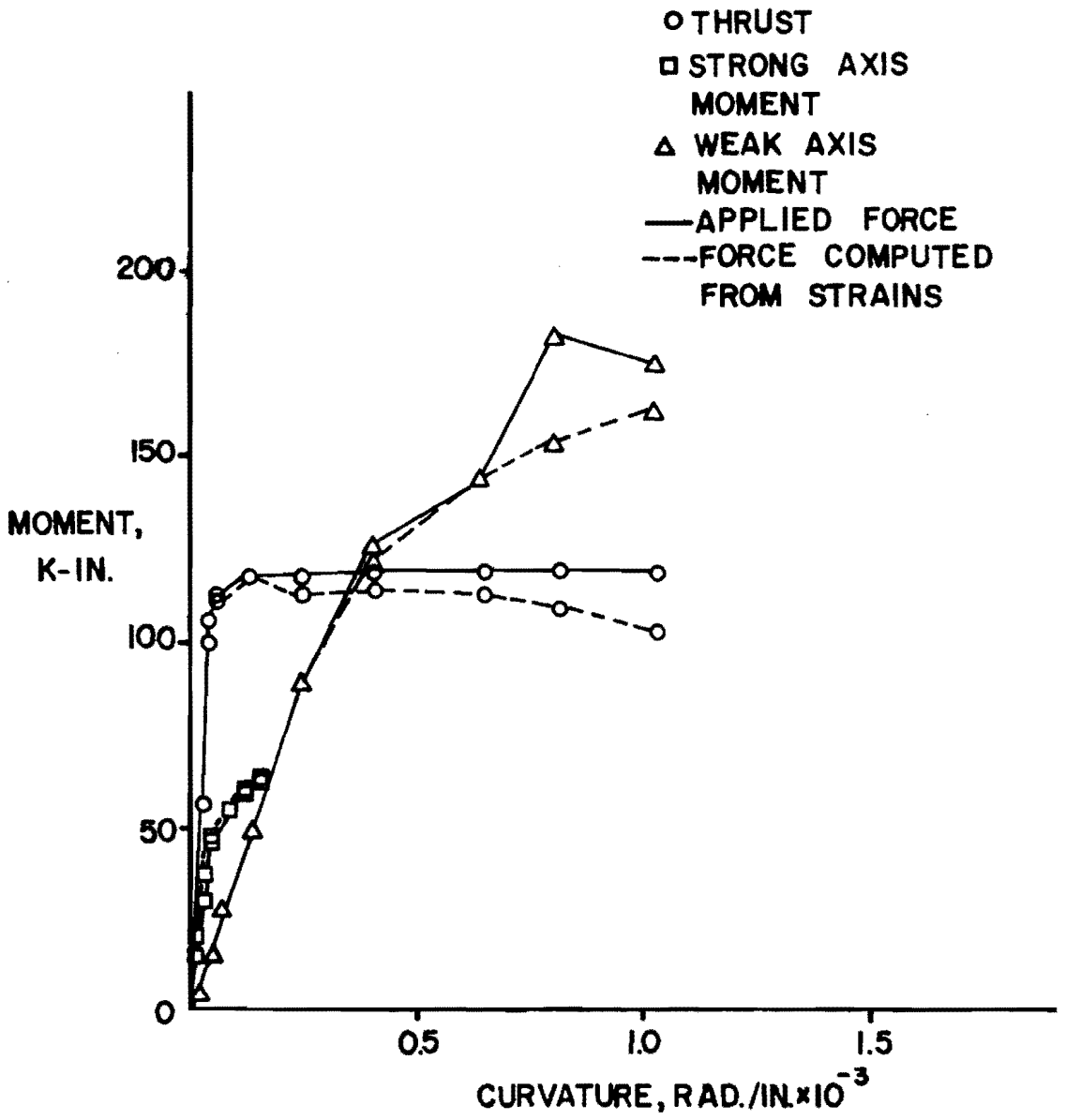

Fig. 3.10 Applied forces and forces computed from strains
Specimen RC-1 (P_u/P_o = 0.472, load angle 22.5°)

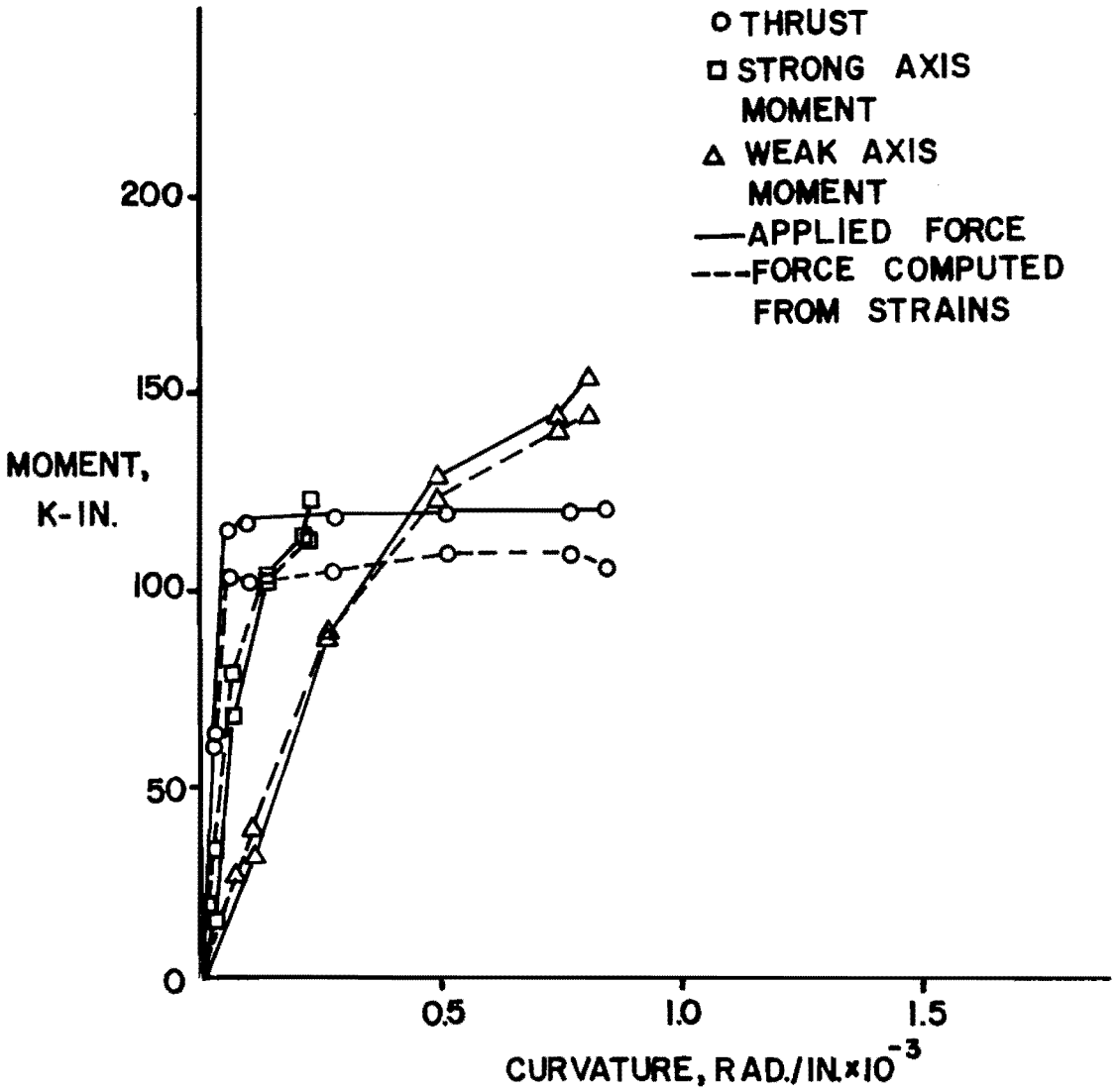

Fig. 3.11 Applied forces and forces computed from strains
Specimen RC-2 (P_u/P_o = 0.478, load angle 45°)

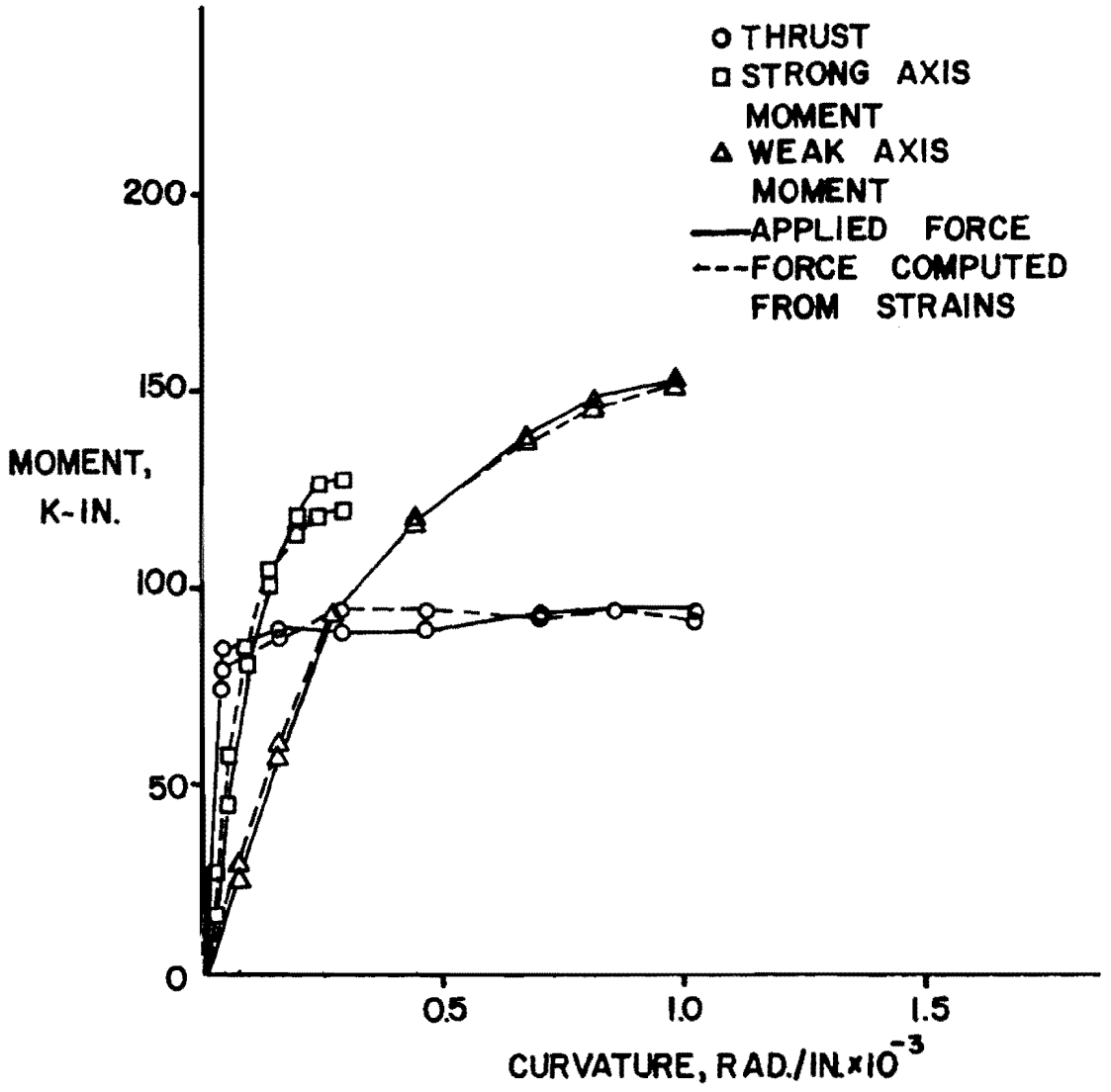

Fig. 3.12 Applied forces and forces computed from strains
Specimen RC-3 (P_u/P_o = 0.353, load angle 45°)

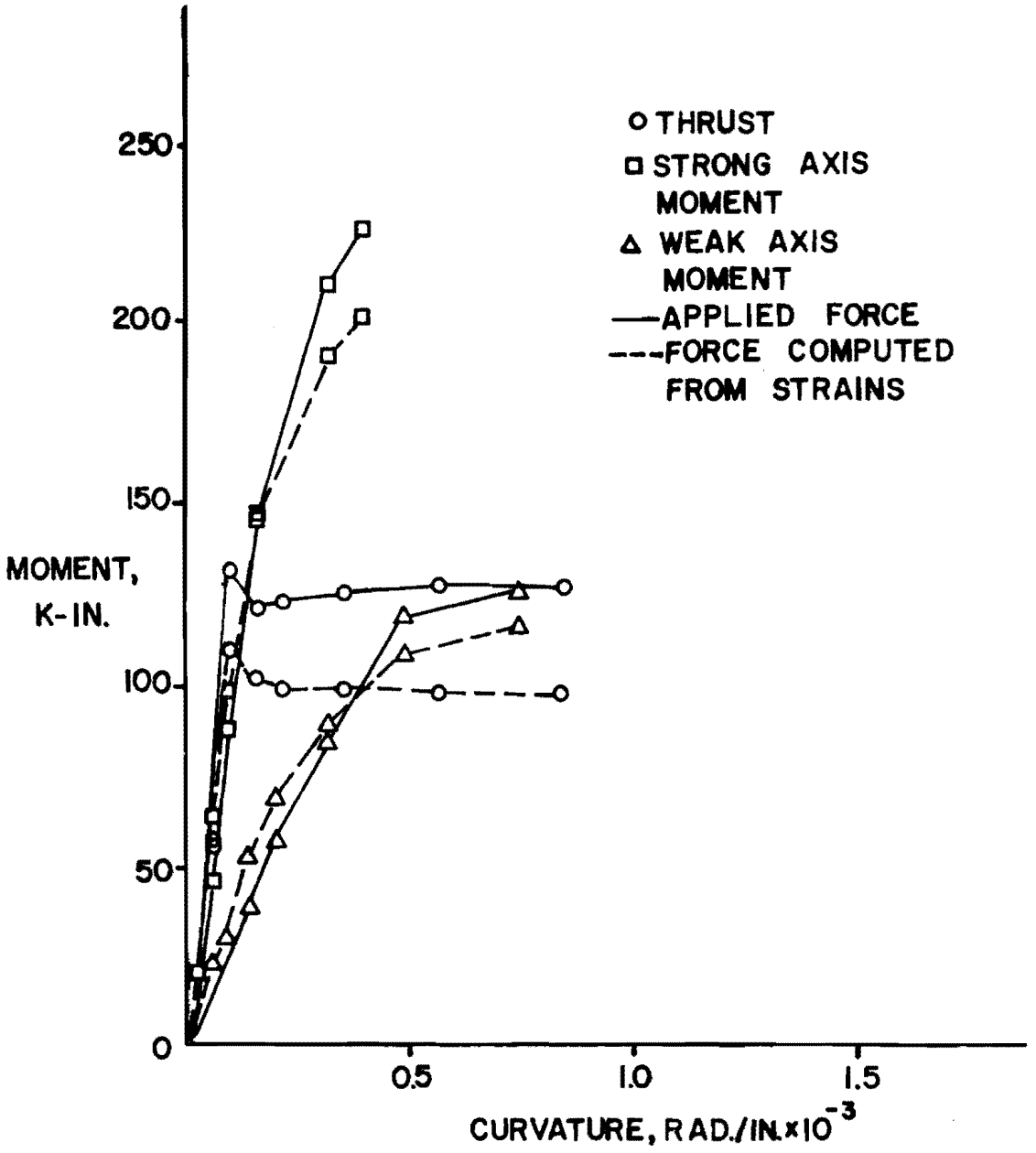

Fig. 3.13 Applied forces and forces computed from strains Specimen RC-4 (P_u/P_o = 0.485, load angle 67.5°)

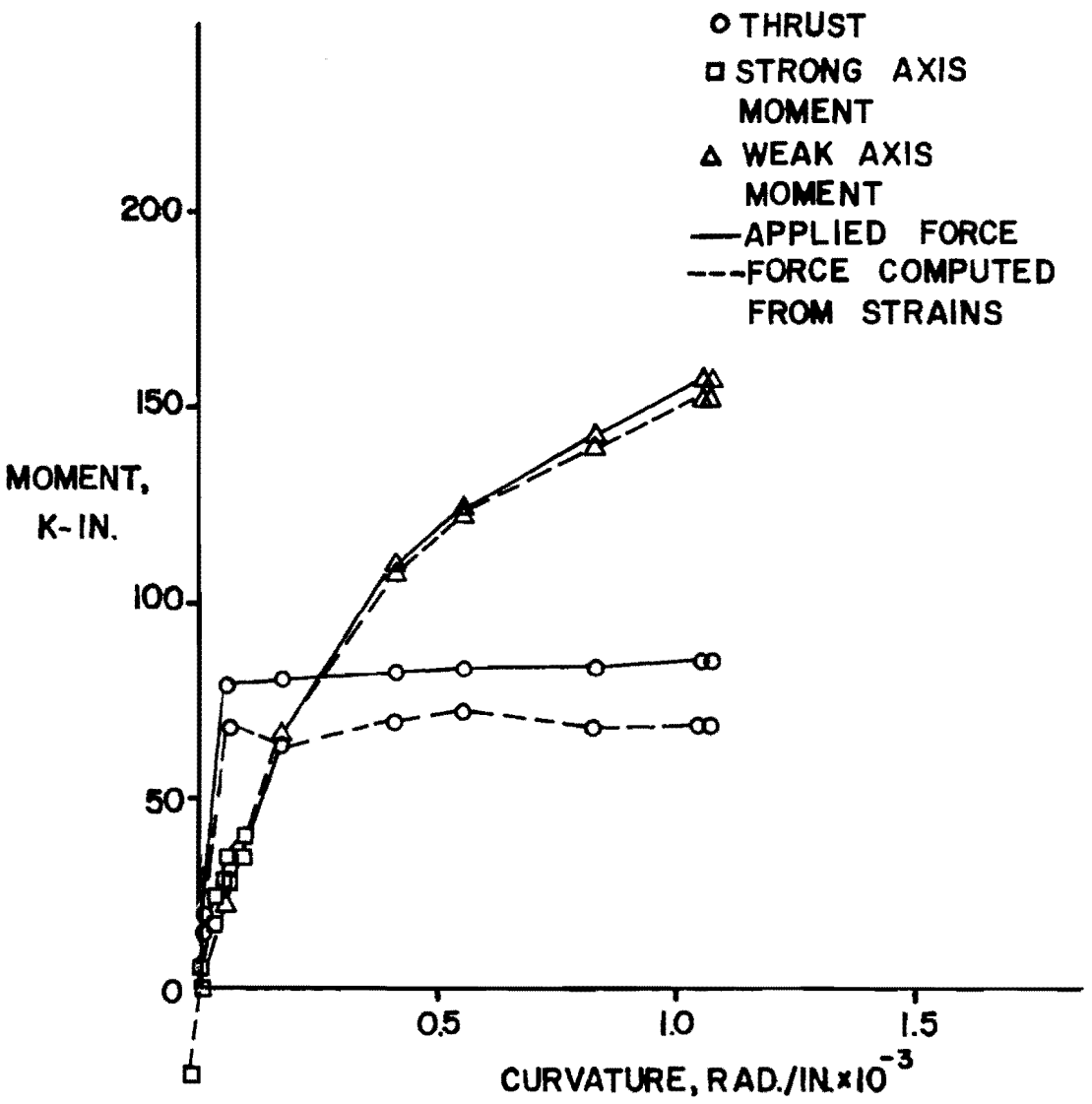

Fig. 3.14 Applied forces and forces computed from strains
Specimen RC-5 (P_u/P_o = 0.337, load angle 22.5°)

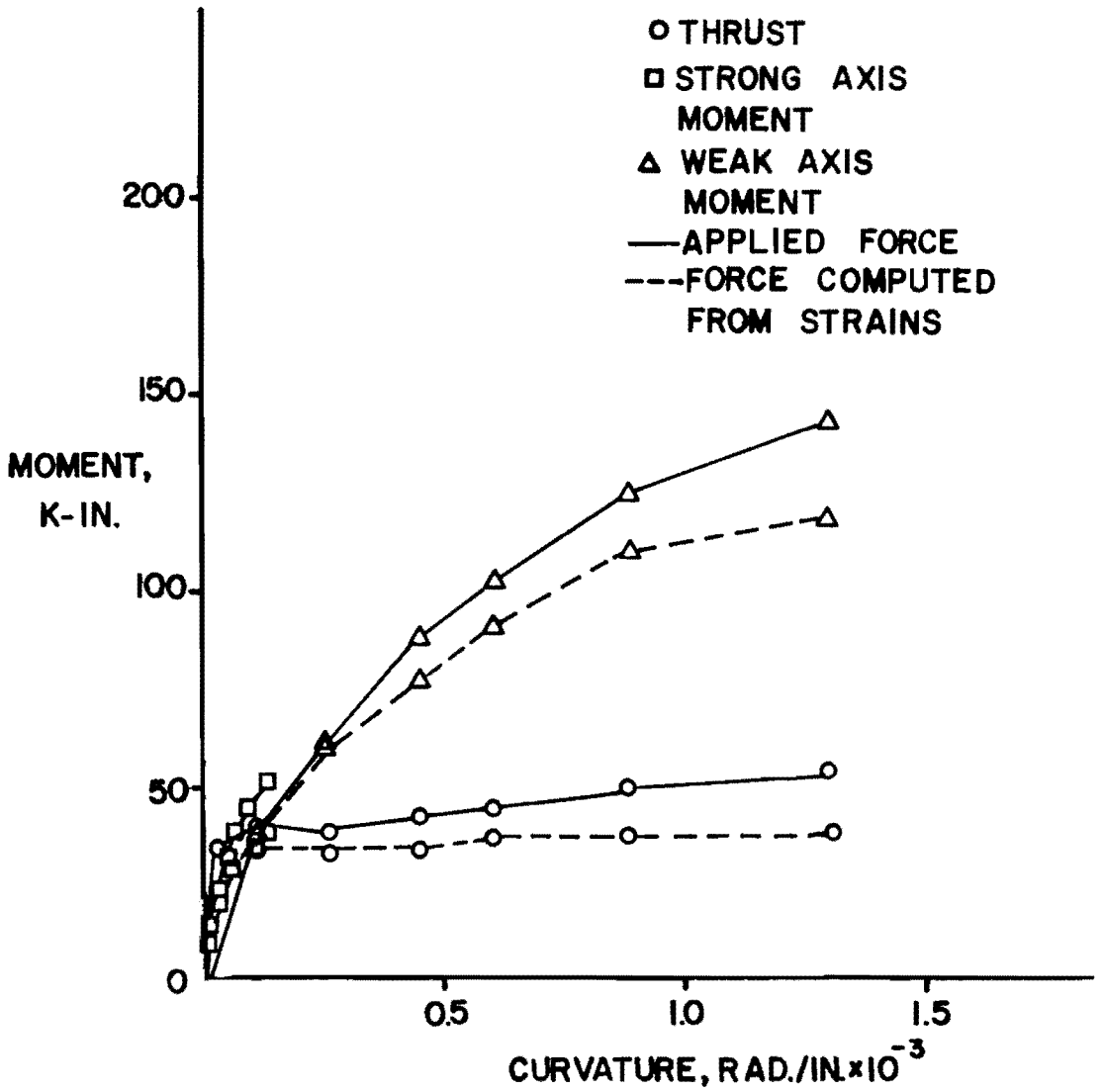

Fig. 3.15 Applied forces and forces computed from strains Specimen RC-6 (P_u/P_o = 0.233, load angle 22.5°)

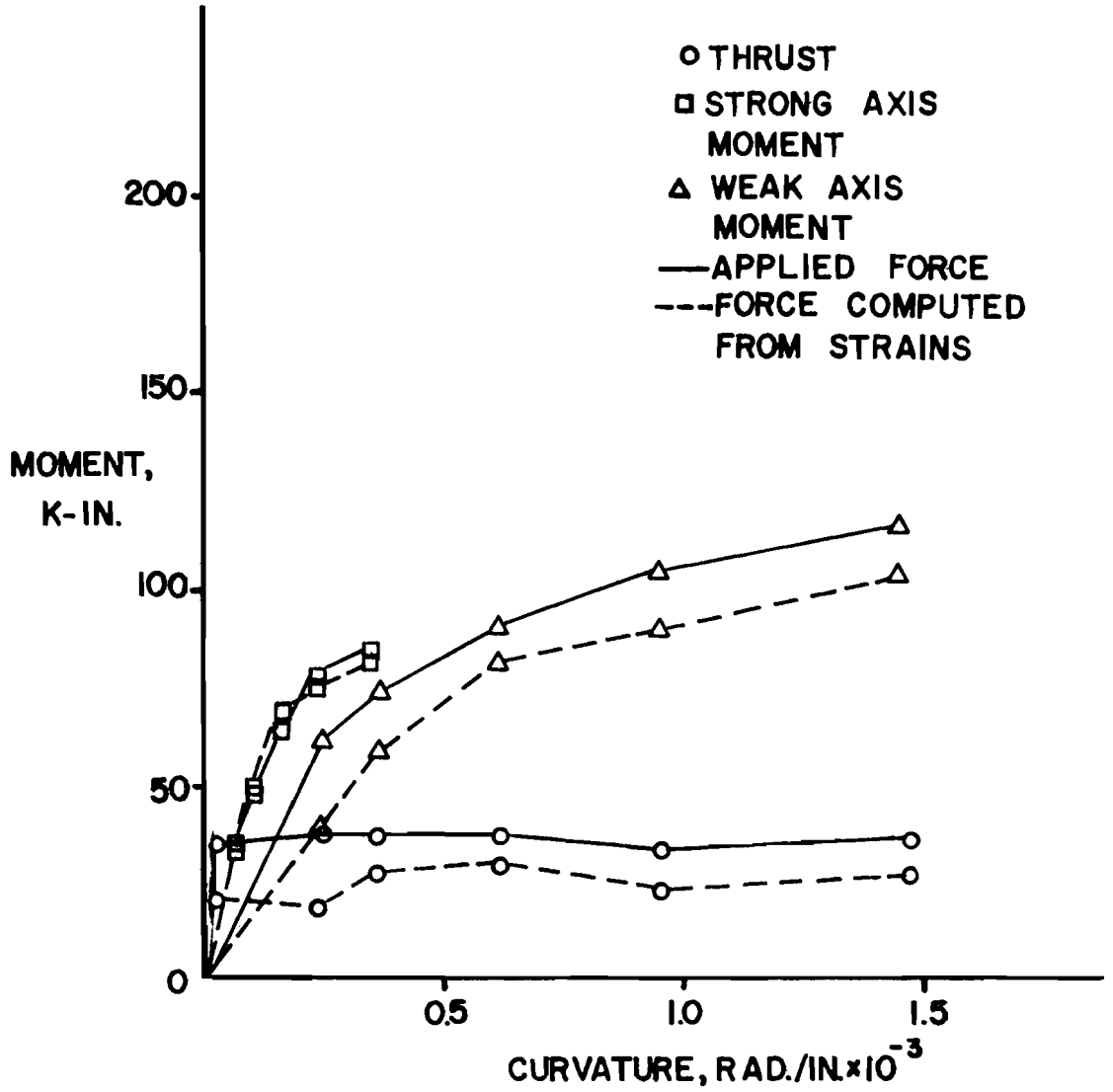

Fig. 3.16 Applied forces and forces computed from strains
Specimen RC-7 (P_u/P_o = 0.177, load angle 45°)

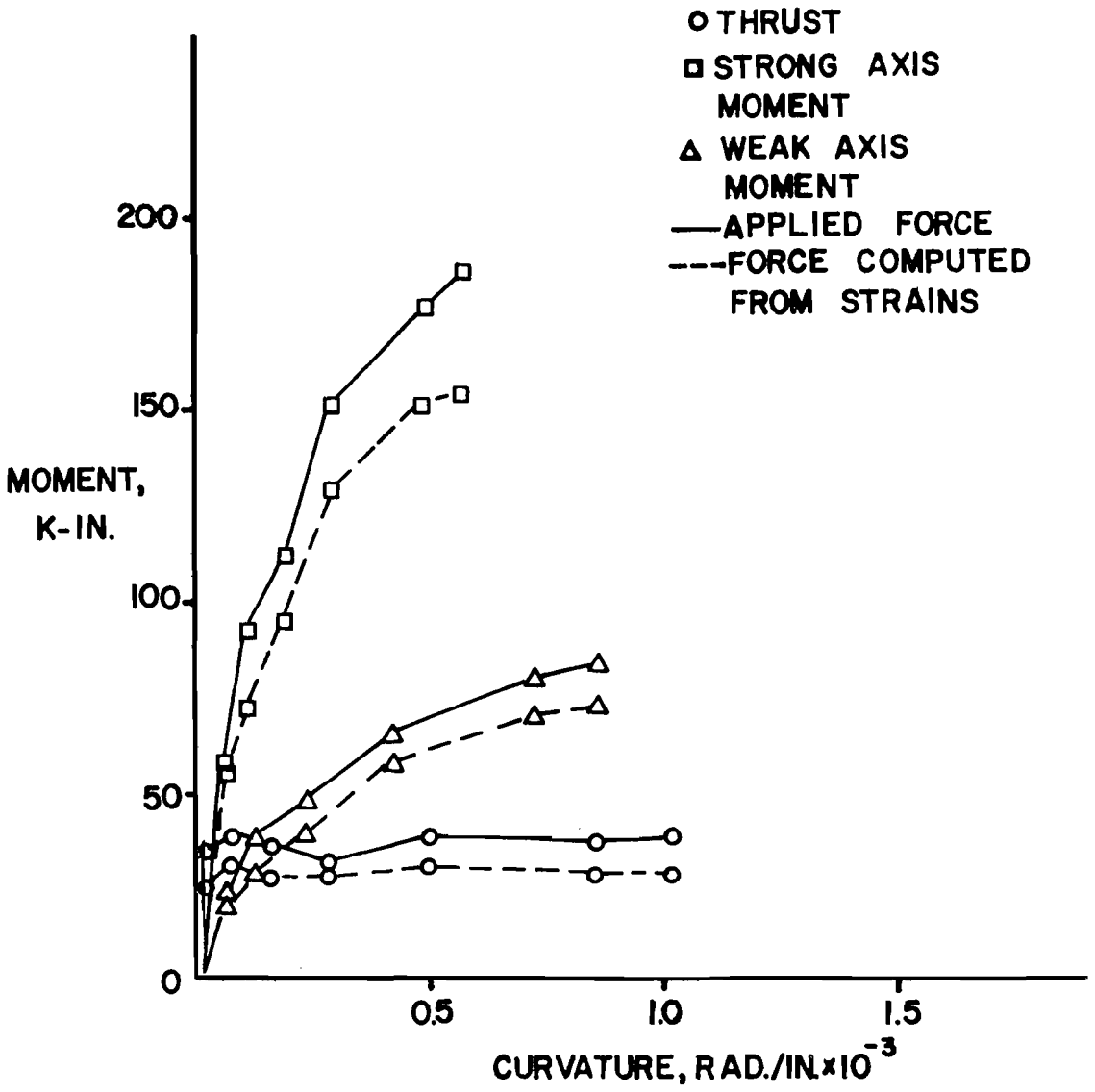

Fig. 3.17 Applied forces and forces computed from strains Specimen RC-8 (P_u/P_o = 0.174, load angle 67.5°)

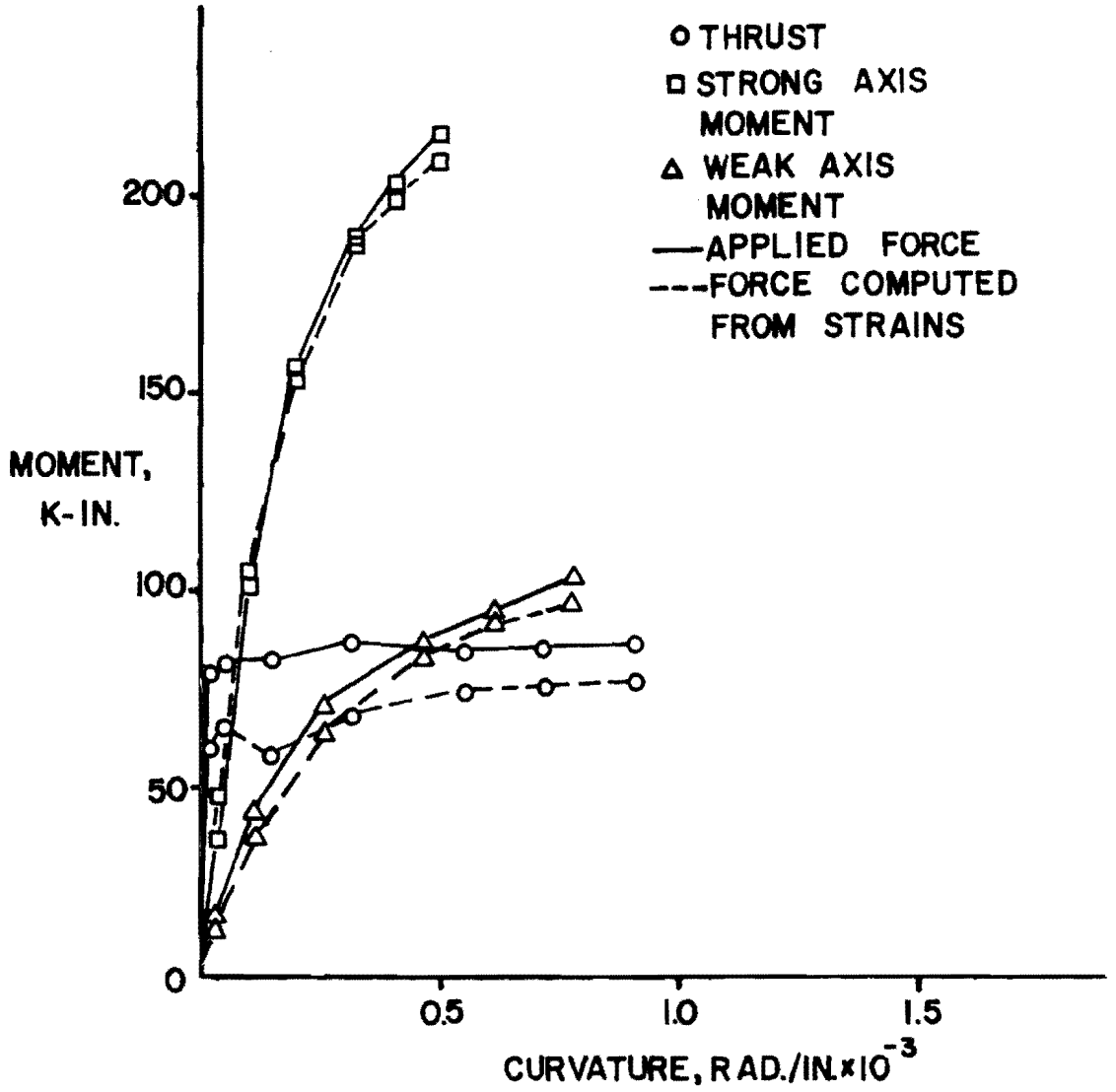

Fig. 3.18 Applied forces and forces computed from strains Specimen RC-9 (P_u/P_o = 0.351, load angle 67.5°)

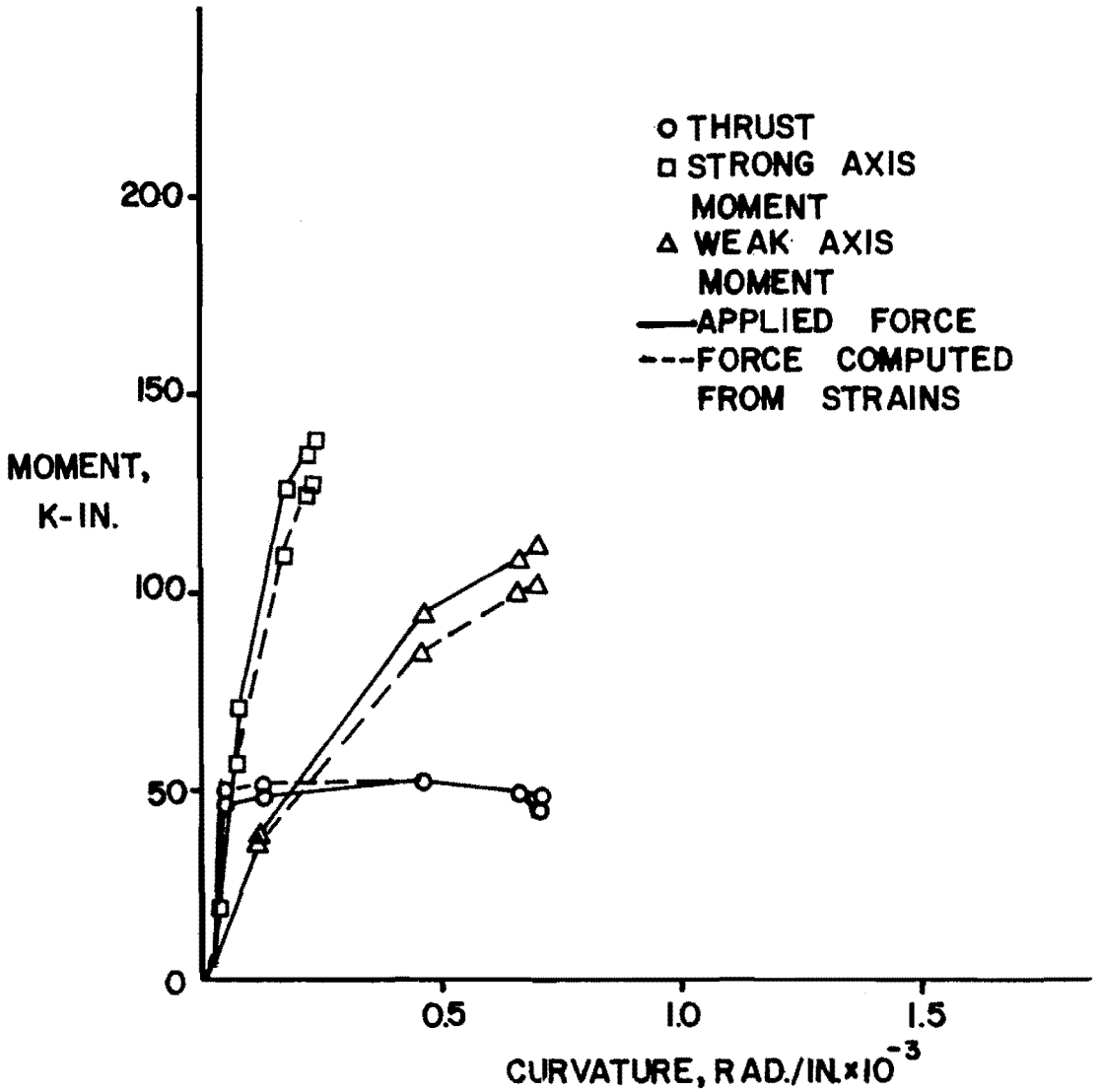

Fig. 3.19 Applied forces and forces computed from strains
Specimen C-5 (P_u/P_o = 0.190, load angle 45°)

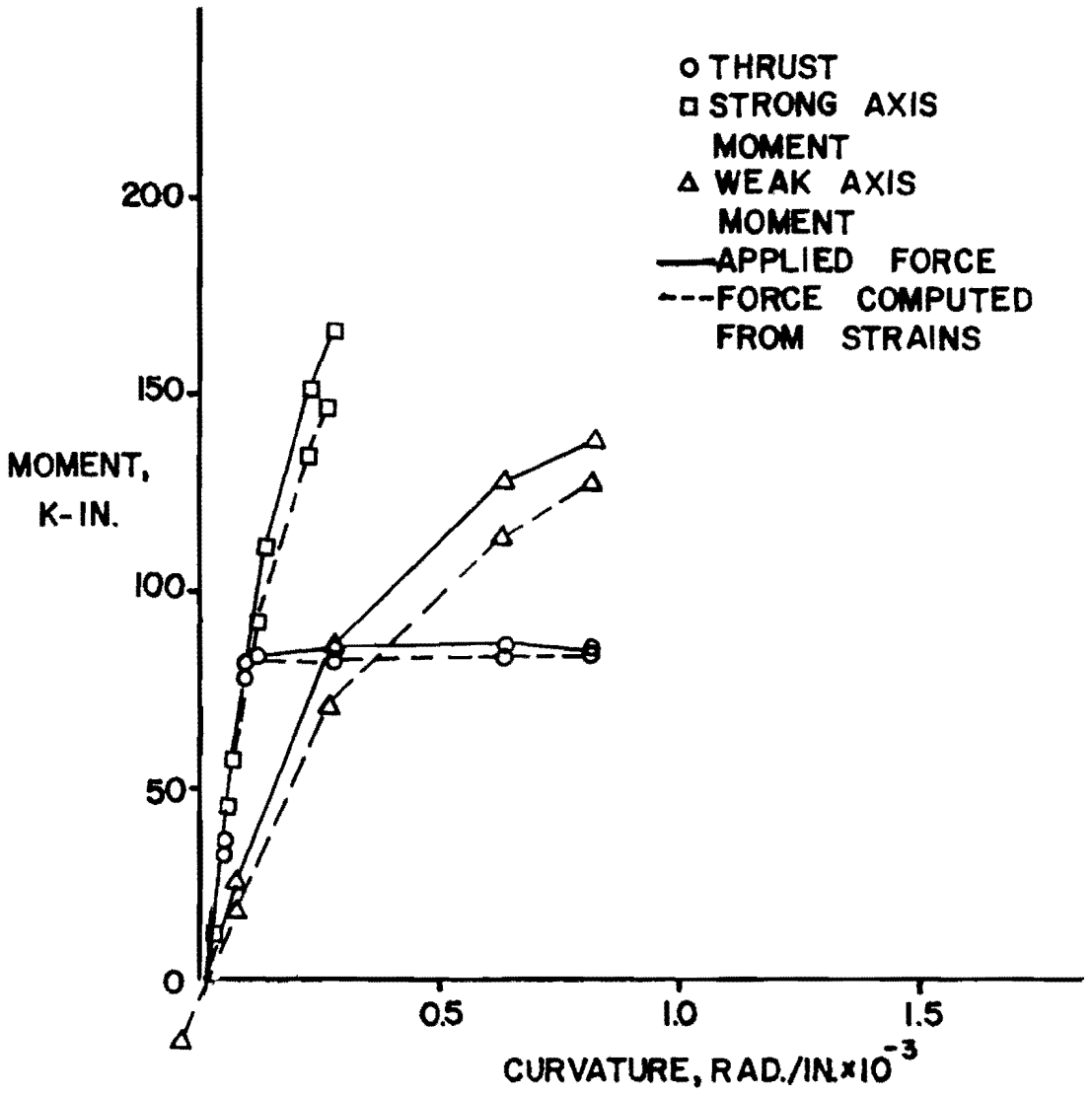

Fig. 3.20 Applied forces and forces computed from strains
Specimen C-6 (P_u/P_o = 0.349, load angle 45°)

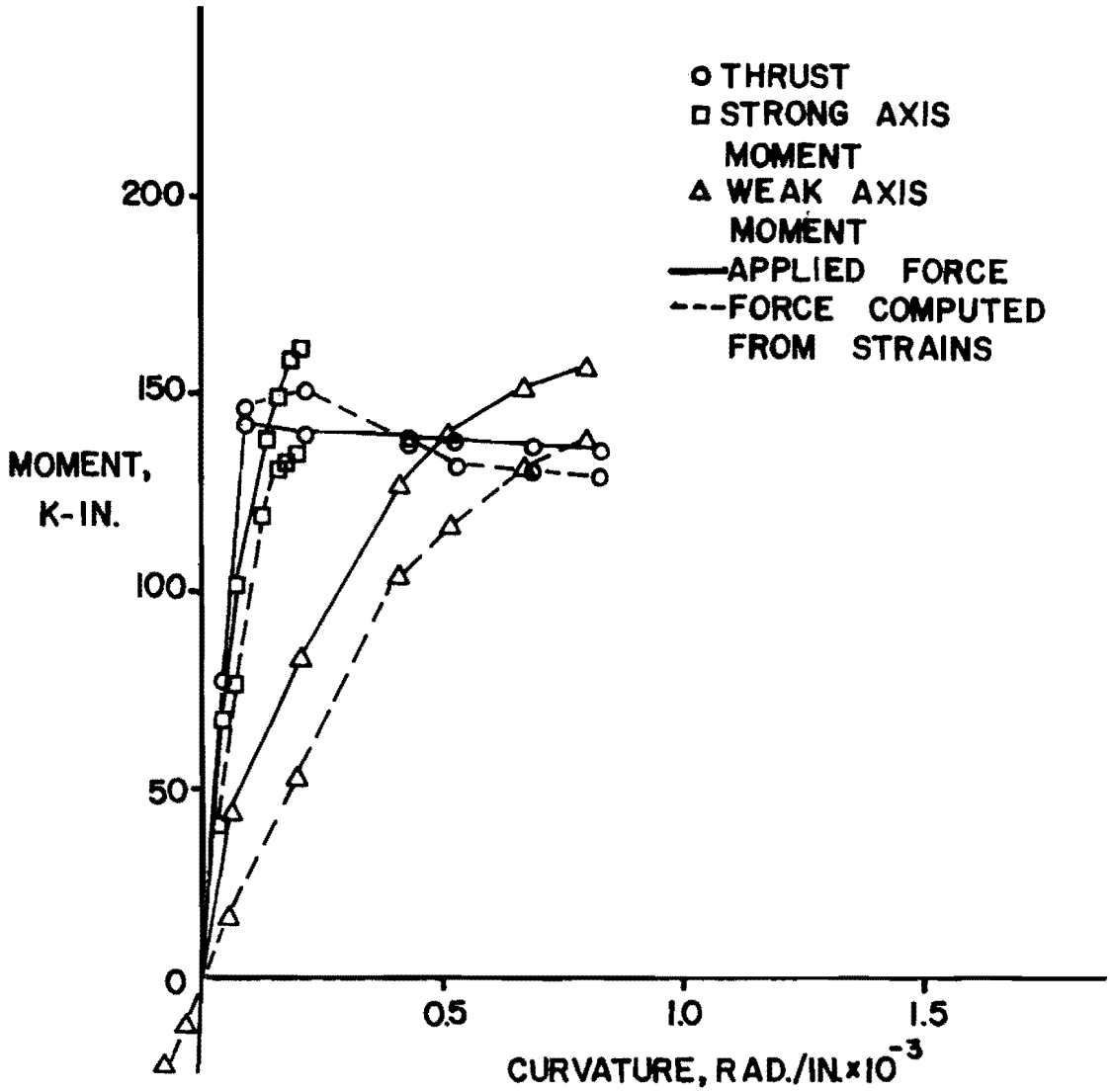

Fig. 3.21 Applied forces and forces computed from strains
Specimen C-7 (P_u/P_o = 0.529, load angle 45°)

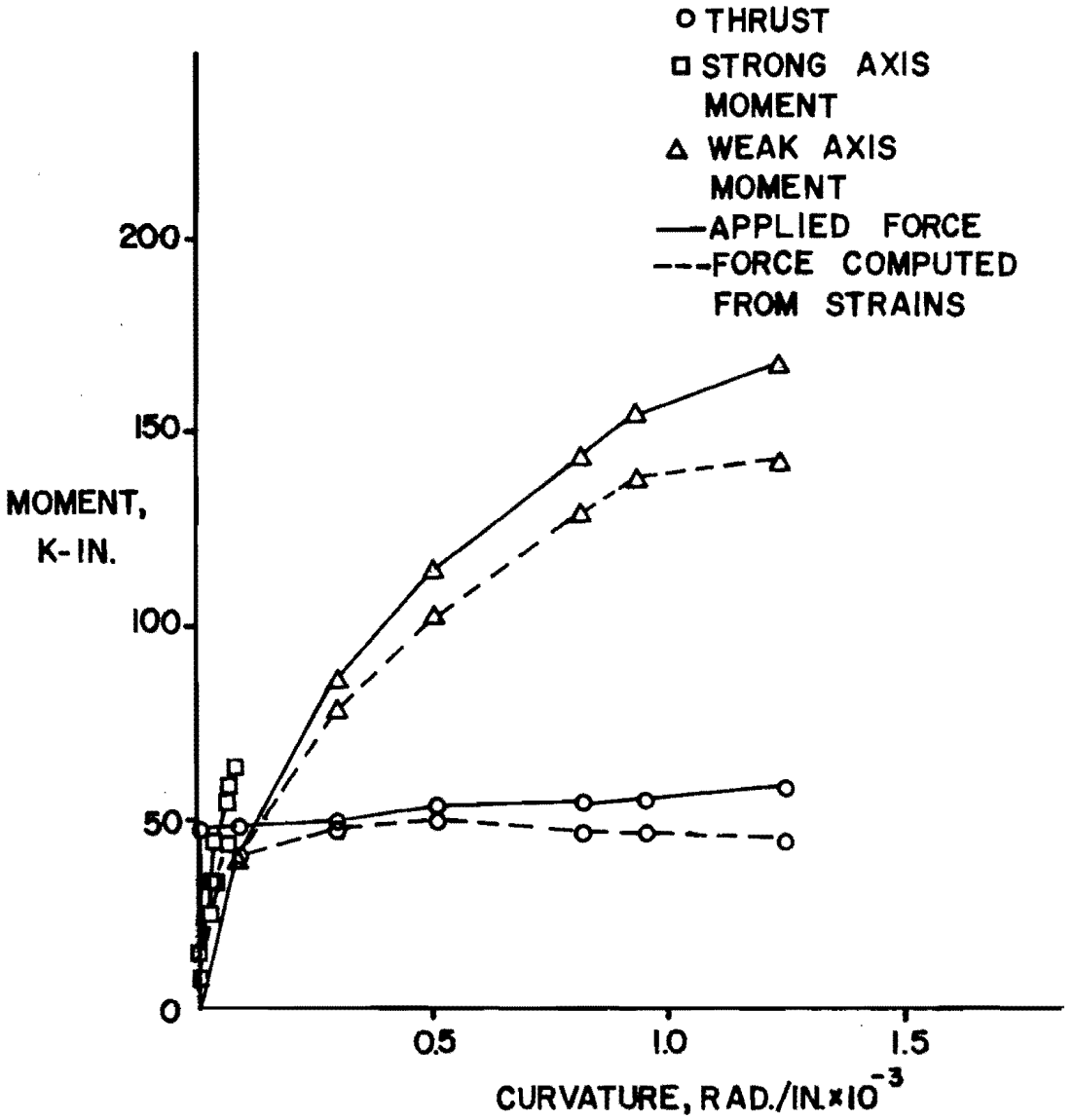

Fig. 3.22 Applied forces and forces computed from strains
Specimen C-8 (P_u/P_o = 0.203, load angle 22.5°)

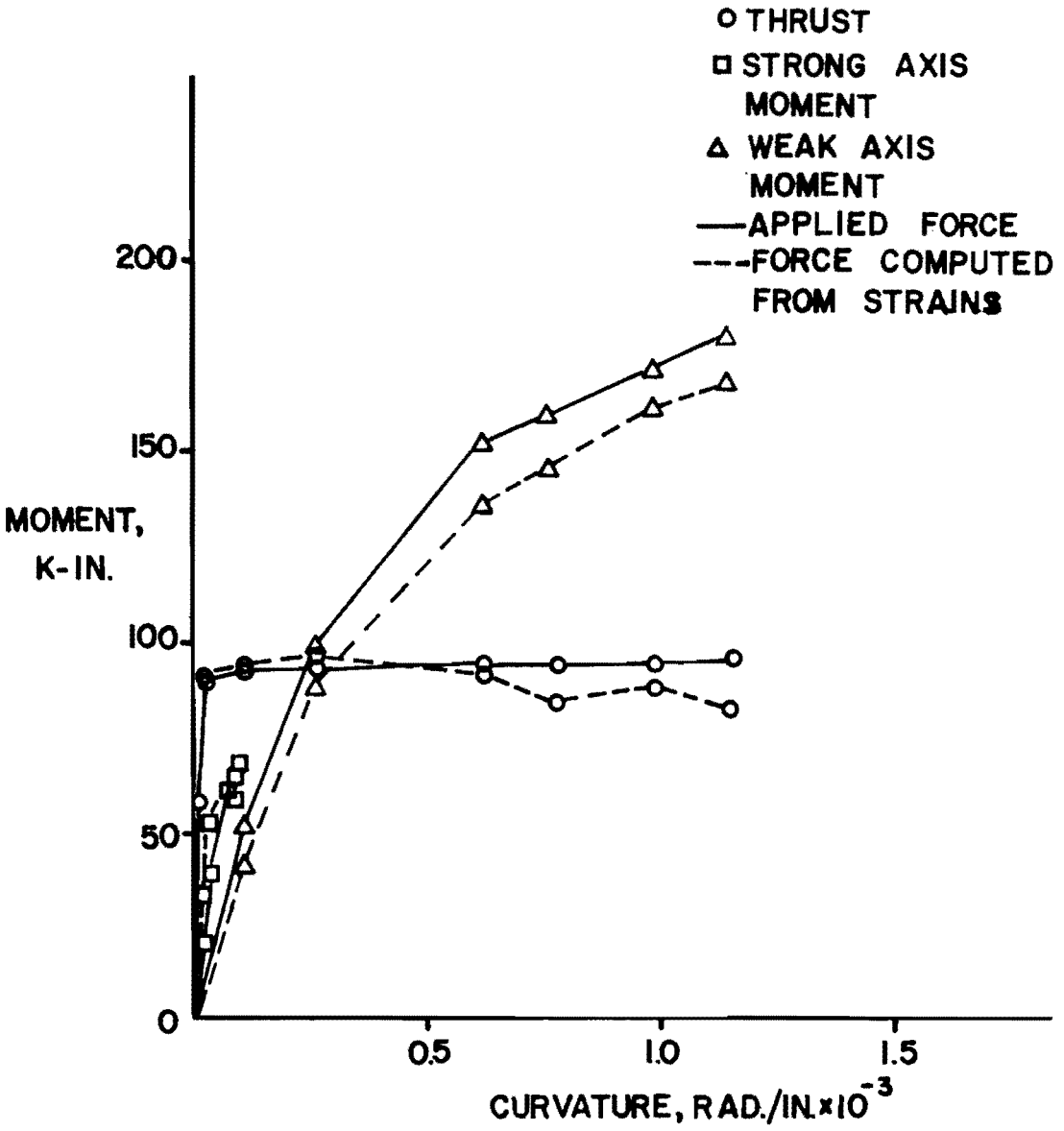

Fig. 3.23 Applied forces and forces computed from strains
Specimen C-9 (P_u/P_o = 0.355, load angle 22.5°)

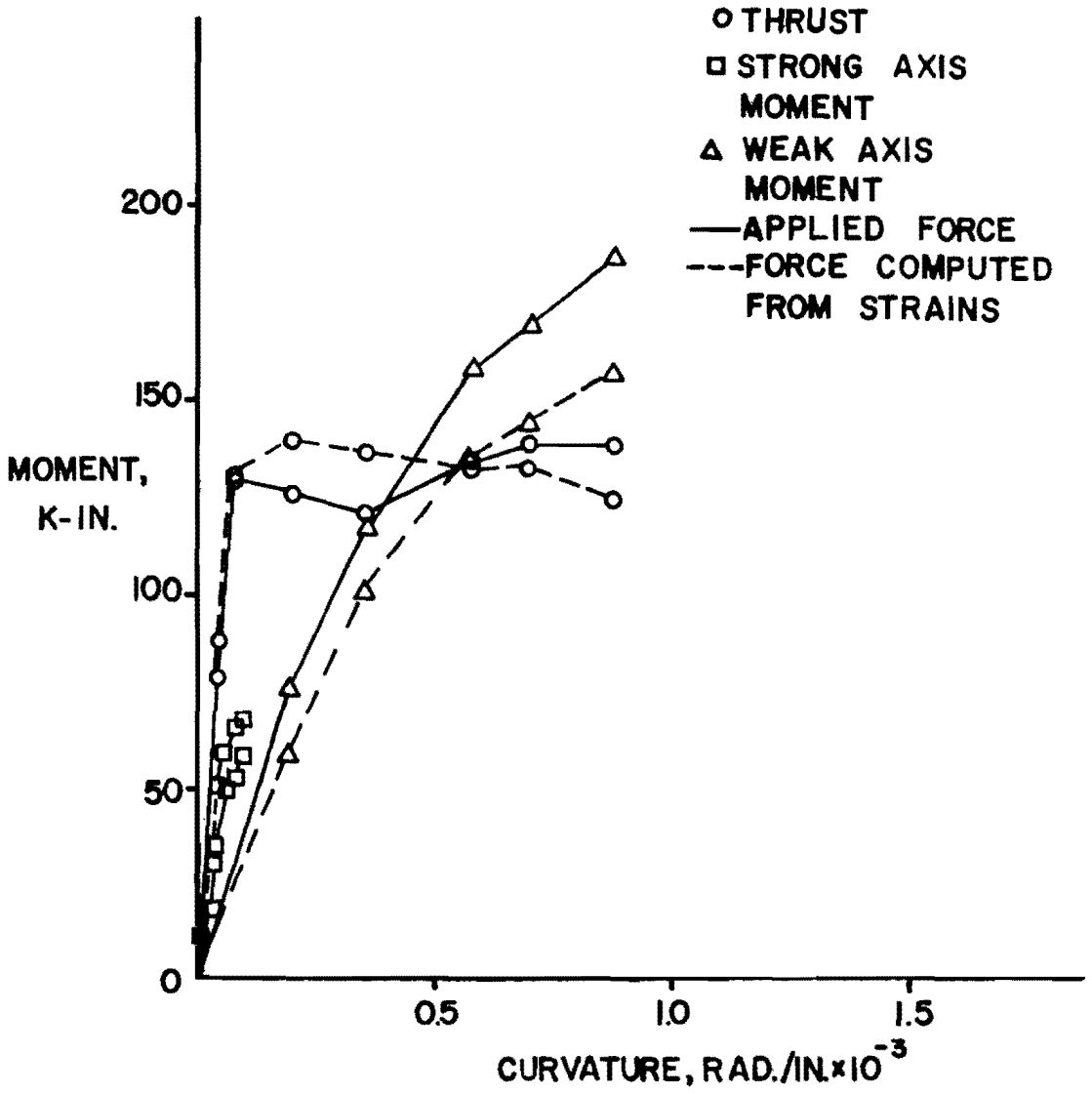

Fig. 3.24 Applied forces and forces computed from strains
Specimen C-10 (P_u/P_o = 0.521, load angle 22.5°)

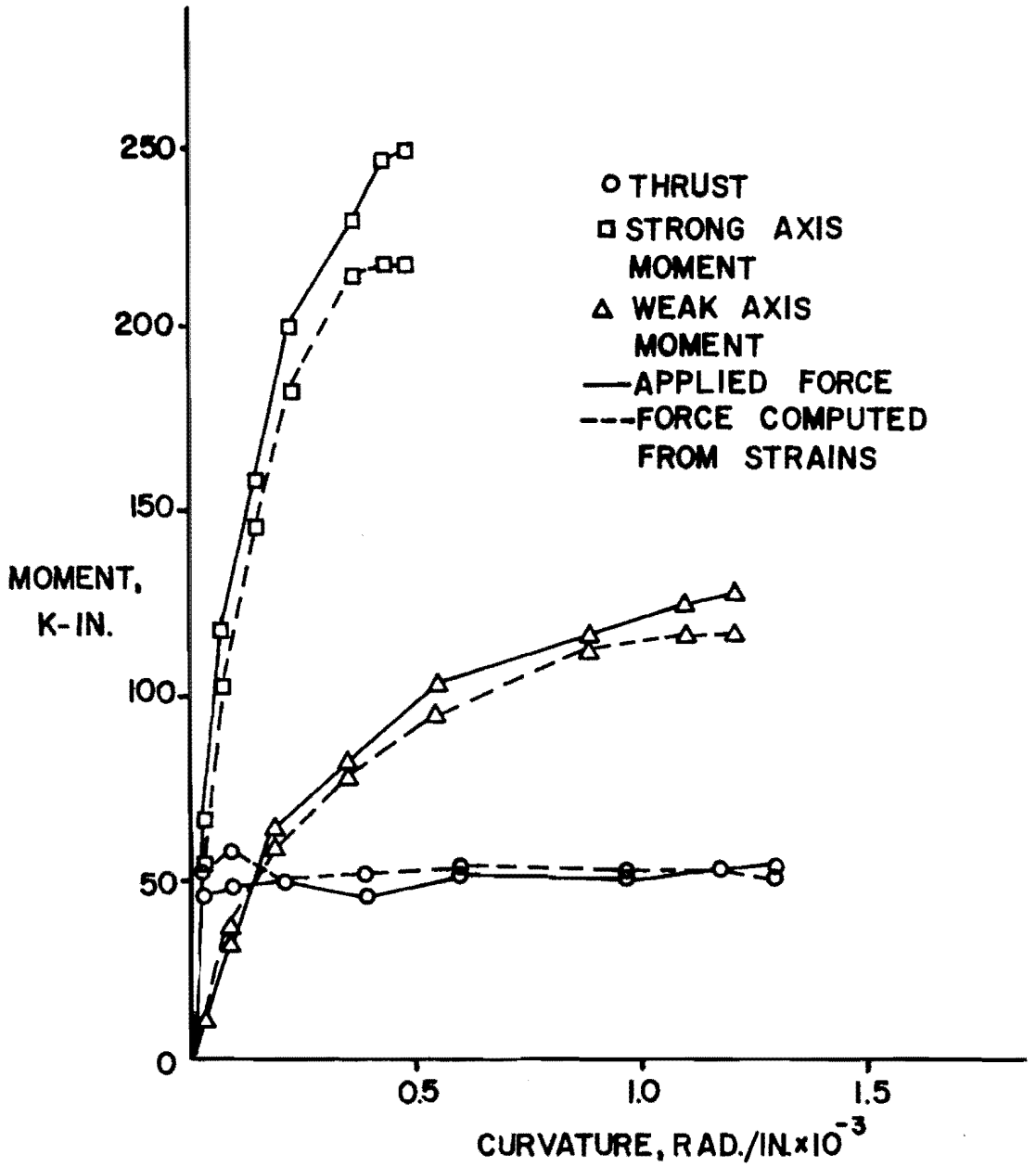

Fig. 3.25 Applied forces and forces computed from strains Specimen C-11 (P_u/P_o = 0.186, load angle 67.5°)

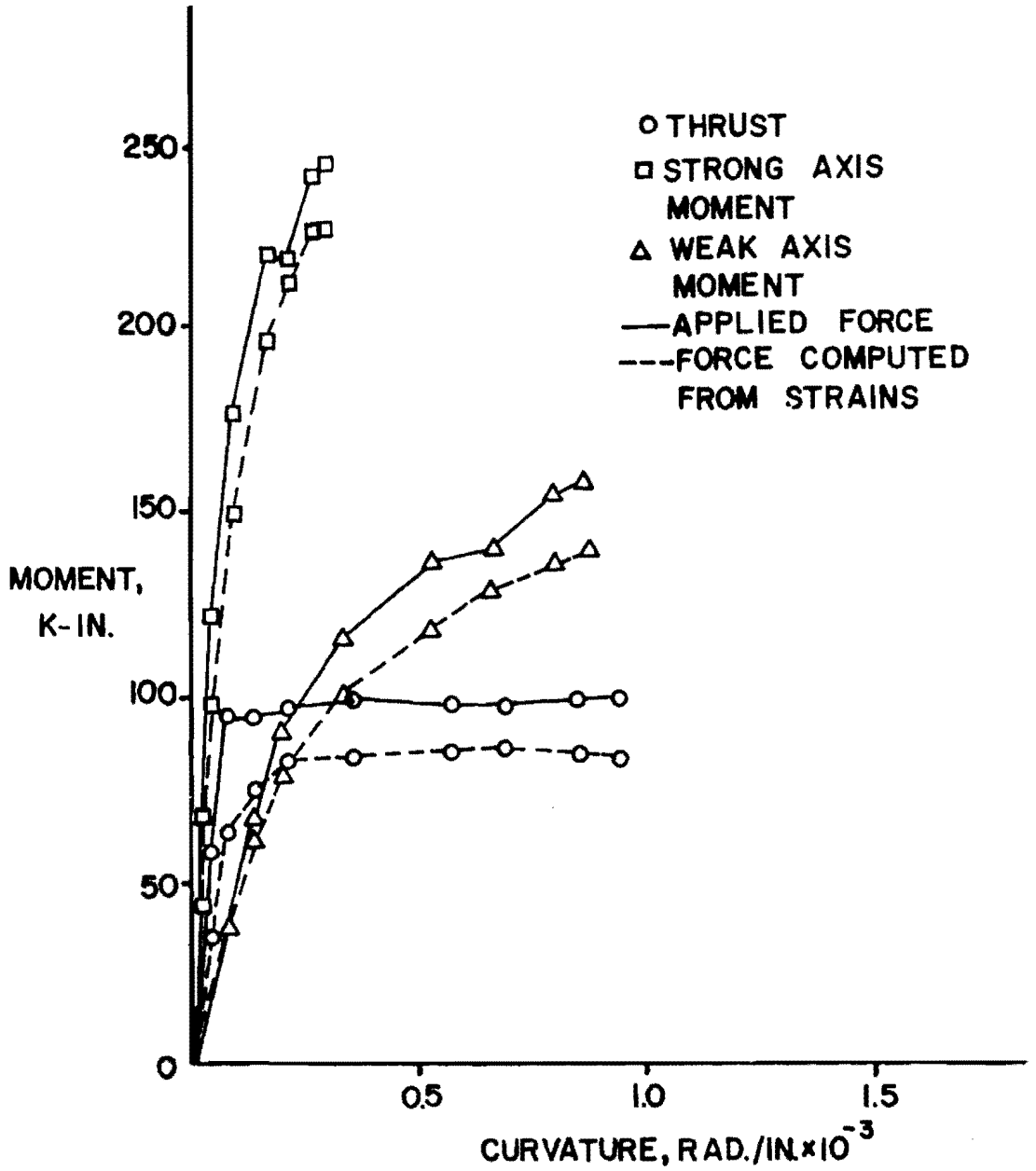

Fig. 3.26 Applied forces and forces computed from strains Specimen C-12 (P_u/P_o = 0.355, load angle 67.5°)

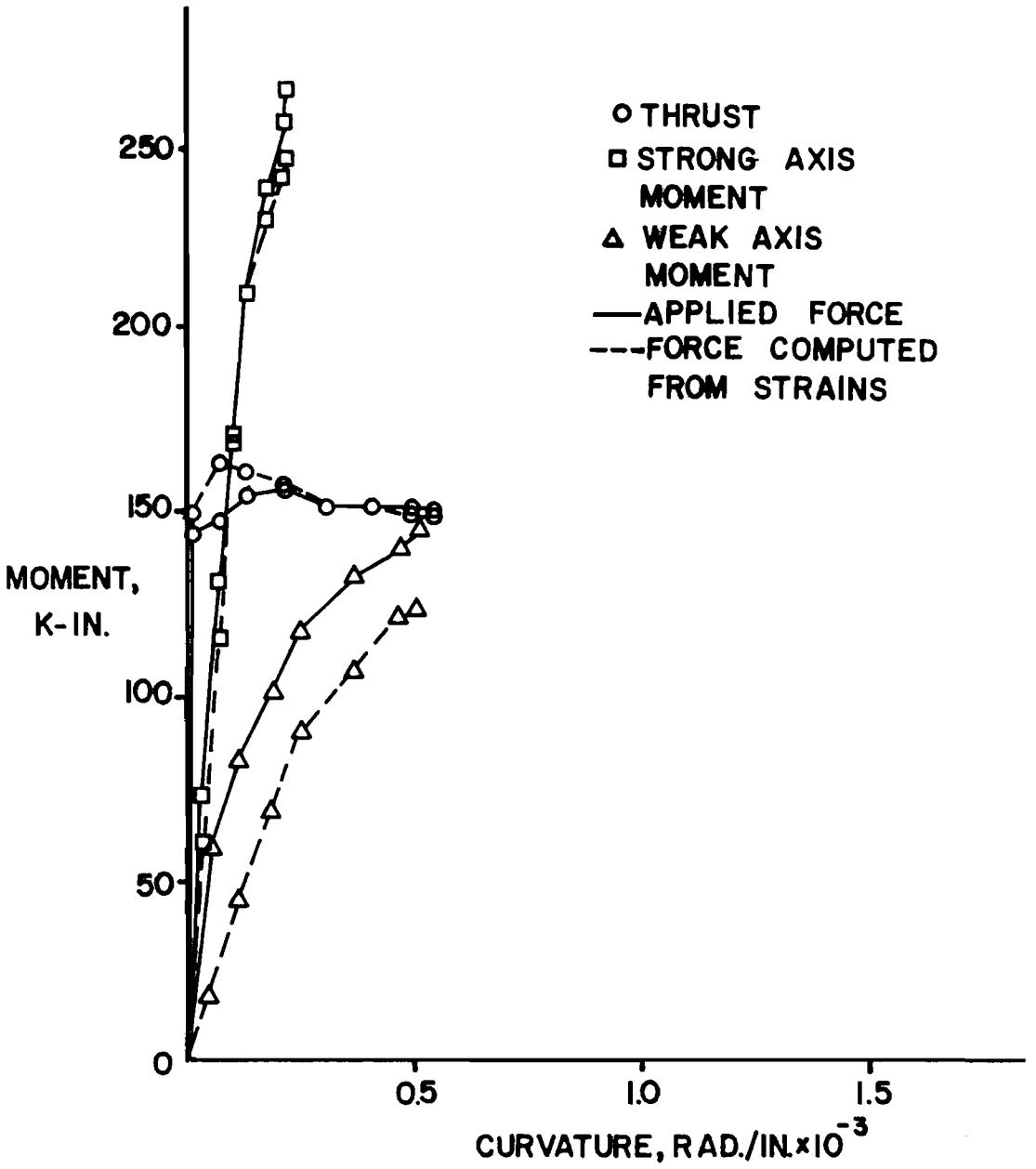

Fig. 3.27 Applied forces and forces computed from strains
Specimen C-13 (P_u/P_o = 0.486, load angle 67.5°)

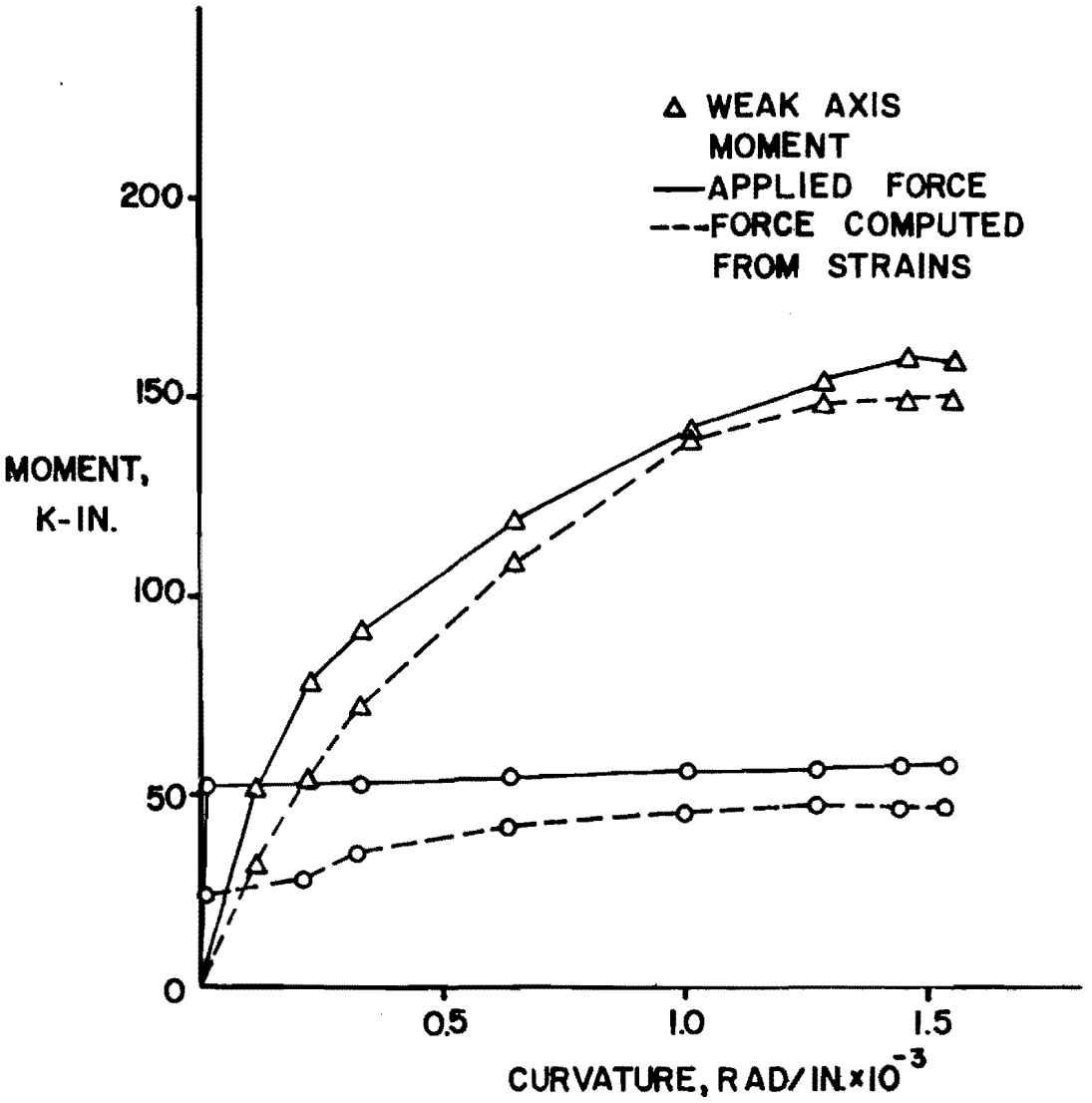

Fig. 3.28 Applied forces and forces computed from strains Specimen C-1 (P_u/P_o = 0.215, weak axis uniaxial bending test)

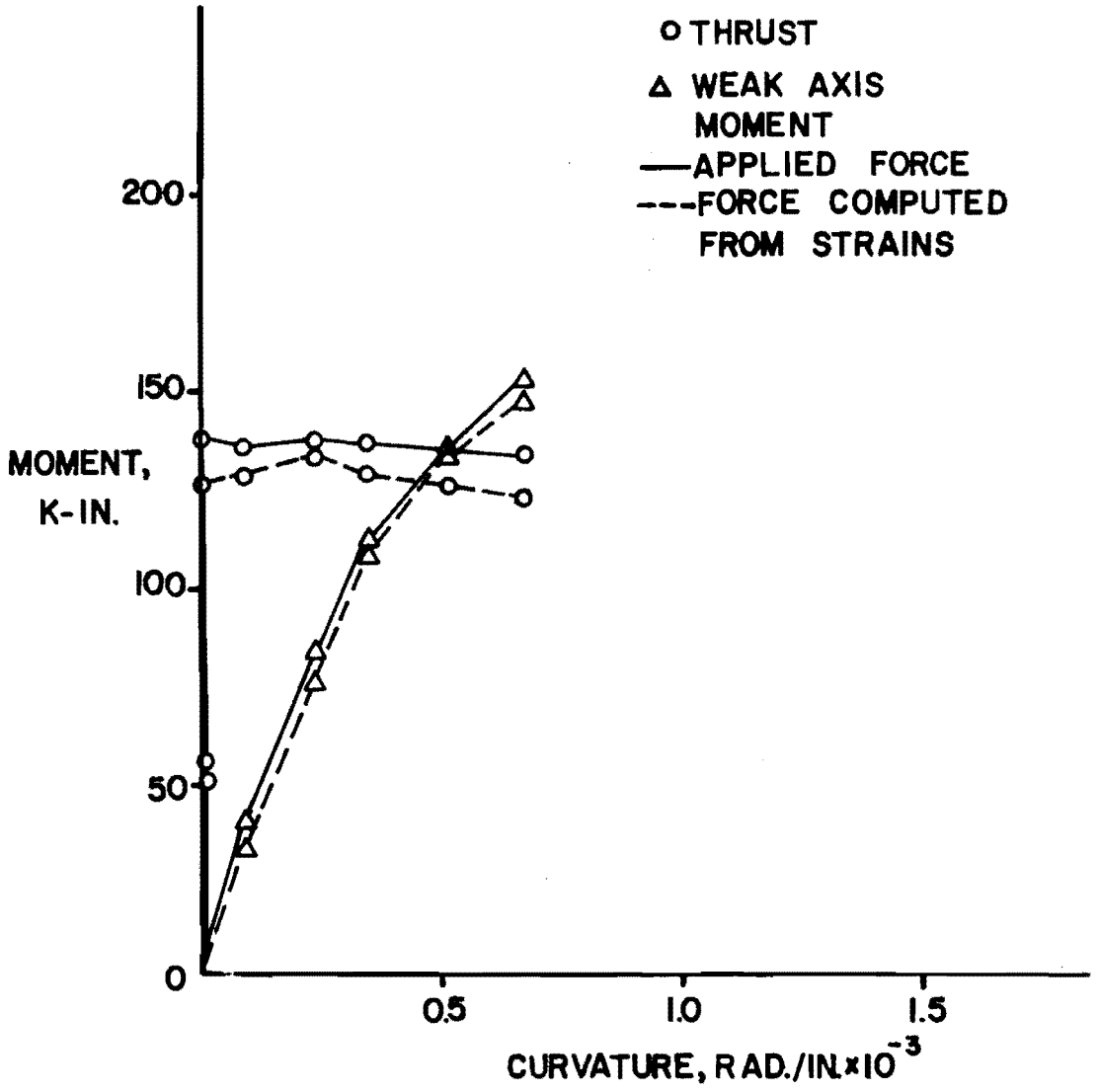

Fig. 3.29 Applied forces and forces computed from strains Specimen C-2 (P_u/P_o = 0.509, weak axis uniaxial bending test)

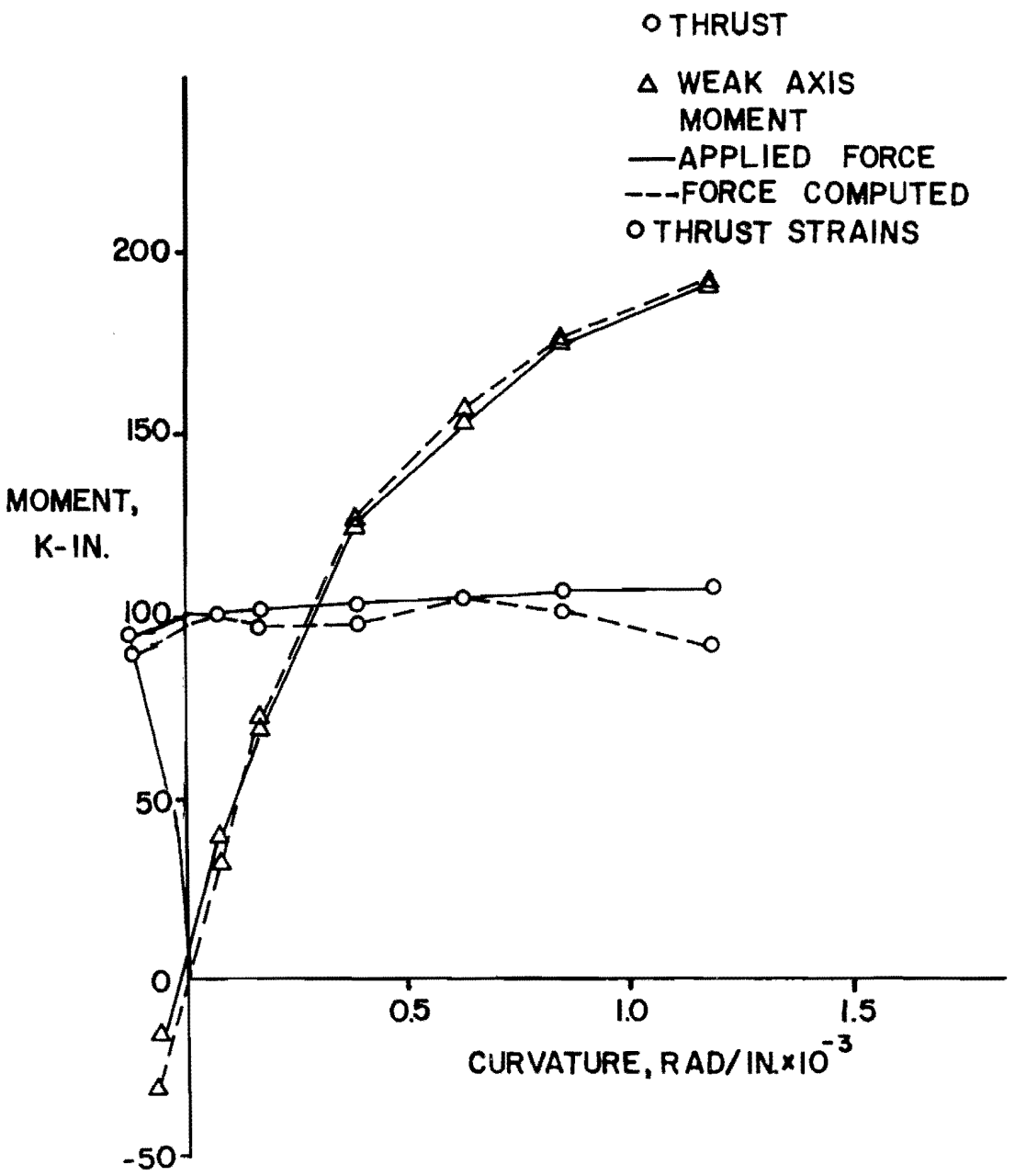

Fig. 3.30 Applied forces and forces computed from strains Specimen C-15 (P_u/P_o = 0.345, weak axis uniaxial bending test)

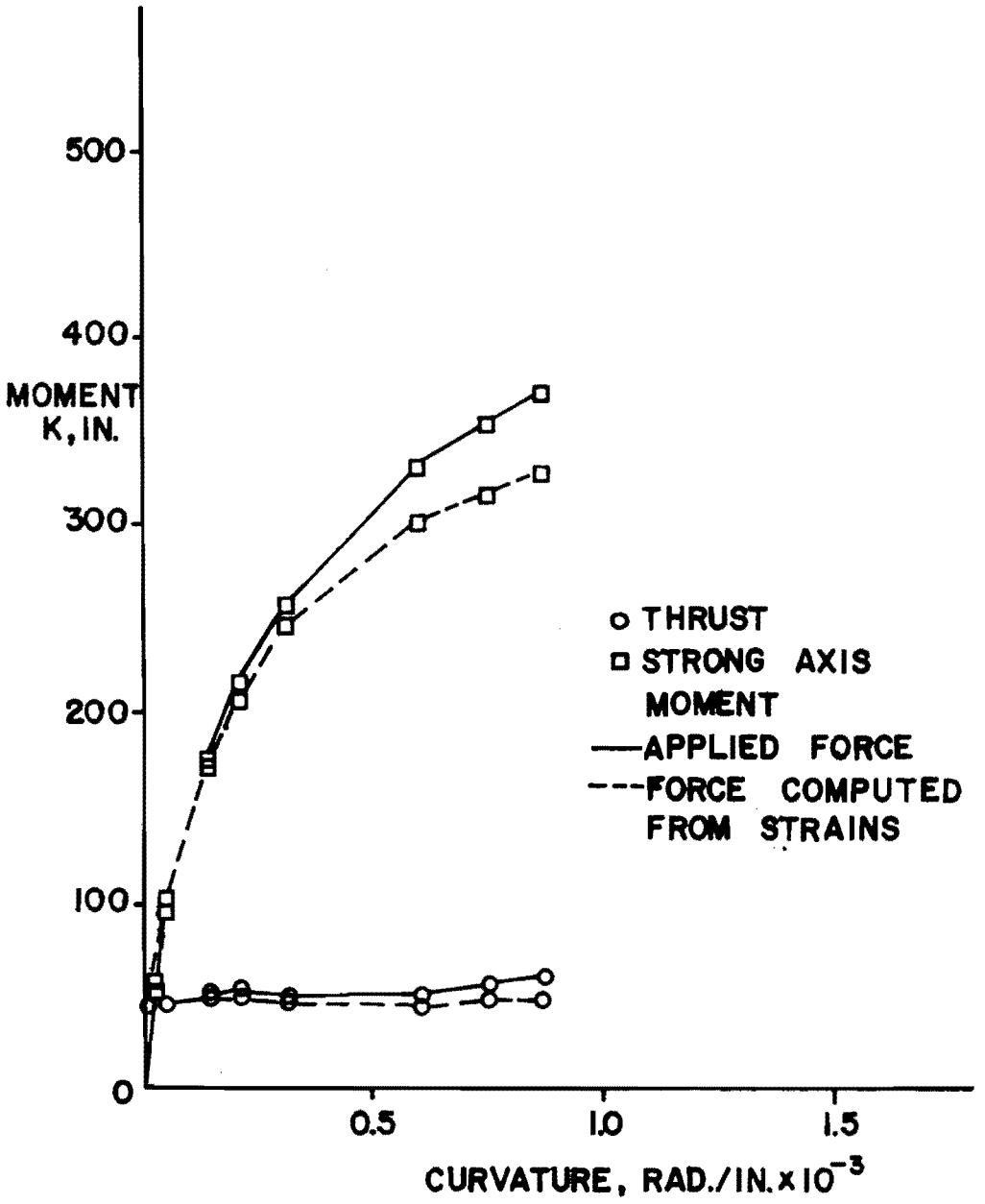

Fig. 3.31 Applied forces and forces computed from strains Specimen C-3 (P_u/P_o = 0.223, strong axis uniaxial bending test)

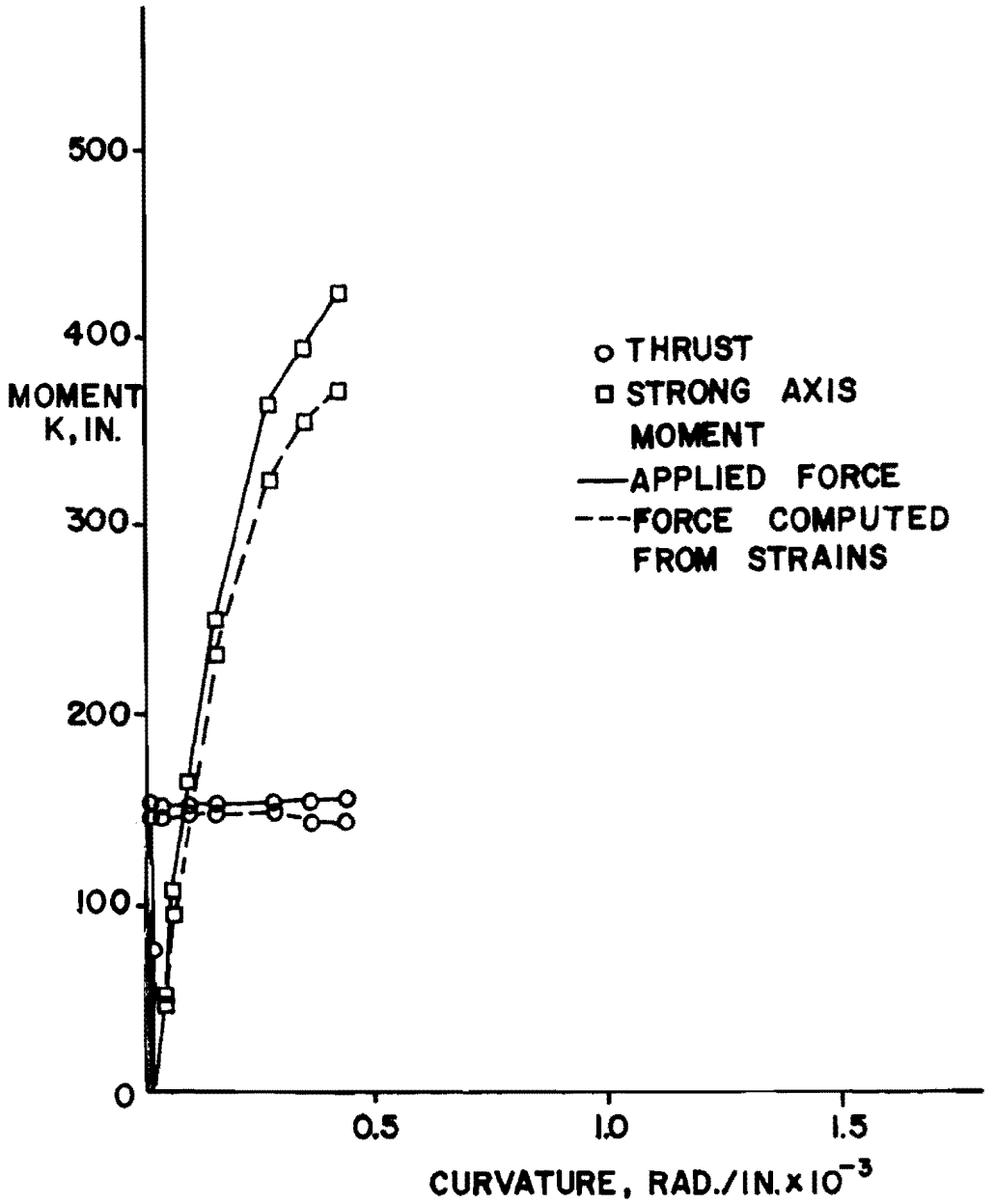

Fig. 3.32 Applied forces and forces computed from strains Specimen C-4 (P_u/P_o = 0.547, strong axis uniaxial bending test)

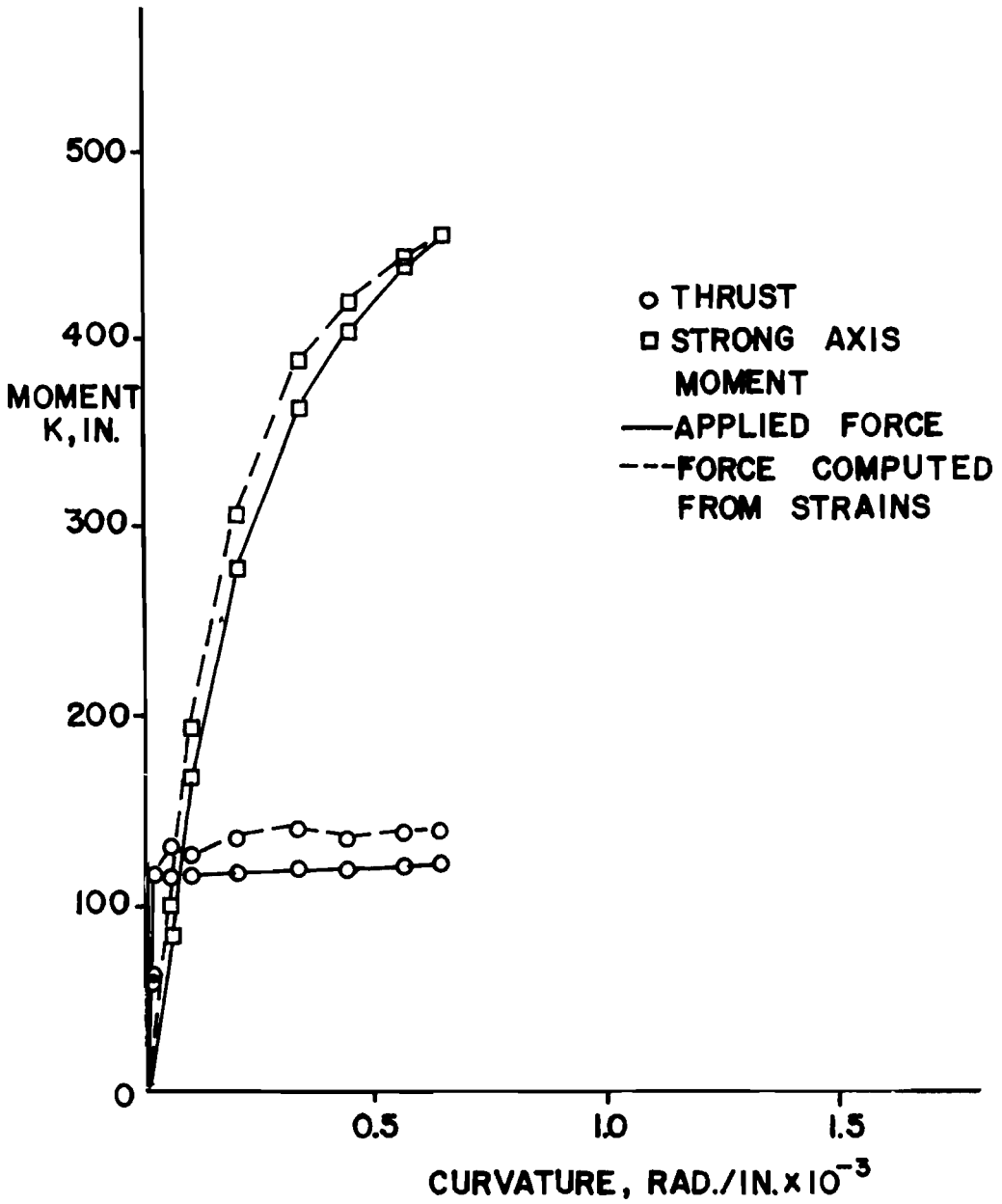

Fig. 3.33 Applied forces and forces computed from strains Specimen C-14 (P_u/P_o = 0.374, strong axis uniaxial bending test)

for the applied thrust of 130 kips on Specimen RC-4, a difference of 23 percent. At the lower level of thrust the percentage difference was higher although the value of the difference was lower. For example, the difference was 18 kips in Specimen RC-7 for a measured thrust of 47 kips, or about 38 percent. Moments computed from strains were always lower than the moments indicated from ram pressures. The analyzed moments gave better agreement with the applied moments than did the thrust, with no difference between moment computed from strain and from the applied moment greater than 20 percent.

Figures 3.19 to 3.27 show the graphs for Specimens C-5 to C-13, the oval-shaped cross section columns under biaxial bending. Again, the values of thrust and moments computed from strains were less than the measured forces for almost all cases. Correspondence between analytic and measured values was not as good as that of rectangular columns. However, all comparisons indicated the same trends of behavior. The maximum difference between the theoretical and the measured thrust was about 32 percent in Specimen C-12. Oval-shaped columns gave better agreement than the rectangular columns for thrust comparisons in specimens with low levels of thrust. No moments analyzed from strain deviated from measured moments by more than 15 percent at failure, except for the strong axis moment of Specimen C-8, for which there was a 30 percent difference. The largest difference between the analyzed moment and measured moment was found at the beginning of the loading of partial circular specimens. A difference as high as 40 percent was found in the weak axis moment of Specimen C-13 at the early stage of loading. These large differences decreased as the loading approached failure.

Thrusts and moments computed from strains were always lower than the observed values for the midheight region. The use of strains averaged over a 30-in. length may account for the lower flexural forces from analysis, but the smaller thrust values imply that the initial slope of the parabolic rectangular stress function may not be high enough.

Thrust and moment versus curvature graphs for uniaxial bending tests are shown in Figs. 3.28 to 3.33. Correspondence between thrust for analyzed results and for the applied thrust was closer in uniaxial specimens than in the biaxial bending specimens. Again, the applied loads were higher than the theoretical load, except for thrust in Specimen C-14. The maximum difference between the analyzed results and the applied loads at failure was less than 20 percent for thrust, 12 percent for strong axis moment, and 17 percent for weak axis moment.

3.6 General Behavior and Mode of Failure of Specimens

The loading system of this test program was operated so that the axial thrust should remain constant as moments or eccentricity increased. The axial load was applied to the designated level first before the moment load gradually was applied until failure. A summary of the failure observations for all specimens is shown in Table 3.8. The load and moment recorded by ram pressure and by load cells are both shown in this table, but the load from ram pressure was used as the capacity of the column throughout this report.

(a) Type of Failure. Two types of failure were observed. Tension failure has been said to occur if the tension steel in the specimen yields before concrete spalls in compression. When the tension steel yielded (computed from the plane of strain), the specimen could carry more load and display large deformation after this stage. Such a column then would fail when concrete in the compression zone crushed and cracks on the tension face could be seen. Compression failure occurred when concrete at the compression face spalled, or crushed before yielding in the tension steel had been reached. For high thrust levels ($0.5P_o$), all specimens failed in the compression mode, and for low axial load, all columns failed in tension. At the load level of $0.35P_o$, a combination of these two modes occurred. Figure 3.34(a) and (b) show the pictures of specimens failed in tension and compression modes.

(a) Tension failure

(b) Compression failure

Fig. 3.34 Type of failure

(b) Location of Failure. Because of the nonuniformity of concrete, columns could fail at any location where the concrete was weak and moments were high. Usually the columns failed near midheight where the maximum moment was measured.

For Specimens C-3 and C-4, which were uniaxial strong axis tests, the secondary moment effect was small, and moments were almost the same along the length of the columns. These columns failed at the position near the top of the specimens. Because of the vertical casting procedure, the top portion of these columns was expected to be weaker than lower portions and failure was considered likely to happen near the top.

Listed in Table 3.8 are the mode of failure and its location for all specimens. For specimens C-5, C-6, C-7, C-11, C-12, C-13, and C-15, no crushing of concrete was reached. As previously explained in Sec. 2.7, the tests were stopped before failure would occur to prevent damage of the measuring devices.

(c) Maximum Strain in Concrete. Maximum compressive strains averaged across five stations (30 in.) along the center portion of the columns are listed in Table 3.8. The maximum strain of all the columns at failure varied from 0.00228 to 0.00393, except for Specimen C-5, for which the maximum strain through the 30-in. region was only 0.00194. The strains across a 30-in. gage length were known to be smaller than the localized values at positions 2 to 8 in. long where concrete actually spalled at failure. The maximum compressive strain at failure measured locally for the five stations at the 6-in. gage length are also shown in Table 3.8 for every specimen. These values ranged from 0.00306 to 0.00526, except for Specimen C-5, for which the maximum strain was 0.00223 locally. The strength study that is described in Chapter 4, together with the low compressive strains indicated here led to the conclusion that the test for Specimen C-5 was stopped before the column actually reached its maximum load.

The shape of the cross section was found to have an influence on the maximum strain at failure. The partial circular specimens

TABLE 3.8 FAILURE SUMMARY

Specimen	Failure Load at Midheight*			Curvature		Maximum Compression Strain		N. A. Angle	Load Angle		θ - φ	Type of Failure	Failure Location
	Thrust	M_{strong}	M_{weak}	Strong Axis	Weak Axis	Avg. along 30" center position (5 stations)	at maximum station		at end	at midheight			
	k	k-in.	k-in.	x 10^{-4}	x 10^{-4}			φ		θ			
RC-1	119.2 (138.7)	60.6 (61.0)	184.0 (188.7)	1.219	8.185	0.00303	0.00324	8.5	21.0	18.2	9.7	Compression	Midheight
RC-2	120.3 (133.9)	124.0 (124.4)	154.1 (155.5)	2.413	8.293	0.00355	0.00438	16.2	50.2	38.8	22.6	Compression	6" above midheight
RC-3	96.3 (107.2)	128.2 (128.5)	150.4 (151.3)	2.791	8.279	0.00328	0.00366	16.1	49.7	40.5	24.4	Compression	Midheight
RC-4	128.8 (141.1)	228.9 (229.6)	127.4 (128.3)	3.984	7.476	0.00386	0.00499	28.1	71.8	60.9	32.8	Compression	6" below midheight
RC-5	87.1 (95.8)	40.3 (40.5)	160.8 (161.9)	0.866	10.710	0.00272	0.00314	4.6	19.1	14.1	9.5	Tension	6" above midheight
RC-6	53.9 (59.9)	52.2 (52.3)	145.9 (146.9)	1.294	13.110	0.00270	0.00313	5.6	25.5	19.7	14.1	Tension	Midheight
RC-7	40.4 (46.3)	86.6 (86.9)	121.3 (122.4)	3.221	14.260	0.00345	0.00467	12.7	42.1	35.5	22.8	Tension	3" above midheight
RC-8	40.4 (45.7)	190.4 (190.8)	86.4 (87.0)	5.434	8.517	0.00339	0.00487	32.5	69.4	65.6	33.1	Tension	Midheight
RC-9	85.8 (100.4)	217.5 (218.5)	102.0 (103.5)	6.821	7.759	0.00402	0.00514	31.9	72.0	64.9	33.0	Compression	12" above midheight
C-5**	49.5 (50.7)	138.3 (138.3)	113.5 (113.6)	1.706	6.520	0.00194	0.00223	14.7	55.7	50.8	36.1	Tension	No crushing, wide cracks
C-6	92.2 (95.3)	171.3 (171.7)	147.1 (147.5)	1.884	7.501	0.00275	0.00306	14.1	56.2	49.4	35.3	Compression	No crushing, comp. steel yielded
C-7	139.7 (142.9)	165.1 (165.7)	161.6 (161.9)	1.762	7.816	0.00332	0.00357	12.7	58.8	45.6	32.9	Compression	No crushing
C-8	57.1 (59.9)	64.4 (64.5)	168.0 (168.5)	0.823	12.590	0.00246	0.00353	3.7	26.0	21.0	17.3	Tension	Midheight
C-9	96.2 (98.9)	67.8 (67.8)	179.1 (179.5)	0.645	10.020	0.00785	0.00357	4.8	28.3	20.7	15.9	Tension + Comp.	12" below midheight
C-10	138.2 (144.2)	57.1 (57.2)	188.0 (188.6)	0.883	8.698	0.00311	0.00435	5.8	22.3	16.9	11.1	Compression	6" above midheight
C-11	53.2 (55.2)	251.9 (252.1)	128.8 (129.0)	4.854	12.200	0.00367	0.00420	21.7	67.7	62.9	41.2	Tension	No crushing
C-12	99.2 (106.9)	243.1 (242.5)	155.6 (156.2)	2.998	8.222	0.00296	0.00390	20.0	64.9	57.6	37.4	Tension + Comp.	No crushing
C-13	152.5 (164.1)	268.2 (269.0)	147.7 (148.3)	2.155	5.037	0.00266	0.00392	23.2	68.6	61.2	38.0	Compression	No crushing
C-1	60.7 (59.4)	-	165.5 (166.3)	-	14.580	0.00256	0.00401	-	-	-	-	Tension	6" above midheight
C-2	135.6 (138.0)	-	154.1 (154.3)	-	6.880	0.00228	0.00526	-	-	-	-	Compression	9" above midheight
C-15	109.2 (113.2)	-	196.2 (196.9)	-	11.950	0.00277	0.00309	-	-	-	-	Tension	No crushing, wide crack
C-3	58.4 (58.3)	372.2 (372.2)	-	8.683	-	0.00328	0.00381	-	-	-	-	Tension	15" below top of column
C-4	155.8 (156.8)	424.2 (424.2)	-	4.330	-	0.00310	0.00347	-	-	-	-	Compression	15" below top of column
C-14	119.2 (120.6)	455.2 (455.3)	-	6.311	-	0.00393	0.00526	-	-	-	-	Tension + Comp.	6" above midheight

*From ram pressure
(value from load cell in parenthesis)

**For C-5 test stopped before column actually failed

had smaller average strains at failure than the rectangular specimens. Rusch's[39] study of maximum strain of various shapes of compression area under flexure indicated that a triangular shape would yield more maximum strain at failure than a rectangular shape. In the case of a rectangular cross section subjected to biaxial bending, the compression area of the cross section would be a triangle as the width of the compression zone reduces from the neutral axis to the maximum compressive fiber. Therefore, in accordance with Rusch's observation a rectangular cross section should have more strain at failure than the partial circular cross sections, in which maximum strain is not at a corner. The average of maximum strain at failure for fourteen specimens of partial circular cross section (all except C-5) was 0.00298, while the average of the maximum strain for all rectangular specimens was 0.00333.

(d) Load Angle and Neutral Axis Angle. Also tabulated in Table 3.8 are the neutral axis angles and the load angles at both top and center of the columns at the failure load stage.

The load angle is defined as

$$\theta = \tan^{-1} \frac{M_{strong}}{M_{weak}} = \tan^{-1} \frac{e_{strong}}{e_{weak}}$$

θ is measured from the strong axis of bending.

The neutral axis angle, φ, is the angle between the weak axis and the neutral axis. The sketch of these two angles is shown in Fig. 3.35.

1. Change of load angle θ from end of the column to to midheight of the column

From Table 3.8 it can be seen that the load angle θ is smaller at midheight than it is at the ends of the column. This difference was due to the secondary effect of the deflection. The column deflected more in the weak direction than in the strong direction, such that the secondary effect was greater in the weak axis direction. This caused the load angle to decrease as the secondary effect increased from the loading point at the end to the

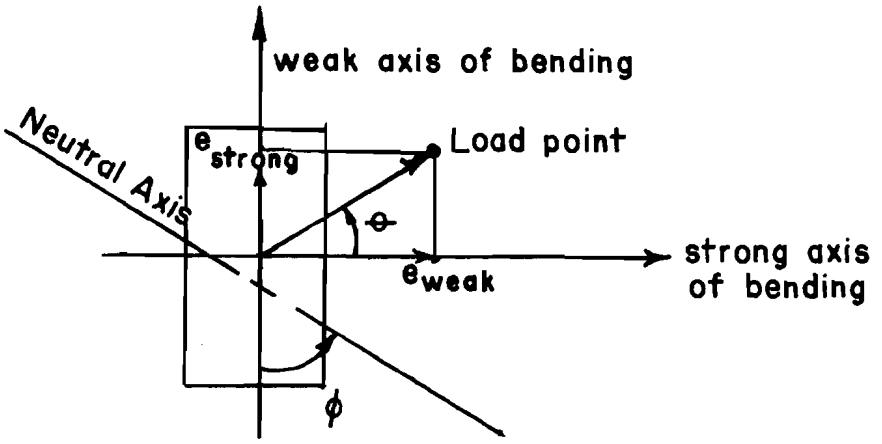

Fig. 3.35 Load angle and N.A. angle

central portion of the column. The deviation of this load angle along the length of the column had no measurable influence on thrust level or the applied moment angle. The maximum change of the load angle was 13.2 degrees and the minimum was 2.8 degrees. The shape of the cross section was not found to effect the amount of change in load angle along the column.

2. Difference between load angle and neutral axis angle

Some research reported by Wu[47] and Ramamurthy[37] neglected the difference of load angle, θ, and neutral axis angle, φ, and used the same angle for their strength analysis. Although Wu observed that there was some difference between θ and φ, he concluded that it was small and neglected the difference in order to simplify his analysis. In this experimental program it was found that there was a significant amount of difference between the load angle and the neutral axis angle.

It was observed that the difference between load angle and neutral axis angle or (θ - φ as shown in Table 3.8) is related to the applied moment angle. As the load angle θ increased the difference of θ-φ increased. The quantity (θ-φ) was greatest for specimens with a nominal load angle of 67-1/2 degrees and smallest for specimens with a nominal load angle of 22-1/2 degrees. No significant effect of thrust level was found to be involved in the angle θ-φ.

Figure 3.36 shows a plot between load angle, θ, and the difference between load angle and neutral axis angle, θ-φ. The plot suggests a linear relationship between θ and θ-φ on the basis of the data available which includes load angles between 15 degrees and 65 degrees. However, when a "90-degree" load angle (major axis flexure) was used for partial circle columns, there was almost no difference between θ and φ.

Redwine[38] studied the problem of the difference between the load angle and neutral axis angle using his analytical model. He concluded that the difference was mainly dependent on the orientation of the neutral axis and the aspect ratio of the section. The axial load level and strain gradient had only a small effect on θ-φ. He also observed that values of θ-φ as large as 38 degrees could be predicted for columns with the same aspect ratio of sections used in these tests.

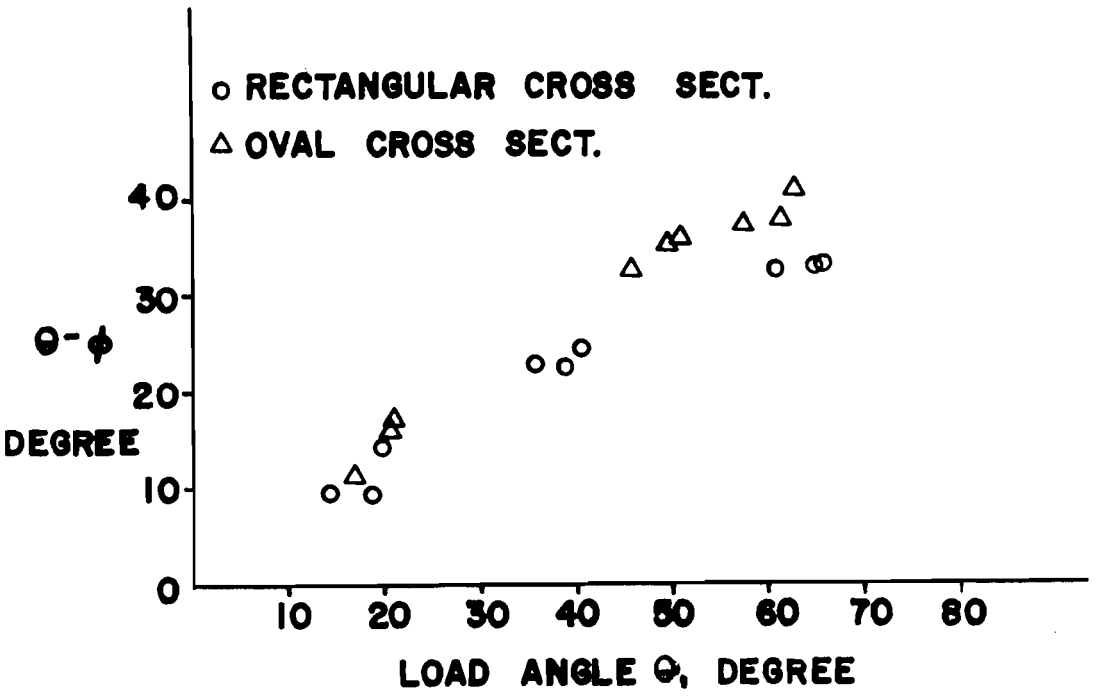

Fig. 3.36 Load angle (θ) vs. the difference between load angle and neutral axis angle (θ-φ)

The practical significance of the real skew angle at midheight involves the estimate of M_y and M_x components that must be checked for strength in the design process. The application of moment magnifier coefficients that increase according to flexibility through a given unsupported length of column produces the same trend of difference between load angle θ at column ends and column midheight as that observed in these tests.

(e) Rotation about Longitudinal Centroidal Axis and Twist. During the test, the specimen was observed to rotate about its longitudinal centroidal axis. Measurements at the top, midheight, and bottom of the columns indicated that before the moment load was applied a very small rotation was recorded, but after moment was applied the rotation increased continually until the failure load. Specimen RC-9 was noted to have the most rotational movement. The maximum rotations of RC-9 after moment was applied were 0.25 degrees at the top, 0.28 degrees at midheight, and 0.43 degrees at the bottom.

Twist of the column is defined here as the change of angle of rotation along the length of the column. For each specimen there were two measurements which indicated the twist, the change of angle of rotation from top to midheight, and from midheight to the bottom of the column. Although Specimen RC-9 was observed to have the maximum rotation, the maximum twist was not obtained from Specimen RC-9. Maximum twist was measured for Specimen RC-2, a rectangular specimen with 0.00746 radian (0.427 degree) of twist from top to midheight, and 0.00311 radian (0.178 degree) from midheight to the bottom. These twist angles were the angle change along a length of 25 in. For partial circular specimens, the maximum twist was found for Specimen C-11 to be 0.00386 radian (0.221 degree) from top to midheight, and 0.00731 radian (0.419 degree) from midheight to the bottom.

Redwine[38] studied the torsion of columns under biaxial bending and concluded that the effect of torsion should be negligible. Green[25] also confirmed that the biaxially column failure was not influenced by torsional effects.

With the maximum angle of twist of 0.0075 radian measured from RC-2, the torsional stress due to this twist can be estimated as follows:

$$\varphi_t = \frac{1}{J}\frac{T}{G}$$

where φ_t = Twist angle per unit length
J = Polar moment of inertia of section
G = Shear modulus
T = Torque on the section

Redwine[38] used the value of J as $0.196bt^3$, where b was the depth and t was the width of the section, and he used G equal to 1.25×10^5 psi for the shear modulus of concrete. These values applied to Specimen RC-2 yield:

$$\varphi_t = \frac{T}{0.196bt^3 \times 1.25 \times 10^5}$$

$$T = \varphi\,[0.196 \times 9 \times 5^3 \times 1.25 \times 10^5]$$

$$T = \frac{0.0075}{25}\,[0.196 \times 9 \times 5^3 \times 1.25 \times 10^5]$$

$$T = 8.2 \text{ k-in.}$$

The allowable shear stress for torsion as specified in the ACI Building Code(ACI 318-71)[1] for plain concrete sections is

$$v_{tc} = 2.4\sqrt{f'_c}$$
$$= 169.7 \text{ psi for 5000 psi concrete}$$

or the allowable torsional moment for concrete is

$$T_c = \frac{x^2 y}{3} v_{tc}$$
$$= \frac{5^2 \times 9}{3} \times 169.7$$
$$= 12.7 \text{ k-in.} > 8.2 \text{ k-in.}$$

The calculation shows that when the column twisted to the maximum angle of twist measured from all tests reported here, less than two-thirds of the allowable torsional shear strength of plain concrete would be generated. The inevitable presence of longitudinal bars and ties in columns should reduce even further any likelihood of torsional strength complications in biaxially loaded concrete columns.

CHAPTER 4

CROSS SECTION STRENGTH AND STIFFNESS

4.1 Introduction

A surface that describes the ultimate capacity of a column under combined axial thrust and flexure can be constructed by plotting an infinite number of points for which thrust is the vertical axis and flexural capacities about each principal axis are the coordinates in the horizontal plane. Any vertical plane contains a thrust-flexure interaction diagram for a specific skew angle. Interaction diagrams for uniaxial bending about a principal axis have been derived on the basis of a limiting strain definition of failure. These uniaxial interaction diagrams have been accepted as accurate enough for design, and functions that relate biaxial capacities to the uniaxial capacities have been proposed by some investigators.

One method of relating the uniaxial capacities of cross sections to biaxial capacities is called "the Load Contour Method." For any levels of axial load the ratios between the component of skew moment about each principal axis to the moment capacities about each principal axis at the same thrust level can be expressed as

$$\left[\frac{M_{xu}}{M_{xo}}\right]^{\alpha_1} + \left[\frac{M_{yu}}{M_{yo}}\right]^{\alpha_1} = 1 \qquad 4.1$$

with M_{xu}, M_{yu} = Components of ultimate moment at the assigned thrust

M_{xo}, M_{yo} = Uniaxial moment capacities about each principal axis for the assigned thrust

α_1 = Exponent that is a function of cross-sectional properties and the ratio between M_{xo} and M_{yo}

Many references[23,33] have contained suggestions for evaluating the exponent α_1, some involving relatively complex relationships among parameters. The "calibration" of analytic functions for α_1 has relied entirely on correlations with results from interaction surfaces that were derived with a rectangular stress block to represent concrete strength prior to failure. In most cases the analytic results that were obtained from the use of Eq. (4.1) after α_1 had been evaluated were not checked against laboratory data from actual resistance to load.[30,32,33]

Another method, "the Reciprocal Load Method" provides a simple relationship between skewed thrust and the uniaxial thrust capacities of the column. In this chapter the Reciprocal Load Method introduced by Bresler[5] will be discussed. This method requires only uniaxial interaction diagrams before a cross section can be analyzed.

4.2 Reciprocal Thrust Equation

The derivation of the reciprocal thrust equation as presented here was described by Bresler.[5] A plane, S′, passing through three points, A, B, and C, which lie on the failure surface S is defined for the surface sketched in Fig. 4.1. A, B, and C have the coordinates:

$$A \quad (e_{xA},\ o,\ \frac{1}{P_y})$$

$$B \quad (o,\ e_{yB},\ \frac{1}{P_x})$$

$$C \quad (o,\ o,\ P_o)$$

The thrust P_o is the axial load capacity without any eccentricity of the section, and P_x and P_y are the load capacity at the uniaxial eccentricity e_{yB} and e_{xA}, respectively. With these definitions point A represents a point (P_y, M_{yu}) on the uniaxial load-moment interaction curve for bending about the y axis, point B is a point on the uniaxial interaction diagram for moment about the x axis and C is a point on the interaction curve with no eccentricity and is the common point of both uniaxial interaction curves.

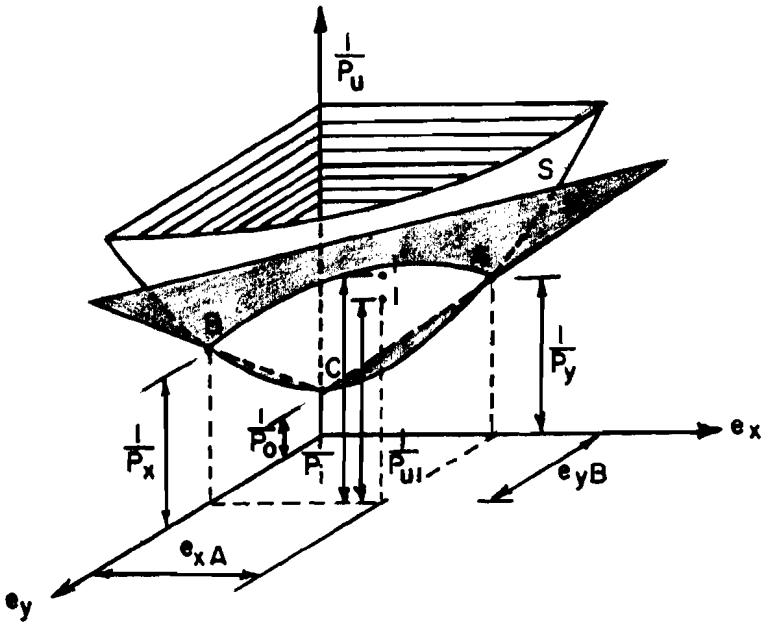

Fig. 4.1 Failure surface for reciprocal load (from Ref. 5)

The general equation for the plane S′ with the same axes $\frac{1}{P_u}$, e_x, e_y is:

$$D_1 e_x + D_2 e_y + D_c \frac{1}{P_u} + D_4 = 0 \qquad 4.2$$

Substituting the coordinates of points A, B, and C which are points that plane S′ passed through gives

$$D_1 e_{xA} + 0 + D \frac{1}{3P_y} + D_4 = 0 \qquad 4.3$$

$$0 + D_2 e_{yB} + D \frac{1}{3P_x} + D_4 = 0 \qquad 4.4$$

$$0 + 0 + D \frac{1}{3P_o} + D_4 = 0 \qquad 4.5$$

Solving Eqs. 4.3, 4.4, 4.5 simultaneously in terms of D_4 yields

$$D_1 = \frac{D_4}{e_{xA}} \left(\frac{P_o}{P_y} - 1\right)$$

$$D_2 = \frac{D_4}{e_{yB}} \left(\frac{P_o}{P_x} - 1\right)$$

$$D_3 = -D_4 P_o$$

Equation 4.2 then can be expressed as

$$D_4\left[\frac{1}{e_{xA}} \left(\frac{P_o}{P_y} - 1\right)e_x + \frac{1}{e_{yB}}\left(\frac{P_o}{P_x} - 1\right)e_y - \frac{P_o}{P_u} + 1\right] = 0 \qquad 4.6$$

Dividing Eq. 4.6 by $D_4 P_o$, the equation for the plane S′ becomes

$$\frac{e_x}{e_{xA}}\left(\frac{1}{P_y} - \frac{1}{P_o}\right) + \frac{e_y}{e_{yB}}\left(\frac{1}{P_x} - \frac{1}{P_o}\right) - \frac{1}{P_u} + \frac{1}{P_o} = 0 \qquad 4.7$$

Point 1, on the failure surface S with the coordinates $e_x = e_{xA}$, $e_y = e_{yB}$ and $1/P_u = 1/P_{u_1}$, is approximately equal to point 1′ on plane S′ with the coordinates $e_x = e_{xA}$, $e_y = e_{yB}$ and $1/P_u = 1/P_i$. Equation 4.7 after substituting coordinates of point 1′ becomes

$$\frac{1}{P_y} - \frac{1}{P_o} + \frac{1}{P_x} - \frac{1}{P_o} - \frac{1}{P_i} + \frac{1}{P_o} = 0 \qquad 4.8$$

or

$$\frac{1}{P_i} = \frac{1}{P_x} + \frac{1}{P_y} - \frac{1}{P_o} \qquad 4.9$$

Equation 4.9 is called the Reciprocal Load Equation where

P_i = Approximate failure load capacity of the section under biaxial bending with eccentricities e_x and e_y

P_x = Uniaxial load capacity of the section under eccentricity e_y only

P_y = Uniaxial load capacity of the section under eccentricity e_x only

P_o = Axial load capacity of the section without any eccentricities

Bresler[5] and Ramamurthy[37] compared results using this equation and physical test results. They concluded that Eq. 4.9 can be used to predict the approximate load capacity of reinforced concrete sections with reasonable accuracy. Pannell[32] indicated that Eq. 4.7 may be inappropriate when small values of axial load are involved ($P/P_o < 0.06$) and the sections should be designed only for flexure in such cases.

4.3 Uniaxial Interaction Diagram

In order to use Eq. 4.9 one must obtain values P_x, e_y and P_y, e_x which are shown on the uniaxial interaction diagram for each major axis of the section. Three types of stress-strain relationships for the ultimate compressive strength of concrete have been considered for derivations of uniaxial interaction functions in this study.

Rectangular Stress Block. The compressive strength of concrete at ultimate load can be represented by a rectangular block of stress. The ACI Building Code[1] (ACI 318-71) permits such a block to be considered if the maximum compression strain at an extreme fiber is taken as 0.003. A uniformly distributed concrete stress of $0.85f'_c$ is assumed to act over a compression region bounded by the extreme compressive fiber and a line parallel to the neutral axis at a distance $a = \beta_o C$ from the extreme fiber of maximum compression strain. The distance, C, is the distance from the neutral axis to the point of maximum compression strain, and β_o is a factor that is used to modify the total magnitude of compression force and to locate the centroid of the force. The factor β_o may be taken as 0.85 for concrete strengths f'_c up to 4000 psi, but it is to be reduced 0.05 for each 1000 psi stress for f'_c greater than 4000 psi. Figure 4.2 shows the strain distribution and the concrete stress related to this distribution. Tension in concrete may be neglected according to the ACI Building Code.

Modified Hognestad Stress-Strain Curve. The second type of concrete stress-strain relationship used was a modified Hognestad

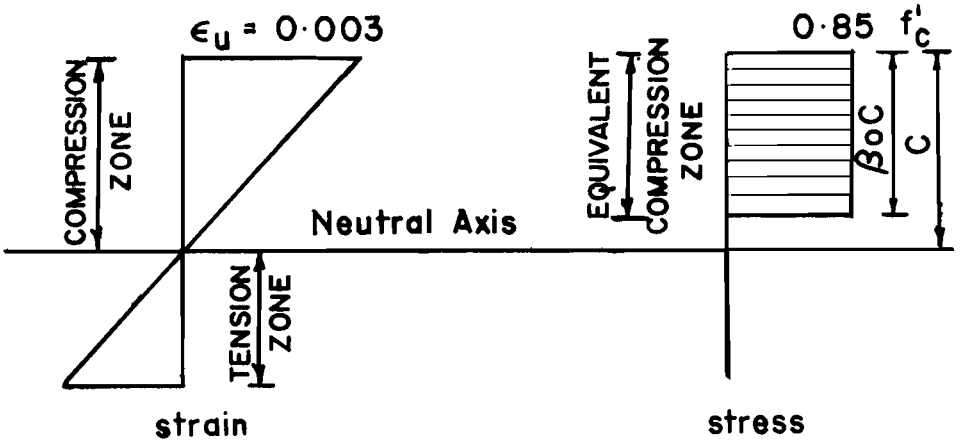

Fig. 4.2 Rectangular stress block

curve which has been described in Chapter 3. The curve consists of two portions, a parabola and a straight line.

For strains less than $\epsilon_o = 2f'_c/E_c$, the curve is a parabola with the equation

$$f_c = f'_c\left[\frac{2\epsilon}{\epsilon_o} - \left(\frac{\epsilon}{\epsilon_o}\right)^2\right] \qquad 4.10$$

where $E_c = 72000\sqrt{f'_c}$

Beyond the strain of ϵ_o, the curve is a straight line with a slope down from stress f'_c at ϵ_o to a stress $0.85f'_c$ at the strain of 0.0038. Failure is assumed to exist when the maximum strain at the extreme compressive fiber reaches 0.0038. No tension is considered for concrete. Strain and stress distribution of this type are shown in Fig. 4.3.

Parabolic-Rectangular Stress-Strain Function. A parabolic-rectangular stress-strain function for concrete was discussed in Chapter 3. In order to construct the interaction diagram between

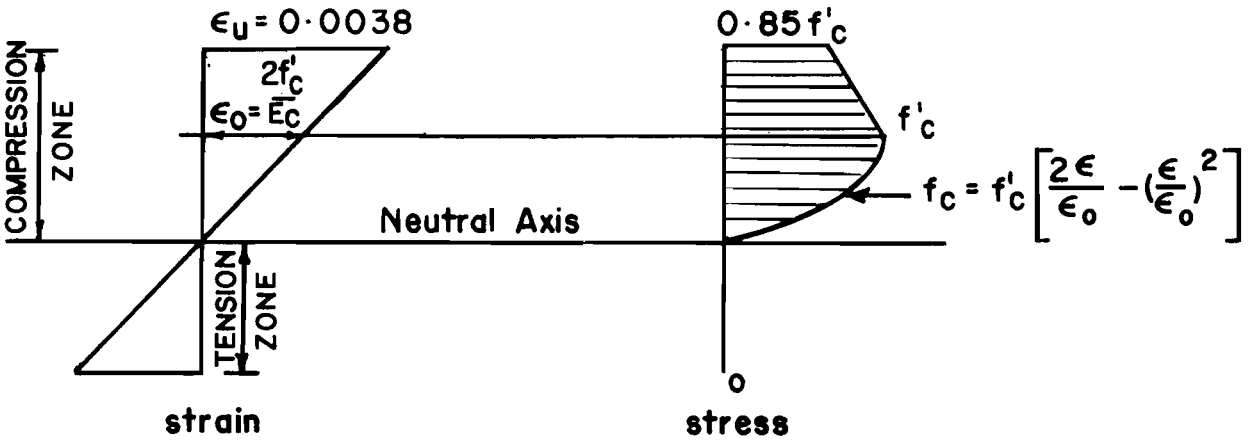

Fig. 4.3 Modified Hognestad stress-strain curve

thrust and moment for uniaxial bending in this chapter, the parabolic curve had the same equation as the Modified Hognestad's curve (Eq. 4.10) but ϵ_o was taken as 0.002 instead of $2f'_c/E_c$. Beyond the strain of 0.002 a constant stress was used up to the failure strain of 0.0035. The failure strain of 0.0035 has been recommended by the Comité Européen de Beton.[10] Figure 4.4 shows the strain distribution and the stress corresponding to the strain on the section. Again no tension stress in concrete was considered.

Points on interaction diagrams were calculated by assuming a neutral axis location and the failure strain on the extreme compressive fiber, strain distribution was assumed to vary linearly acorss the section. The stress-strain relationships for concrete were used to determine stresses and forces in the segments of the section. These forces were integrated to get normal forces and moments about the centroid of the section. The same procedure was used for reinforcing steel except that the elastic-purely plastic stress-strain function for steel was used.

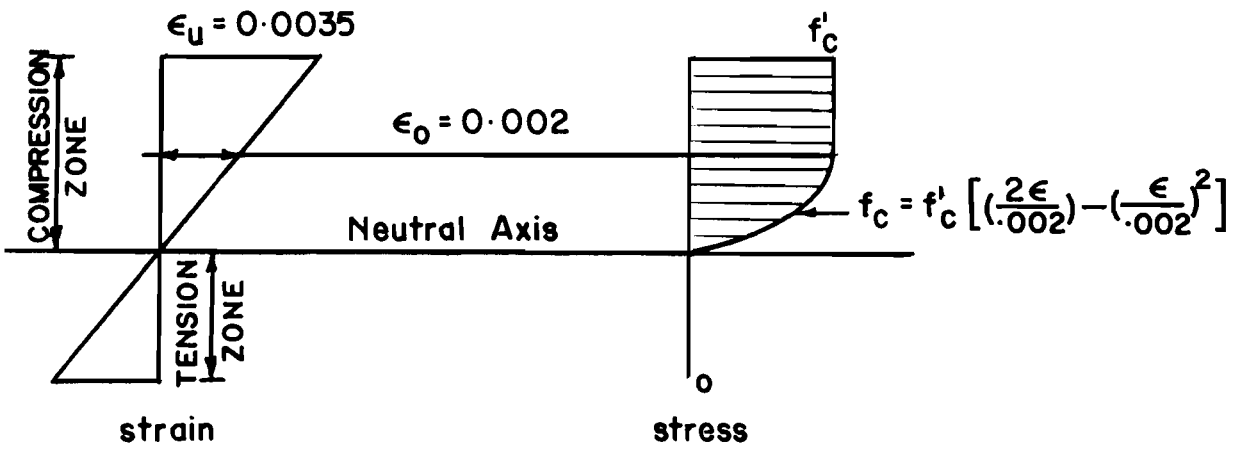

Fig. 4.4 Parabolic-rectangular stress-strain curve

4.4 Approximate Strength of the Section by Reciprocal Thrust Equation

With the eccentricities specified about both axes, the uniaxial strengths corresponding to those eccentricities can be found from uniaxial interaction diagrams. The approximate strength of the section under biaxial eccentricities e_x, e_y can be determined by using Eq. 4.9.

In this section, the moments and axial load at the failure load stage of every specimen were used as the actual load capacity of the cross section. Eccentricity of the axial load on the cross section was taken as the ultimate moment divided by the axial load. All the given values are based on the thrusts and moments for the center portion of the members.

With these "measured" eccentricities, the predicted strength was calculated using Eq. 4.9 and the uniaxial interaction diagrams. Table 4.1 displays three values of the approximate strength of the

TABLE 4.1 COLUMN STRENGTH USING RECIPROCAL LOAD EQUATION

Specimen	f'_c	Eccentricity		P_{test}	Rectangular Stress Block			Modified Hognestad's Stress-Strain Curve			Parabolic-Rectangular Stress-Strain Curve			P_u/P_o**
	psi	ECC_s in.	ECC_w in.	k	P_o* k	P_i k	P_i/P_u	P_o** k	P_i k	P_i/P_u	P_o** k	P_i k	P_i/P_u	
C-8	4760	1.128	2.940	57.1	246.4	49.3	0.863	282.0	51.6	0.904	282.0	53.1	0.930	0.2025
C-5	4340	2.796	2.295	49.5	228.7	53.6	1.083[1]	261.1	56.2	1.135[1]	261.1	58.5	1.182[1]	0.1896
C-11	4830	4.735	2.420	53.2	249.4	42.1	0.791	285.5	44.8	0.842	285.5	46.0	0.865	0.1863
C-9	4830	0.704	1.861	96.2	236.9	84.5	0.878	270.8	88.1	0.916	270.8	91.4	0.950	0.3552
C-6	4396	1.859	1.595	92.2	231.1	78.0	0.846	264.0	83.8	0.909	264.0	88.1	0.956	0.3492
C-12	5091	2.451	1.568	99.2	260.4	81.0	0.817	298.4	87.3	0.880	298.4	91.3	0.920	0.3324
C-10	4425	0.413	1.360	138.2	232.3	106.2	0.768	265.4	107.5	0.778	265.4	118.3	0.856	0.5207
C-7	4403	1.182	1.157	139.7	231.4	107.0	0.766	264.3	111.1	0.795	264.3	118.0	0.845	0.5286
C-13	5397	1.759	0.968	152.5	273.3	124.0	0.813	313.6	130.3	0.854	313.6	138.5	0.908	0.4863
RC-1	4886	0.508	1.543	119.2	219.5	92.8	0.779	252.6	97.4	0.817	252.6	104.9	0.880	0.4719
RC-2	4871	1.031	1.281	120.3	218.9	98.3	0.817	251.9	101.9	0.847	251.9	109.7	0.912	0.4776
RC-4	5181	1.777	0.989	128.8	230.4	102.4	0.795	265.4	106.5	0.827	265.4	114.5	0.889	0.4853
RC-5	5012	0.463	1.845	87.1	224.3	82.2	0.944	258.2	86.2	0.990	258.2	92.5	1.062	0.3373
RC-3	5210	1.360	1.594	94.3	231.9	84.7	0.898	267.2	90.0	0.954	267.2	95.8	1.016	0.3529
RC-9	4700	2535	1.189	85.8	212.4	73.9	0.861	244.2	78.7	0.917	244.2	83.0	0.967	0.3514
RC-6	4425	0.968	2.705	53.9	201.8	46.4	0.861	231.7	48.2	0.894	231.7	49.9	0.926	0.2326
RC-7	4350	2.144	3.003	40.4	199.0	36.2	0.896	228.5	37.9	0.938	228.5	39.3	0.973	0.1768
RC-8	4446	4.716	2.141	40.4	202.6	35.3	0.874	232.7	36.4	0.901	232.7	37.7	0.933	0.1736
					Mean		0.8392			0.8802			0.9287	
					Standard Deviation		0.0497			0.0560			0.0548	
					Coef. of Variation		0.0592			0.0636			0.0590	

*For rectangular stress block type $P_o = 0.85f'_c A_c + A_s f_y$

**For parabolic stress-strain type $P_o = 1.0f'_c A_c + A_s f_y$

[1]Specimen C-5 not included in statistical analysis.

section, one value for each type of stress-strain relationship of concrete. Table 4.1 shows the comparisons of these values and also the observed thrust P_i when ultimate moments occurred. The ratios of the calculated strengths and the observed strength are listed in Table 4.1.

It has been noted that for Specimen C-5 the approximate value from Eq. 4.9 predicted much higher strength than the actual test strength. This indicated that the test on Specimen C-5 had not reached a failure load stage at the end of testing, and the column would carry higher moments than the moments recorded when the test was stopped. The results from Sec. 3.6 indicated that the maximum compressive strain at the final load stage was lower than the strain in other tests and no yielding in the reinforcing bars was observed when strains in the bars were calculated from the equation of the plane of deformation. With the observations both in Sec. 3.6 and in this section, it was concluded that for Specimen C-5 the test result did not represent the "failure load".

As indicated in Table 4.1, the results from the rectangular and Hognestad stress-strain functions are lower than the observed strengths. For the parabolic rectangular stress-strain curve, the results indicate lower analytic values except for two specimens, RC-3 and RC-5. The average of the ratio between P_i and P_u for all specimens shows that with rectangular stress block stress diagram the result was least accurate and parabola-rectangle function gave the best agreement between analysis and test results. The standard deviation of the ratio of P_i/P_u is between 5 percent and 5.6 percent, and the coefficient of variation is between 5.9 percent to 6.4 percent for all three types of stress-strain curves of concrete. The highest and best mean value that was determined was 0.929 from the modified CEB curve with the standard deviation of only 5.5 percent and a coefficient of variation of 5.9 percent.

4.5 Strength of Section on Uniaxial Tests

Six specimens with a partial circular cross section were tested in bending about only one major axis at a time. Listed in Table 4.2 are the results from the tests and the predicted failure moments from three types of interaction diagram analyzed for the same axial load level as the tests. The results indicate again that the parabolic-rectangular stress-strain function for concrete gave the most favorable agreement between test values and analytic values. The mean value of the ratio between the moment from this interaction diagram and the actual failure moment was 0.996 with the standard deviation of 7.3 percent and a coefficient of variation of 7.33 percent. It should be noted that this interaction function gave failure estimates higher than those measured for load about the weak axis, but the excess was less than 4 percent.

The parabola-rectangle (Modified CEB) stress-strain function was used for the strength investigation that follows.

4.6 Study of Other Experimental Results

Data from two other investigators were used for further evidence of the reliability of the reciprocal load equation. The data include four rectangular columns tested by Bresler[5] and 55 square and rectangular columns tested by Ramamurthy.[37] The 18 biaxial tests reported here make the specimen sample total 77 for this investigation.

The approximate strength P_i was calculated by using the reciprocal load equation for every sample. The ratio of P_i and the actual tested strength P_u for each column was used as an index of the accuracy of the reciprocal load method. The mean value of the ratio between P_i and P_u taken from all samples was 0.9428. The standard deviation was 0.0689, and the coefficient of variation was 7.31 percent.

These results indicate that the reciprocal load equation with a proper thrust-moment interaction diagram for uniaxial bending

TABLE 4.2 FAILURE LOAD OF THE UNIAXIAL TESTS

Specimen	f'_c	P_u	Actual Moment		From Interaction Diagram			M_a/M_u	M_c/M_u	M_b/M_u
			M_u weak	M_u strong	Rect. Stress Block (M_a)	Parabolic Rect. (M_c)	Modified Hognestad (M_b)			
	psi	k	k-in.	k-in.	k-in.	k-in.	k-in.			
C-1	4783	60.7	165.5	-	160	169	166.5	0.9668	1.0211	1.0060
C-15	5468	109.2	194.2	-	181	208	202	0.9320	1.0711	1.0402
C-2	4460	135.6	154.1	-	140	167	157	0.9805	1.0837	1.0188
C-3	4386	58.4	-	372.2	331	350	346.5	0.8893	0.9404	0.9310
C-14	5514	119.2	-	455.2	387	447	436.5	0.8502	0.9820	0.9589
C-4	4831	155.8	-	424.2	304.5	371	348	0.7178	0.8746	0.8204
							$\bar{x}$	0.8894	0.9955	0.9626
							σ	0.0886	0.0730	0.0734
					Coefficient of Variation			0.0996	0.0733	0.0762

gives a good prediction for cross section capacity under biaxial bending and compression. Further studies of the influence on accuracy from variables such as axial load level, percentage of steel and section shape will be described.

4.6.1 Influence of Axial Load Level. Figure 4.5 shows data points comparing values of the ratio P_i/P_u with the relative thrust level P_u/P_o for all 77 data points. More data fell below the average value of $P_i/P_u = 0.9428$ for the thrust level greater than 0.4, but one cannot conclude that the axial load level has any apparent trend that affects the accuracy of the reciprocal thrust strength calculation because of the lack of data at thrust levels higher than $0.6P_o$.

4.6.2 Influence of Percentage of Reinforcement, Aspect Ratio and Load Angle. The accuracy of strength predictions was not found to be influenced by the amount of reinforcement. The data included specimens with reinforcement ratios of 1 percent to 4.5 percent. Table 4.3 shows the list of percentage of reinforcement on the cross section and the average ratio of P_i/P_u for each percentage. These data show that the accuracy or inaccuracy of the reciprocal thrust estimate of P_i was independent of the amount of reinforcement.

Table 4.4 compares the relationship between the aspect ratio (depth/width) of the section and the predicted strength P_i/P_u. Again there is no evidence that the aspect ratio influences the accuracy of strength calculated from the reciprocal load equation. The limited number of specimens with partial circular cross sections showed the most inaccurate result, suggesting that there might be some influence from the shape of the cross section. However, the low estimates of strength may be due not to the reciprocal thrust equation, but instead due to the uniaxial strength estimates.

The relationship between P_i/P_u and the aspect ratio d/b is also shown graphically in Fig. 4.6. A linear regression analysis of data points gives the relationship as

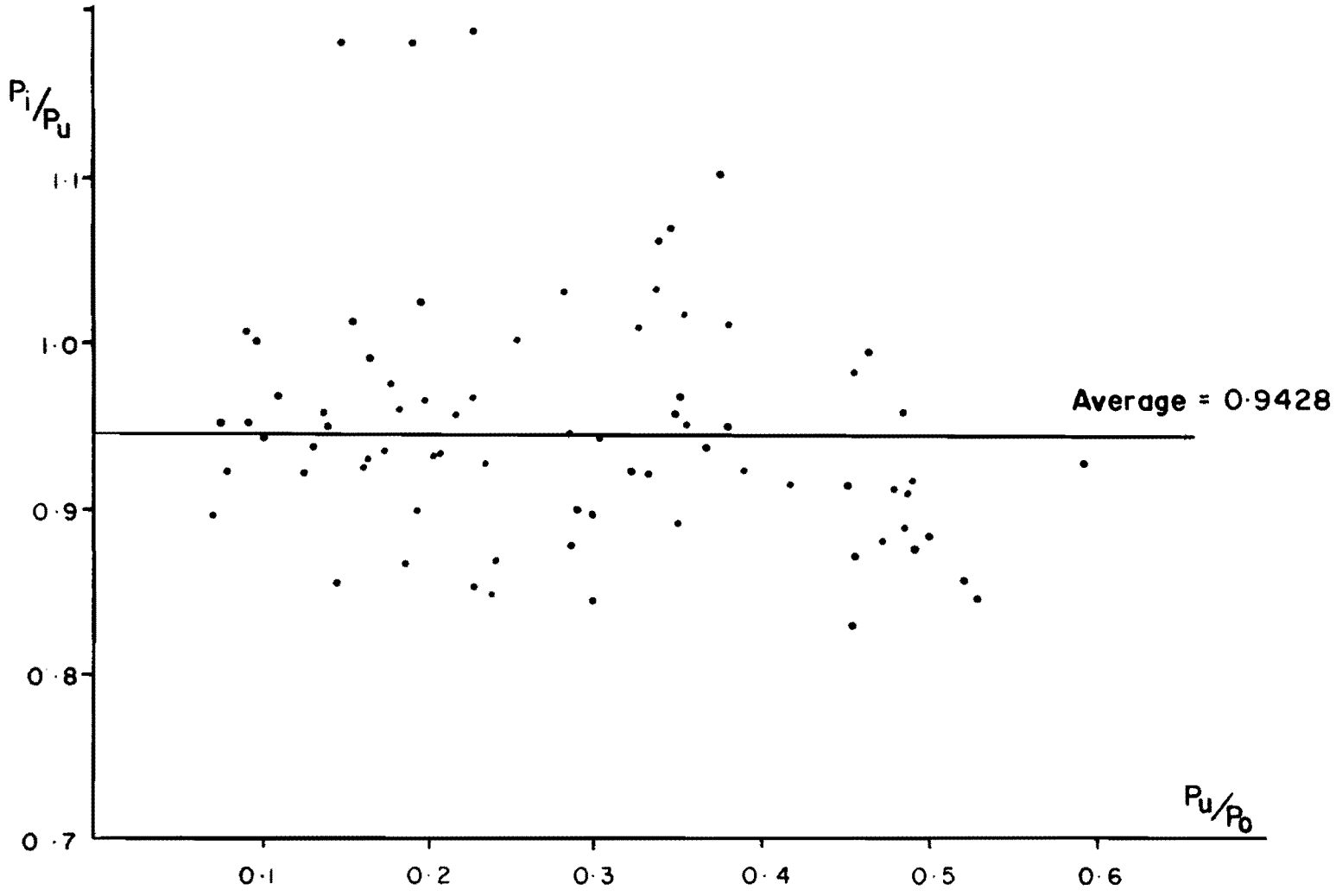

Fig. 4.5 Approximate strength P_i/P_u (from Reciprocal Load Equation) and failure load level P_u/P_o

TABLE 4.3 INFLUENCE OF PERCENTAGE OF REINFORCEMENT

Percentage of Steel,	Number of Specimens	Average P_i/P_u
0.0109	9	0.951
0.138	8	0.904
0.0218	5	0.943
0.0245	19	0.952
0.0256	4	1.005
0.0291	5	0.998
0.0341	4	0.926
0.0383	8	0.944
0.0430	8	0.947
0.0455	6	0.867

TABLE 4.4 INFLUENCE OF ASPECT RATIO

Aspect Ratio d/b	Number of Specimens	Average P_i/P_u
1.0	35	0.949
1.33	4	1.005
1.5	11	0.926
1.8	9	0.951
2.0	9	0.936
2.2*	8	0.904

*Partial Circular Cross Section

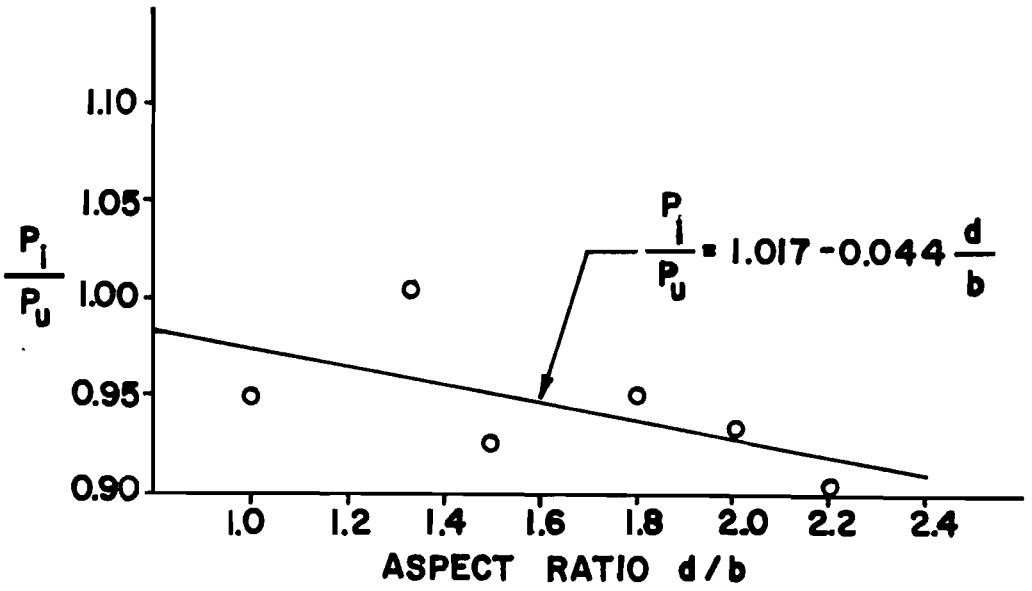

Fig. 4.6 Influence of aspect ratio

$$P_i/P_u = 1.017 - 0.044\ d/b \qquad 4.11$$

with the coefficient of correlation equal to r = -0.577. From the low coefficient of correlation, one could not conclude that there was any influence of aspect ratio on the accuracy of the reciprocal load approximation. But the trend showed that at higher aspect ratios there might be some influence on the accuracy of the calculation.

Listed in Table 4.5 are the skew angles and the average ratio of P_i/P_u at those load angles. No unique relationship between skew angle and the reciprocal load equation is apparent.

None of the parameters studied, reinforcement ratio, aspect ratio, thrust level, or load angle, appeared to have a predictable influence on the relative accuracy of the reciprocal thrust equation for estimating the biaxial bending strength P_i. The accuracy of the reciprocal thrust equation is dependent only on the accuracy of uniaxial strength estimates for P_x and P_y that act at the specified eccentricities e_y and e_x.

TABLE 4.5 INFLUENCE OF LOAD ANGLE

Skew Angle	Number of Specimens	Average P_i/P_u
10^o-20^o	21	0.945
20^o-30^o	15	0.929
30^o-40^o	12	0.966
over 40^o	28	0.934

4.7 Stiffness of the Cross Section

The relationship between the measured moments about both principal axes and the corresponding curvatures were studied with graphs shown in Figs. 4.7 to 4.30. These graphs show the measured moment-curvature (M-φ) results of all the columns tested. The moment values were the midheight moments computed from the ram pressure readings, and the curvatures were the average values obtained from five stations along the center portion of the column as described in Chapter 3. These average moment-curvature graphs represent the column section at midheight. The slope of the M-φ curve would represent the flexural stiffness EI of the cross section at midheight.

The nominal computed values of EI about each axis for uncracked sections and for cracked sections are also shown as lines of constant slope in Figs. 4.7 to 4.30. The uncracked section nominal EI was computed as $E_c I_g + E_s I_s$ where $E_c = 57000 \sqrt{f'_c}$, $E_s = 30000$ ksi, I_g = gross moment of inertia of the section about the axis of bending, and I_s = moment of inertia of the reinforcing steel about the appropriate axis of bending. Because of the low percentage of steel (0.011 and 0.013), the cracked section EI values were estimated as 40 percent of the gross stiffness $E_c I_g$ of the section on the basis of the approximation in ACI[1,2] Eq. (10-8), $EI = E_c I_g/2.5$ Values of $E_c I_g$, $E_s I_s$ and $E_c I_g/2.5$

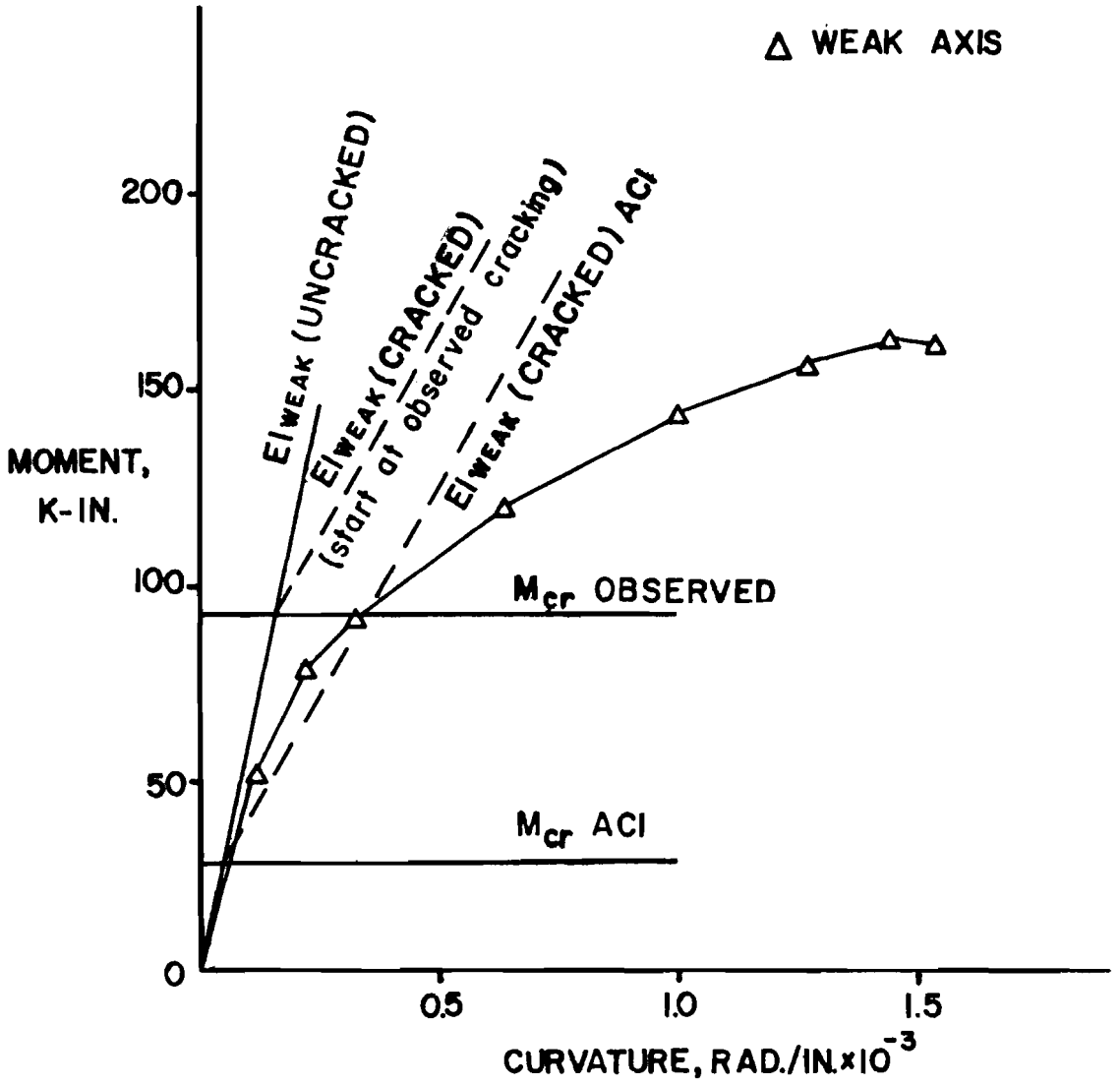

Fig. 4.7 Moment-curvature relationship, Specimen C-1 $(P_u/P_o = 0.125$, weak axis uniaxial bending test)

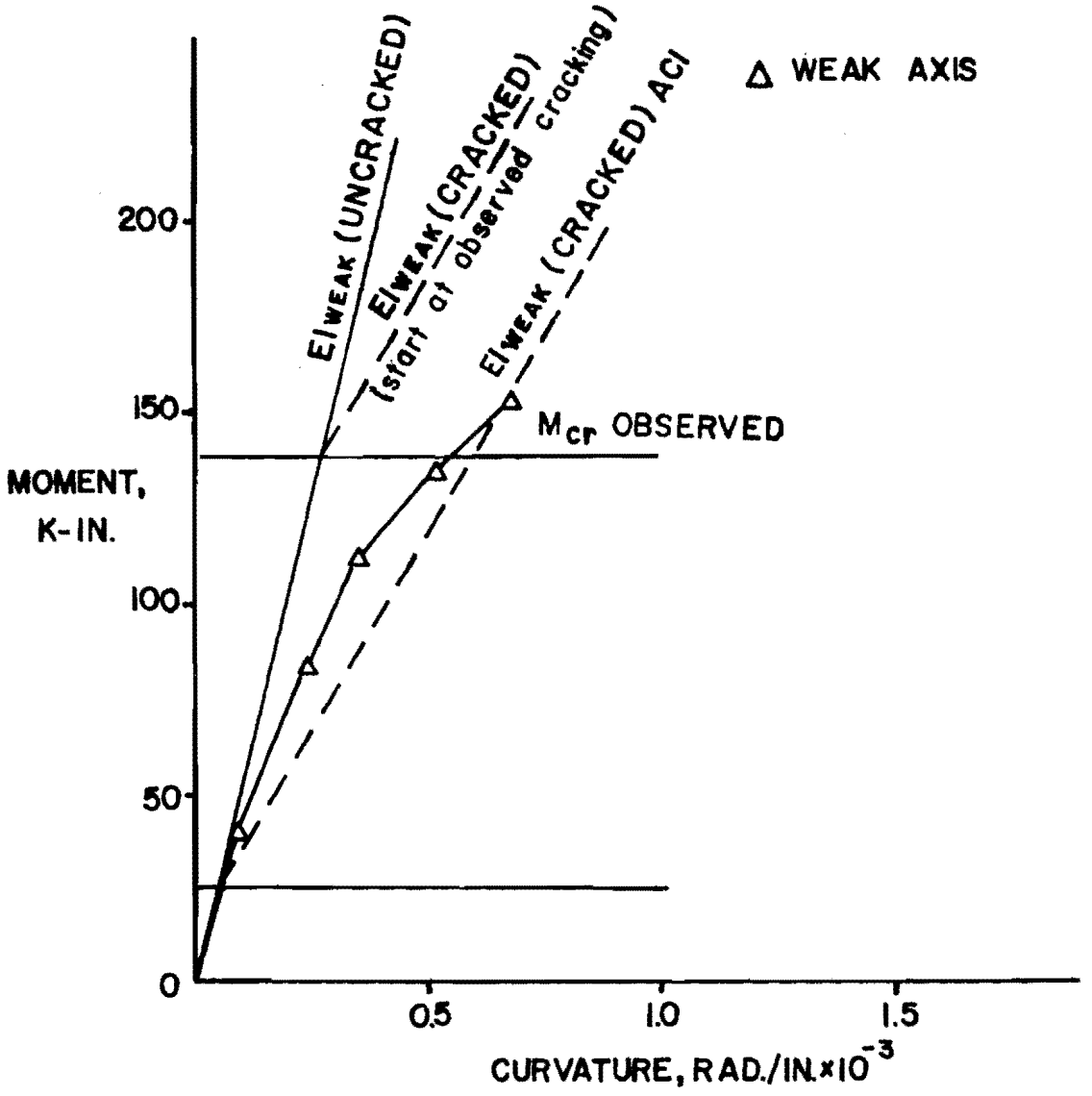

Fig. 4.8 Moment-curvature relationship, Specimen C-2 $(P_u/P_o)_{test} = 0.509$, weak axis uniaxial bending

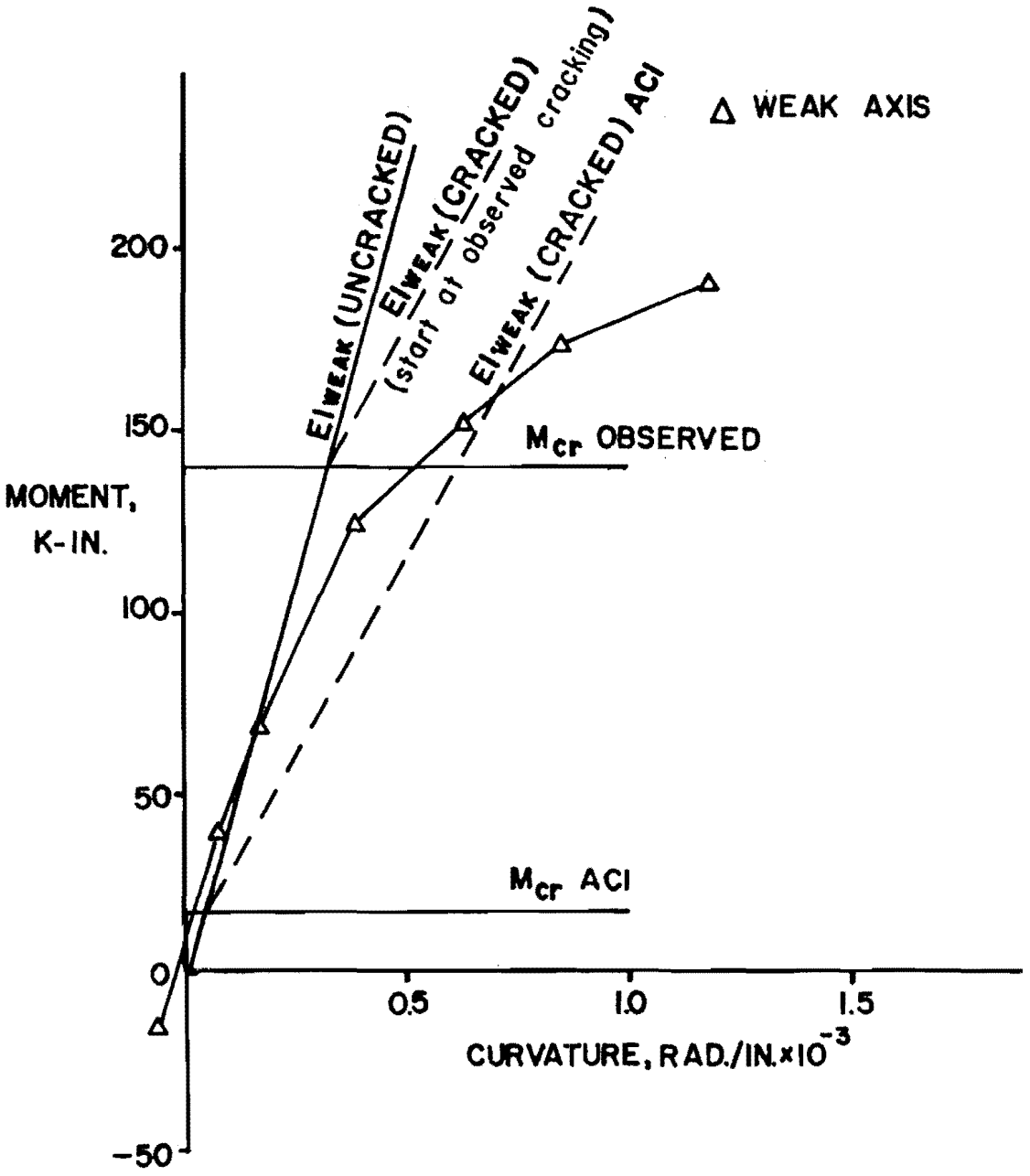

Fig. 4.9 Moment-curvature relationship, Specimen C-15 $(P_u/P_o$ test$)^o$ = 0.345, weak axis uniaxial bending

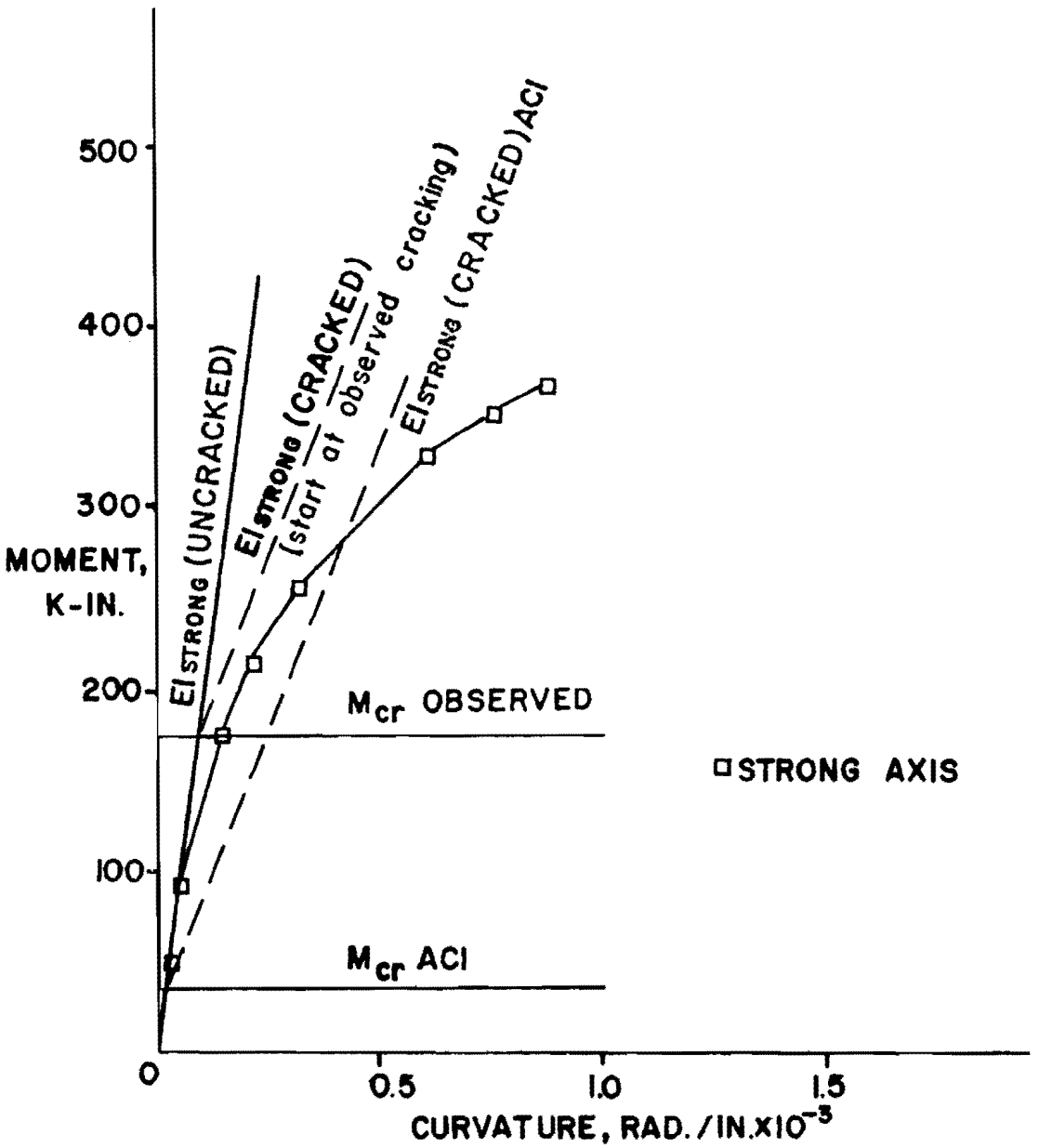

Fig. 4.10 Moment-curvature relationship, Specimen C-3 (P_u/P_o = 0.223, strong axis uniaxial bending test)

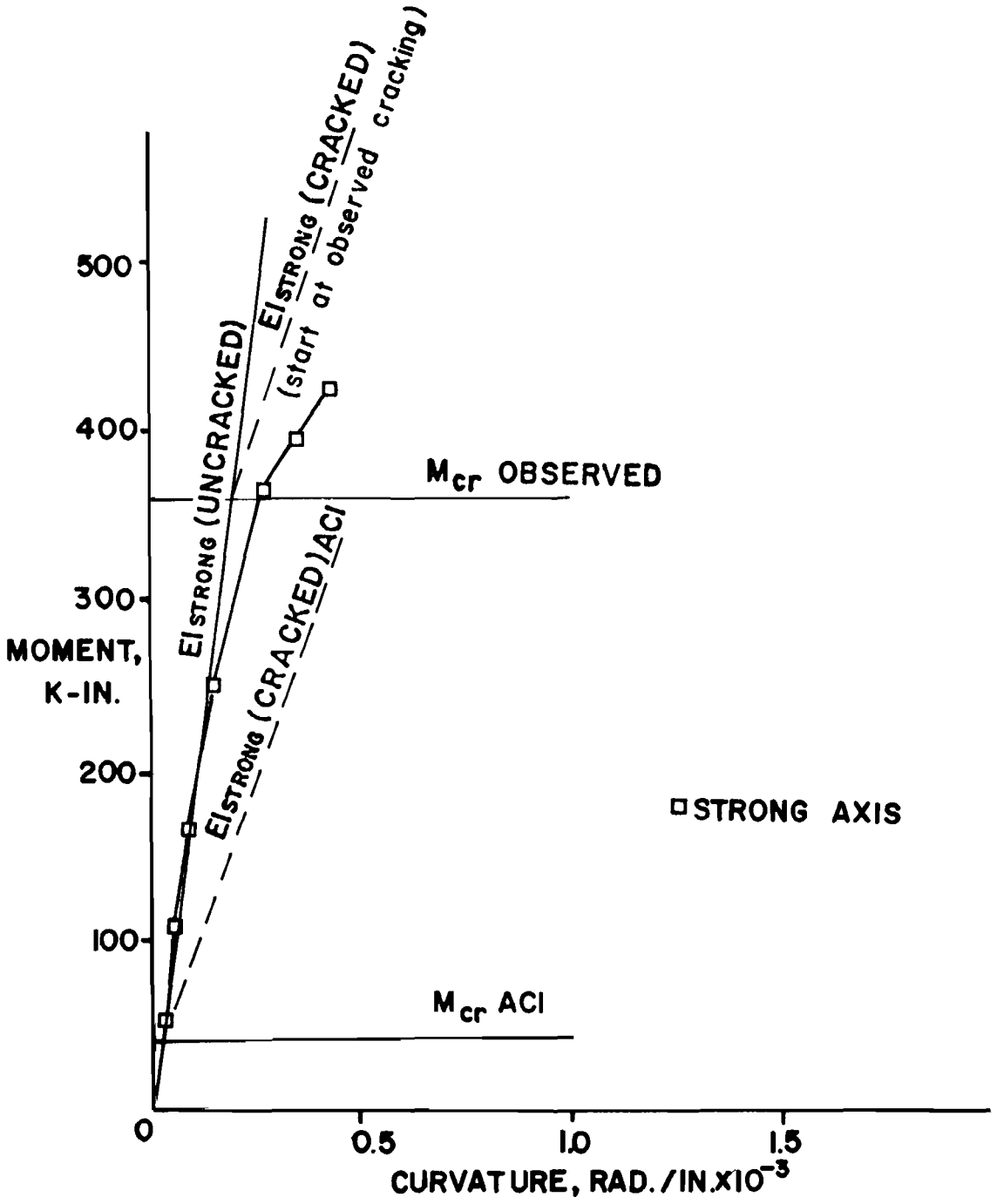

Fig. 4.11 Moment-curvature relationship, Specimen C-4 (P_u/P_o = 0.547, strong axis uniaxial bending test)

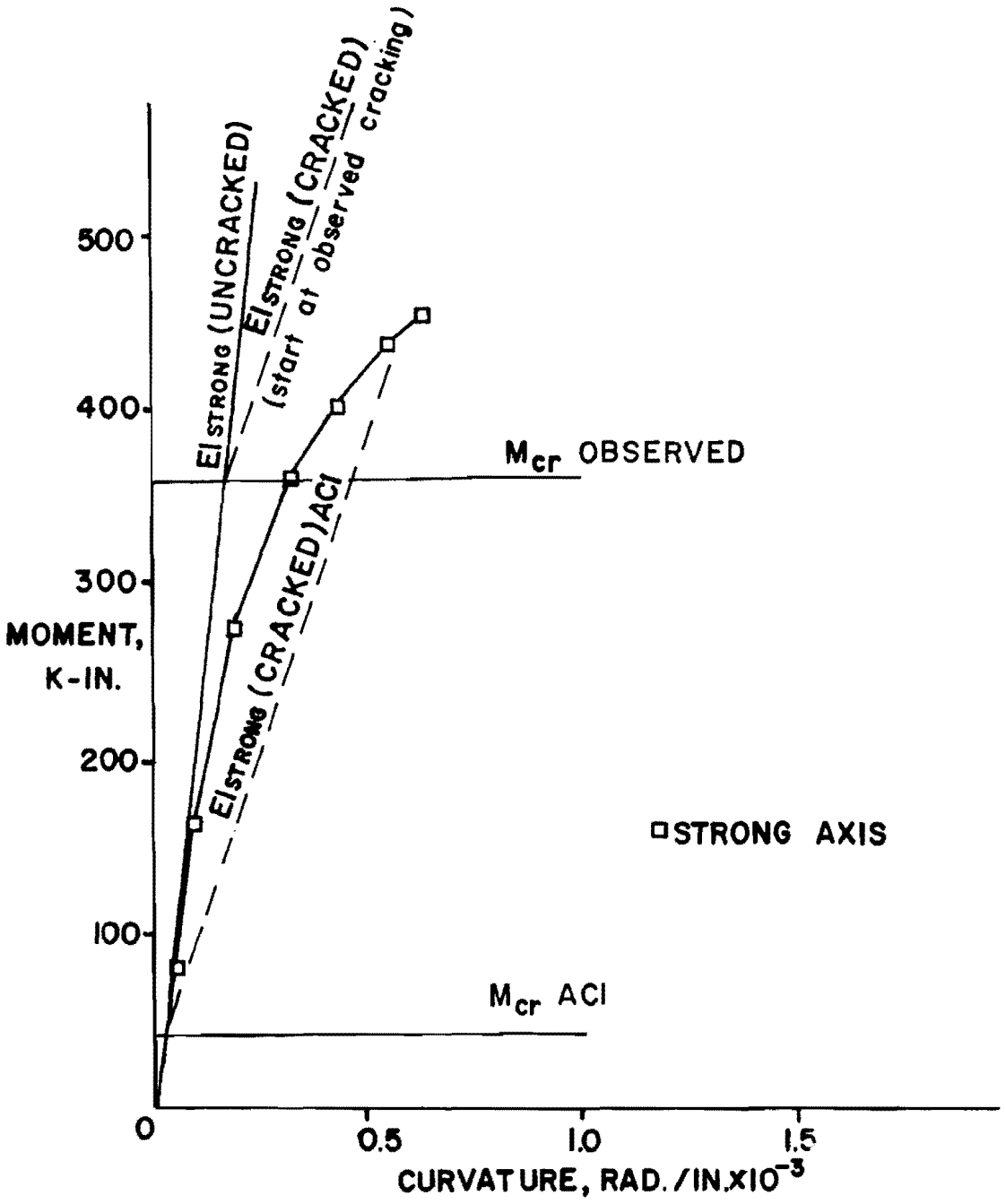

Fig. 4.12 Moment-curvature relationship, Specimen C-14 (P_u/P_o = 0.374, strong axis uniaxial bending test)

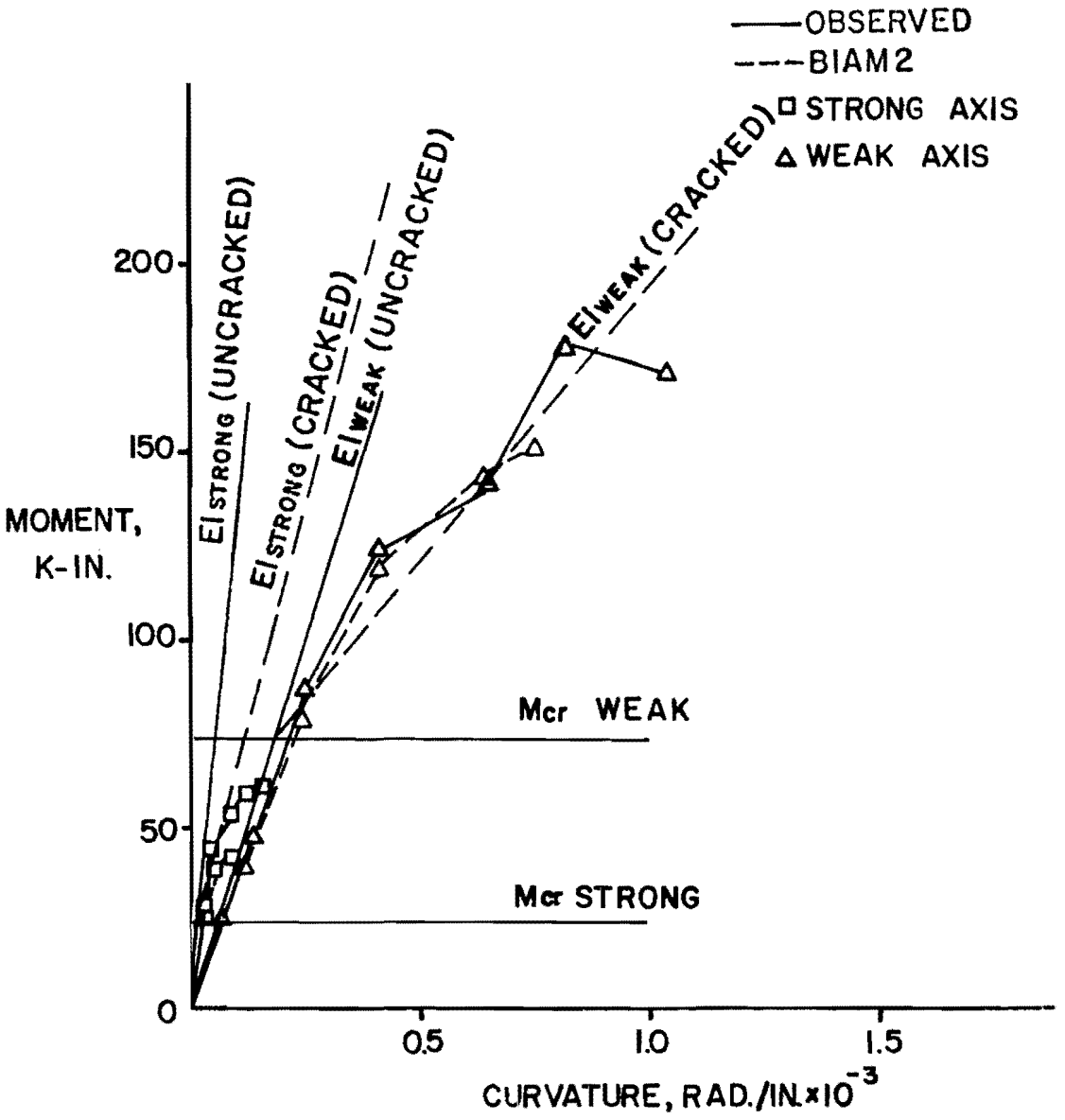

Fig. 4.13 Moment-curvature relationship, Specimen RC-1 (P_u/P_o = 0.472, load angle 22.5°)

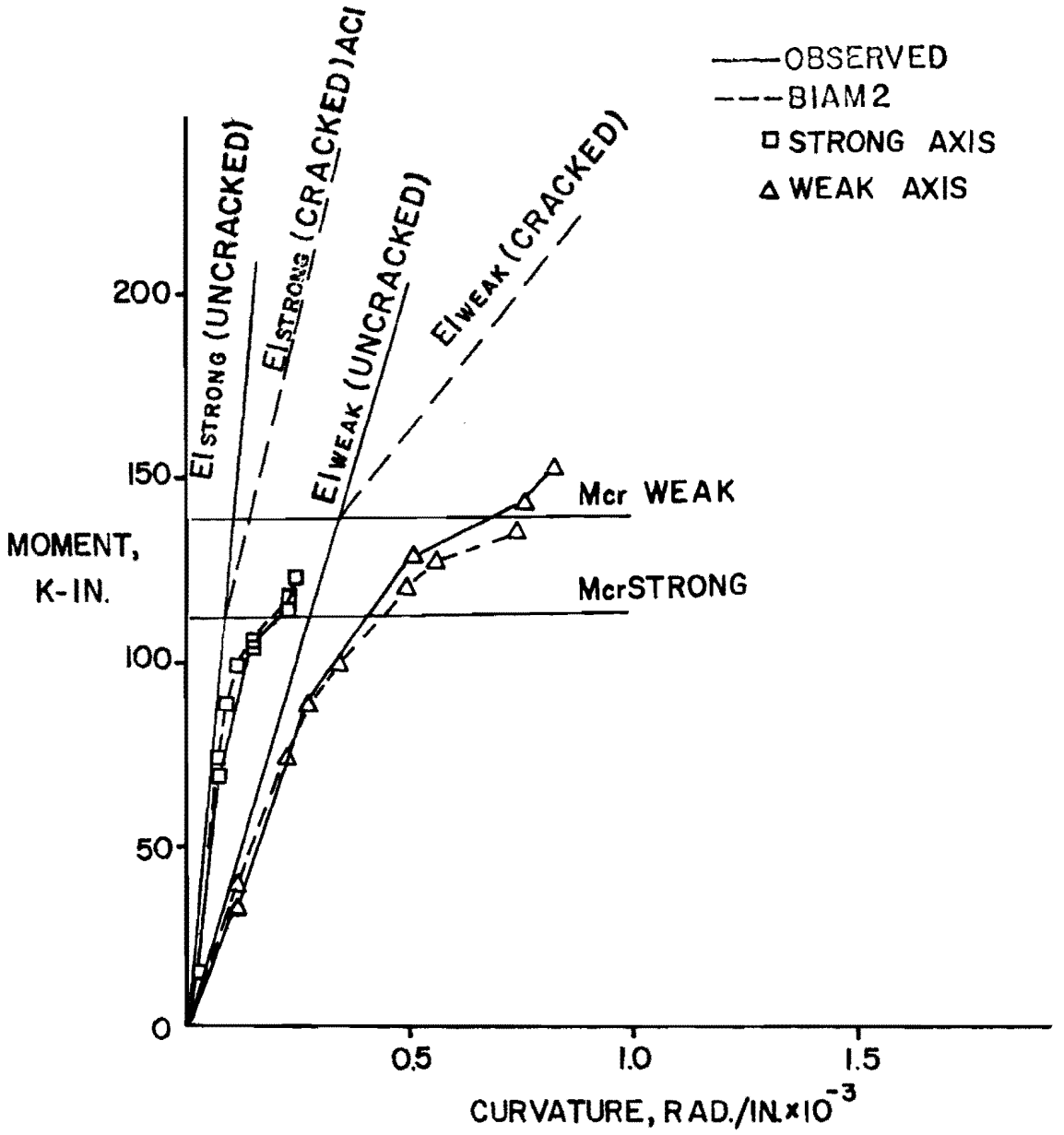

Fig. 4.14 Moment-curvature relationship, Specimen RC-2 (P_u/P_o = 0.478, load angle 45°)

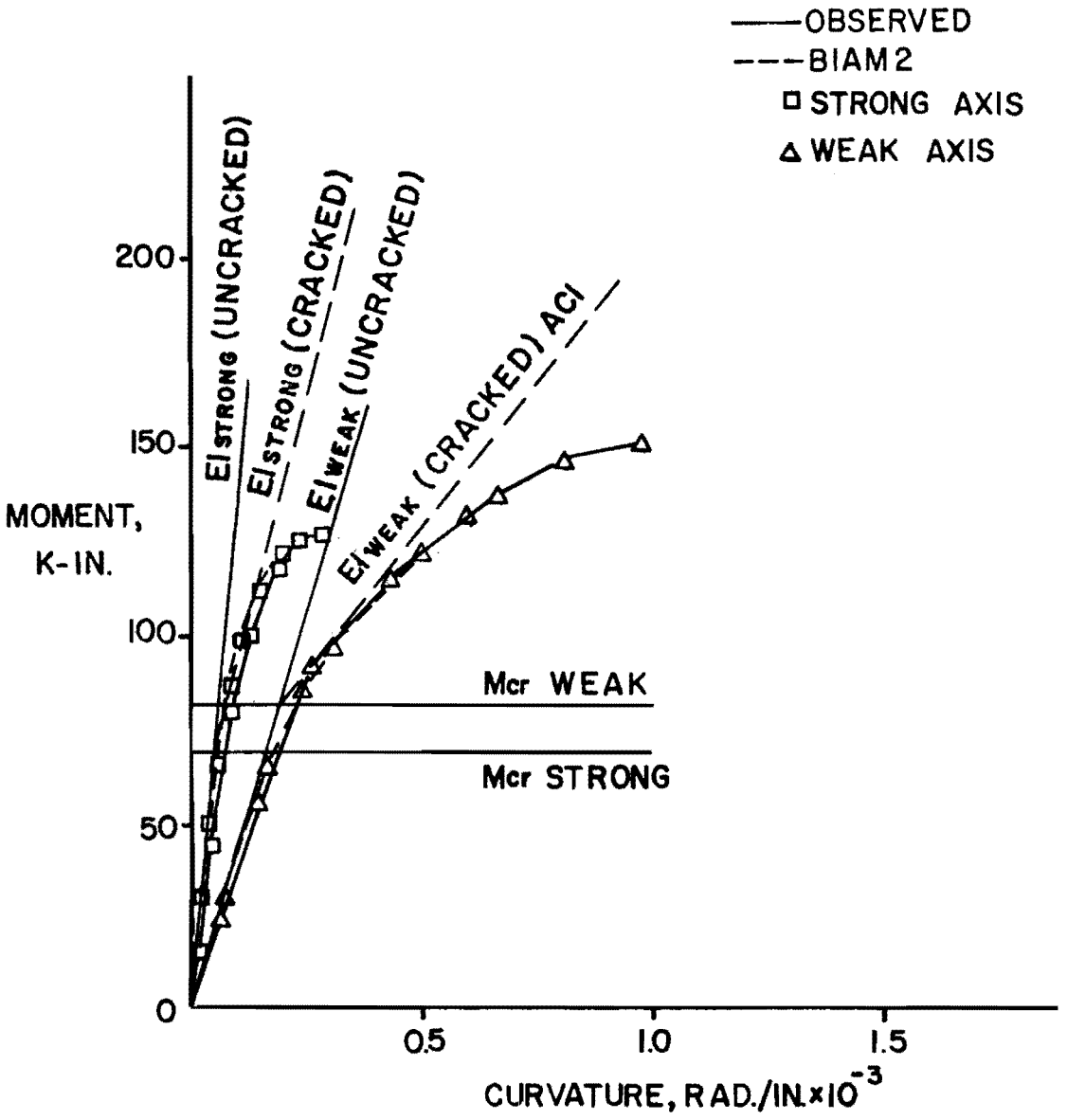

Fig. 4.15 Moment-curvature relationship, Specimen RC-3 (P_u/P_o = 0.353, load angle 45°)

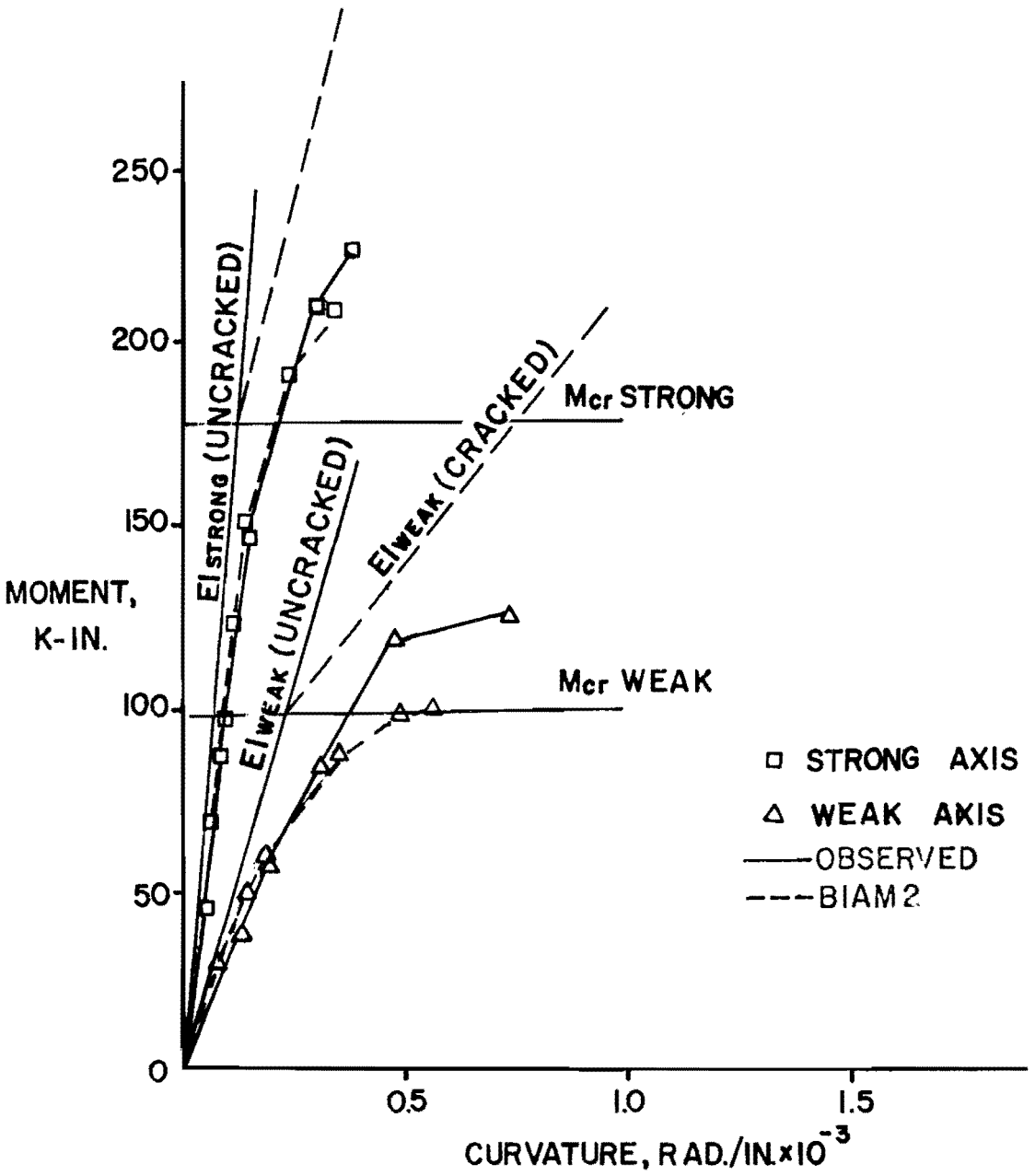

Fig. 4.16 Moment-curvature relationship, Specimen RC-4 (P_u/P_o = 0.485, load angle 67.5°)

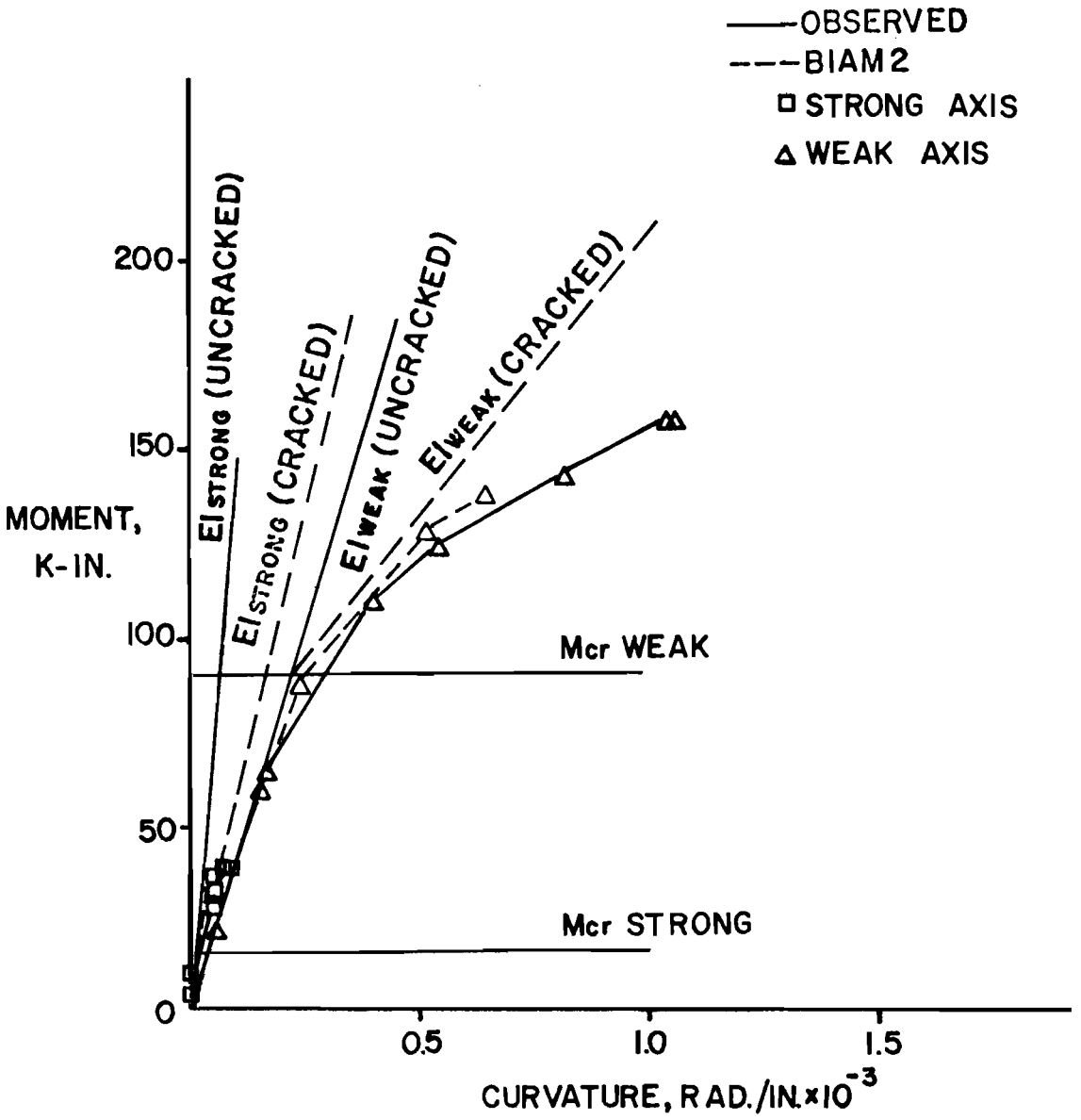

Fig. 4.17 Moment-curvature relationship, Specimen RC-5 (P_u/P_o = 0.337, load angle 22.5°)

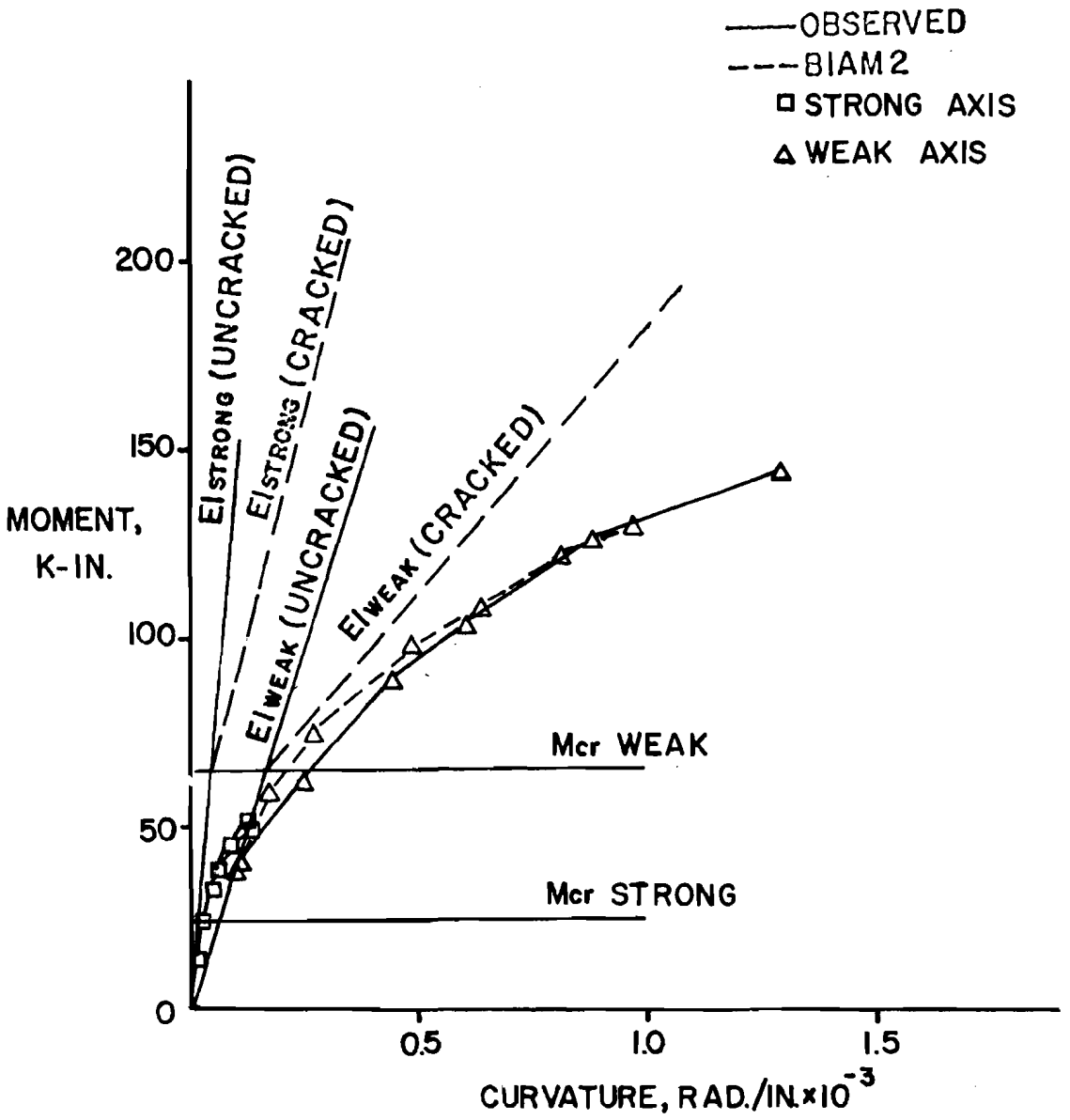

Fig. 4.18 Moment-curvature relationship, Specimen RC-6 (P_u/P_o = 0.233, load angle 22.5°)

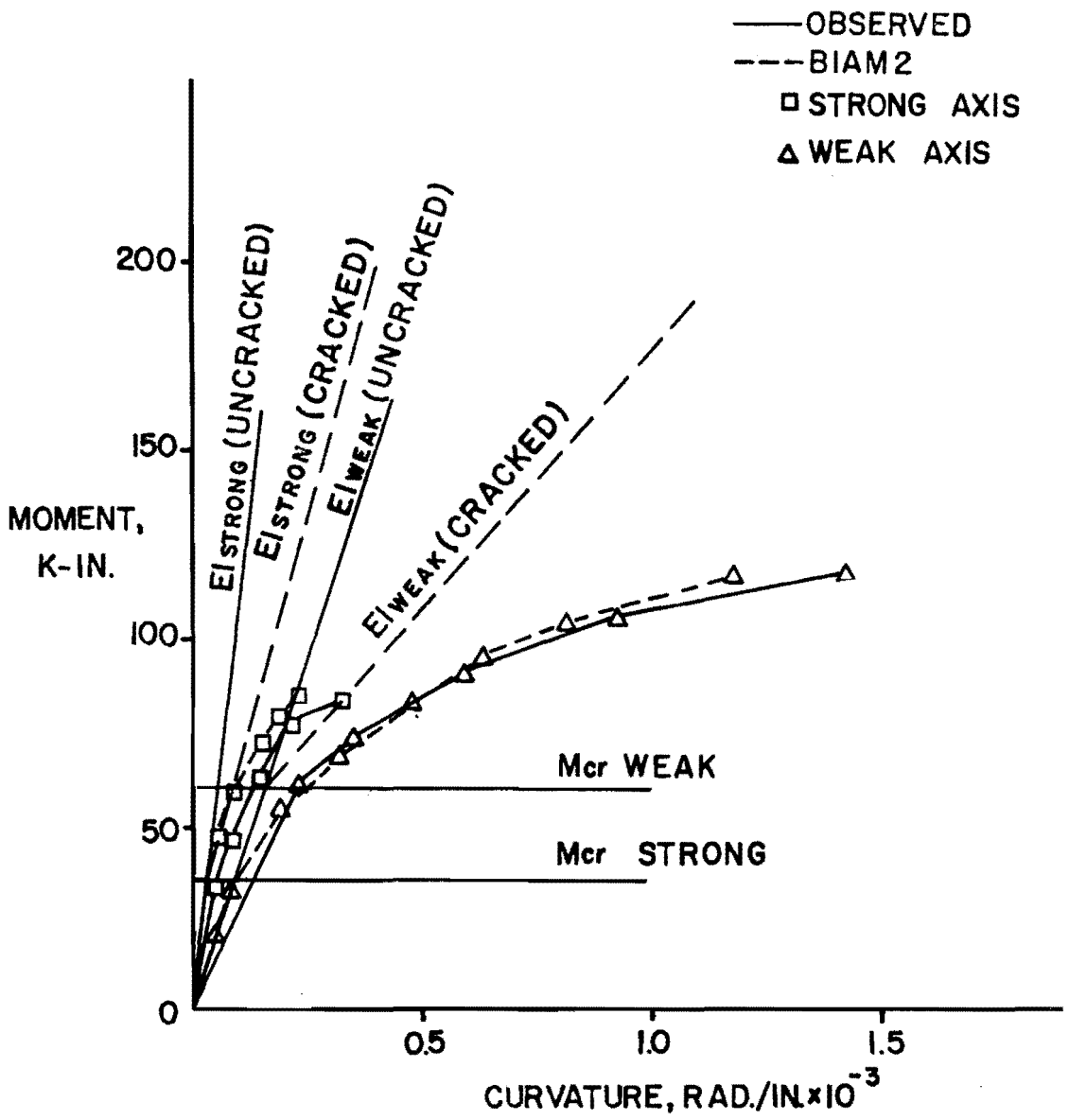

Fig. 4.19 Moment-curvature relationship, Specimen RC-7 (P_u/P_o = 0.177, load angle 45°)

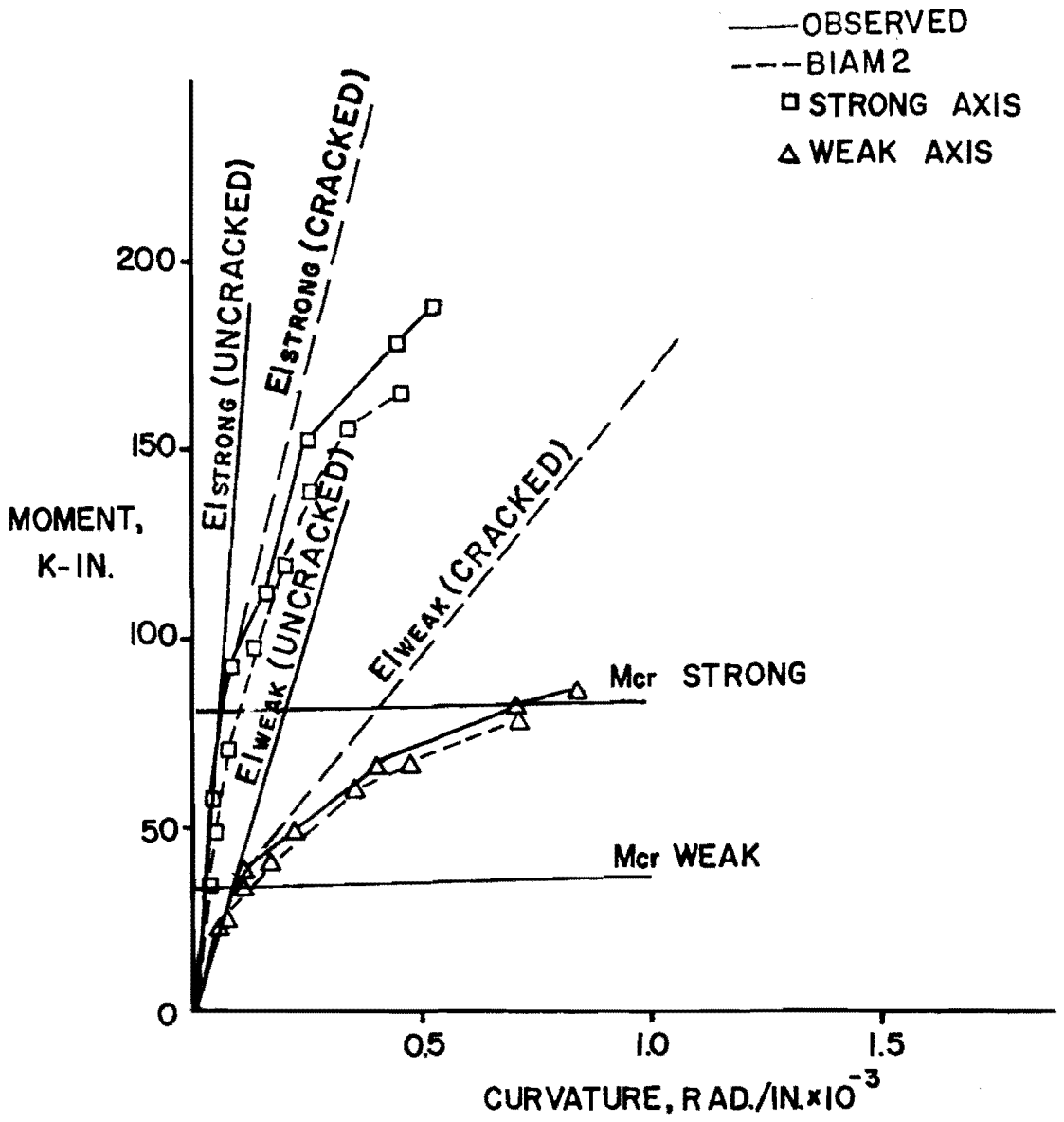

Fig. 4.20 Moment-curvature relationship, Specimen RC-8 (P_u/P_o = 0.174, load angle 67.5°)

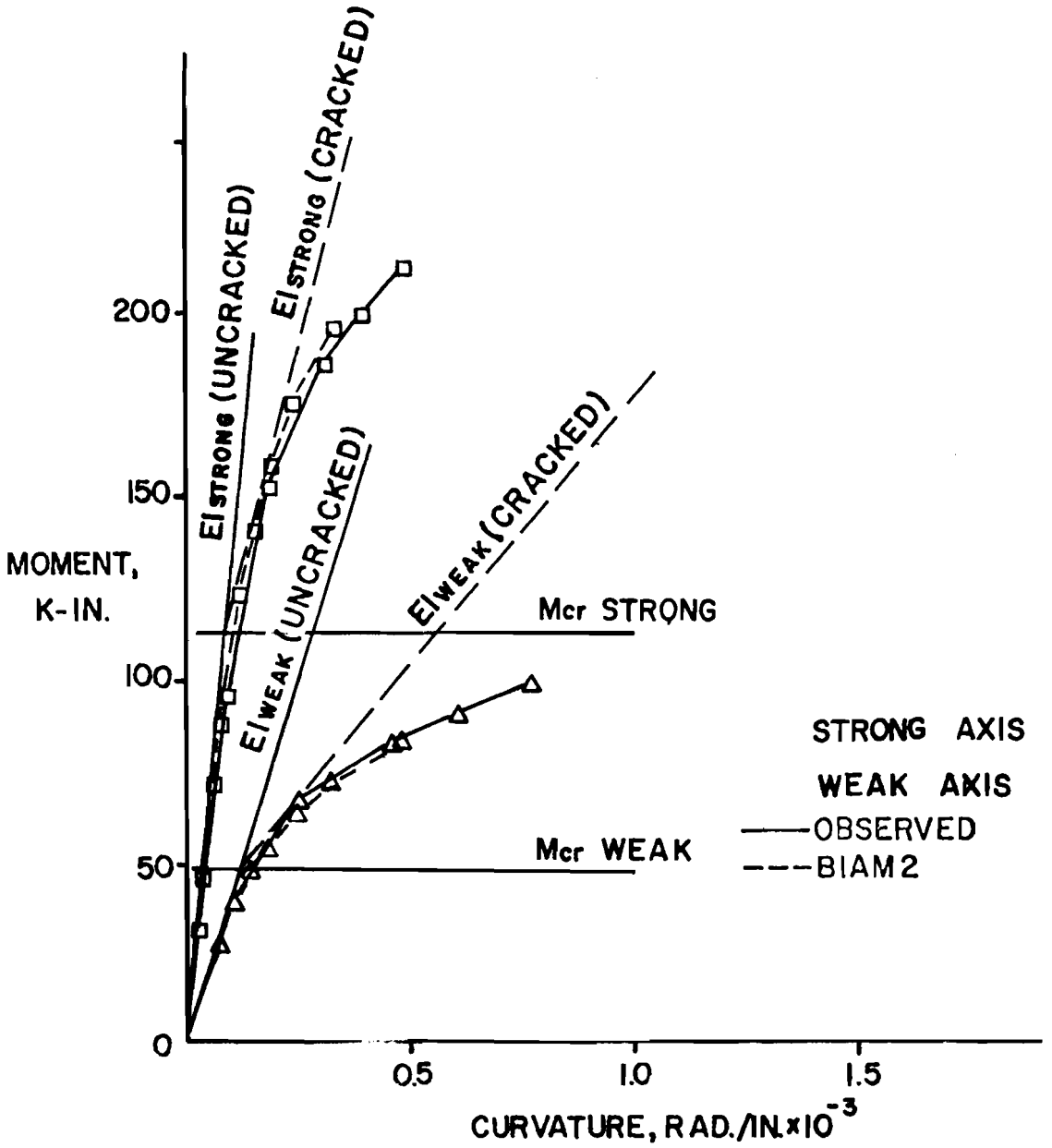

Fig. 4.21 Moment-curvature relationship, Specimen RC-9 (P_u/P_o = 0.351, load angle 67.5°)

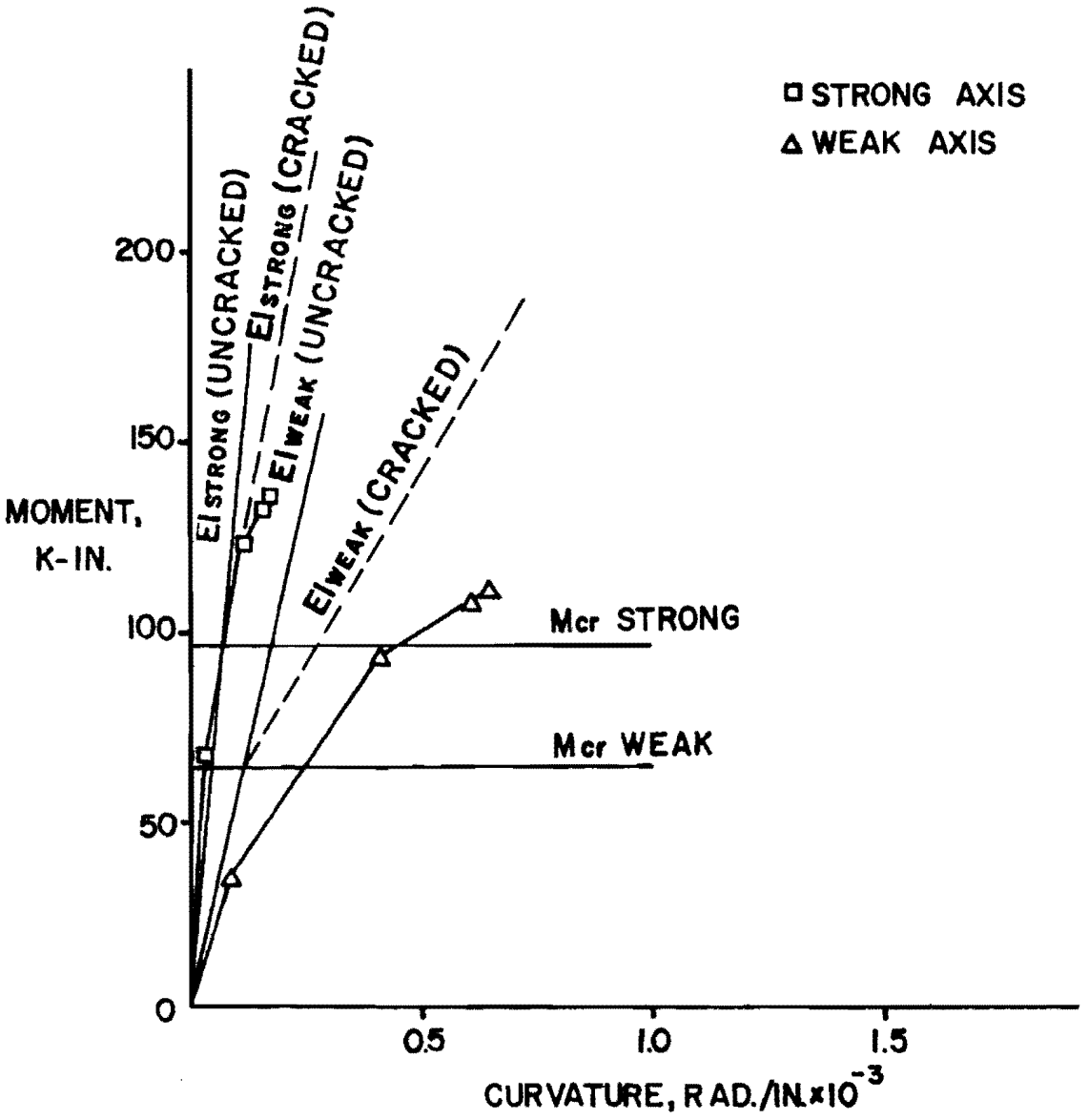

Fig. 4.22 Moment-curvature relationship, Specimen C-5 (P_u/P_o = 0.190, load angle 45°)

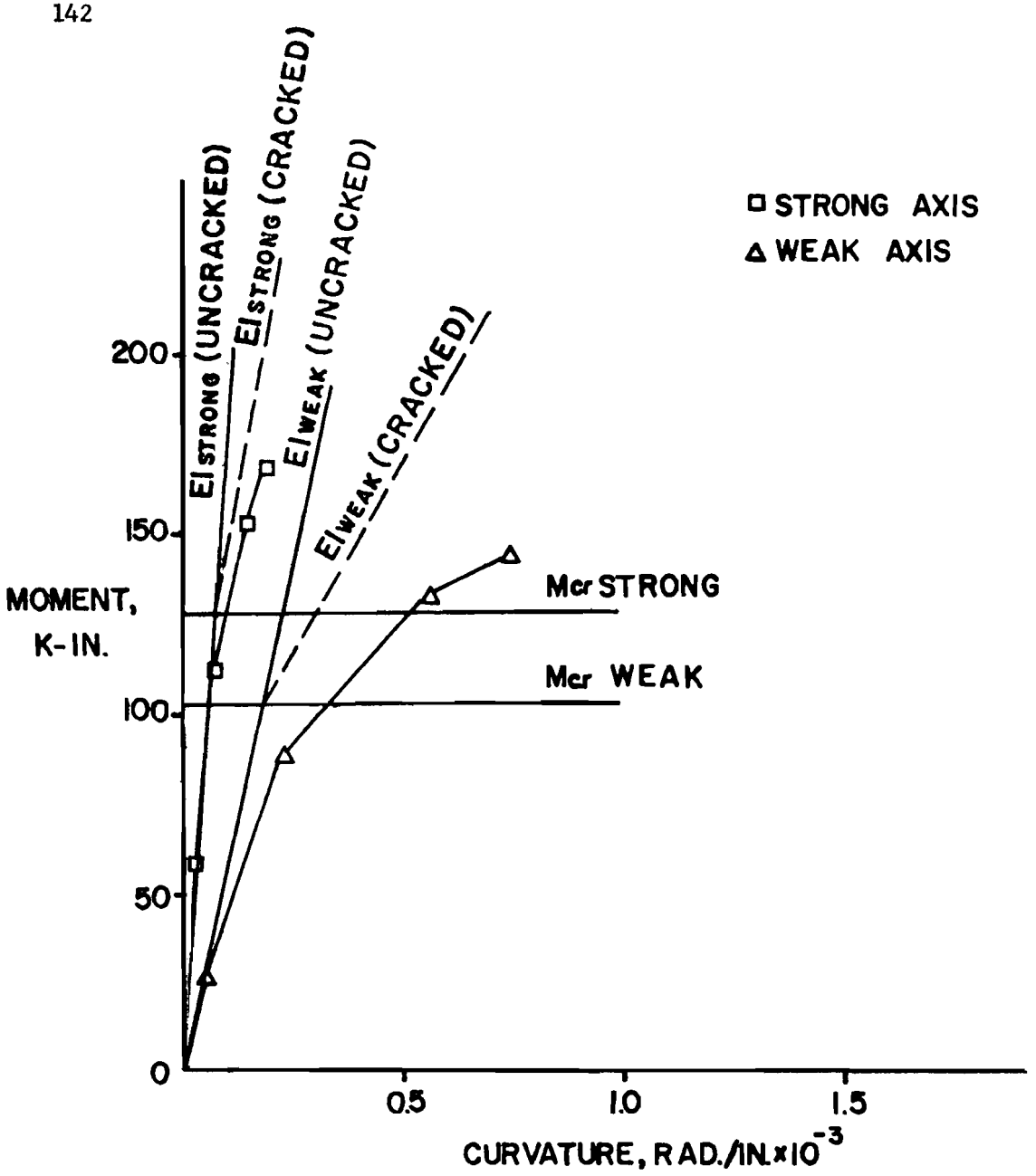

Fig. 4.23 Moment-curvature relationship, Specimen C-6 (P_u/P_o = 0.349, load angle 45°)

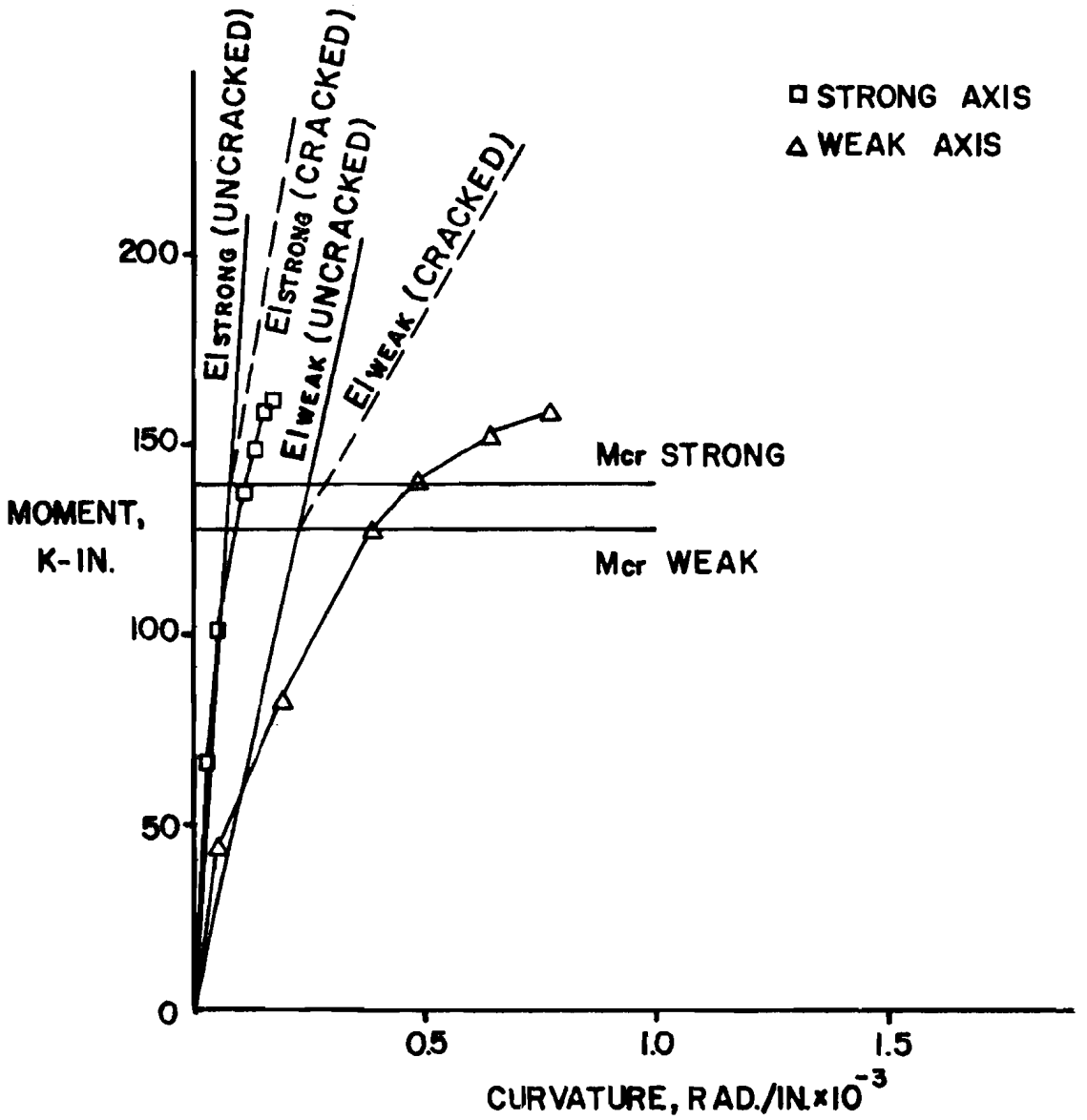

Fig. 4.24 Moment-curvature relationship, Specimen C-7 (P_u/P_o = 0.529, load angle 45°)

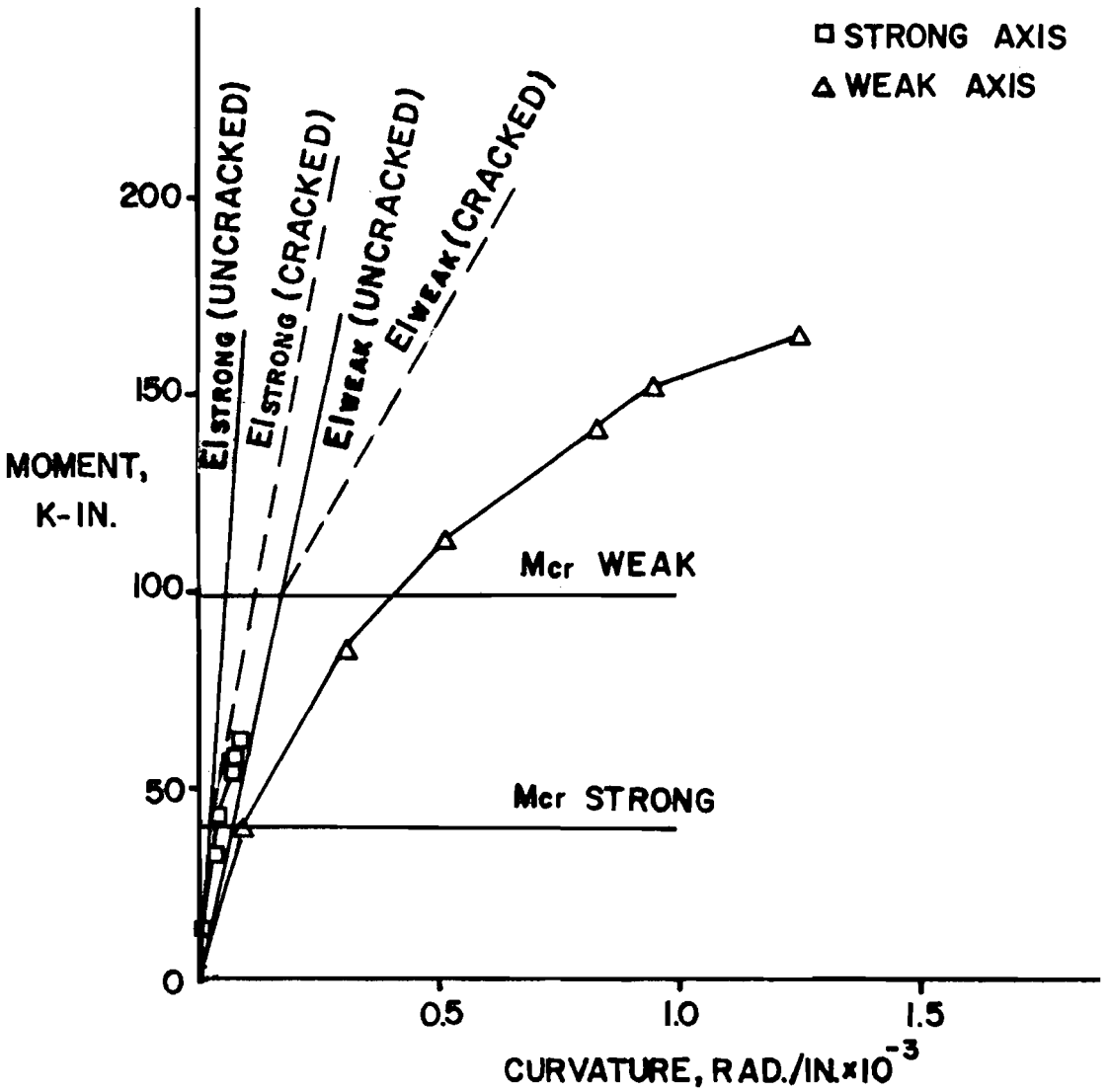

Fig. 4.25 Moment-curvature relationship, Specimen C-8 (P_u/P_o = 0.203, load angle 22.5°)

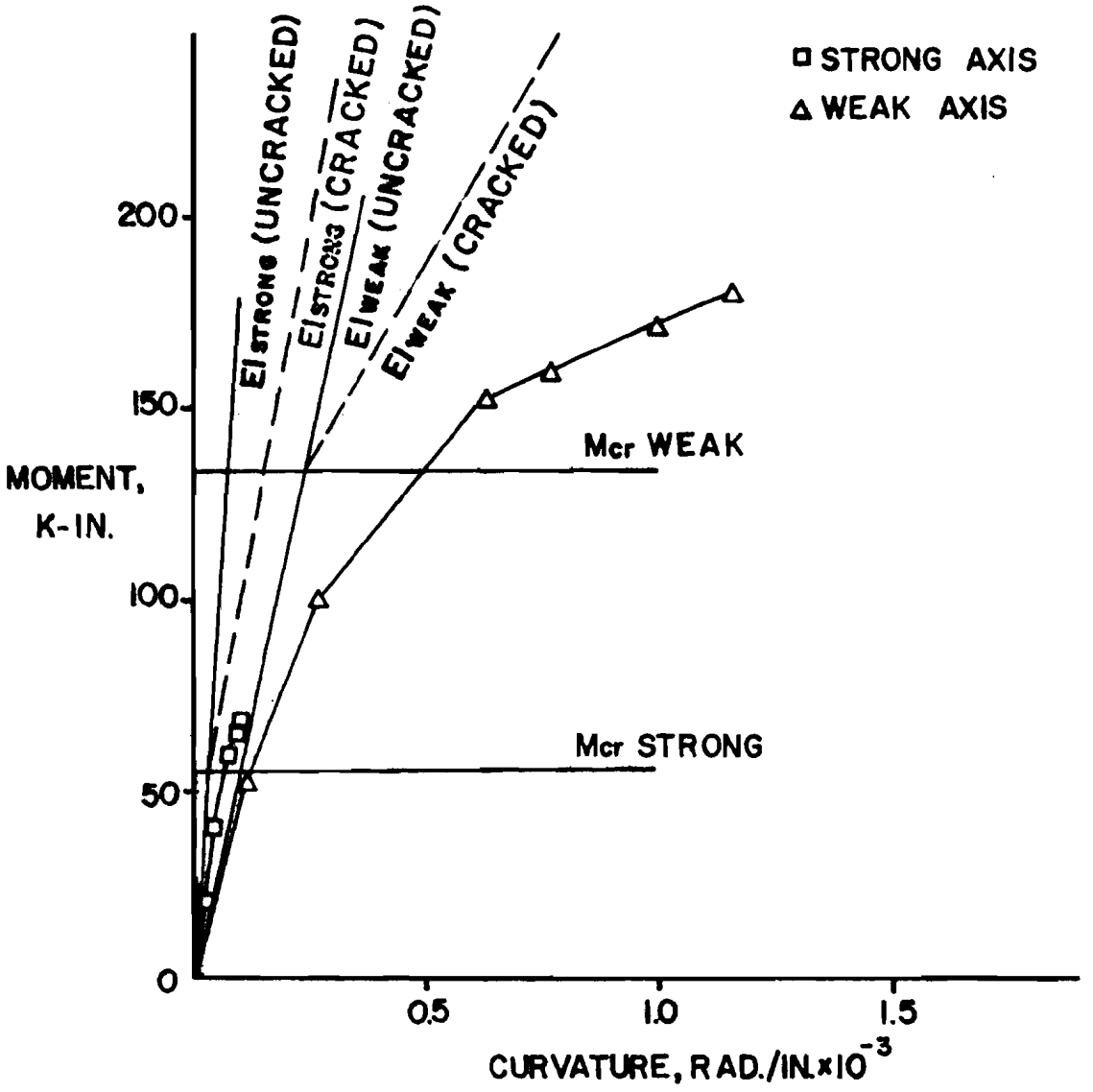

Fig. 4.26 Moment-curvature relationship, Specimen C-9 (P_u/P_o = 0.355, load angle 22.5°)

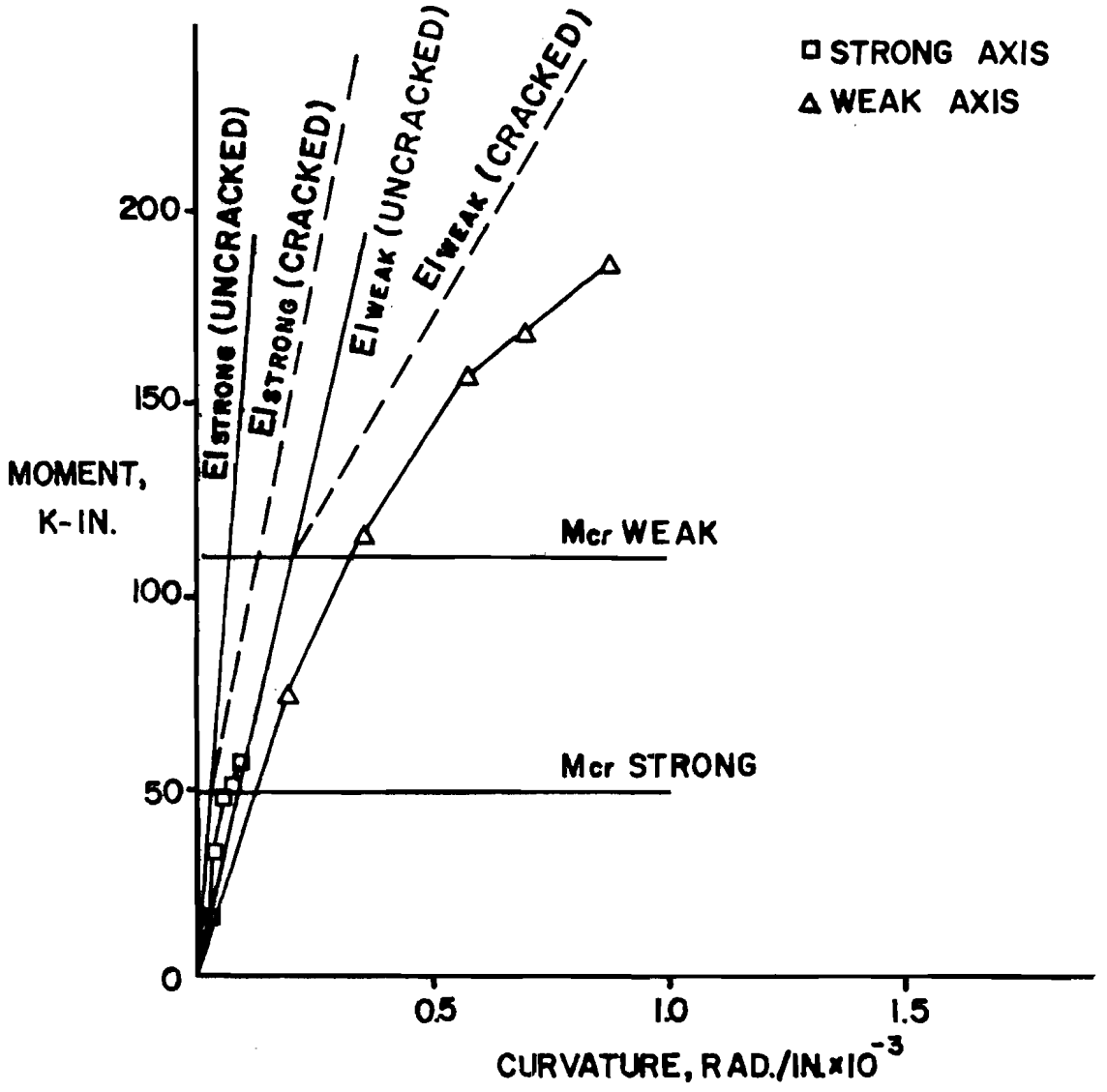

Fig. 4.27 Moment-curvature relationship, Specimen C-10 (P_u/P_o = 0.521, load angle 22.5°)

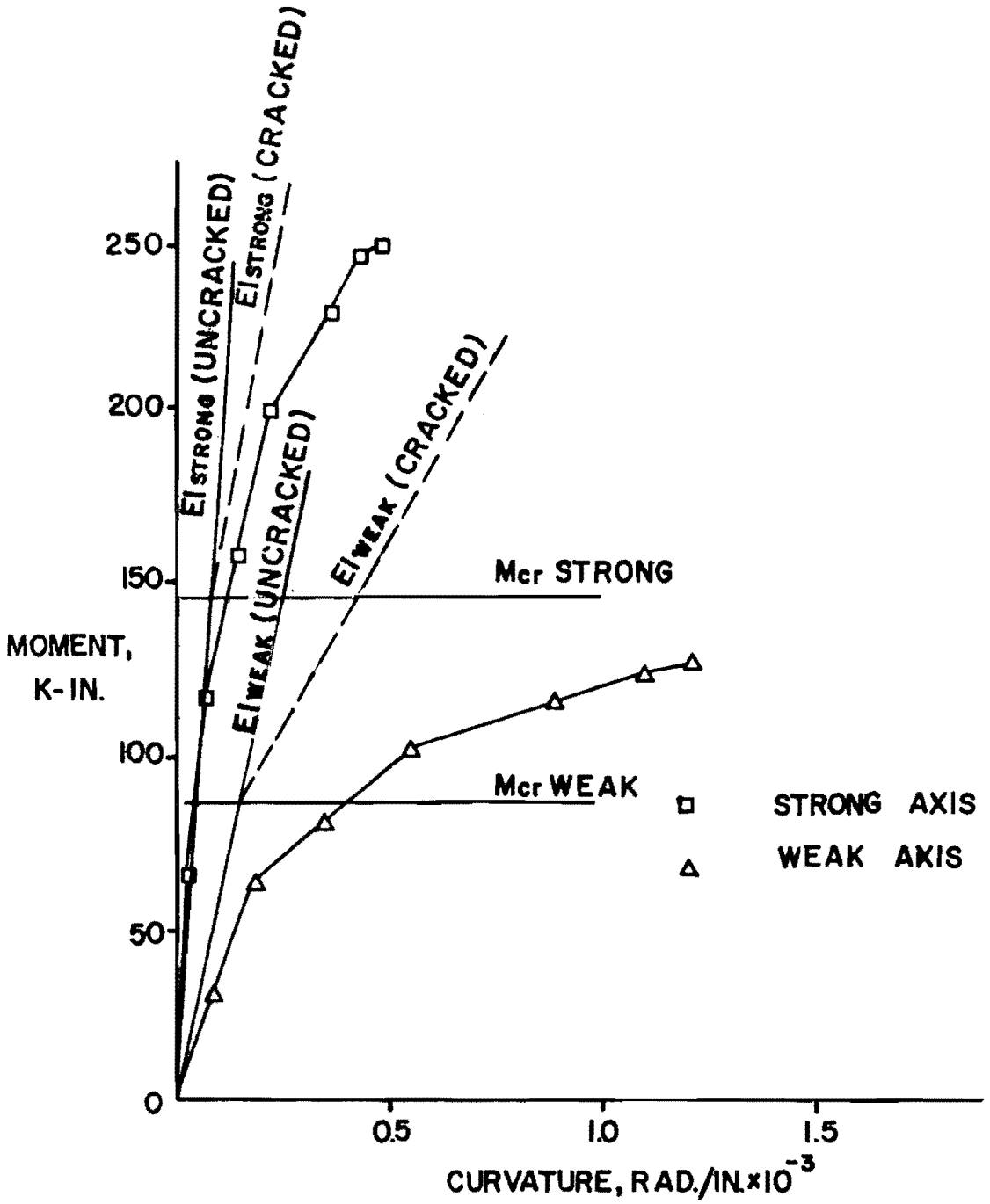

Fig. 4.28 Moment-curvature relationship, Specimen C-11 (P_u/P_o = 0.186, load angle 67.5°)

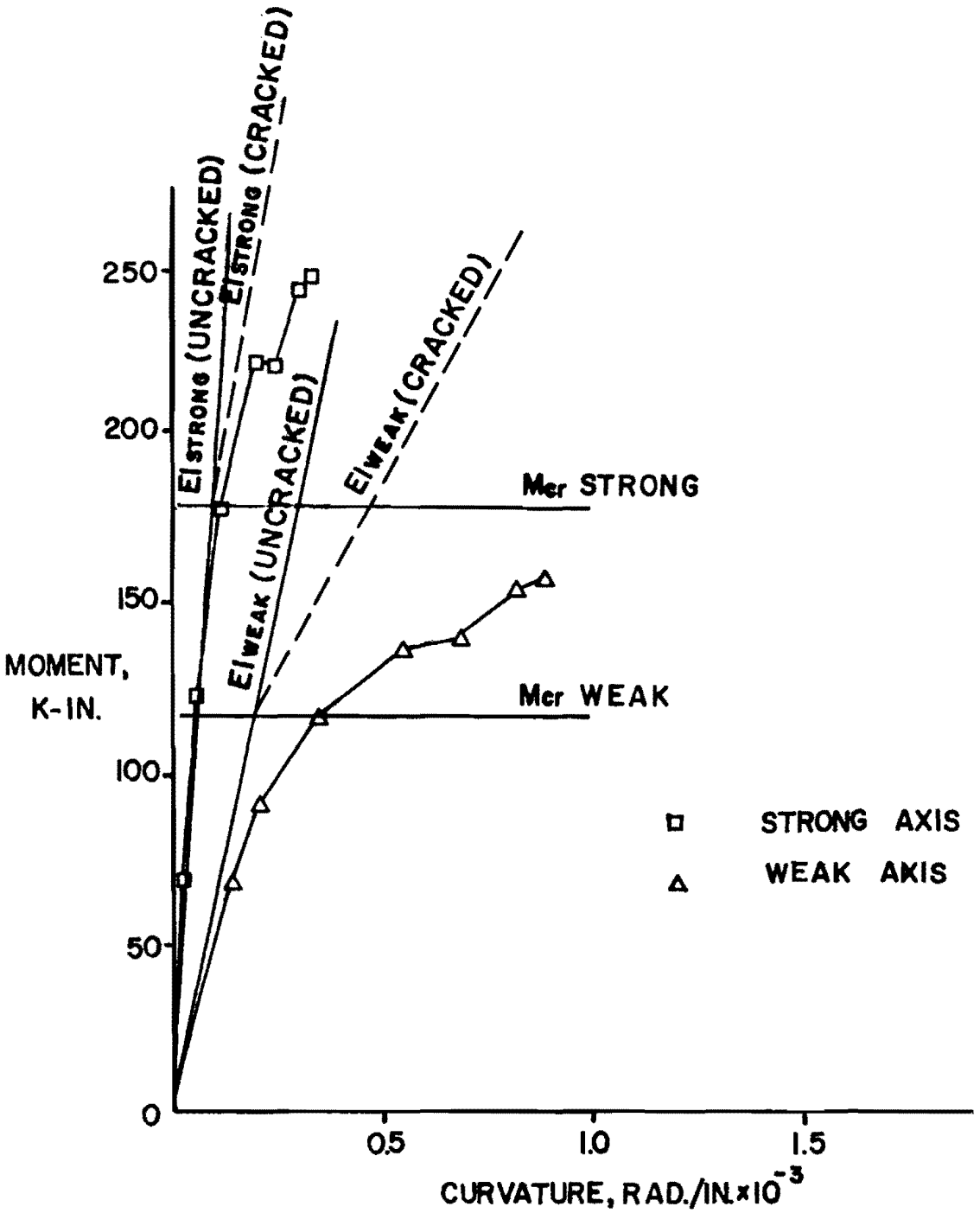

Fig. 4.29 Moment-curvature relationship, Specimen C-12 (P_u/P_o = 0.332, load angle 67.5°)

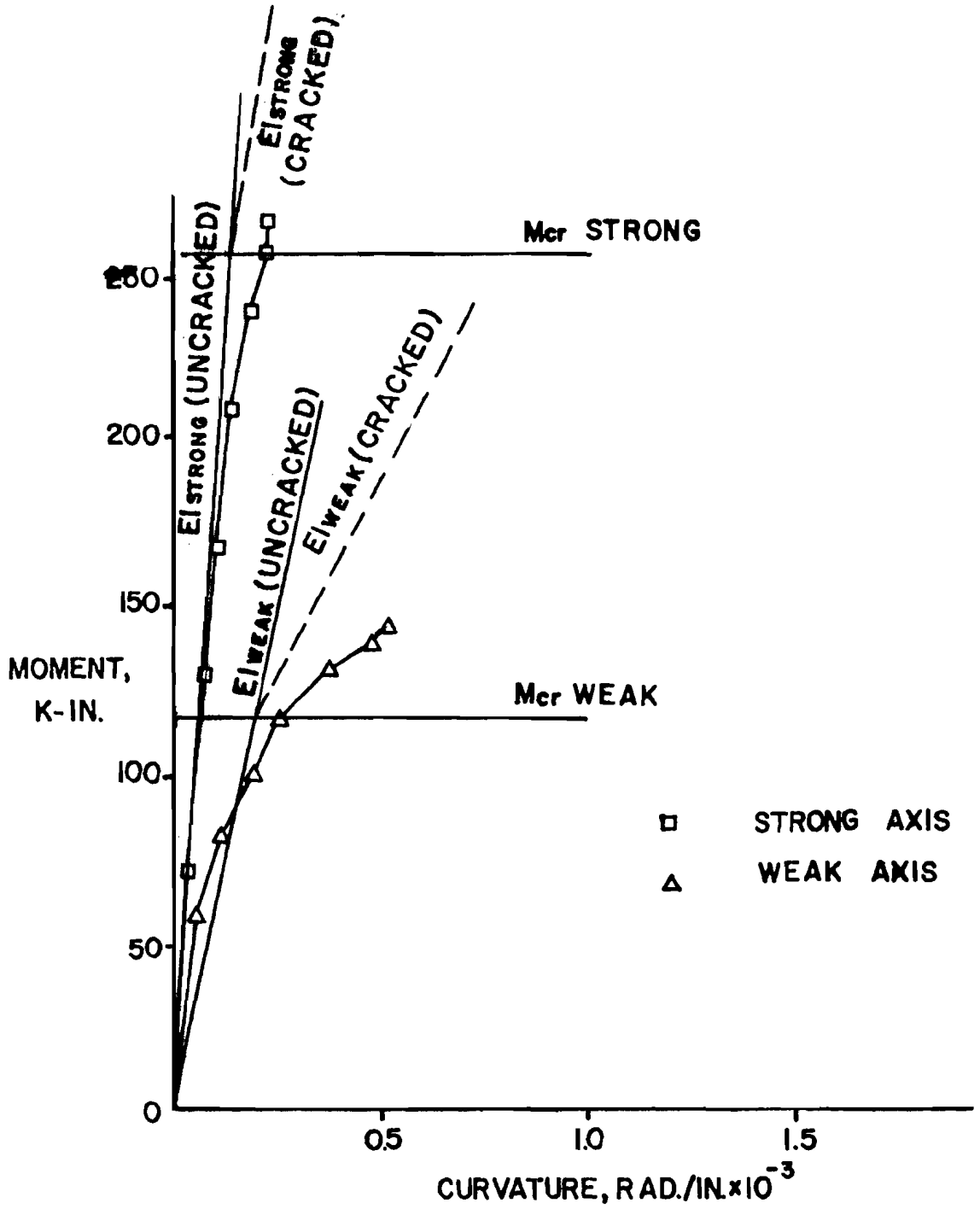

Fig. 4.30 Moment-curvature relationship, Specimen C-13 (P_u/P_o = 0.486, load angle 67.5°)

for all specimens are shown in Table 5.1 in Chapter 5. Cracked section estimates of EI are shown by dashed lines in Figs. 4.7 to 4.30. The initial slope of the graph representing uncracked EI was changed to the cracked EI slope at the moment for which cracking was observed visually during the loading sequence. The ACI[1] Building Code recommends in Sec. 9.5.2.2 the estimation of cracking moment, $M_{cr} = \frac{f_r I_g}{y_t}$ where $f_r = 7.5\sqrt{f'_c}$, I_g = gross moment of inertia of the section, and y_t = distance from centroidal axis of gross section to extreme fiber in tension. Table 4.6 shows the values of the computed cracking moment for each axis and the cracking moment as observed for every specimen. The comparison between the computed and observed cracking moments indicated either that the ACI Code formula underestimated the cracking moment or visual evidences existed well after theoretical cracking both for strong axis and weak axis. Only in Specimens RC-1, RC-5, and RC-6 were the observed strong axis cracking moments lower than the moments computed according to the ACI Code equation. Lower observed values were recorded with the load angle of $22\text{-}1/2^{o}$ (i.e., the weak axis moment was greater than the strong axis moment). Specimens with load angles of $22\text{-}1/2^{o}$ on both oval-shaped and rectangular columns had observed cracking moments closer to the computed values for strong axis bending. For other load angles the observed moment was significantly higher than the computed moment for strong axis bending. The differences were greater for weak axis moment on all specimens.

For uniaxial moment tests, the computed cracking moment was also less than the observed value. Observed and computed cracking moments of uniaxial test specimens are shown in Figs. 4.7 to 4.12. The graphs show that the slope of the M-ϕ relationship began to decrease at a moment between the observed and computed cracking moments. This observation indicates that the ACI Code equation underestimates the cracking moment, and the crack should occur before becoming a visible crack, so that the observed values were too high. In this report the cracking moments which are shown in Figs. 4.13 to 4.30 are the moments

TABLE 4.6 CRACKING MOMENT

Specimen	$f_r = 7.5\sqrt{f'_c}$	$M_{cr} = f_r I_g / y_t$*		M_{cr} observed**	
	psi	M_{cr} strong k-in.	M_{cr} weak k-in.	M_{cr} strong k-in.	M_{cr} weak k-in.
RC-1	524.2	35.4	19.7	24.7	75.5
RC-2	523.4	35.3	19.6	113.0	139.8
RC-3	541.4	36.5	20.3	69.6	82.4
RC-4	539.8	36.4	20.2	180.7	100.7
RC-5	531.0	35.8	19.9	16.3	91.2
RC-6	498.9	33.7	18.7	24.2	65.7
RC-7	494.7	33.4	18.6	36.0	61.9
RC-8	500.1	33.8	18.8	81.5	33.8
RC-9	514.2	34.7	19.3	116.9	50.0
C-5	494.1	37.9	27.2	97.5	65.8
C-6	497.3	38.2	27.3	128.8	103.8
C-7	497.7	38.2	27.4	141.5	129.0
C-8	517.4	39.7	28.4	40.2	100.7
C-9	505.0	38.8	27.8	54.0	134.3
C-10	498.9	38.3	27.4	49.0	161.4
C-11	521.2	40.0	28.6	147.3	75.7
C-12	535.1	41.1	29.4	179.0	117.2
C-13	551.0	42.3	30.3	257.8	118.7
C-1	518.7	-	28.5	-	93.3
C-2	500.9	-	27.5	-	140.2
C-15	554.6	-	30.5	-	143.0
C-3	496.7	38.1	-	177.5	-
C-4	521.3	40.0	-	395.9	-
C-14	556.9	42.8	-	360.0	-

*From ACI Code, Sec. 9.5.2.2.

**Moment at load stage when first visible crack was noticed.

which were determined from ram pressures at the load stage at which the first visible crack was detected during the test.

Behavior of column stiffness as influenced by various parameters is discussed on the basis of the M-φ plots in Figs. 4.7 to 4.30. The influence of the thrust level and the load angle on the stiffness of columns will be discussed together with a comparison between the slope of the M-φ curve and the computed EI values before and after cracks occurred.

Influence of Thrust Level. Before cracking, the nominal EI for bending about the strong axis agrees well with the initial slope of the measured M-φ curve for both rectangular-shaped and oval-shaped columns in every level of thrust, as shown by virtually identical slopes to observed and analytical graphs at precracking stages. The slope of the M-φ curve decreased before reaching the observed cracking moment, as has been discussed, suggesting that cracking occurred and column stiffness decreased before visible cracks could be seen. The same phenomenon was observed for the weak axis stiffness of specimens under low thrust ($0.2P_o$ - $0.35P_o$) on both rectangular columns and oval-shaped columns with uniaxial eccentricities.

For weak axis bending, as thrust levels increased for rectangular columns, the nominal uncracked stiffness for bending about the weak axis suggested stiffer EI values than the measured values. The initial slope of the M-φ curve for bending about the weak axis on the oval-shaped columns was smaller than the nominal EI value at every thrust level.

For the cracked section, the strong axis stiffness for columns of both shapes showed obvious similarities between measured and estimated values of EI, although the computed EI was greater than the slope of the M-φ curve after cracking. The slope of the M-φ curve for bending about the weak axis after cracking showed that the nominal EI overestimated the section stiffness for both rectangular and oval columns at all levels of thrust.

Influence of Nominal Load Angle. The nominal initial stiffness (uncracked EI) for strong axis bending showed good agreement with the initial slope of M-φ curves at large moment angles. The load angle as used here refers to the angle for which the tangent equals the ratio of moment about the strong axis and weak axis. At a moment angle of $22\text{-}1/2^{o}$, the measured slopes deviated from the nominal EI and showed stiffness softer than calculated, especially on oval-shaped columns. For weak axis stiffness of biaxial bending specimens, no unique influence of load angle could be detected. All specimens showed that the initial slope of M-φ curves was smaller than the computed EI. However, better agreement was found for the weak axis uncracked stiffness of the uniaxial test specimens.

The observation of stiffness after cracking indicated reasonable agreement between measured and nominal EI values for bending about the strong axis. For weak axis values of EI, a smaller stiffness was detected from the slope of the measured M-φ curves than from the estimated cracked section stiffness. Specimens with small load angles ($22\text{-}1/2^{o}$) showed better agreement than specimens with large load angles, although no consistent relationship was apparent between load angle and the cracked section changes in EI.

The investigation of the stiffness of the columns could be summarized with the observation that before cracking, the nominal uncracked section was in good agreement with the EI measured from M-φ curves especially for strong axis bending. The observed cracking moment was higher than the moment at which the initial slope of the M-φ curve started to change to indicate softer or cracked section stiffness. After cracking, the nominal stiffness calculation overestimated the EI of the section, but it was within reasonable agreement for strong axis bending. Better results were observed for columns under low thrust than under high thrust. The nominal uncracked section EI gave a better estimation for columns with larger moment angles than those

with the smaller load angles. No relationship between stiffness and load angle could be observed after columns cracked.

M-φ Curve by BIAM2.[38] A computer program called BIAM2 prepared by Redwine[38] was used to predict the strength and stiffness behavior of rectangular columns in this test program. BIAM2 was coded to analyze pinned end columns loaded with biaxial bending with equal end eccentricities. For consistency of the analytical results and experimental results BIAM2 was modified to use the parabolic-rectangular stress-strain curve for concrete as previously described. A grid system to discretize the cross section was also used. Failure of columns was defined analytically to occur when the maximum strain of 0.0035 on any section was reached. The loading input was specified so that the axial thrust was applied first before the eccentricities on each major axis were made to increase gradually at a constant load angle the same as in the test specimen. Total thrust was maintained constant throughout. The tolerance limit for deflection, which was the control of convergence in BIAM2, was increased from 0.01 in. at early loads up to 0.05 in. near failure in order to improve the rate of convergence and the computational stability of the analytical model.

Analytical moment-curvature relationships for the midheight section of each rectangular column were plotted with dashed lines in Figs. 4.13 to 4.21. The M-φ plots from BIAM2 followed almost the same path as the observed M-φ curves. The failure moments at midheight from BIAM2 were lower than the observed moments in every specimen with the maximum difference not greater than 20 percent. The convergence procedure did not allow BIAM2 to approach the same ultimate limit as that observed. A summary of the end eccentricities from BIAM2 at failure is shown in Table 5.8 for a comparison with the results from the actual test.

CHAPTER 5

MEMBER STRENGTH

5.1 Introduction

The strength analysis in Chapter 4 considered only the cross-sectional strength of the columns. Data were taken from short column tests or from the position in which maximum moments were measured. No slenderness effect was included in the investigations that were reported in Chapter 4. Member strength is differentiated from cross section strength in that slenderness affects member strength.

In this chapter the strength of columns subjected to biaxial bending will be discussed with length effects included. In general, the methods that use moment amplification, such as required in the ACI Building Code,[1] will be employed in order to predict slenderness effects. Member strength as determined according to an analysis that employs the reciprocal thrust equation (Eq. 4.9) will be used in conjunction with moment magnification as recommended by the ACI Building Code for biaxial bending in slender columns, in order to compare analytic predictions with test results. Data from Drysdale[14] and from Wu[47] for short term loading tests of slender columns will be included in the data as well as a set of analytical model column variable lengths, but with the same cross-sectional properties as the rectangular columns of this test report. Recommended procedures for handling the effect of length will conclude this chapter.

5.2 Moment Magnification Required in the ACI Building Code

When a column is loaded with end eccentricity, supplementary moment must be considered along the column length in addition to the moment due to end eccentricity alone. In Fig. 5.1 a column with equal

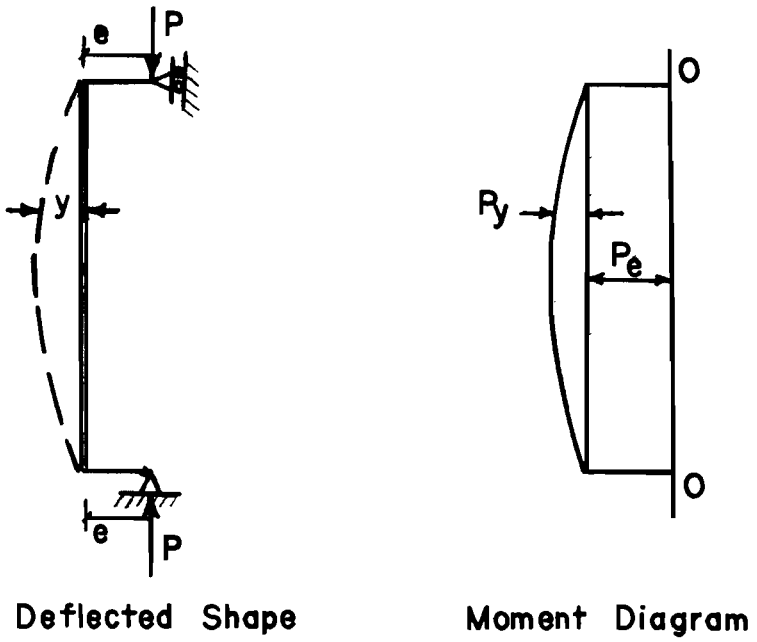

Fig. 5.1 Column subjected to end eccentricities

end eccentricities, e, is shown subjected to a moment Pe at each end. Secondary moments Py due to lateral displacements of the column axis will increase the magnitude of moment between column ends. The deflection y is greatly dependent on the overall length, so that this secondary effect is called a "long column effect".

If cross section strength is uniformly constant, the capacity of a column will decrease as length increases, because between the ends of the column the secondary moment Py must be sustained in addition to the end moment Pe. The amount of secondary moment Py increases with length.

The three curves A, B, and C in Fig. 5.2 show graphs of maximum (midheight) moment and thrust in short, intermediate, and long columns under the same end eccentricity e.

Curve 1 illustrates the strength interaction diagram for failure thrust and moment at all cross sections. When the thrust moment condition at any point along the column intersects the interaction curve,

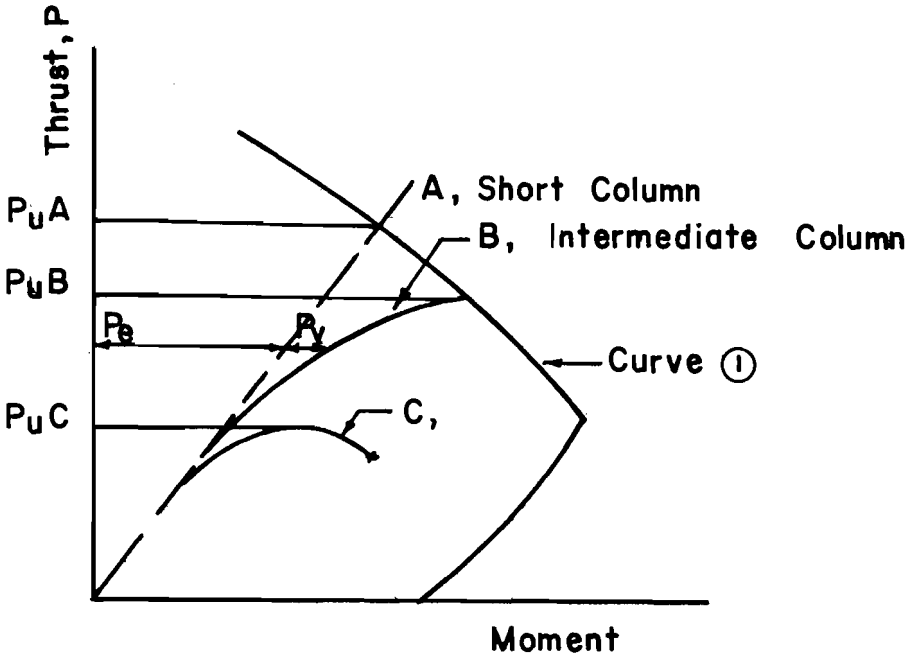

Fig. 5.2 Interaction diagram and load-moment patterns of columns

material failure (defined as the stage at which crushing and spalling of concrete occurred on extreme compression fibers) of the column can be assumed to have occurred. The load-moment curve A for a very short column is a straight line. For intermediate length columns, the auxiliary or secondary moments Py increase nonlinearly as P increases, and the column fails at an axial load lower than the short column capacity, because of the larger moment at the failure section. Long column instability is represented by curve C, which suggests that a maximum thrust cannot be sustained until moments increase enough to reach the interaction diagram for strength.

The ACI Building Code (ACI 318-71)[1] requires that secondary or Py moments be considered for the design of slender compression members. The Code groups columns into three slenderness categories based on the slenderness ratio $k\ell/r$ (effective length of column to radius of gyration of cross section). A short single curvature column is said to

have a slenderness ratio less than 22 for which the effect of slenderness may be neglected. At the other extreme, for all compression members with $k\ell/r$ greater than 100, a special analysis that includes the influence of axial load, variable moment of inertia or member stiffness and the affect of lateral deflection on force and moment must be made. Columns with $k\ell/r$ less than 100 can be designed using the design axial load and a magnified design moment, M_c, defined as (quoted from ACI 318-71, Chap. 10)

$$M_c = \delta M_2 \qquad 5.1$$

where

$$\delta = \frac{C_m}{1 - \frac{P_u}{\varphi P_c}} \geq 1.0 \qquad 5.2$$

and

$$P_c = \frac{\pi^2 EI}{(k\ell)^2} \qquad 5.3$$

in which

M_c = Moment to be used for design of compression members

M_2 = Value of larger design end moment on compression member

δ = Moment magnification factor

C_m = A factor relating the actual moment diagram to an equivalent uniform moment diagram

$$C_m = 0.6 + 0.4\, M_1/M_2 \geq 0.4$$

M_1 = Value of smaller design end moment on compression member, positive if member is bent in single curvature, negative if bent in double curvature

P_u = Axial design load in compression member

φ = Capacity reduction factor

P_c = Critical load

EI = Flexural stiffness of compression members

$k\ell$ = Effective length of compression members

In this report the columns to be analyzed are assumed to be pinned at their ends and subjected to equal end moments that create a deflected shape that is called symmetric single curvature. Single

curvature simply indicates curvature of a single direction as opposed to double curvature which would involve a point of inflection between ends of the column. The factor C_m in Eq. 5.2 is 1.0 for symmetric single curvature, and the effective length coefficient k is also 1.0. Since laboratory studies will involve measured material strengths and dimensions, no capacity reduction factor φ should be applicable, and φ will be taken as unity. The moment magnification factor δ should be applied to moments that have been computed on the basis of a first order frame analysis. First order analysis is an analysis performed without considering secondary effects of lateral displacements of joints or members.

For members subjected to bending about both principal axes, the ACI Building Code requires the amplification of moments in both directions, each δ factor determined as if bending occurred separately about each axis. With C_m, k, and φ equal to 1.0, the magnified factor can be expressed as

$$\delta = \frac{1}{1 - P_u/P_c} \qquad 5.4$$

where

$$P_c = \frac{\pi^2 EI}{\ell^2} \qquad 5.5$$

There may be differences in the cross section stiffness factor EI values for each axis of bending and corresponding differences in δ values for each axis of bending.

5.2.1 EI Computed from ACI Code. The value of compression member flexural stiffness EI, as specified by the ACI Building Code[1] may be taken either as

$$EI = \frac{\frac{E_c I_g}{5} + E_s I_s}{1 + \beta_d} \qquad \text{ACI (10-7)}$$

or $$EI = \frac{\frac{E_c I_g}{2.5}}{1 + \beta_d} \qquad \text{ACI (10-8)}$$

where β_d = the sustained load factor which for short term loading can be taken as zero

E_c = the modulus of elasticity of concrete
= $57000\sqrt{f'_c}$ in psi

E_s = the modulus of elasticity of steel

I_g = the gross moment of inertia of the concrete cross section about the centroidal axis of bending

I_s = the moment of inertia of reinforcement about the centroidal axis of bending of the member cross section

The discussion in the Commentary of the ACI Building Code[2] and in Chapter 14.18 of Ref. 18 recommends that for small percentages of reinforcement (ρ_t about 0.01 to 0.02), Eq. ACI(10-8) gives a good approximation of EI, while Eq. ACI(10-7) is preferable for larger percentages of reinforcement. The approximate EI from these two equations when compared to the theoretical EI computed from the slopes of thrust-moment-curvature functions gives a variety of results. The variety, however, tends always to predict EI softer than that measured. Since the EI values as computed from these equations are lower than measured values, the size of δ should be larger than those determined from tests or from more accurate estimates of EI. No published discussions of the moment magnifier for columns under biaxial bending have been found. The study in this chapter includes the observation of moment magnifiers for columns under compression with bending about both axes.

Table 5.1 contains calculated values that were used to determine EI from Building Code Eqs. (10-7) and (10-8) applied to the cross section properties of all 24 specimens in the test series reported here. Because the percentage of steel ρ_t was only 0.011, Eq. (10-8) gives larger values of EI than Eq. (10-7) for both strong axis and weak axis bending.

5.2.2 Moment Magnifiers According to ACI Code Compared with Tests. With the stiffness listed in Table 5.1, the critical loads, P_c,

TABLE 5.1 FLEXURAL STIFFNESS ACCORDING TO ACI BULIDING CODE

Specimen	E_c ksi	I_s	I_w	Specimen Data: Strong Axis E_cI_g	Specimen Data: Strong Axis E_sI_s	Specimen Data: Weak Axis E_cI_g	Specimen Data: Weak Axis E_sI_s	ACI Eq. (10-7) $EI = E_cI_g/5+E_sI_s$: Strong	ACI Eq. (10-7): Weak	ACI Eq. (10-8) $EI = E_cI_g/2.5$: Strong	ACI Eq. (10-8): Weak
C-8	3933	I_{gs} = 422.39 in.^{4}, I_{ss} = 7.67 in.^{4}	I_{gw} = 137.40 in.^{4}, I_{sw} = 1.51 in.^{4}	1.66×10^6	2.301×10^5	5.404×10^5	4.53×10^4	5.623×10^5	1.534×10^5	6.644×10^5	2.162×10^5
C-5	3755			1.586		5.159		5.473	1.485	6.344	2.064
C-11	3961			1.673		5.442		5.647	1.541	6.692	2.177
C-9	3838			1.621		5.273		5.543	1.508	6.484	2.109
C-6	3779			1.596		5.191		5.493	1.491	6.384	2.076
C-12	4067			1.718		5.588		5.737	1.571	6.872	2.235
C-10	3792			1.602		5.210		5.505	1.495	6.408	2.084
C-7	3782			1.597		5.196		5.495	1.492	6.388	2.078
C-13	4187			1.769		5.753		5.839	1.604	7.076	2.301
RC-1	3984	I_{gs} = 303.75 in.^{4}, I_{ss} = 4.44 in.^{4}	I_{gw} = 93.75 in.^{4}, I_{sw} = 1.20 in.^{4}	1.210×10^6	1.332×10^5	3.735×10^5	3.60×10^4	3.752×10^5	1.107×10^5	4.840×10^5	1.494×10^5
RC-2	3978			1.208		3.729		3.748	1.106	4.832	1.492
RC-4	4103			1.246		3.847		3.824	1.129	4.984	1.539
RC-5	4035			1.226		3.783		3.784	1.117	4.904	1.513
RC-3	4114			1.250		3.857		3.832	1.131	5.000	1.543
RC-9	3908			1.187		3.664		3.706	1.093	4.748	1.466
RC-6	3792			1.152		3.555		3.636	1.071	4.608	1.422
RC-7	3759			1.142		3.524		3.616	1.065	4.568	1.410
RC-8	3801			1.155		3.563		3.642	1.073	4.620	1.425
C-1	3942	I_{gs} = 422.39 in.^{4}, I_{ss} = 7.67 in.^{4}	I_{gw} = 137.4 in.^{4}, I_{sw} = 1.51 in.^{4}	-	2.301×10^5	5.416×10^5	4.53×10^4	-	1.536×10^5	-	2.166×10^5
C-15	4215			-		5.791		-	1.611	-	2.316
C-2	3807			-		5.231		-	1.499	-	2.092
C-3	3775			1.595×10^6		-		5.491×10^5	-	6.380×10^5	-
C-14	4233			1.788		-		5.877	-	7.152	-
C-4	3962			1.674		-		5.649	-	6.696	-

of each column for bending about each axis were computed according to Eq. 5.5 and a length $k\ell = 76.25$ in. The moment magnifier for bending about each axis was then computed using Eq. 5.4 with P_u taken as the thrust that measured from ram pressure at failure. Moment magnifiers computed by Eqs. ACI (10-7) and (10-8) are listed in Table 5.2.

Also included in Table 5.2 are the measured compression force, the end eccentricities and midheight eccentricities for both axes of bending. The maximum deflection and consequent maximum secondary moment was expected at midheight due to symmetrical loading. The measured moment magnifier was taken as the eccentricity at midheight divided by end eccentricity.

$$\delta_{test} = \frac{M_{max}}{M_{end}} = \frac{P_u e_{max}}{P_u e_{end}} = \frac{e_{max}}{e_{end}} \qquad 5.6$$

The comparisons between δ_{ACI} and δ_{test} in Table 5.2 indicated that with low compression forces ACI Eq. (10-8) gave some unsafe values of magnifier ($\delta_{ACI}/\delta_{test} < 1.0$), the lowest values underestimating weak axis magnifiers by 22 percent. For the higher axial loads, ACI Eq. (10-7) exaggerated the values of weak axis magnifier by as much as 80 percent, while ACI Eq. (10-8) gave a maximum value only 27 percent higher than that which was measured. The comparison showed that for strong axis moment magnifiers both ACI Eq. (10-7) and ACI Eq. (10-8) gave good agreement with the test values. The mean value for $\delta_{ACI}/\delta_{test}$ for strong axis was 0.997 for ACI Eq. (10-7) and 0.971 for ACI Eq. (10-8), with the standard deviation of 0.041 and 0.037 respectively. Less favorable results were found for weak axis moment magnifiers. The mean value of $\delta_{ACI}/\delta_{test}$ was 1.171 for ACI Eq. (10-7) and 0.94 for ACI Eq. (10-8), with the standard deviation of 0.244 and 0.103, respectively.

The shape of the column also had some influence on the moment magnifier comparison. It can be seen that larger ratios of $\delta_{ACI}/\delta_{test}$ were obtained from rectangular shaped columns than those from the oval shaped columns at the same thrust level.

TABLE 5.2 MOMENT MAGNIFICATION FACTOR

(Measured from Test and Computed Based on ACI Building Code)

Specimen	Test Data						Moment Magnifier δ						P_u/P_o	Load Angle	$\delta_{ACI}/\delta_{test}$ [ACI Eq. (10-7)]		$\delta_{ACI}/\delta_{test}$ [ACI Eq. (10-8)]	
			Strong Axis Ecc. (in.)		Weak Axis Ecc. (in.)		About Strong Axis			About Weak Axis								
	f'_c (psi)	P_u (kips)	End	Midheight	End	Midheight	ACI Eq. (10-7)	ACI Eq. (10-8)	Test	ACI Eq. (10-7)	ACI Eq. (10-8)	Test		(degree)	Strong Axis	Weak Axis	Strong Axis	Weak Axis
C-8	4760	57.1	1.036	1.128	2.128	2.940	1.064	1.053	1.089	1.281	1.184	1.382	0.2025	22-1/2	0.977	0.927	0.967	0.857
C-5	4340	49.5	2.644	2.796	1.803	2.295	1.056	1.048	1.057	1.244	1.165	1.273	0.1896	45	0.999	0.977	0.991	0.915
C-11	4830	53.2	4.354	4.735	1.787	2.420	1.059	1.049	1.088	1.255	1.168	1.354	0.1863	67-1/2	0.973	0.927	0.964	0.863
C-9	4534	96.2	0.614	0.704	1.414	1.861	1.114	1.096	1.147	1.602	1.367	1.316	0.3552	22-1/2	0.971	1.217	0.955	1.039
C-6	4396	92.2	1.594	1.859	1.066	1.595	1.110	1.093	1.166	1.573	1.354	1.496	0.3492	45	0.952	1.051	0.937	0.905
C-12	5091	99.2	2.131	2.451	1.000	1.568	1.113	1.093	1.150	1.592	1.354	1.568	0.3324	67-1/2	0.968	1.015	0.950	0.864
C-10	4425	138.2	0.315	0.413	0.767	1.360	1.174	1.146	1.311	2.196	1.641	1.773	0.5207	22-1/2	0.895	1.239	0.874	0.926
C-7	4403	139.7	1.018	1.182	0.616	1.157	1.176	1.148	1.161	2.230	1.656	1.878	0.5286	45	1.013	1.187	0.989	0.882
C-13	5397	152.5	1.529	1.759	0.599	0.968	1.182	1.145	1.150	2.273	1.640	1.616	0.4863	67-1/2	1.028	1.407	0.996	1.015
RC-1	4886	119.2	0.399	0.508	1.038	1.543	1.230	1.170	1.273	2.735	1.887	1.487	0.4719	22-1/2	0.966	1.839	0.919	1.269
RC-2	4871	120.3	0.893	1.031	0.744	1.281	1.233	1.172	1.155	2.785	1.905	1.722	0.4776	45	1.067	1.617	1.015	1.106
RC-4	5181	128.8	1.514	1.777	0.499	0.989	1.248	1.180	1.174	3.048	1.972	1.982	0.4853	67-1/2	1.063	1.538	1.005	0.995
RC-5	5012	87.1	0.390	0.463	1.127	1.845	1.157	1.117	1.187	1.850	1.513	1.637	0.3373	22-1/2	0.975	1.130	0.941	0.924
RC-3	5210	94.3	1.211	1.360	1.026	1.594	1.170	1.114	1.123	1.830	1.498	1.554	0.3529	45	1.042	1.178	0.992	0.964
RC-9	4700	85.8	2.222	2.535	0.723	1.189	1.158	1.119	1.141	1.861	1.526	1.645	0.3514	67-1/2	1.015	1.131	0.981	0.928
RC-6	4425	53.9	0.888	0.968	1.860	2.705	1.096	1.074	1.090	1.421	1.287	1.454	0.2326	22-1/2	1.006	0.977	0.985	0.883
RC-7	4350	40.4	1.935	2.144	2.141	3.003	1.070	1.055	1.108	1.288	1.203	1.403	0.1768	45	1.014	1.071	0.952	0.857
RC-8	4446	40.4	4.349	4.716	1.632	2.141	1.070	1.054	1.084	1.285	1.200	1.312	0.1736	67-1/2	0.987	0.979	0.972	0.915
C-1	4783	60.7	-	-	1.990	2.728	-	-	-	1.304	1.198	1.371	0.2150	0	-	0.951	-	0.874
C-15	5468	109.2	-	-	0.999	1.778	-	-	-	1.665	1.385	1.780	0.3450	0	-	0.935	-	0.778
C-2	4460	135.6	-	-	0.692	1.136	-	-	-	2.140	1.618	1.642	0.5090	0	-	1.303	-	0.985
C-3	4386	58.4	5.782	6.375	-	-	1.067	1.057	1.103	-	-	-	0.2230	90	0.967	-	0.958	-
C-14	5514	119.2	3.377	3.813	-	-	1.136	1.109	1.129	-	-	-	0.3740	90	1.006	-	0.982	-
C-4	4831	155.8	2.416	2.723	-	-	1.194	1.159	1.127	-	-	-	0.5470	90	1.059	-	1.059	-
														Mean	0.9973	1.1712	0.9707	0.9402
														Standard Deviation	0.0405	0.2437	0.0368	0.1030

5.3 Method of Computing Measured EI

Having observed that for the biaxial bending problem in columns, the moment magnifier procedure of the ACI Code with simplified relationships for flexural stiffness gave inconsistent results, alternate relationships were considered. The stiffness EI was overestimated for low axial loads and underestimated at high axial loads and appeared to be shape sensitive. The ACI Commentary[2] and the discussion of Ref. 18 included thrust levels higher than the axial loads in this test program.

The measured moment at the end and the moment at midheight of the column were calculated. The measured moment magnifiers for the two major axes were computed. The reverse procedure was then used in order to calculate a flexural stiffness of each column under the actual loading conditions. Rearranging Eq. 5.4 gives:

$$\frac{P_u}{P_c} = 1 - \frac{1}{\delta} \qquad 5.7$$

or

$$P_c = \frac{P_u}{1 - \frac{1}{\delta}} \qquad 5.8$$

But

$$P_c = \frac{\pi^2 EI}{\ell^2}$$

so

$$EI = \frac{P_u}{1 - \frac{1}{\delta}} \cdot \frac{\ell^2}{\pi^2} \qquad 5.9$$

The measured EI at the failure load stage was determined with Eq. 5.9. Table 5.3 shows intermediate calculations in this procedure and the resulting value of EI. Also tabulated in Table 5.3 is the ratio between EI_g and the computed EI, where EI_g is the gross flexural stiffness based on the product of concrete stiffness and the gross moment of inertia of the cross section. This EI_g ratio was plotted against the axial load ratio P_u/P_o in Fig. 5.3. The data are rather

TABLE 5.3 FLEXURAL STIFFNESS COMPUTED FROM TEST DATA

Specimen	P_u/P_o	P_u	Strong Axis			Weak Axis			EI_g/EI	
			δ_s	$P_c = \frac{P_u}{1-\frac{1}{\delta}}$	EI_s	δ_w	$P_c = \frac{P_u}{1-\frac{1}{\delta}}$	EI_w	Strong Axis	Weak Axis
		kips	in.	kips	k-in.^{2}	in.	kips	k-in.^{2}		
C-8	0.2025	57.1	1.089	698.7	4.116×10^5	1.382	206.6	1.217×10^5	4.035	4.440
C-5	0.1896	49.5	1.057	917.9	5.407	1.273	230.8	1.360	2.933	3.793
C-11	0.1863	53.2	1.088	657.7	3.874	1.354	203.5	1.199	4.319	4.539
C-9	0.3552	96.2	1.147	750.6	4.422	1.316	400.6	2.360	3.666	2.234
C-6	0.3492	92.2	1.166	647.6	3.815	1.496	278.1	1.638	4.183	3.169
C-12	0.3324	99.2	1.150	760.5	4.480	1.568	273.8	1.613	3.835	3.464
C-10	0.5207	138.2	1.311	582.6	3.432	1.773	317.0	1.867	4.668	2.791
C-7	0.5286	139.7	1.161	1007.4	5.934	1.878	298.8	1.760	2.691	2.952
C-13	0.4863	152.5	1.150	1169.2	6.888	1.616	400.1	2.357	2.568	2.441
RC-1	0.4719	119.2	1.273	555.8	3.274	1.487	364.0	2.144	3.696	1.742
RC-2	0.4776	120.3	1.155	896.4	5.281	1.722	286.9	1.690	2.287	2.207
RC-4	0.4853	128.8	1.174	869.0	5.119	1.982	260.0	1.532	2.434	2.919
RC-5	0.3373	87.1	1.187	552.9	3.257	1.637	223.8	1.318	3.764	2.870
RC-3	0.3529	94.3	1.123	861.0	5.072	1.554	264.5	1.558	2.465	2.476
RC-9	0.3514	85.8	1.141	694.3	4.090	1.645	218.8	1.289	2.902	2.843
RC-6	0.2326	53.9	1.090	652.8	3.846	1.454	172.6	1.017	2.995	3.496
RC-7	0.1768	40.4	1.108	414.5	2.442	1.403	140.6	0.828	4.676	4.256
RC-8	0.1736	40.4	1.084	521.4	3.072	1.312	169.9	1.001	3.760	3.559
C-1	0.215	60.7	-	-	-	1.371	224.3	1.321	-	4.100
C-15	0.345	109.2	-	-	-	1.780	249.2	1.468	-	3.945
C-2	0.509	135.6	-	-	-	1.640	347.5	2.047	-	2.555
C-3	0.223	58.4	1.103	625.4	3.684	-	-	-	4.330	-
C-14	0.374	119.2	1.129	1043.2	6.145	-	-	-	2.910	-
C-4	0.547	155.8	1.127	1382.6	8.145	-	-	-	2.022	-

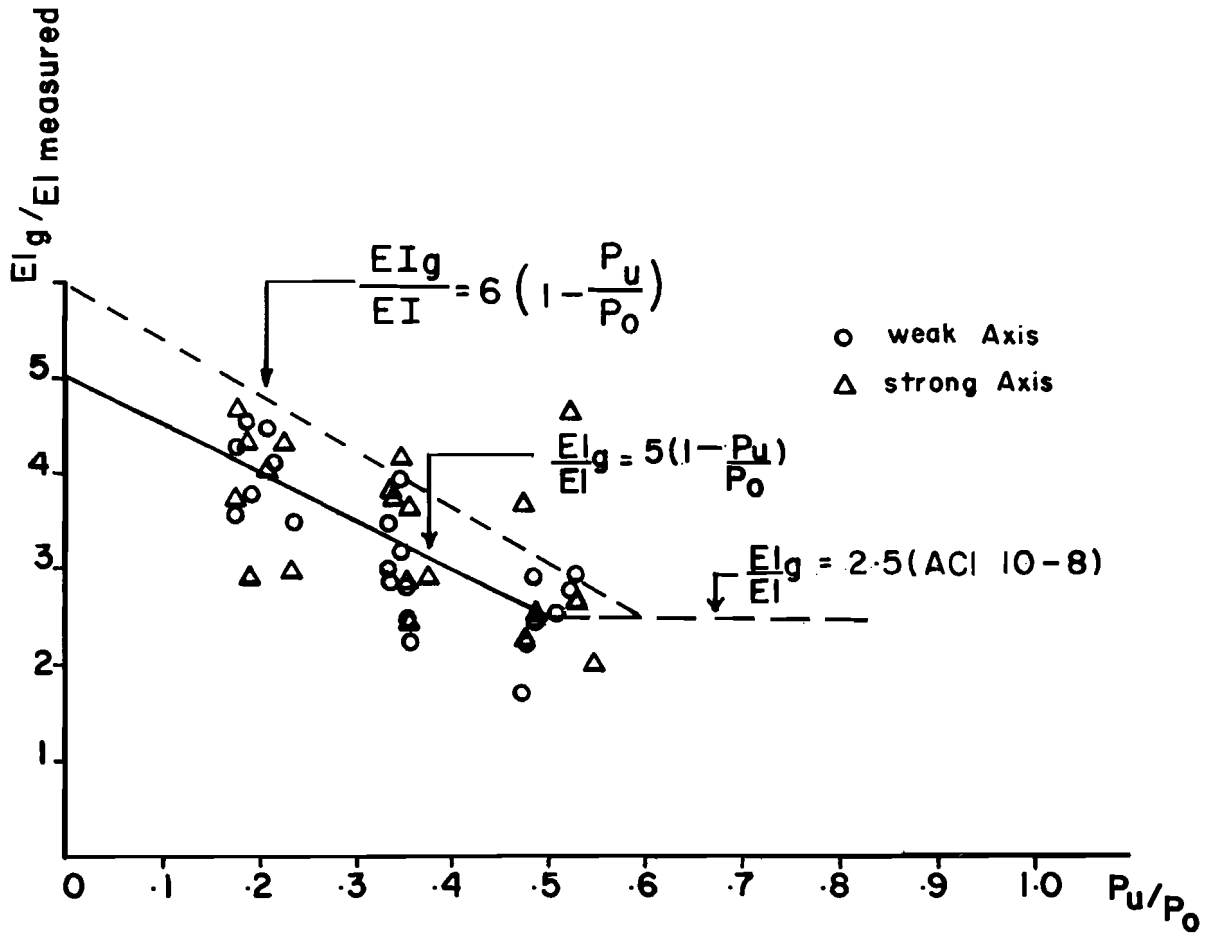

Fig. 5.3 Relationship between flexural stiffness and relative thrust level

scattered, but a trend of the relationship between $EI_g/EI_{measured}$ and P_u/P_o can be observed.

A linear regression analysis was made using P_u/P_o as an independent variable and $EI_g/EI_{measured}$ as a dependent variable. The results showed that the relationship between $EI_g/EI_{measured}$ and P_u/P_o could be approximated.

$$EI_g/EI_{measured} = 5.017 - 4.958\ P_u/P_o \qquad 5.10$$

or approximately

$$EI = \frac{EI_g}{5(1 - P_u/P_o)} \qquad 5.11$$

With the adjustment of EI using Eq. 5.11, when P_u/P_o is less than 0.5, the computed value of EI will be less than that computed from ACI Eq. (10-8). The values in Table 5.2 show that for higher levels of thrust, ACI Eq. (10-8) gave a safe estimation of moment magnifiers, so ACI Eq. (10-8) may be applied for the thrust levels greater than 0.5. The dotted line graph of Fig. 5.3 indicates that a value 6 instead of 5 in the denominator of Eq. 5.11 provides a lower bound for all data.

Table 5.4 contains a list of the stiffness and moment magnifier values computed from Eq. 5.11 plus the ratios between computed and measured values. The ratio $\delta_{Eq.\ 5.11}/\delta_{measured}$ gave a mean value of 0.994 for strong axis and 1.033 for weak axis, with the standard deviation of 0.0296 and 0.1087, respectively. The overall average ratio on both axes was 1.0135, with a standard deviation of 0.08

5.4 Column Strength Analysis Including Length Effects Using Moment Magnifier Method

5.4.1 Specimens in This Test Program. The 24 specimens of this series of tests consisted of intermediate length columns with

TABLE 5.4 MOMENT MAGNIFIER BASED ON FLEXURAL STIFFNESS FROM EQ. 5.11

$$EI_{5.11} = \frac{EI_g}{5(1 - P_u/P_o)}$$

Specimen	P_u	P_u/P_o	Strong Axis				Weak Axis				$\delta_{5.11}/\delta_{test}$	
			$EI_{5.11}$	$P_{C\ 5.11}$	$\delta_{5.11}$	δ_{test}	$EI_{5.11}$	$P_{C\ 5.11}$	$\delta_{5.11}$	δ_{test}	Strong	Weak
C-8	57.1	0.2025	4.166×10^5	707.2	1.088	1.089	1.355×10^5	230.0	1.330	1.382	0.999	0.962
C-5	49.5	0.1896	3.914	664.4	1.081	1.057	1.273	216.1	1.297	1.273	1.023	1.019
C-11	53.2	0.1863	4.112	698.0	1.083	1.088	1.338	227.1	1.306	1.354	0.995	0.965
C-9	96.2	0.3552	5.028	853.5	1.127	1.147	1.636	277.7	1.530	1.316	0.983	1.163
C-6	92.2	0.3492	4.905	832.6	1.125	1.166	1.595	270.8	1.516	1.496	0.965	1.013
C-12	99.2	0.3324	5.147	873.7	1.128	1.150	1.674	284.2	1.536	1.568	0.981	0.980
C-10	138.2	0.5207	4.799	814.6	1.204	1.311	2.174	369.0	1.599	1.773	0.918	0.902
C-7	139.7	0.5286	6.776	1150.3	1.138	1.161	2.204	374.1	1.596	1.878	0.980	0.849
C-13	152.5	0.4863	6.887	1169.1	1.150	1.150	2.240	380.2	1.670	1.616	1.000	1.033
RC-1	119.2	0.4719	4.582	777.8	1.181	1.273	1.415	240.2	1.985	1.487	0.928	1.335
RC-2	120.3	0.4776	4.625	785.1	1.181	1.555	1.428	242.4	1.901	1.722	1.023	1.104
RC-4	128.8	0.4853	4.842	821.9	1.186	1.174	1.495	253.8	2.030	1.982	1.010	1.024
RC-5	87.1	0.3373	3.700	628.1	1.161	1.187	1.142	193.9	1.816	1.637	0.978	1.109
RC-3	94.3	0.3529	3.863	655.8	1.168	1.123	1.192	202.3	1.873	1.554	1.040	1.205
RC-9	85.8	0.3514	3.660	621.3	1.160	1.141	1.130	191.8	1.809	1.645	1.018	1.100
RC-6	53.9	0.2326	3.002	509.6	1.118	1.090	0.9265	157.3	1.521	1.454	1.026	1.046
RC-7	40.4	0.1768	2.775	471.1	1.094	1.108	0.8562	145.3	1.385	1.403	0.987	0.987
RC-8	40.4	0.1736	2.795	474.5	1.093	1.084	0.8623	146.4	1.381	1.312	1.008	1.053
C-1	60.7	0.2150	-	-	-	-	1.3799	234.2	1.350	1.371	-	0.985
C-15	109.2	0.345	-	-	-	-	1.768	300.1	1.572	1.780	-	0.883
C-2	135.6	0.509	-	-	-	-	2.131	361.7	1.600	1.642	-	0.974
C-3	58.4	0.223	4.106	697.0	1.091	1.103	-	-	-	-	0.989	-
C-14	119.2	0.374	5.712	969.6	1.140	1.129	-	-	-	-	1.010	-
C-4	155.8	0.547	7.391	1254.7	1.142	1.124	-	-	-	-	1.016	-

two types of cross-sectional shapes. Nine rectangular shaped columns and nine oval shaped specimens were tested under biaxial bending moment and compression. The slenderness ratio ℓ/r of rectangular shaped columns was 27.5 for strong axis bending and 50 for weak axis bending, if r is taken as the radius of gyration of the uncracked transformed cross section. The oval shaped columns had slenderness ratios of 24.3 and 43 in the strong and weak axis directions, respectively, if r were taken again as the radius of gyration of the uncracked transformed section.

Moment magnifiers computed from the use of ACI Eq. (10-7) and ACI Eq. (10-8) were used to magnify the measured end eccentricities at the failure thrust stage. Then column strength according to these eccentricities was computed with the reciprocal load equation discussed in Chapter 4 as rewritten below:

$$\frac{1}{P_i} = \frac{1}{P_x} + \frac{1}{P_y} - \frac{1}{P_o} \qquad 5.12$$

Also determined were the column capacities using moment magnifiers as proposed by Eq. 5.11. The computed strengths are listed in Table 5.5 for comparison with the actual test loads. The measured end eccentricities and moment magnifiers were already shown in Table 5.2 and Table 5.4.

From Table 5.5, the computed strength of C-5 is included even though the capacity was felt to be larger than the maximum test value, as previously mentioned in Chapters 4. The strength of C-5 was the only overestimated strength obtained from the use of Eq. 5.11. The EI value from ACI Eq. (10-7) gave good results at lower levels of axial load, but grossly underestimated the strength at higher thrusts. The use of ACI Eq. (10-8) gave good approximations at high axial loads, but overestimated the strength when the thrust was low. Overoptimistic strength estimates cannot be tolerated for design purposes. The EI values from Eq. 5.11 resulted in estimates of member strength closer to measured values and also predicted less strength than any of the observed values except the

TABLE 5.5 COLUMN STRENGTH USING MOMENT MAGNIFIER METHOD

Specimen	P_i			P_{test}	P_{test}/P_i			P_u/P_0
	ACI Eq. (10-7)	ACI Eq. (10-8)	Eq. 5.11		ACI Eq. (10-7)	ACI Eq. (10-8)	Eq. 5.11	
C-8	58.74	65.26	55.77	57.1	0.972	0.875	1.024	0.2025
C-5	59.49	63.12	56.76	49.5	0.832	0.784	0.872	0.1896*
C-11	49.86	52.84	47.53	53.2	1.067	1.007	1.119	0.1863
C-9	74.99	88.84	78.93	96.2	1.283	1.083	1.219	0.3552
C-6	85.93	95.22	87.84	92.2	1.073	0.968	1.050	0.3492
C-12	91.25	101.18	92.78	99.2	1.087	0.980	1.069	0.3324
C-10	101.31	126.37	128.32	138.2	1.364	1.094	1.077	0.5207
C-7	106.31	126.47	129.00	139.7	1.314	1.105	1.083	0.5286
C-13	114.96	137.91	136.61	152.5	1.327	1.106	1.116	0.4863
RC-1	51.24	85.17	80.14	119.2	2.326	1.400	1.487	0.4719
RC-2	74.39	102.78	102.80	120.3	1.617	1.170	1.170	0.4776
RC-4	89.89	114.37	112.86	128.8	1.433	1.126	1.141	0.4853
RC-5	80.41	99.26	82.27	87.1	1.083	0.877	1.059	0.3373
RC-3	83.45	98.17	81.58	94.3	1.130	0.961	1.156	0.3529
RC-9	77.92	86.43	78.92	85.8	1.101	0.993	1.087	0.3514
RC-6	52.11	59.54	47.35	53.9	1.034	0.905	1.138	0.2326
RC-7	44.03	48.06	39.97	40.4	0.918	0.841	1.011	0.1768
RC-8	39.12	41.35	36.57	40.4	1.033	0.977	1.105	0.1736
				Mean	1.2448	1.0275	1.1242	
			Standard Deviation		0.324	0.218	0.104	

*C-5 did not fail according to Sec. 4.4.

aforementioned C-5 result. The average ratio between P_{test} and P_i using Eq. 5.11 (excluding Specimen C-5) was 1.124 with a maximum value of 1.49 and a minimum of 1.01, the standard deviation was 0.104. ACI Eq. (10-8) gave better mean values of P_{test}/P_i than did Eq. 5.11, but with more scatter in the data (mean = 1.028 and standard deviation = 0.218). ACI Eq. (10-7) gave the worst comparison. The maximum ratio for Specimen RC-1 involved a measured weak axis magnifier that was 33 percent greater than that predicted by the use of Eq. 5.11 for EI.

5.4.2 Slender Columns Tested by Others. Thirty-three slender column test results reported by others were analyzed, twenty-two columns were from the experiments reported by Drysdale[14] and eleven reported by Wu.[47] All columns were square columns with the same slenderness ratio of $\ell/r = 105$ and with approximately a 3 percent reinforcement ratio. The details of cross section properties and loading conditions for these columns are given in Appendix A.

Another set of imaginary columns named RC-1A to RC-9A were modeled in a computer aided analysis, so that they had the same dimensions and reinforcement as the rectangular specimens described in Chapter 2, but with the length increased to 108 inches. The longer length gave a slenderness ratio of 75 about the weak axis. The computer program BIAM2 written by Redwine[38] was used to provide the analytical predictions for these columns. The nominal loadings for the column were input so that there were three load levels, $0.2P_o$, $0.4P_o$, and $0.6P_o$, and nominal moment angles of 22-1/2, 45, and 67-1/2 degrees for each load level. These imaginary column loadings were the same as the proposed loadings of the actual test program reported here. The concrete strength $f'_c = 4500$ psi was assumed to possess a parabola-straight line stress-strain relationship.

(a) The Computation of Column Flexural Stiffness. Flexural stiffness of columns described in Sec. 5.4.2 were computed using ACI Eq. (10-7), Eq. (10-8), and Eq. 5.11. The calculated stiffnesses

are tabulated in Table 5.6, as well as the critical load P_c computed from Eq. 5.5.

From Table 5.6, the stiffnesses computed from ACI Eqs. (10-7) and (10-8) and Eq. 5.11 can be called conservative, because each gives very large moment magnifiers δ. With the "soft" EI values and large slenderness ratio, the computed critical loads shown in Table 5.6 were lower than the actual failure loads reported from experiments. This indicates that the moment magnifier method cannot be applied to these long columns under biaxial bending unless an appropriate adjustment for the stiffness of columns can be made. These results do indicate that design applications of ACI Eq. (10-7), (10-8), or Eq. 5.11 would give "too safe" results at least for the very slender columns.

(b) Strength of Columns Predicted by BIAM2. The strength of Drysdale and Wu specimens were computed analytically using computer program BIAM2.[38] For a very slender column such as the Drysdale[14] and Wu[47] specimens, the analysis converged slowly. It was noted that the control tolerance limit for deflections which were the control of convergence in BIAM2 needed to be increased up to 0.1 in. in order to let the program converge. With the control deflection tolerance of 0.1 in., the analytical results of strength of Drysdale and Wu specimens are shown in Table 5.7. Comparing to the test strength, BIAM2 gave a reasonable result although for the 6-1/4 and 7-1/2 in. column from Wu specimens the program overestimated the strength of the columns as much as 17 percent.

The BIAM2 analysis also was used to predict the strength of rectangular columns tested in this report. Input for that study was adjusted so that the axial thrust could remain constant at the failure thrust while the eccentricities about each principal axis were increased gradually until failure was predicted. The results from BIAM2 for RC-1 to RC-9 are recorded in Table 5.8. The predicted member strength from BIAM2 showed good agreement with test results,

TABLE 5.6 FLEXURAL STIFFNESS

Specimen	P/P_o	EI* ACI Eq. (10-7) $\times 10^5$	EI* ACI Eq. (10-8) $\times 10^5$	EI* Eq. 5.11 $\times 10^5$	$P_c = \pi^2 EI/L^2$ ACI Eq. (10-7) k	$P_c = \pi^2 EI/L^2$ ACI Eq. (10-8) k	$P_c = \pi^2 EI/L^2$ Eq. 5.11 k	P_u k	$\frac{1}{1 - P_u/P_c}$ $\delta_{ACI\ 10-7}$	$\delta_{ACI\ 10-8}$	δ_{5-11}
Drysdale Specimens											
A1C	0.2647	1.0808	0.7406	0.5036	43.83	30.04	20.43	37.6	7.035	**	**
A1D	0.2842	1.0803	0.7396	0.5166	43.81	29.99	20.95	40.3	12.481	**	**
A2A	0.2788	1.0794	0.7377	0.5114	43.78	29.92	20.74	39.4	9.995	**	**
A2B	0.2831	1.0794	0.7377	0.5145	43.78	24.92	20.87	40.0	11.582	**	**
A3C	0.2650	1.0869	0.7529	0.5122	44.08	30.53	20.77	38.5	7.900	**	**
A3D	0.2588	1.0869	0.7529	0.5079	44.08	30.53	20.60	37.6	6.802	**	**
B1C	0.2565	1.0622	0.7035	0.4731	43.08	28.53	19.19	34.0	4.744	**	**
B1D	0.2595	1.0622	0.7035	0.4750	43.08	28.53	19.26	34.4	4.963	**	**
B2C	0.2761	1.0702	0.7194	0.4969	43.40	29.18	20.16	37.7	7.614	**	**
B2D	0.2761	1.0702	0.7194	0.4969	43.40	29.18	20.16	37.7	7.614	**	**
C2A	0.2791	1.0798	0.7387	0.5123	43.79	29.96	20.78	39.5	10.207	**	**
C2B	0.2769	1.0798	0.7387	0.5108	43.79	29.96	20.72	39.2	9.540	**	**
C3A	0.2815	1.0916	0.7622	0.5304	44.27	30.91	21.51	41.6	16.581	**	**
C3B	0.2686	1.0916	0.7622	0.5211	44.27	30.91	21.13	39.7	9.687	**	**
E1C	0.2296	1.0808	0.7406	0.4807	43.83	30.04	19.50	32.6	3.903	**	**
E1D	0.2365	1.0808	0.7406	0.4850	43.83	30.04	19.67	33.6	4.284	**	**
E2A	0.2177	1.1043	0.7876	0.5034	44.79	31.94	20.41	33.7	4.039	**	**
E2B	0.2158	1.1043	0.7876	0.5022	44.79	31.94	20.37	33.4	3.932	**	**
F1A	0.3965	1.0920	0.7631	0.6322	44.29	30.95	25.64	58.7	**	**	**
F1B	0.3762	1.0920	0.7631	0.6117	44.29	30.95	24.81	55.7	**	**	**
F2A	0.3799	1.0957	0.7704	0.6212	44.44	31.24	25.19	57.0	**	**	**
F2B	0.3799	1.0957	0.7704	0.6212	44.44	31.24	25.19	57.0	**	**	**
Wu Specimens											
1	0.2291	0.3424	0.2394	0.1553	25.01	17.48	11.34	19.0	4.161	**	**
2	0.2207	1.0300	0.7566	0.4854	41.77	30.68	19.68	31.8	4.187	**	**
3	0.1973	2.5539	1.8566	1.1565	67.14	48.81	30.40	45.0	3.033	12.811	**
4	0.2065	5.4252	3.8681	2.4374	99.05	70.62	44.50	69.0	3.296	43.593	**
10	0.2117	1.0300	0.7566	0.4799	41.77	30.68	19.46	30.5	3.706	170.444	**
16	0.2093	1.0286	0.7538	0.4767	41.72	30.57	19.33	30.0	3.560	53.632	**
16	0.2239	1.0220	0.7406	0.4771	41.45	30.04	19.35	31.3	4.084	**	**
26	0.1783	0.3615	0.2776	0.1689	26.40	20.27	12.33	18.3	3.259	10.289	**
27	0.1871	1.0904	0.8774	0.5397	44.22	35.58	21.89	33.5	4.125	17.106	**
28	0.1700	2.6968	2.1425	1.2907	70.90	56.33	33.93	47.8	3.069	6.604	**
29	0.1535	5.7123	4.4421	2.6238	104.30	81.10	47.90	62.7	2.507	4.408	**

*ACI Eq. (10-7) $EI = E_c I_g/5 + E_s I_s$ **$P_u > P_c$

ACI Eq. (10-8) $EI = E_c I_g/2.5$

Eq. 5.11 $EI = E_c I_g/5(1 - P/P_o)$

TABLE 5.6 (Continued)

	P_u/P_o	End Ecc.*** (in.) e_{strong}	e_{weak}	EI (k-in.^{2}) ACI Eq. (10-7)	ACI Eq. (10-8)	P_c (kips) ACI Eq. (10-7)	ACI Eq. (10-8)	Eq. 5.11	P_u***	$\delta = \frac{1}{P_u/P_c}$ ACI 10-7	ACI 10-8	Eq. 5.11
Analytical Model of RC Specimens with Length of 108 in.												
RC-6A	0.2	2.89	1.19708	Strong Axis = 3.655×10^5 Weak Axis = 1.077×10^5	Strong Axis = 4.64616×10^5 Weak Axis = 1.434×10^5	P_c Strong = 309.27 P_c Weak = 91.13	P_c Strong = 393.14 P_c Weak = 121.34	Strong Axis = 5.8077×10^5 Weak Axis = 1.7925×10^5	140.76	δ_{Strong} = 1.835 δ_{Weak} = **	δ_{Strong} = 1.558 δ_{Weak} = **	δ_{Strong} = 1.753 δ_{Weak} = **
RC-7A	0.2	1.50	1.50						140.76			
RC-8A	0.2	0.6627	1.60						140.76			
RC-5A	0.4	1.37	0.56749					Strong Axis = 3.8718×10^5 Weak Axis = 1.195×10^5	93.84	δ_{Strong} = 1.436 δ_{Weak} = **	δ_{Strong} = 1.314 δ_{Weak} = 4.412	δ_{Strong} = 1.401 δ_{Weak} = 13.890
RC-3A	0.4	0.71	0.71						93.84			
RC-9A	0.4	0.32728	0.79						93.84			
RC-1A	0.6	0.64	0.26507					Strong Axis = 2.9039×10^5 Weak Axis = 0.89625×10^5	46.92	δ_{Strong} = 1.179 δ_{Weak} = 2.061	δ_{Strong} = 1.136 δ_{Weak} = 1.630	δ_{Strong} = 1.236 δ_{Weak} = 2.622
RC-2A	0.6	0.31	0.31						46.92			
RC-4A	0.6	0.13258	0.32						46.92			

P_c Strong = 491.45
P_c Weak = 151.68

P_c Strong = 327.63
P_c Weak = 101.12

P_c Strong = 245.73
P_c Weak = 75.84

***From RIAM2

TABLE 5.7 STRENGTH OF COLUMN FROM BIAM2, DRYSDALE AND WU SPECIMENS

Specimen	End Eccentricity		P_u (from test)	P_u (BIAM2)	$\frac{P_{BIAM2}}{P_{test}}$
	e_x in.	e_y in.	kips	kips	
Drysdale*					
f'_c = 4000 psi	0.707	0.707	37.0	36.9	0.997
	0.383	0.924	40.0	36.9	0.923
	0.574	1.386	38.6	30.0	0.777
	0.191	0.462	57.0	51.9	0.911
Wu					
1	0.662	0.662	19.0	19.1	1.005
26	0.563	0.975	18.3	19.5	1.066
2,10,16	0.885	0.885	31.8	31.6	0.994
27	0.750	1.300	33.5	32.5	0.970
3	1.110	1.110	45.0	49.7	1.104
28	0.938	1.625	47.8	51.0	1.067
4	1.325	1.325	69.0	73.75	1.069
29	1.125	1.950	62.7	72.0	1.148

*All Drysdale specimens were the same dimension with small variation of concrete strength (3500 psi to 4400 psi). Concrete strength of 4000 psi was assumed in the input data for BIAM2 to represent all the Drysdale specimens.

TABLE 5.8 STRENGTH OF RC COLUMNS FROM BIAM2

Specimen	Axial Load (kips)	Test End Ecc.		BIAM2 End Ecc.		$\frac{Ecc_{BIAM2}}{Ecc_{test}}$
		e_s	e_w	e_s	e_w	
RC1	119.2	0.399	1.038	0.320	0.8336	0.802
RC2	120.3	0.893	0.744	0.880	0.7330	0.985
RC3	94.3	1.211	1.026	1.250	1.0600	1.032
RC4	128.8	1.514	0.499	1.480	0.4869	0.978
RC5	87.1	0.390	1.127	0.440	1.2707	1.128
RC6	53.9	0.888	1.860	0.890	1.8663	1.002
RC7	40.4	1.935	2.141	1.970	2.1808	1.018
RC8	40.4	4.349	1.632	4.090	1.5378	0.940
RC9	85.8	2.222	0.723	2.260	0.7345	1.017

involving a maximum overestimate of 13 percent and an underestimate not greater than 20 percent of the observed strength. For an overall comparison with Wu, Drysdale, and the rectangular columns reported here, the average ratio between analytical strength and test strength was 0.997 with the standard deviation of 0.091 indicating good agreement.

5.5 Member Strength Using Deflection Limit

It has been observed that the moment magnifier method for column strength is not an accurate approach for the biaxial bending problem with very slender columns. In this section another study is reported using the available experimental data to substantiate an alternate approach.

With seventeen of the Drysdale and Wu specimen tests on square columns subjected to equal eccentricities on both axes (i.e., load angle = 45^{o}), a backward computation was performed as follows:

(1) The test strength was taken as P_i, and P_o was computed from reported section properties. P_x and P_y could be determined from the reciprocal load equation.

$$\frac{1}{P_i} = \frac{1}{P_x} + \frac{1}{P_y} - \frac{1}{P_o} \tag{5.12}$$

If $P_x = P_y$ (Load angle = 45^{o})

$$\frac{2}{P_x} = \frac{1}{P_i} + \frac{1}{P_o} \tag{5.13}$$

$$P_x = \frac{2}{\frac{1}{P_i} + \frac{1}{P_o}} \tag{5.14}$$

(2) With the calculated P_x, the failure eccentricity e_x could be located on the interaction diagram for the section.

(3) Assuming that the column fails at midheight where the maximum moment was expected, the deflection at midheight becomes

TABLE 5.9 COLUMN STRENGTH OF DRYSDALE AND WU SPECIMENS WITH EQUAL END ECCENTRICITIES

Specimen	P_u	P_o	$\frac{1}{\frac{1}{P_u}+\frac{1}{P_o}}$	P_x	e_x	e_{end}	$\frac{\Delta}{L_x}=\frac{e_x-e_{end}}{L}$	Δ/L total	P/P_o	δ	P/P_c	P_c	EI_{test} ($\times 10^5$)	$\frac{EI_{10-7}}{EI_{test}}$
A1C	37.6	142.05	29.73	59.46	2.050	0.707	0.0086	0.01216	0.2647	2.90	0.655	57.4	1.4153	0.7637
A1D	40.3	141.8	31.38	62.76	1.886	0.707	0.0076	0.01075	0.2842	2.668	0.625	64.48	1.5899	0.6795
A2A	39.4	141.3	30.81	61.26	1.930	0.707	0.0078	0.01103	0.2788	2.730	0.634	62.15	1.5325	0.7043
A2B	40.0	141.3	31.17	68.34	1.897	0.707	0.0078	0.01103	0.2831	2.683	0.627	63.80	1.5731	0.6862
A3C	38.5	145.3	30.44	60.88	2.039	0.707	0.0085	0.01202	0.2650	2.884	0.653	58.96	1.4538	0.7476
A3D	37.6	145.3	29.87	59.74	2.098	0.707	0.0089	0.01259	0.2588	2.967	0.663	56.71	1.3983	0.7773
B1C	34.0	132.55	27.06	54.12	2.154	0.707	0.0093	0.01315	0.2565	3.047	0.672	50.60	1.2477	0.8513
B1D	34.4	132.55	27.31	54.62	2.123	0.707	0.0091	0.01287	0.2595	3.003	0.667	51.57	1.2716	0.8353
B2C	37.7	136.55	29.54	59.08	1.964	0.707	0.0081	0.01146	0.2761	2.778	0.640	58.91	1.4526	0.7367
B2D	37.7	136.55	29.54	59.08	1.964	0.707	0.0081	0.01146	0.2761	2.778	0.640	58.91	1.4526	0.7367
1	19.0	82.95	15.46	30.92	1.808	0.662	0.0099	0.01400	0.2291	2.731	0.634	29.97	0.4104	0.8343
2	31.8	144.06	26.05	52.10	2.477	0.885	0.0102	0.01442	0.2207	2.799	0.643	49.46	1.2196	0.8445
3	45.0	228.1	37.59	75.18	3.518	1.110	0.0124	0.01754	0.1973	3.440	0.709	63.47	2.4141	1.0579
4	69.0	334.21	57.19	114.38	4.039	1.325	0.0117	0.01655	0.2065	3.048	0.672	102.68	5.6238	0.9647
10	30.5	144.06	25.17	50.34	2.603	0.885	0.0110	0.01556	0.2117	2.941	0.660	46.21	1.1394	0.9040
16	30.0	143.31	24.81	49.62	2.639	0.885	0.0112	0.01584	0.2093	2.981	0.665	45.11	1.1123	0.9248
16	31.3	139.81	25.57	51.14	2.459	0.885	0.0101	0.01428	0.2239	2.779	0.641	48.83	1.2040	0.8488

$$\Delta_x = e_x - e_{end}$$

(4) Moment magnification was taken as the ratio e_x/e_{end}

(5) Computed flexural stiffness: EI was computed using the same procedure described in Sec. 5.3 (the reverse procedure with Eqs. 5.7 - 5.9).

(6) Values of Δ/L for both axes were computed using Δ from step 3 to find the total Δ/L, Δ/L total = $\sqrt{(\Delta_x/L)^2 + (\Delta_y/L)^2}$

A step-by-step computation is tabulated in Table 5.9. The study on these slender columns subjected to biaxial bending then was considered with two different column behavior parameters, the column stiffness EI and a deflection limit at failure, Δ/L.

5.5.1 Column Stiffness EI. Table 5.9 contains the list of EI values computed backward from failure loads of Drysdale and Wu square columns loaded by equal eccentricities on both principal axes. A ratio between EI_{test} and EI computed according to ACI Eq. (10-7) was found and also tabulated in Table 5.9. A linear relationship between the ratio EI_{10-7}/EI_{test} and the relative thrust level was found to be

$$\frac{EI_{10-7}}{EI_{test}} = 1.6(1 - 2\,P_u/P_o) \qquad 5.15$$

or

$$EI_{test} = \frac{EI_{10-7}}{1.6(1 - 2\,P_u/P_o)} \qquad 5.16$$

Using Eq. 5.16 to compute the moment magnifier for specimens with unequal eccentricities, the reciprocal load method for column strength then was applied in order to calculate the column strength P_i. The calculated strength P_i and the actual strength P_{test} for Drysdale and Wu slender columns are shown in Table 5.10. The results obtained using Eq. 5.16 for the flexural stiffness showed inconsistent accuracy of the computed strength. The result of using Eq. 5.16 was good for calculating the strength of columns under equal eccentricities. For Drysdale columns with unequal moments, Eq. 5.16 overestimated the

TABLE 5.10 COLUMN STRENGTH BY MOMENT MAGNIFIER METHOD USING EQ. 5.16

$$EI = \frac{EI_{10\text{-}7}}{1.6(1 - 2P_u/P_o)}$$

Specimen	f'_c	P_o	Eccentricity e_c	Eccentricity e_y	δ	P_x	P_y	P_i	P_{test}	$\frac{P_i}{P_{test}}$
Drysdale Specimens										
A1C	3890	142.05	0.707	0.707	2.8244	60.43	60.43	38.4	37.6	1.021
A1D	3880	141.8	0.707	0.707	2.7408	61.62	61.62	39.4	40.3	0.978
A2A	3860	141.3	0.707	0.707	2.7558	61.21	61.21	39.1	39.4	0.992
A2B	3860	141.3	0.707	0.707	2.7339	61.55	61.55	39.3	40.0	0.983
A3C	4020	145.3	0.707	0.707	2.9145	60.46	60.46	38.2	38.5	0.992
A3D	4020	145.3	0.707	0.707	2.9272	60.29	60.29	38.0	37.6	1.011
B1C	3510	132.55	0.707	0.707	2.5970	60.08	60.08	38.8	34.0	1.141
B1D	3510	132.55	0.707	0.707	2.5948	60.11	60.11	38.9	34.4	1.131
B2C	3670	136.55	0.707	0.707	2.6477	60.98	60.98	39.3	37.7	1.042
B2D	3690	136.55	0.707	0.707	2.6477	60.98	60.98	39.3	37.7	1.042
C2A	3870	141.55	0.383	0.924	2.7595	86.42	50.90	41.4	39.5	1.048
C2B	3870	141.55	0.383	0.924	2.7706	86.27	50.75	41.3	39.2	1.053
C3A	4120	147.8	0.383	0.924	2.9153	87.90	50.71	41.1	41.6	0.988
C3B	4120	147.8	0.383	0.924	2.9761	87.04	49.95	40.4	39.7	1.018
E1C	3890	142.05	0.574	1.386	2.8071	69.40	34.19	27.3	32.6	0.837
E1D	3890	142.05	0.574	1.386	2.8281	69.09	33.89	27.1	33.6	0.807
E2A	4400	154.80	0.574	1.386	3.1222	70.18	30.82	24.9	33.7	0.739
E2B	4400	154.8	0.574	1.386	3.1073	70.40	31.02	25.0	33.4	0.749
F1A	4130	148.05	0.191	0.462	1.7825	124.61	100.06	88.8	58.7	1.513
F1B	4130	148.05	0.191	0.462	1.9930	122.29	95.89	84.4	55.7	1.515
F2A	4210	150.05	0.191	0.462	1.9724	124.19	97.57	85.9	57.0	1.507
F2B	4210	150.05	0.191	0.462	1.9724	124.19	97.57	85.9	57.0	1.507
Wu Specimens										
1	4060	82.95	0.662	0.662	2.9289	29.33	29.33	17.8	19.0	0.937
2	4060	144.06	0.885	0.885	3.1285	48.03	48.03	28.8	31.8	0.906
3	4100	228.10	1.110	1.110	2.8503	81.36	81.36	49.5	45.0	1.100
4	4140	334.21	1.325	1.325	2.8920	118.71	118.71	72.2	69.0	1.046
10	4060	144.06	0.885	0.885	3.0636	48.83	48.83	29.4	30.5	0.964
16	4030	143.31	0.885	0.885	3.0216	49.13	49.13	29.6	30.0	0.987
16	3890	139.81	0.885	0.885	3.0051	48.31	48.31	29.2	31.3	0.933
26	5460	102.64	0.563	0.975	3.4898	34.64	16.11	12.3	18.3	0.672
27	5460	179.06	0.750	1.300	4.1396	48.88	22.25	16.7	33.5	0.499
28	5460	281.23	0.938	1.625	3.4716	94.47	45.72	34.6	47.8	0.724
29	5460	408.46	1.125	1.950	2.9994	154.48	84.20	62.9	62.7	1.003

TABLE 5.11 COLUMN STRENGTH USING DEFLECTION CONTROL--DRYSDALE AND WU SPECIMENS WITH UNEQUAL END ECCENTRICITY

Specimen	P/P_o	Δ/L Total	Ecc/r		Δ/L		End Ecc.		End Ecc. + Δ		P_x	P_y	P_o	P_1	P_u	P_1/P_u
			e/r_x	e/r_y	Δ/L^x	Δ/L^y	e_x	e_y	e_x	e_y						
C2A	0.2791	0.0125	0.265	0.640	0.004782	0.011549	0.383	0.924	1.1290	2.7257	83.89	48.45	141.55	39.2	39.5	0.992
C2B	0.2769	0.0125	0.265	0.640	0.004782	0.011549	0.383	0.924	1.1290	2.7257	83.89	48.45	141.55	39.2	39.2	1.000
C3A	0.2815	0.0125	0.265	0.640	0.004782	0.011549	0.383	0.924	1.1290	2.7257	87.44	50.28	147.8	40.72	41.6	0.979
C3B	0.2686	0.0125	0.265	0.640	0.004782	0.011549	0.383	0.924	1.1290	2.7257	87.44	50.28	147.8	40.72	39.7	1.026
E1C	0.2295	0.0140	0.398	0.961	0.005357	0.012935	0.574	1.386	1.4097	3.4038	75.00	40.00	142.05	31.96	32.6	0.980
E1D	0.2365	0.0140	0.398	0.961	0.005357	0.012935	0.574	1.386	1.4097	3.4038	75.00	40.00	142.05	31.96	33.6	0.951
E2A	0.2177	0.0140	0.398	0.961	0.005357	0.012935	0.574	1.386	1.4097	3.4038	81.19	41.74	154.8	33.54	33.7	0.995
E2B	0.2158	0.0140	0.398	0.961	0.005357	0.012935	0.574	1.386	1.4097	3.4038	81.19	41.74	154.8	33.54	33.4	1.004
F1A	0.3965	0.0095	0.132	0.320	0.003623	0.008782	0.191	0.462	0.7561	1.8320	103.18	66.48	148.05	55.62	58.7	0.948
F1B	0.3762	0.0095	0.132	0.320	0.003623	0.008782	0.191	0.462	0.7561	1.8320	103.18	66.48	148.05	55.62	55.7	0.999
F2A	0.3799	0.0095	0.132	0.320	0.003623	0.008782	0.191	0.462	0.7561	1.8320	104.56	67.28	150.05	56.30	57.0	0.989
F2B	0.3799	0.0095	0.132	0.320	0.003623	0.008782	0.191	0.462	0.7561	1.8320	104.56	67.28	150.05	56.30	57.0	0.988
26	0.1783	0.0175	0.520	0.900	0.008748	0.015157	0.563	0.975	1.5800	2.7370	40.88	23.42	102.64	17.42	18.3	0.952
27	0.1871	0.0175	0.520	0.901	0.008748	0.015157	0.750	1.300	2.11469	3.6645	70.54	39.18	179.06	29.31	33.5	0.875
28	0.1700	0.0175	0.520	0.901	0.008748	0.015157	0.938	1.625	2.6324	4.5617	111.39	62.56	281.23	46.72	47.8	0.977
29	0.1535	0.0175	0.520	0.901	0.008748	0.015157	1.125	1.950	3.1589	5.4740	162.38	92.37	408.46	68.79	62.7	1.097

column strength on columns with small eccentricities and underestimated the column strength on columns with large eccentricities. The equation underestimated the strength of columns tested by Wu, but better agreement was found on large cross section columns than on the small cross section columns.

5.5.2 Deflection Limit at Failure. A study on the deflection limit of long columns was conducted. In Table 5.9, a relationship between Δ/L total and P_u/P_o was observed, with the average of P_u/P_o at 0.2703 and Δ/L total equal to 0.01183 for Drysdale specimens. Average values P_u/P_o were 0.2141 in the Wu specimens, with Δ/L total equal to 0.01546. These values indicated that as the relative thrust level increased, the failure deflection Δ/L decreased.

An analysis of results for columns subjected to unequal eccentricities was made to study whether the deflection control would give satisfactory results. A deflection control was assigned for each principal axis proportional to the e/r ratio (ratio of eccentricity to radius of gyration) of the cross section about the centroidal axis such that the total amount of deflection should equal Δ/L total (i.e., $\sqrt{(\Delta_x/L)^2 + (\Delta_y/L)^2} = \Delta/L$ total). The Drysdale and Wu test data with unequal end eccentricities of columns were grouped according to their relative thrust level. An arbitrary deflection limit Δ/L total was assigned to each group on a trial and error basis, from which the most satisfactory deflection for each group is shown in Table 5.11. Values of Δ_x/L and Δ_y/L were computed and also the mid-height eccentricities e = End Ecc + Δ. The reciprocal load method was applied and the computed strength P_i was tabulated. The assigned Δ/L total for each group was changed until a result was obtained for which P_i was within 5 percent of the reported failure load P_u.

From the results in Table 5.9 and Table 5.11, the average value of P_u/P_o and the deflection limit Δ/L total assigned for each group was found, and the average values are listed in Table 5.12 below.

Graphs displaying Δ/L total as a function of the inverse of P_u/P_o are shown in Fig. 5.4, and the linear relation between these two variables can be observed. Using the same procedure, values of Δ/L total were assigned to other specimens with different slenderness ratios. By trial and error an assigned Δ/L was selected to give a a computed value of P_i nearest to the actual test P_u.

TABLE 5.12 LOAD LEVEL P_u/P_o AND ASSIGNED DEFLECTION LIMIT

P_u/P_o	Δ/L total	$\frac{1}{P_u/P_o}$
0.1722	0.01750	5.807
0.2140	0.01546	4.673
0.2249	0.01400	4.446
0.2703	0.01183	3.700
0.2765	0.01250	3.617
0.3831	0.00950	2.610

The assigned Δ/L total and P_u/P_o for each specimen are also plotted in Fig. 5.4. For each group of slenderness ratios, a linear regression analysis was made, and the relationship between Δ/L total and P_u/P_o were computed as follows:

$$\Delta/L \text{ total} = 0.00293 + 0.00259 \frac{1}{P_u/P_o} \quad \text{for specimens with } \ell/r_{weak} = 105 \qquad 5.17(a)$$

$$\Delta/L \text{ total} = 0.00274 + 0.00193 \frac{1}{P_u/P_o} \quad \text{for specimens with } \ell/r_{weak} = 75 \qquad 5.17(b)$$

$$\Delta/L \text{ total} = 0.00372 + 0.00107 \frac{1}{P_u/P_o} \quad \text{for specimens with } \ell/r_{weak} = 52.8 \qquad 5.17(c)$$

$$\Delta/L \text{ total} = 0.00340 + 0.00078 \frac{1}{P_u/P_o} \quad \text{for specimens with } \ell/r_{weak} = 45.8 \qquad 5.17(d)$$

From Eq. 5.17(a) to Eq. 5.17(d) it was found that the first term of the right-hand side of these equations changed only slightly, and thereafter the first term was assumed to be constant. The coefficient of the second term varied in the proportion of ℓ/r_{weak}. For

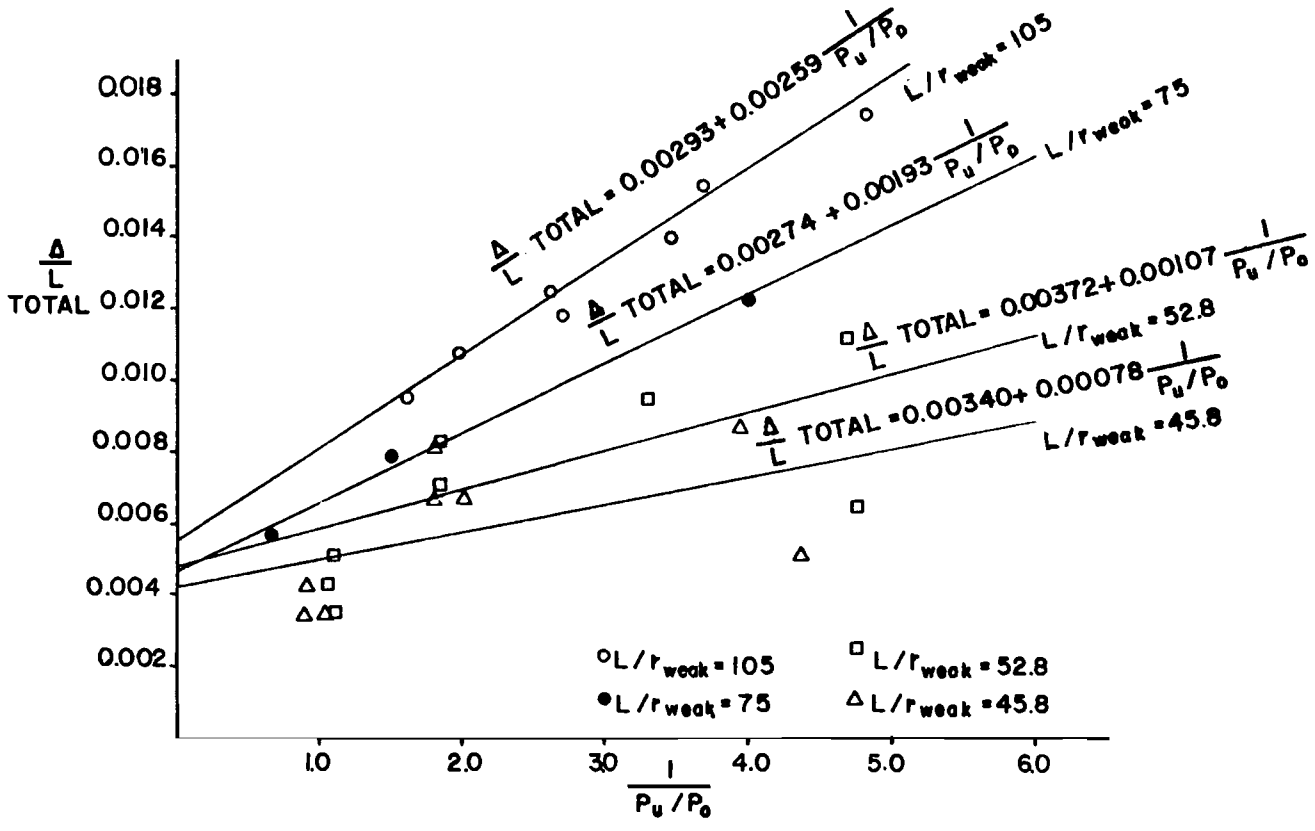

Fig. 5.4 Relationship between Δ/L total and P_u/P_o

specimens with different ℓ/r ratios, the ratio of the coefficients of different groups was close to the ratio of the corresponding slenderness ratios. Eq. 5.18 was then proposed, using the most conservative values from Eq. 5.17(a) to Eq. 5.17(d) (the coefficient that would give the largest Δ/L total):

$$\Delta/L \text{ total} = 0.00372 + [0.00270 \frac{1}{P_u/P_o}] \frac{\ell/r_{weak}}{105} \qquad 5.18$$

Table 5.13 shows the calculation of column strength using Eq. 5.18 for all 59 specimens reported in this chapter. The comparison between P_i and the actual P_u was calculated as P_i/P_u and also has been shown in Table 5.13. The mean value of P_i/P_u for all specimens was 0.9397, with the standard deviation of 0.046 and the coefficient of variation of 0.049. It should be noted that there were a few specimens that gave unconservative results; i.e., $P_i/P_u > 1.0$. The maximum P_i/P_u was 1.13, or a 13 percent overestimate, while the minimum was 0.848, or a 15 percent underestimate of the actual strength.

In conclusion it has been demonstrated that a method of strength analysis more consistent than the moment magnification analysis for the length effect of reinforced concrete columns under biaxial bending can be developed in terms of a deflection limit, Δ/L total, as in Eq. 5.18. The method of assigning a deflection limit to calculate an additional bending moment or eccentricity has been called an additional moment or complementary moment method.[26,49]

The deflection limit is a function of axial load level P_u/P_o and slenderness ratio $k\ell/r$. For each axis of bending, the limit is proportioned according to the ℓ/r ratio on the weak axis and the strong axis. The term relative eccentricity was defined as the ratio of the eccentricity to the radius of gyration of the same direction of bending, so the relative skew angle was the fictitious angle between the relative eccentricities. The eccentricity to be calculated for estimating the column strength is simply the end eccentricity plus the deflection Δ from the deflection limit. With this procedure, the approximation

TABLE 5.13 COLUMN STRENGTH USING DEFLECTION CONTROL

$$\left(\frac{\Delta}{L}\right) \text{Total} = 0.00372 + \left[0.00270 \frac{1}{P_u/P_o}\right] \frac{\ell/r}{105}$$

Specimen	P_u/P_o	Δ/L Total	Ecc/r		Δ/L		End Ecc		End Ecc + δ		P_x	P_y	P_o	P_t	P_u	P_t/P_u
			e_x/r_x	e_y/r_y	Δ/L x	Δ/L y	$e_{end\ x}$	$e_{end\ y}$	e_x	e_y						
RC-6A	0.2	0.013363	1.11239	0.82958	0.010712	0.007989	2.890	1.197	4.067	2.060	71.1	79.5	234.6	44.7	46.92	0.953
RC-7A	0.2	0.013363	0.57737	1.03950	0.006489	0.011682	1.500	1.500	2.201	2.762	125.2	52.8	234.6	44.1	46.92	0.940
RC-8A	0.2	0.013363	0.25508	1.10880	0.002996	0.013023	0.663	1.600	0.987	3.006	178.8	46.6	234.6	43.9	46.92	0.936
RC-5A	0.4	0.008541	0.52733	0.39271	0.006850	0.005101	1.370	0.567	2.110	1.118	128.7	131.3	234.6	89.9	93.84	0.958
RC-3A	0.4	0.008541	0.27329	0.49203	0.004147	0.007467	0.710	0.710	1.158	1.516	170.6	105.8	234.6	90.5	93.84	0.964
RC-9A	0.4	0.008541	0.12597	0.54747	0.001915	0.008326	0.327	0.790	0.534	1.689	202.0	96.9	234.6	90.8	93.84	0.968
RC-1A	0.6	0.006934	0.24634	0.18369	0.005559	0.006145	0.640	0.265	1.240	0.713	166.7	163.5	234.6	127.3	140.76	0.904
RC-2A	0.6	0.006934	0.11932	0.21483	0.003367	0.006062	0.310	0.310	0.674	0.965	194.3	142.9	234.6	126.9	140.76	0.902
RC-4A	0.6	0.006934	0.05103	0.22176	0.001555	0.006757	0.133	0.320	0.301	1.050	215.5	136.4	234.6	129.7	140.76	0.921
RC-6	0.2326	0.009557	0.3418	1.2890	0.002450	0.009238	0.888	1.860	1.075	2.564	172.1	58.5	231.16	53.8	53.9	0.998
RC-7	0.1768	0.011399	0.7448	1.4837	0.005114	0.010187	1.935	2.141	2.325	2.918	117.3	47.9	227.79	40.0	40.4	0.990
RC-8	0.1736	0.011541	1.6740	1.1310	0.009563	0.006461	4.349	1.632	5.078	2.125	52.1	75.8	232.11	35.6	40.4	0.881
RC-5	0.3373	0.007745	0.1501	0.7810	0.001462	0.007606	0.390	1.127	0.501	1.707	223.8	104.4	257.61	98.4	87.1	1.130
RC-3	0.3579	0.007567	0.4661	0.7110	0.006149	0.006328	1.211	1.026	1.527	1.509	174.0	119.6	266.53	96.6	94.3	1.024
RC-9	0.3514	0.007584	0.8553	0.5010	0.006544	0.003833	2.222	0.723	2.721	1.015	111.1	144.3	243.55	84.6	85.8	0.986
RC-1	0.4730	0.006593	0.1536	0.7193	0.001376	0.006448	0.399	1.038	0.504	1.530	218.7	112.3	251.93	105.2	119.2	0.883
RC-2	0.4776	0.006563	0.3437	0.5156	0.003640	0.005461	0.893	0.744	1.171	1.160	182.1	137.2	251.25	113.6	120.3	0.944
RC-4	0.4853	0.006518	0.5828	0.3458	0.005606	0.003326	1.514	0.499	1.961	0.753	152.7	181.0	265.22	120.4	128.8	0.935
C-8	0.7025	0.009536	0.3552	1.2789	0.002552	0.009188	1.036	2.128	1.231	2.829	207.0	59.6	281.40	55.4	57.1	0.970
C-11	0.1863	0.010062	1.4926	1.0739	0.008151	0.005865	4.354	1.787	4.976	2.234	78.6	83.5	284.87	47.2	53.2	0.887
C-9	0.3552	0.007036	0.2105	0.6856	0.002065	0.006726	0.614	1.141	0.771	1.654	222.6	108.9	270.16	100.3	96.2	1.043
C-6	0.3492	0.007093	0.5465	0.6406	0.004603	0.005396	1.594	1.066	1.965	1.477	161.1	116.7	263.30	91.1	92.2	0.988
C-12	0.3324	0.007263	0.7306	0.6010	0.005609	0.004614	2.131	1.000	2.559	1.352	154.1	140.3	297.85	97.5	99.2	0.983
C-10	0.5207	0.005982	0.1090	0.4609	0.001365	0.005824	0.315	0.767	0.419	1.211	238.2	136.0	264.74	128.6	138.2	0.931
C-7	0.5286	0.005948	0.3496	0.3702	0.004084	0.004324	1.018	0.616	1.329	0.946	189.2	157.5	263.65	127.5	139.7	0.913
C-13	0.4863	0.006142	0.5242	0.3600	0.005063	0.003477	1.579	0.599	1.915	0.864	192.5	195.7	313.06	140.6	152.5	0.922
Drysdale's Specimens																
A1C	0.2647	0.013920	0.488	0.488	0.009843	0.009843	0.707	0.707	2.243	2.243	55.9	55.9	142.05	34.8	37.6	0.926
B1D	0.2842	0.013220	0.488	0.488	0.009348	0.009348	0.707	0.707	2.165	2.165	57.2	57.2	141.8	35.8	40.3	0.888
A2A	0.2788	0.013404	0.488	0.488	0.009478	0.009478	0.707	0.707	2.186	2.186	56.7	56.7	141.3	35.5	39.4	0.901
A2B	0.2831	0.013257	0.488	0.488	0.009376	0.009374	0.707	0.707	2.169	2.169	57.0	57.0	141.3	35.7	40.0	0.893
A3C	0.2650	0.013909	0.488	0.488	0.009835	0.009835	0.707	0.707	2.241	2.241	57.0	57.0	145.3	35.5	38.5	0.922
B1C	0.2565	0.014246	0.488	0.488	0.010073	0.010073	0.707	0.707	2.278	2.278	52.1	52.1	132.55	32.4	34.0	0.953
B1D	0.2595	0.014125	0.488	0.488	0.009988	0.009988	0.707	0.707	2.265	2.265	52.3	52.3	132.55	32.6	34.4	0.948
B2C	0.2761	0.013499	0.488	0.488	0.009545	0.009545	0.707	0.707	2.196	2.196	54.8	54.8	136.55	34.3	37.7	0.910
B2D	0.2761	0.013499	0.488	0.488	0.009545	0.009545	0.707	0.707	2.196	2.196	54.8	54.8	136.55	34.3	37.7	0.910
A3D	0.2588	0.014153	0.488	0.488	0.010008	0.010008	0.707	0.707	2.268	2.268	56.5	56.5	145.3	35.1	37.6	0.934

TABLE 5.13 (Continued)

Specimen	P_u/P_o	Δ/L Total	Ecc/r		Δ/L		End Ecc		End Ecc + δ		P_x	P_y	P_o	P_i	P_u	P_i/P_u
			e_x/r_x	e_y/r_y	Δ/L x	Δ/L y	$e_{end\ x}$	$e_{end\ y}$	e_x	e_y						
Dryadale's Specimens (Continued)																
C2A	0.2791	0.013394	0.265	0.640	0.005124	0.012375	0.384	0.924	1.183	2.855	82.0	46.9	141.55	37.8	39.5	0.957
C2B	0.2769	0.013471	0.265	0.640	0.005154	0.012446	0.384	0.924	1.188	2.866	81.8	46.7	141.55	37.6	39.2	0.959
C3A	0.2815	0.013311	0.265	0.640	0.005092	0.012298	0.384	0.924	1.178	2.842	85.6	48.7	147.80	39.3	41.6	0.945
C3B	0.2686	0.013772	0.265	0.640	0.005269	0.012724	0.384	0.924	1.206	2.909	84.6	47.8	147.80	38.5	39.7	0.970
E1C	0.2295	0.015485	0.398	0.961	0.005925	0.014307	0.574	1.386	1.498	3.618	72.4	37.3	142.05	29.8	32.6	0.914
E1D	0.2365	0.015136	0.398	0.961	0.005792	0.013984	0.574	1.386	1.478	3.568	72.9	37.9	142.05	30.2	33.6	0.899
E2A	0.2177	0.016122	0.398	0.961	0.006169	0.014895	0.574	1.386	1.536	3.710	77.3	37.6	154.80	30.2	33.7	0.896
E2B	0.2158	0.016232	0.398	0.961	0.006211	0.014997	0.574	1.386	1.543	3.726	77.1	37.4	154.80	30.1	33.4	0.901
F1A	0.3965	0.010530	0.132	0.320	0.004015	0.009734	0.191	0.462	0.817	1.981	100.4	63.1	148.05	52.5	58.7	0.894
F1B	0.3762	0.010897	0.132	0.320	0.004155	0.010074	0.191	0.462	0.839	2.034	99.3	62.0	148.05	51.4	55.7	0.923
F2A	0.3799	0.010827	0.132	0.320	0.004129	0.010009	0.191	0.462	0.835	2.023	100.8	63.0	150.05	52.3	57.0	0.918
F2B	0.3799	0.010827	0.132	0.320	0.004129	0.010009	0.191	0.462	0.835	2.023	100.8	63.0	150.05	52.3	57.0	0.918
Wu's Specimens																
1	0.2291	0.015505	0.611	0.611	0.010964	0.010964	0.662	0.662	1.937	1.937	29.3	29.3	82.95	17.8	19.0	0.937
2	0.2207	0.015954	0.614	0.614	0.011281	0.011281	0.885	0.885	2.645	2.645	50.0	50.0	144.06	30.2	31.8	0.950
3	0.1973	0.017405	0.615	0.615	0.012307	0.012307	1.110	1.110	3.494	3.494	75.6	75.6	228.10	45.3	45.0	1.007
4	0.2065	0.016795	0.612	0.612	0.011876	0.011876	1.325	1.325	4.086	4.086	113.4	113.4	334.21	68.3	69.0	0.990
10	0.2117	0.016474	0.614	0.614	0.011649	0.011649	0.885	0.885	2.702	2.702	49.0	49.0	144.06	29.5	30.5	0.967
16	0.2093	0.016628	0.614	0.614	0.011752	0.011752	0.885	0.885	2.718	2.718	48.5	48.5	143.31	29.2	30.0	0.973
16	0.2239	0.015779	0.614	0.614	0.011157	0.011157	0.885	0.885	2.625	2.625	48.8	48.8	139.81	29.6	31.3	0.946
26	0.1783	0.018863	0.520	0.900	0.009437	0.016333	0.563	0.975	1.660	2.874	39.4	21.9	102.64	16.3	18.3	0.891
27	0.1871	0.018151	0.520	0.901	0.009073	0.015721	0.750	1.300	2.165	3.752	69.3	37.9	179.06	28.4	33.5	0.848
28	0.1700	0.019602	0.520	0.901	0.009798	0.016977	0.938	1.625	2.836	4.914	105.4	56.2	281.23	42.1	47.8	0.881
29	0.1535	0.021310	0.520	0.901	0.010602	0.018370	1.125	1.950	3.590	6.221	147.8	76.8	408.46	57.7	62.7	0.920

$\Sigma \frac{P_i}{P_u}$	55.443
No. of data	59
Mean	0.9397
Standard deviation	0.0462
Coefficient of variation	0.0492

of member strength of pinned-end columns with equal end moments that cause columns to deflect in single curvature can be estimated more accurately than the approximation of strength derived only on the basis of moment magnifiers and the strength of cross sections. The moment magnifier method was found less effective for the estimation of column strength in biaxial bending because of its inconsistency in the calculation of column stiffness.

5.6 Procedure to Calculate Column Strength Using Deflection Control

A column can be analyzed for capacity to support a given condition of thrust and moment about each principal axis using the deflection control procedure. A step-by-step outline of the procedure is described as follows:

1. Compute the end eccentricities under the load conditions given, and then calculate the relative eccentricity e/r about each principal axis.
2. Find the relative skew angle according to the relative eccentricities.
3. Use Eq. 5.18 and compute the total deflection ratio, Δ/L, for the relative thrust level P_u/P_o.
4. Proportion the deflection ratio components to each principal axis according to the relative skew angle in step 2.
5. Determine the deflection limit Δ about each axis by multiplying Δ/L values from step 4 by the column length.
6. The failure eccentricity for each axis is the end eccentricity plus the deflection limit in step 5.
7. Apply the failure eccentricity in step 6 to the uniaxial interaction diagram and locate the uniaxial failure thrust values P_x and P_y for each axis.

8. Use the Reciprocal Load Equation (Eq. 5.12) to predict the strength of the column P_i.

9. Compare P_i to the given thrust P_u. If $P_i > P_u$ the column is safe under the loading condition given. If $P_u > P_i$ the column is not strong enough to carry the loads assigned.

An example for the above procedure is illustrated step by step, using Specimen RC-1:

The details of the problem

Failure thrust	119.2 kips
Strong axis moment	47.6 k-in.
Weak axis moment	123.8 k-in.
f'_c	4.886 ksi
f_y	65.5 ksi
Column length	76.25 in.

Column dimension and reinforcement were shown in Chapter 2 (i.e., 5 in. by 9 in. rectangular column with 10 - 8mm diameter deformed bars).

Strength Analysis

The step numbers are the same as previously described above.

1. End eccentricity $e_s = 0.399$ in.
   $e_w = 1.038$ in.
   Radius of gyration $r_s = 2.598$ in.
   $r_w = 1.443$ in.
   Relative eccentricity $\frac{e_s}{r} = \frac{399}{2.598} = 0.1536$
   $\frac{e_w}{r} = \frac{1.038}{1.443} = 0.7193$

2. Relative skew angle $= \tan^{-1}(\frac{0.1536}{0.7193})$
   $= 12.05$ degree

3. Squash strength $P_o = A_c f'_c + A_s f_y$
   $= 252.0$ k
   Relative thrust level $\frac{P_u}{P_o} = \frac{119.2}{252.0} = 0.473$

Deflection limit from Eq. 5.18

$$\Delta/L = 0.00372 + [0.00270 \frac{1}{P_u/P_o}] \frac{\ell/r_{weak}}{105}$$

$$\Delta/L = 0.00372 + [0.00270 \frac{1}{0.473}] \frac{76.25}{1.443 \times 105}$$

$$\Delta/L = 0.006593$$

4. Proportion for weak axis and strong axis

$$\frac{\Delta}{L}s = 0.006593 \sin (12.05^o)$$
$$= 0.001376$$

$$\frac{\Delta}{L}w = 0.006595 \cos (12.05^o)$$
$$= 0.006448$$

5,6 Maximum eccentricity $e = e_{end} + \frac{\Delta}{L} \cdot L$

Strong axis $e_s = 0.399 + 0.001376 \times 76.25 = 0.504$ in.

Weak axis $e_w = 1.038 + 0.006448 \times 76.25 = 1.530$ in.

7. With $e_s = 0.504$, $e_w = 1.530$ from interaction diagram for uniaxial bending of RC-1 in Fig. 5.5

$P_s = 218.7$ k

$P_w = 112.3$ k

8. From Eq. 5.12 $\frac{1}{P_i} = \frac{1}{P_s} + \frac{1}{P_w} - \frac{1}{P_o}$

$$\frac{1}{P_i} = \frac{1}{218.7} + \frac{1}{112.3} - \frac{1}{252.0}$$

$$P_i = 105.2 \text{ k}$$

The analyzed strength was 105.2, which was about 12 percent lower than the actual strength of 119.2 k.

The sensitivity of the computation procedure for changes of the relative load level P_u/P_o in Eq. 5.18 was investigated. When the actual failure strength P_u is not known, it was found that even with inaccurate estimates of P_u used in Eq. 5.18, the resulting predicted strength P_i was found to converge toward the "correct" value. Convergence was more rapid for an iteration method that started with

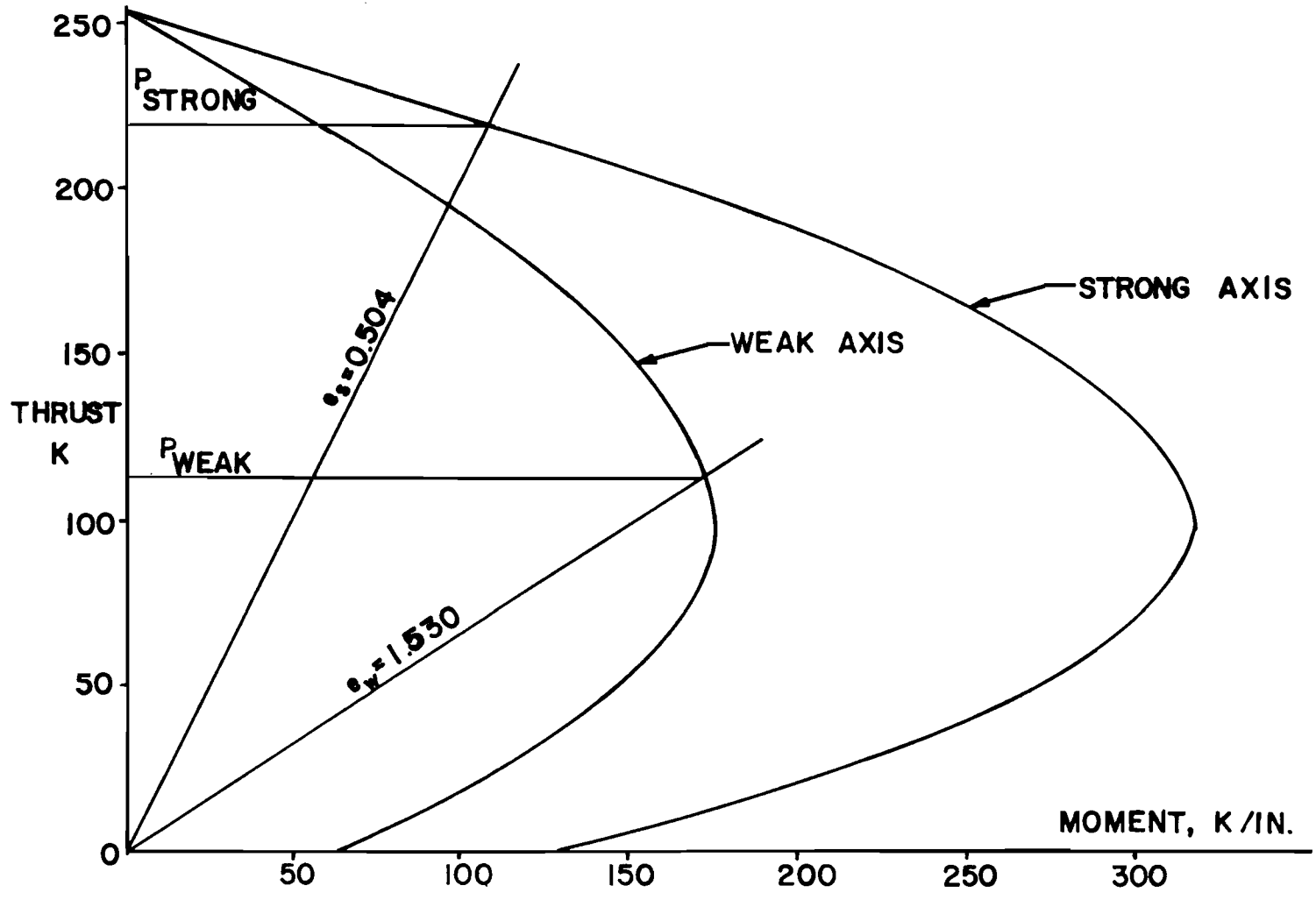

Fig. 5.5 Uniaxial interaction diagram for thrust and moment
Specimen RC-1 (f'_c = 4.886 ksi)

values P_u greater than P_i and the rate of convergence was slowest for low ratios P_i/P_o. For Specimen RC-1 as an example if the first estimate of P_u = 200 k, the resulting P_i = 110.1 k, and then using 110.1 k as P_u for the next calculation, P_i = 104.2 k. If the procedure had started first with P_u = 70 k, the resulting P_i = 81.5 k, and the second iteration yields P_i = 84.0 k. A review of values from Drysdale and Wu specimens showed that if the iteration procedure were used to compute the column strength with unknown values of P_u, convergence should not be assumed unless the computed value of P_i is less than the initial value P_u used in the calculation of Δ/L in Eq. 5.18. The assumed P_u at the start should be greater than the actual strength of the column for the quickest convergence. Of course, if P_i is greater than P_u, the P_i estimate does represent at least a lower bound on the maximum or "correct" value.

Data from very slender columns that were tested by Saenz and Martin[48] were used to test the deflection limit method for long concentrically loaded columns. Equation 5.18 was used to calculate Δ/L and the total deflection was assigned to the weak axis deflection. With concentric loading the end eccentricity was considered zero and the maximum analytic eccentricity used was taken as the total deflection. The predicted failure thrust was determined from the uniaxial interaction diagram with thrust and moment acting about the weak axis. End conditions of the specimens were assumed partially fixed such that the effective length used in the computation was 0.75L. Three types of specimens were selected in the study: specimens with lengths of 7-1/2, 9, and 12 ft. with concrete strengths of 3350, 4930, and 5590 psi, respectively. The column cross section was 5 in. by 3-9/16 in., with four #2 bars as longitudinal reinforcing steel. The deflection limit method gave the strength of the columns as 53.4, 67.5, and 55.3 kips for 7-1/2, 9, and 12 ft. specimens, respectively. The average test strengths of these specimens were 54.3, 72.0, and 54.2 kips. The results showed that deflection limit procedures may also apply for predicting the strength of columns under concentric

load, even without an initial or arbitrary eccentricity specified for analysis.

CHAPTER 6

CONCLUSIONS

6.1 Summary of the Investigation

The purpose of the investigation reported herein was to study the behavior of reinforced concrete columns subject to loads that cause bending moments about two principal axes plus compression in the longitudinal direction. A general review on column strength included data available from previous studies by other investigators. Additional data were obtained from physical tests on columns with rectangular and partial circle cross sections. Strengths estimated from an approximate method of calculation were compared with the experimental data, and the influence of parameters that would affect the accuracy of the method was studied. Secondary effects of lateral deformation were included in the investigation of member strength.

A moment magnifier method was used also for comparing results with the experimental data. Methods of computing member stiffness as recommended by the ACI Building Code[1] were included in the comparisons with test data. A numerical analysis method was also used after it was adjusted to agree with test results and it was used to develop more analytical data for comparison with the approximate methods of analysis. Member strength for very slender columns could be estimated from a deflection control method which was introduced. An empirical equation for column strength was proposed on the basis of its favorable comparison with experimental results.

6.2 Results of the Investigation from Physical Tests

(a) The assumption that plane sections remain plane before and after loading was examined and was found to be acceptable. On the basis of correspondence between a fourth point measurement and a plane section analytical prediction, test data showed that the distribution of the average cross-sectional strain was within 10 percent of being a plane when long gage-lengths (5 thicknesses of the member) were used, although the local strain differences for each 6-in. gage length showed greater values. The variations overall at less than 10 percent were considered accurate enough for computing forces compatible with plane strain distribution. This assumption was used with average strains through a 30-in. length of specimen in all the strength analyses throughout this report.

(b) In the analyses of forces that were consistent with strain measurements, the stress-strain functions for concrete that used a full cylinder strength f'_c as the maximum stress gave better correlation than stress-strain functions that used reduced maximum strength such as $0.85f'_c$ as the maximum compressive stress. The integration of stresses consistent with strains that were determined from measured longitudinal displacements indicated that a parabolic rectangular stress-strain function for concrete gave values of force and moment in better agreement with measured loads than any other form of stress-strain functions for concrete that were investigated.

(c) Load angle and neutral axis angle were found not to be equal. The difference between the load angle and the neutral axis angle always showed that the neutral axis shifted toward the weak axis of bending. The difference was significant enough that it should not be neglected in the analysis when both the neutral axis angle and load angle are required such as in numerical analysis. The difference between these angles tended to increase as the nominal angle increased. No effect of thrust level was observed to be

involved in this difference. Secondary deflections caused the net value of load angle ($M_{\text{strong axis}}/M_{\text{weak axis}}$) to vary along the length of a slender column. The load angle change indicated that columns deflected more in the weak axis direction than in the strong axis direction. The deflection caused more secondary moment about weak axis than about the strong axis. Thus the load angle decreased from end to midheight of the column where the maximum deflection occurred.

(d) Torsional effects from twisting of the member were small and could be neglected in the analysis.

6.3 Results of the Study of Cross Section Strength and Stiffness

6.3.1 Strength. The strength of short columns can be approximated using the reciprocal load equation:

$$\frac{1}{P_i} = \frac{1}{P_x} + \frac{1}{P_y} - \frac{1}{P_o}$$

This equation requires uniaxial interaction diagrams of thrust and moment about each principal axis. The investigation of strength revealed that:

(a) The reciprocal load equation could be used to predict the strength of the column cross section (with the average of less than 6 percent difference from the test results) when the accurate uniaxial interaction diagrams were used.

(b) Interaction diagrams of ultimate thrust and moment derived with the rectangular stress block for concrete strength showed generally less strength than that obtained in measured tests. Consequently, when the interaction diagrams derived from the rectangular stress block assumption are used, the biaxial column strength was underestimated by the reciprocal load equation.

(c) The stress-strain function that best represented the concrete behavior in constructing the uniaxial interaction diagram was the parabolic rectangular function. The stress-strain curve consisted of a parabola with a maximum stress of f'_c at a strain of

0.002, and beyond the strain of 0.002 the concrete stress remained constant at f'_c until the failure strain was reached. The actual maximum strain across a 30-in. gage length at failure from tests varied from 0.00228 to 0.00393; the maximum strain up to 0.00525 was found locally in the 6 in. segment of the column. In the construction of interaction diagrams for failure thrust and uniaxial moment, the failure strain of 0.0035 was assumed for every specimen.

(d) The amount of reinforcement, aspect ratio, and load angle were not found to be factors that influenced the calculation of strength with the reciprocal load method. The accuracy of the equation depended on the accuracy of the interaction diagram of thrust and moments about each principal axis.

6.3.2 Stiffness. The slope of the graphs of moment and curvature (M-φ curve) at the middle portion of the column represented the stiffness EI of the section. The study of stiffness of the section showed that:

(a) Before cracking the computed stiffness EI based on an uncracked cross section agreed well with the initial slope of the measured M-φ curve for strong axis bending of both rectangular and oval-shaped sections. For weak axis flexural stiffness, the computation of a nominal uncracked section stiffness overestimated the stiffness of the oval-shaped column. At low levels of thrust ($P_u = 0.2P_o$) the computed uncracked section stiffness for bending about the weak axis of rectangular cross sections compared well with the initial slope of the M-φ curves, but at higher thrust levels the same computation again overestimated the cross section stiffness.

(b) After each specimen cracked the nominal cracked section EI was assumed to be equal to 40 percent of the uncracked stiffness. The comparison with graphs from tests showed that the nominal cracked stiffness for bending about the strong axis was larger than the slope of the measured M-φ curve, but still in reasonable agreement. For bending about the weak axis, the computed uncracked section

EI overestimated the column stiffness at every level of thrust for both rectangular and oval-shaped columns.

6.4 Results of the Study of Slenderness Effects on Member Strength

6.4.1 The study on length effects showed that the moment magnification method would not give accurate results in predicting the member strength if the flexural stiffness EI of the member was inaccurately computed. The recommended stiffnesses in the ACI Building Code[1] were used in the investigation. It was found that for the test specimens reported, ACI Eq. (10-7) underestimated weak axis stiffness at high levels of thrust ($0.5P_o$), but better agreement with test results were obtained at lower levels of thrust. However, ACI Eq. (10-7) gave good agreement with the tests for calculating strong axis stiffness at every level of thrust. The stiffness computed with ACI Eq. (10-8) overestimated the column stiffness at low thrust levels ($0.2P_o$), but gave reasonable values at higher thrust levels. The data from experiments suggested that member stiffness should reflect the influence of the level of thrust. A graph of measured flexural stiffness and the thrust level showed that the effective stiffness EI increased as the thrust level increased for thrust values as high as $0.55P_o$. The study of long columns tested by other investigators showed that a different relationship exists between thrust level and stiffness. It was concluded that simplified estimates of stiffness were inconsistent; each method of calculating stiffness might be good for one specimen but might not be accurate for others that had a different overall slenderness or load angle.

6.4.2 The numerical analysis of column strength using computer program BIAM2 gave favorable results compared with the experimental data (average of 0.997 with a maximum of 13 percent overestimate and 23 percent underestimate when compared to the observed strength). The convergence of the iteration method was found to be the main problem in the BIAM2 analysis. The iteration could

not converge if tolerance limits were too small, but when larger tolerances were used the problem converged slowly.

6.4.3 Although intentional underestimations of stiffness are generally safe for design, for the most slender columns in this report the method of computing column stiffness from the ACI Code formulas could not be applied because the formulas indicated that columns failed in instability at loads lower than the actual failure load (i.e., $P_{cr} < P_u$). It was found that in addition to the slenderness ratio the thrust level should be a factor in the complementary moment or deflection control. An empirical equation for the deflection limit was derived from the data available. The assigned deflection then was distributed to each principal axis according to the nominal ratio of eccentricity about each axis of bending. The reciprocal load equation then was applied to calculate the column strength after the additional deflection had been added to the end eccentricity (if any). Predictions of column strength from the method were found to be within 15 percent of measured values from tests.

6.5 Conclusions and Recommendations

The reciprocal load equation provides a good method for estimating approximate column strength for biaxial bending problems. This method requires only uniaxial interaction diagrams for bending about two major axes and it is independent of other biaxial bending parameters such as percentage of steel, load angle, and column shape aspect ratio. Accurate results require the use of interaction diagrams that are accurate. A parabola-rectangle function for concrete stress-strain behavior with a full cylinder strength f'_c for maximum compressive stress gave results less likely to underestimate strength than did the use of rectangular stress block. Eccentrically loaded columns can be designed for specified thrust and eccentricities plus additional eccentricities that accommodate length effects. The moment magnifier method for biaxial bending problems is accurate only if the flexural stiffness is accurately computed. More consistent results were found using the deflection limit to assign the

additional eccentricity to the column. No computation of flexural stiffness EI is required for using the deflection limit method. Also the neutral axis angle was not required in the deflection limit procedure, so that the relationship between load angle and neutral axis angle is not involved in the computation.

In this test series only columns with pinned-ends subjected to equal end moments that caused the columns to bend in single curvature were studied. Further work on columns with other end conditions and different end moments should be observed. It is recommended that further studies of stiffness of members be conducted. The existing computer program BIAM2, with possible modifications for more rapid convergence, can be used as a "true" strength predictor when no physical test data are available. Simplified general forms of equations to predict EI can be studied systematically in order to determine the domains of accuracy for the simplified equations. The biaxial bending capacity of unique shapes of cross section such as L, T, or hollow boxes can be studied also.

APPENDIX A

DRYSDALE AND WU SPECIMENS

A P P E N D I X A

DRYSDALE AND WU SPECIMENS

(a) Dimensions and Properties

Drysdale Specimens

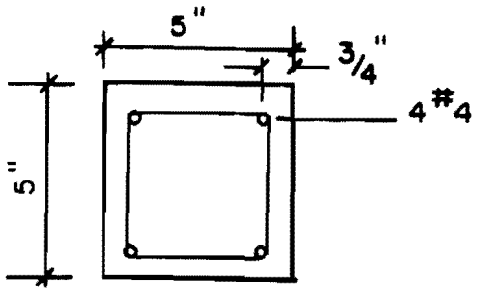

Length = 13'0"

Reinforcement 4 - #4

f_y = 56.0 ksi

A_s = 0.2 $in.^2$ each

E_s = 29000 ksi

Wu Specimens

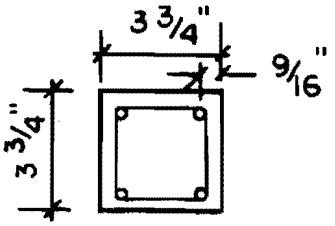

Length = 9'8-1/4"

Reinforcement 4 - #3

f_y = 57.2 ksi

A_s = 0.113 $in.^2$ each

E_s = 28600 ksi

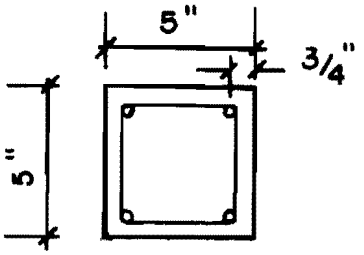

Length = 13'0"

Reinforcement 4 - #4

f_y = 57.2 ksi

A_s = 0.186 $in.^2$ each

E_s = 28600 ksi

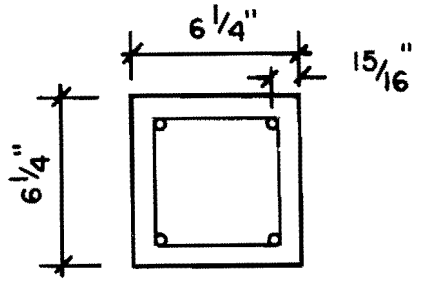

Length = 16'1-3/4"

Reinforcement 4 - #5

f_y = 57.0 ksi

A_s = 0.298 $in.^2$ each

E_s = 28500 ksi

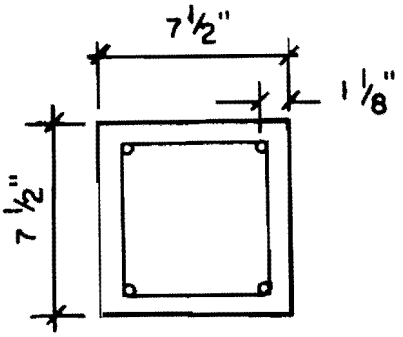

Length = 19'4-1/2"

Reinforcement 4 - #6

f_y = 56.8 ksi

A_s = 0.446 $in.^2$ each

E_s = 28400 ksi

(b) Concrete Strength and Loading Information

Specimen	f'_c psi	Failure Load kips	End Eccentricity e_x in.	End Eccentricity e_y in.
Drysdale Specimens				
A1C	3890	37.6	0.707	0.707
A1D	3880	40.3	0.707	0.707
A2A	3860	39.4	0.707	0.707
A2B	3860	40.0	0.707	0.707
A3C	4020	38.5	0.707	0.707
A3D	4020	37.6	0.707	0.707
B1C	3510	34.0	0.707	0.707
B1D	3510	34.4	0.707	0.707
B2C	3670	37.7	0.707	0.707
B2D	3670	37.7	0.707	0.707
C2A	3870	39.9	0.383	0.924
C2B	3870	39.2	0.383	0.924
C3A	4120	31.6	0.383	0.924
C3B	4120	39.7	0.383	0.924
E1C	3890	32.6	0.574	1.386
E1D	3890	33.6	0.574	1.386
E2A	4400	33.7	0.574	1.386
E2B	4400	33.7	0.574	1.386
F1A	4130	58.7	0.191	0.462
F1B	4130	55.7	0.191	0.462
F2A	4210	57.0	0.191	0.462
F2B	4210	57.0	0.191	0.462

Specimen	Size	f'_c psi	Failure Load kips	End Eccentricity e_x in.	End Eccentricity e_y in.
Wu Specimens					
1	3-3/4"x3-3/4"	4060	19.0	0.662	0.662
2	5"x5"	4060	31.8	0.885	0.885
3	6-1/4"x6-1/4"	4100	45.0	1.110	1.110
4	7-1/2"x7-1/2"	4140	69.0	1.325	1.325
10	5"x5"	4060	30.5	0.885	0.885
16	5"x5"	4030	30.0	0.885	0.885
16	5"x5"	3890	31.3	0.885	0.885
26	3-3/4"x3-3/4"	5460	18.3	0.563	0.975
27	5"x5"	5460	33.5	0.750	1.300
28	6-1/4"x6-1/4"	5460	47.8	0.938	1.625
29	7-1/2"x7-1/2"	5460	62.7	1.125	1.950

APPENDIX B

STRESS-STRAIN RELATIONSHIP OF CONCRETE

A P P E N D I X B

STRESS-STRAIN RELATIONSHIP OF CONCRETE

The stress-strain functions of concrete used in the strain analysis in Chapter 3 were the functions which were proposed by Hognestad, Todeschini, et al., Kent and Park, and Chang. The details of these functions are described below.

(a) Hognestad Stress-Strain Function. The function consists of two parts, the first part is a parabola with an equation of

$$f_c = f_c''\left[\frac{2\epsilon}{\epsilon_o} - \left(\frac{\epsilon}{\epsilon_o}\right)^2\right]$$

where f_c = Concrete stress at strain ϵ

f_c'' = Maximum compressive stress at strain ϵ_o, equals $0.85f_c'$

f_c' = Concrete cylinder strength

ϵ = Strain of concrete associate with stress f_c

ϵ_o = Strain of concrete at maximum stress

$\epsilon_o = 2\frac{f_c''}{E_c}$

E_c = Modulus of elasticity of concrete

The functions were quoted from Fowler's report.

The latter part was a straight line with the stress of f_c'' at strain ϵ_o and a decrease to $0.85f_c''$ at a strain of 0.0038 which is considered the maximum strain of concrete at failure.

(b) Todeschini, et al. Stress-Strain Function. The function proposed by Todeschini is a continuous curve with the equation

$$f_c = 2f_c''\frac{\epsilon}{\epsilon_o\left[1 + \left(\frac{\epsilon}{\epsilon_o}\right)^2\right]}$$

with the same notation as (a).

(c) Kent and Park Stress-Strain Function. The Kent and Park stress-strain function has two parts as does Hognestad's function, but the full concrete cylinder strength, f'_c is used. The equation for the parabola is

$$f_c = f'_c \left[\frac{2\epsilon}{\epsilon_o} - \left(\frac{\epsilon}{\epsilon_o} \right)^2 \right]$$

with the same notation as function (a), but ϵ_o is taken as 0.002 instead of $2f'_c/E_c$.

For strains greater than ϵ_o the function is also a straight line which is represented by the following equations:

for confined concrete and $\epsilon > 0.002$

$$f_c = f'_c [1 - Z(\epsilon - \epsilon_o)]$$

$$Z = \frac{0.5}{\epsilon_{5oh} + \epsilon_{5ou} - \epsilon_o}$$

$$\epsilon_{5oh} = \frac{3}{4} \rho'' \sqrt{\frac{b''}{s}}$$

$$\rho'' = \frac{2(b'' + d'')A''_s}{b''d''s}$$

$$\epsilon_{5ou} = \frac{3 + 0.002f'_c}{f'_c - 1000}$$

where A''_s = Area of hoop bar

s = Spacing of hoop reinforcement

b'', d'' = Width and depth of the confined area, $b'' \leq d''$

Z = Slope of the straight line portion of the function

In the calculation in Chapter 3, Z was calculated and approximated as 260.

(d) Chang Stress-Strain Function. Chang modified the Kent and Park stress-strain function by including the compression steel effect in the slope of the straight line. The first portion of the function

is the same as Kent and Park except that Chang used $\epsilon_o = 2f'_c/E_c$ instead of 0.002. The tail of the function has the same equation as function C, but the calculation for ρ'' contains also the effect of compression steel,

$$\rho'' = \frac{2(b'' + d'')A''_s}{b''s''s} + \frac{A'_s}{b''d''}$$

where A'_s = Area of steel under compression

The calculation of Z by Chang's method for the specimen in this test program gave a Z value of 68 which was used in Chapter 3.

Two more stress-strain functions were introduced in Chapter 3, the Modified Hognestad Stress-Strain Function and the Parabolic-Rectangular Stress-Strain Function. Details of these two functions are explained in Chapter 3 and will not be repeated here. The graphical expression of all these stress-strain functions are shown in Fig. 3.7 for the concrete strength of 5000 psi.

REFERENCES

1. ACI Committee 318, Building Code Requirements for Reinforced Concrete (ACI 318-71), American Concrete Institute, Detroit, 1971.

2. ACI Committee 318, Commentary on Building Code Requirements for Reinforced Concrete (ACI 318-71), Detroit, 1971.

3. Au, Tung, "Ultimate Strength Design of Reinforced Concrete Members Subject to Unsymmetrical Bending," Journal of the American Concrete Institute, Vol. 29, No. 8, February 1958, pp. 657-674.

4. Breen, J. E., "The Restrained Long Concrete Column as a Part of a Rectangular Frame," unpublished Ph.D. dissertation, The University of Texas at Austin, June 1962.

5. Bresler, B., "Design Criteria for Reinforced Columns under Axial Load and Biaxial Bending," Journal of the American Concrete Institute, Vol. 32, No. 5, November 1960, pp. 481-490.

6. Brettle, H. J., and Warner, R. F., "Ultimate Strength Design of Rectangular Reinforced Concrete Sections in Compression and Biaxial Bending," Civil Engineering Transactions (Australia), Vol. CE10, No. 6, April 1968, pp. 101-110.

7. Chang, W. F., "Long Restrained Reinforced Concrete Columns," unpublished Ph.D. dissertation, The University of Texas at Austin, June 1961.

8. Chang, D. C., Computer program for calculating interaction diagram using maximum moment from P-M-ϕ relationship, The University of Texas at Austin.

9. Chu, K. K., and Pubarcius, A., "Biaxially Loaded Reinforced Concrete Columns," Journal of the Structural Division, ASCE, Proc. V. 84, No. ST8, December 1958.

10. Comite Europeen du Beton, Recommendation for an International Code of Practice for Reinforced Concrete, American Concrete Institute, London, 1970.

11. Craemer, H., "Skew Bending in Reinforced Concrete Computed by Plasticity," Journal of the American Concrete Institute, Vol. 23, No. 6, February 1952, pp. 516-519.

12. Concrete Reinforcing Steel Institute, CRSI Handbook Based Upon the 1971 ACI Building Code, Concrete Reinforcing Steel Institute, Chicago, 1972.

13. Desai, J. A., "Strength and Stiffness of Reinforced Concrete Rectangular Columns under Biaxially Eccentric Thrust," unpublished M.S. thesis, The University of Texas at Austin, December 1975.

14. Drysdale, R. G., "The Behavior of Slender Reinforced Concrete Columns Subjected to Sustained Biaxial Bending," unpublished Ph.D. dissertation, University of Toronto, Canada, 1967.

15. Drysdale, R. G., and Huggins, M. W., "Sustained Biaxial Load on Slender Concrete Columns," Journal of the Structural Division, ASCE, Proc. V. 97, No. ST5, May 1971, pp. 1423-1443.

16. Eloseily, H., "Ultimate Strength of Rectangular Reinforced Concrete Sections under Biaxially Eccentric Loads," Swiss Federal Institute of Technology, Zurich, December 1967.

17. Farah, A., and Huggins, M. W., "Analysis of Reinforced Concrete Columns Subjected to Longitudinal Load and Biaxial Bending," Journal of the American Concrete Institute, Vol. 66, No. 7, July 1969, pp. 569-575.

18. Ferguson, P. M., Reinforced Concrete Fundamentals, Third Edition, John Wiley & Sons, Inc., New York, 1973.

19. Fleming, J. F., and Warner, S. D., "Design of Columns Subjected to Biaxial Bending," Journal of the American Concrete Institute, Vol. 63, No. 3, March 1965, pp. 1205-1230.

20. Fleming, R. J., "Ultimate Strength Analysis for Skew Bending of Reinforced Concrete Columns," unpublished M.S. thesis, The University of Texas at Austin, May 1974.

21. Fowler, T. J., "Reinforced Concrete Columns Governed by Concrete Compression," unpublished Ph.D. dissertation, The University of Texas at Austin, January 1966.

22. Furlong, R. W., "Long Columns in Single Curvature as Part of Concrete Frames," unpublished Ph.D. dissertation, The University of Texas at Austin, June 1963.

23. Furlong, R. W., "Ultimate Strength of Square Columns under Biaxially Eccentric Loads," Journal of the American Concrete Institute, Vol. 32, No. 9, March 1961, pp. 1129-1140.

24. Green, R., "Behavior of Unrestrained Reinforced Concrete Columns under Sustained Load," unpublished Ph.D. dissertation, The University of Texas at Austin, January 1966.

25. Green, D. J., "Physical Testing of Reinforced Concrete Columns in Biaxial Bending," unpublished M.S. thesis, The University of Texas at Austin, May 1975.

26. Hage, S. E., and MacGregor, J. G., "The Second-Order Analysis of Reinforced Concrete Frames," Structural Engineering Report No. 49, Department of Civil Engineering, University of Alberta, Edmonton, Alberta, Canada, October 1974.

27. Hognestad, E., "A Study of Combined Bending and Axial Load in Reinforced Concrete Members," Bulletin No. 399, University of Illinois Engineering Experiment Station, Urbana, November 1951.

28. Kent, D. C., and Park, R., "Flexural Members with Confined Concrete," Journal of the Structural Division, ASCE, Proc. V. 97, No. ST7, July 1971, pp.1969-1990.

29. Meek, D. C., "Ultimate Strength Design Charts for Columns with Biaxial Bending," Journal of the American Concrete Institute, Vol. 60, No. 8, August 1963, pp. 1035-1064.

30. Pannell, F. N., "The Design of Biaxially Loaded Columns by Ultimate Load Methods," Magazine of Concrete Research (London), Vol. 12, No. 35, July 1960, pp. 99-108.

31. Pannell, F. N., "Biaxially Loaded Reinforced Concrete Columns," Discussion of Proceedings, Journal of the Structural Division, ASCE, Proc. V. 85, No. ST6, June 1959, pp. 47-54.

32. Pannell, F. N., "Failure Surface for Members in Compression and Biaxial Bending," Journal of the American Concrete Institute, Vol. 60, No. 1, January 1963, pp. 129-140.

33. Parme, A. L., Neives, J. M., and Gouwens, A., "Capacity of Reinforced Rectangular Columns Subject to Biaxial Bending," Journal of the American Concrete Institute, Vol. 63, No. 9, September 1966, pp. 911-923.

34. Portland Cement Association, "Capacity of Reinforced Rectangular Columns Subject to Biaxial Bending," Advanced Engineering Bulletin No. 18, Portland Cement Association, Skokie, Illinois, 1966.

35. Portland Cement Association, "Biaxial and Uniaxial Capacity of Rectangular Columns," Advanced Engineering Bulletin No. 20, Portland Cement Association, Skokie, Illinois, 1967.

36. Portland Cement Association, "IBM 1130 Computer Program for the Ultimate Strength Design of Reinforced Concrete Columns," CEPA Library No. 03.0140, Skokie, Illinois, December 1967.

37. Ramamurthy, L. N., "Investigation of the Ultimate Strength of Square and Rectangular Columns under Biaxially Eccentric Loads," Symposium on Reinforced Concrete Columns, ACI publication SP-13, Detroit, 1966, pp. 263-298.

38. Redwine, R. B., "The Strength and Deformation Analysis of Rectangular Reinforced Concrete Columns in Biaxial Bending," unpublished M.S. thesis, The University of Texas at Austin, May 1974.

39. Rusch, H., "Research Toward a General Flexural Theory for Structural Concrete," Journal of the American Concrete Institute, Vol. 57, No. 1, July 1960, pp. 1-28.

40. Sargin, M., "Stress-Strain Relationship for Concrete and the Analysis of Structural Concrete Sections," Study No. 4, Solid Mechanics Division, University of Waterloo, Waterloo, Ontario, Canada, 1971.

41. Texas Highway Department, Standard Specifications for Road and Bridge Construction, 1962, pp. 473-487.

42. Timoshenko, S. P., and Gere, J. M., Theory of Elastic Stability, Second Edition, McGraw-Hill Book Co., Inc., New York, 1961.

43. Todeschini, C. E., Bianchini, A. C., and Kesler, C. E., "Behavior of Concrete Columns Reinforced with High Strength Steels," Journal of the American Concrete Institute, Vol. 61, No. 6, June 1964, pp. 701-716.

44. Warner, R. F., "Biaxial Moment Thrust Curvature Relations," Journal of the Structural Division, ASCE, Proc. V. 95, No. ST5, May 1969, pp. 923-940.

45. Weber, D. C., "Ultimate Strength Design Charts for Columns with Biaxial Bending," Journal of the American Concrete Institute, Vol. 63, No. 11, November 1966, pp. 1205-1230.

46. Whitney, C. S., and Cohen, E., "Guide for Ultimate Strength Design of Reinforced Concrete," Journal of the American Concrete Institute, Vol. 53, No. 5, November 1956, pp. 455-490.

47. Wu, H., "The Effect of Volume/Surface Ratio on the Behavior of Reinforced Concrete Columns under Sustained Loading," unpublished Ph.D. dissertation, University of Toronto, Ontario, Canada, 1973.

48. Saenz, L. P., and Martin, I., "Test of Reinforced Concrete Columns with High Slenderness Ratios," Journal of the American Concrete Institute, Vol. 60, No. 5, May 1963, pp. 589-616.

49. Planning and Design of Tall Buildings, Draft 2, Chapter 23 "Stability," Lehigh University, Bethlehem, Pennsylvania, September, 1976.